Synthesis, Characterization, and Reactivity of Transition Metal Complexes Supported by Heteropolydentate Ligation

by

Adam J. Ruddy

Submitted for partial fulfillment of the requirements
for the degree of Doctor of Philosophy

at

Dalhousie University
Halifax, Nova Scotia
August 2014

Table of Contents

List of Tables

List of Figures

List of Schemes

Abstract

Pincer complexes of the platinum group metals have been the subject of intense research in recent years, owing to the remarkable stoichiometric and catalytic reactivity exhibited by such complexes. In this context, research previously reported by the Turculet group has focused on developing the reactivity of new bis(phosphino)silyl pincer complexes that feature tridentate ligands of the type [R-PSiP] (R = alkyl or aryl). In an effort to further expand the scope of silyl pincer ligation, the study of complexes supported by new PSiN mixed donor ligands of the type [R-PSiN-R'] (R, R' = alkyl or aryl) has been undertaken. This document details the synthesis of such PSiN ligand precursors, as well as the synthesis, characterization, and reactivity of platinum group metal complexes featuring such PSiN ligands.

In an effort to further expand the scope of silyl pincer ligation to non platinum-group metals, the study of Co complexes supported by PSiP ligation was undertaken. It was anticipated that such Co complexes featuring highly donating PSiP ligands could be able to mimic two-electron redox chemistry of the platinum group metals. The synthesis and characterization of [Cy-PSiP]Co complexes in both the Co^{I} and Co^{II} oxidation states is described, as well as an investigation of the ability of [Cy-PSiP]Co^{I} to undergo two-electron oxidative addition reactions with substrates such as iodobenzene, and H_2.

In order to further develop the applications of heteropolydentate ligands in transition metal chemistry, *N*-phosphinoamidine/amidinate ligands were identified as targets of inquiry. The exploration of the ability of sterically demanding *N*-phosphinoamidine/amidinate ligands to support reactive, low-coordinate complexes for use in catalytic applications is detailed. Of particular interest was the design of low-coordinate complexes that will be active in the iron and cobalt catalyzed reduction of unsaturated substrates. This thesis details the synthesis of novel sterically demanding *N*-phosphinoamidine/amidinate ligands and their corresponding low-coordinate iron and cobalt complexes. The remarkable activity of such iron and cobalt complexes in the catalytic hydrosilylation of carbonyl substrates as well as the catalytic hydroboration of alkenes is also discussed.

List of Abbreviations and Symbols Used

Anal. Calcd = Analysis Calculated
Ar = aryl group
Bpy-PNN =

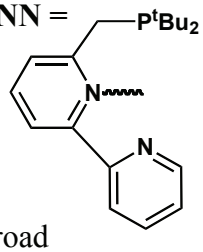

br = broad
COE = cyclooctene
COD = 1,5-cyclooctadiene
COSY = Homonuclear Shift *CO*rrelation *S*pectroscop*Y*
Cy = cyclohexyl
[Cy-PSiP] =

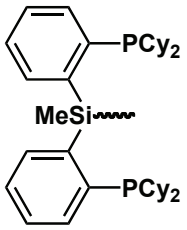

d = doublet
δ = chemical shift
DEPT = *D*istortionless *E*nhancement by *P*olarization *T*ransfer
η = indicator of hapticity in π-bonding ligands
E = main group element
equiv = equivalents
fac = facial
h = hour
HMBC = *H*eteronuclear *M*ultiple *B*ond *C*orrelation
HSQC = *H*eteronuclear *S*ingle *Q*uantum *C*orrelation
IR = infrared
$^{n}J_{XX'}$ = n bond coupling constant
between atom X and atom X`
κ = indicator of hapticity in σ-bonding ligands
L = neutral two electron donor ligand
μ = descriptor for a bridging ligand
m = multiplet
m = meta
M = generic transition metal *or* mol/L
mer = meridional
NMR = *N*uclear *M*agnetic *R*esonance

NSiN =

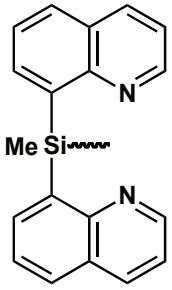

o = ortho

ORTEP = Oak Ridge Thermal Ellipsoid Plot

p = para

PCN =

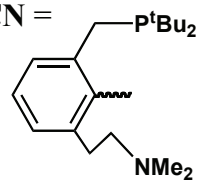

PNN =

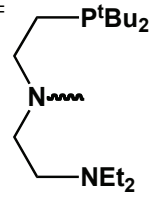

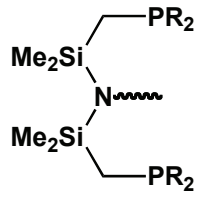

PNP =

POCOP =

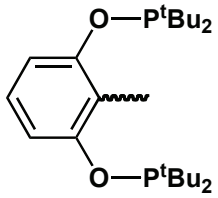

ppm = parts per million

PSiN =

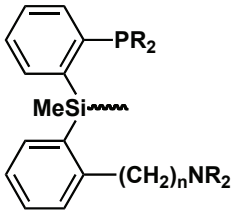

Py-PNN =

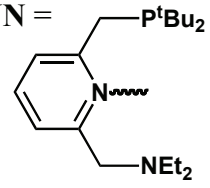

s = singlet
t = triplet
^{t}Bu = tert-butyl
THF = tetrahydrofuran
X = anionic donor ligand

Acknowledgments

First off I would like to thank my advisor Dr. Laura Turculet for her help and support throughout the course of my graduate studies. Her advice and guidance have been invaluable over the last five years. Because of your help I have managed to surpass any expectations that I ever had for myself, and I am grateful for everything you have done for me.

I would like to thank my supervisory committee (past and present), Drs. Neil Burford, Kevin Grundy, Peng Zhang, Jean Burnell, Norm Schepp, and Mark Stradiotto for their support and guidance throughout my studies. I would like to especially thank Mark for all of his support throughout the years, you have absolutely inspired me to be a better scientist. I'd also like to thank Mike Lumsden who has always been very helpful with various NMR experiments. Thank you to Drs. Robert McDonald and Mike Ferguson from the University of Alberta for X-ray crystallography experiments reported in this thesis. Furthermore, the entire staff of the department of chemistry at Dalhousie University also needs to be thanked for helping me with various problems I have encountered, both mechanical and logistical. A special thanks goes to the office staff that managed to bail me out of a number of precarious situations that I seem to find myself in often. Furthermore, I would like to thank Chevron Phillips Chemical Company for their support of my research and our research program in general. The opportunity to work on this project was absolutely my favorite part of my PhD research.

A big thank you is owed to the Turculet group members (past and present) over the years. In particular I'd like to thank Morgan MacInnis, Erin Morgan, and Sam Mitton. You guys were the ones that got me going on the right path and you will always be at least partially responsible for whatever success I have in the future. Also, I need to thank the Stradiotto group (past and present) for very helpful and entertaining conversations, as well as also allowing me to borrow seemingly anything I want from their lab.

My family has always supported me throughout my academic endeavors, graduate studies included. Despite not really understanding what it is I've been doing for the last five years, their unwavering support is appreciated. I'd also like to thank all my friends and extended family that has always supported me. I assure everyone that all of the encouragement and support I have received over the years has been noticed and appreciated, thank you.

CHAPTER 1: Introduction

1.1 Overview

The ability to catalyze chemical reactions in an efficient and selective manner remains one of the greatest challenges in chemistry. Organometallic chemists have made large strides in this area of chemistry in recent years by using transition metal complexes as homogeneous catalysts. In this context, the 2001, 2005, and 2010 Nobel Prizes in Chemistry have been awarded for advancements in the fields of asymmetric catalysis,[1] olefin metathesis,[2] and transition metal mediated coupling reactions,[3] respectively. Although much progress has been made in the area of transition metal mediated catalysis, the ability to catalytically functionalize readily available and abundant substrates (eg. CO, H_2O, NH_3, CH_4, CO_2, O_2) and the ability to use abundant base metals as efficient catalysts remain as significant challenges in both laboratory and industrial settings.

Although the Nobel Prize winning reactions mentioned above have been shown to have wide ranging applications, significant breakthroughs of this type are often rooted in the fundamental study of the reactivity of transition metal complexes. Advances in catalytic methods are often made by designing metal complexes that exhibit novel reactivity, and then attempting to develop this reactivity into catalytic reactions. One highly effective way to access new reaction pathways in transition metal chemistry is to design new ancillary ligands that are able to stabilize reactive metal centers and that provide unique coordination environments.

In this regard, the research described in this document aims to develop the synthesis and reactivity of transition metal complexes that feature novel ancillary ligation. In one project, new phosphinoamino silyl (PSiN) 'pincer'-type ligands were

developed, with the goal of accessing new and highly reactive platinum group metal species that may be able to mediate novel chemical transformations. More specifically, the synthesis of new tridentate PSiN ancillary ligands and the resulting synthesis, characterization and reactivity of platinum group metal complexes featuring such ancillary ligands will be described. In another related project, the synthesis of base metal complexes featuring bis(phosphino)silyl (PSiP) ligation was targeted. The application of previously reported PSiP ligation in the stabilization of low oxidation state cobalt complexes will be detailed. To put this work into context, an overview of previous noteworthy advances in the chemistry of pincer ligated transition metal complexes is discussed herein, with a focus on surveying the stoichiometric and catalytic reactivity of mixed donor pincer complexes that feature potentially hemilabile donors.

A third project detailed herein was pursued in collaboration with Chevron Philips Chemical Company, and involved developing the catalytic application of low-coordinate base metal complexes featuring *N*-phosphinoamidinate ligation. The isolation of low-coordinate iron and cobalt complexes featuring *N*-phosphinoamidinate ligation will be detailed, as well as their application as pre-catalysts in the hydrosilylation and hydroboration of unsaturated substrates. To put this work into context, a brief overview of P,N ligation and monoanionic bidenate ligands will be discussed herein.

1.2 Pincer Ligand Design and Influence on Metal Reactivity

Pincer ligands are tridentate species that typically coordinate to a metal center in a meridional fashion (Figure 1-1). Traditionally, such ligands feature a central anionic donor (X) flanked by two neutral donors (L). These different donors can be connected

using a number of different organic fragments including aliphatic, aromatic, and other heteroatom containing frameworks.[4]

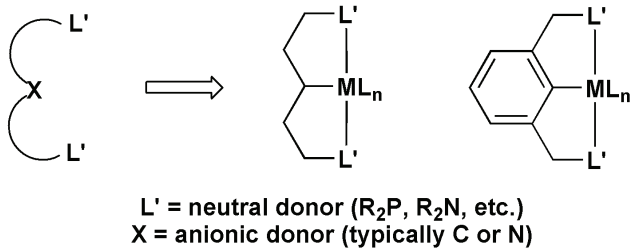

Figure 1-1. Traditional pincer ligand complexes.

Upon coordination to a metal center, pincer ligands confer enhanced stability to the resulting transition metal complex. The stability of these complexes can be attributed partially to the chelating nature of such ligands, where typically five or six membered metallacycles are formed upon metalation. The enhanced stability of the resulting complexes can lead to enhanced reactivity, especially in comparison to monodentate, non-chelating ligands, as reactive intermediates are more effectively stabilized from possible decomposition routes.[4f, 5]

A large advantage of pincer ligands is their modular design, which provides the ability to alter the steric and electronic environments of the resulting metal complexes. This can be achieved by changing the nature of the central anionic donor (X), the neutral donors (L), as well as by modification of the organic backbone of the ligand.[4a-d] Traditionally, phosphine and amine groups have been employed as neutral donors in the context of pincer design,[4] however other neutral donors such as OR_2,[6] SR_2,[7] SeR_2,[8] and CR_2[9] have also been reported. The electronic and steric features of such neutral L donors can be greatly altered by varying the nature of their corresponding R substituents. For example, bulky alkyl substituents can be used to promote the formation of electron rich, monomeric complexes due to their electron donating properties and large size.

Alternatively, the nature of the central anionic donor X can be modified, however C (alkyl, aryl) and N (amido) anionic donors are by far the most common.[4] Furthermore, the ligand backbone connecting the three donor groups can be altered (eg. by using aliphatic versus aromatic moieties), which can greatly alter the ligand rigidity as well as the electronic properties of the anionic and neutral donors.[4]

1.3 Development of PCP and PNP Pincer Chemistry

As discussed above, pincer ligand architecture is highly modular. However, the majority of pincer complexes that have been reported involve tridentate ligands that feature central carbon and nitrogen based anionic donors with flanking phosphine based neutral donors. A brief history of these PCP and PNP complexes will be presented in this section.

Over thirty years ago Shaw and co-workers pioneered the field of pincer chemistry by synthesizing a number of PCP-ligated complexes with group 8, 9 and 10 metals via chelate assisted C-H bond cleavage (Figure 1-2).[11] In subsequent years, PCP complexes related to those reported by Shaw have demonstrated the ability to perform a number of challenging transformations both stoichiometrically and catalytically, including the catalytic dehydrogenation of alkanes[12] and the activation of N-H bonds in aniline and ammonia by oxidative addition.[13]

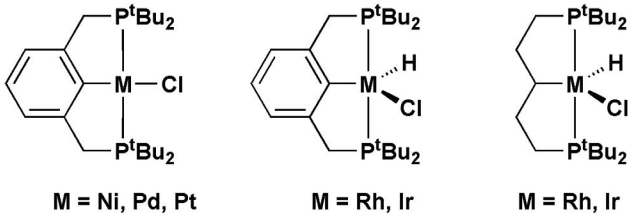

Figure 1-2. PCP-ligated complexes synthesized by Shaw and co-workers.

More recently, PNP pincer chemistry has become prominent in the literature (Figure 1-3). It has been proposed that PNP-ligated complexes should exhibit different reactivity relative to the related PCP species due to the ability of the lone pair of electrons on the central N donor to interact with the metal center. Complexes featuring PNP ligation have been shown to exhibit unique chemistry such as the formation of a formally 14-electron Ru complex,[14] intermolecular activation of arene C-H bonds,[15] and the activation of N-H bonds in amines and ammonia.[16]

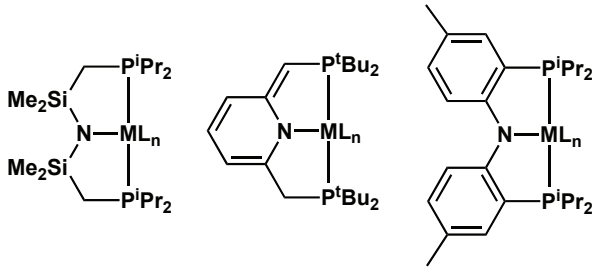

Figure 1-3. Examples of PNP-ligated transition metal complexes.

1.4 Mixed Donor Pincer Complexes

Recently there has been increased interest in pincer complexes supported by tridentate ligands that contain a mixed set of neutral donors. As opposed to the more traditional bis(phosphino) PCP or PNP complexes, mixed donor species feature two different neutral donors (typically a phosphino and amino group) that flank a central anionic donor X. Amines are classified as hard donors, meaning they participate in weaker interactions with soft electron rich late metals centers. This is in contrast to phosphines, which are classified as soft donors that participate in very strong interactions with soft late transition metals. The introduction of an amino neutral donor into the pincer framework was proposed to have a profound effect on the electronic features and

the coordination environment of the resulting pincer ligated complexes, as the amine could act as a hemilabile donor. A hemilabile donor is a weakly bound ligand that can undergo reversible coordination and dissociation from the metal center, resulting in the transient formation of coordinatively unsaturated complexes (Scheme 1-1). The formation of coordinatively unsaturated complexes of this type is highly desirable, as such complexes are typically highly reactive.[17]

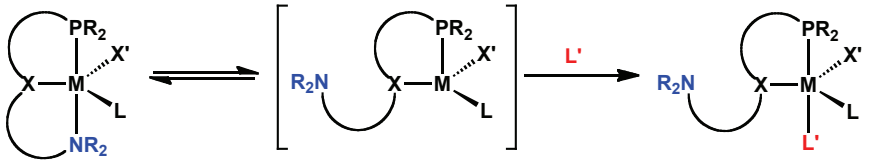

Scheme 1-1. Hemilability of mixed donor pincer complexes.

The use of hemilabile P,N ligands has become well established in organometallic chemistry as an important strategy for accessing highly active catalyst species. A classic example of such ligands are the bidentate phosphinooxazoline (PHOX) ligands developed by Pfaltz and coworkers (Figure 1-4).[18] Such PHOX-ligated complexes of Ru, Ir, Pd, and Cu have demonstrated catalytic reactivity in a large number of transformations, including enantioselective allylic substitution reactions,[19] Heck reactions,[20] transfer hydrogenation of ketones,[21] and asymmetric hydrogenation of olefins.[22] In many cases, the catalytic activity of P,N complexes outperformed analogous P,P and N,N complexes, suggesting that the mixed donor set is key to the increased reactivity observed. Since the initial reports of the catalytic activity of PHOX ligated-complexes, numerous examples of bidentate, potentially hemilabile ligands have been reported in the literature.[23]

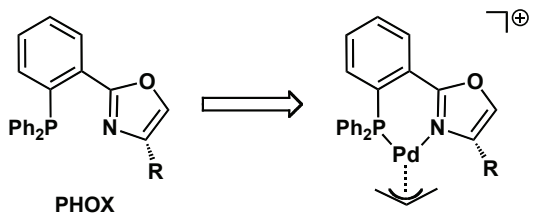

Figure 1-4. PHOX pro-ligand and a PHOX-ligated Pd allyl complex.

The study of mixed donor (phosphinoamino) pincer chemistry has largely been pioneered by Milstein and co-workers. A number of mixed donor pincer complexes have been reported, with PNN[24] and PCN[25] systems being by far the most common (Figure 1-5). Typically, such mixed donor pincers feature *tert*-butyl substitution on the phosphine donor, which helps promote the synthesis of monomeric, electron rich complexes due to the steric bulk and electron donating ability of the *tert*-butyl groups. Substitution at the amine donor is mostly limited to small alkyl groups, however a PNN pincer containing a pyridine neutral donor has been reported by Milstein and co-workers (Figure 1-5).[24d] Examples of the reactivity of PNN and PCN pincer complexes will be discussed in the following sections.

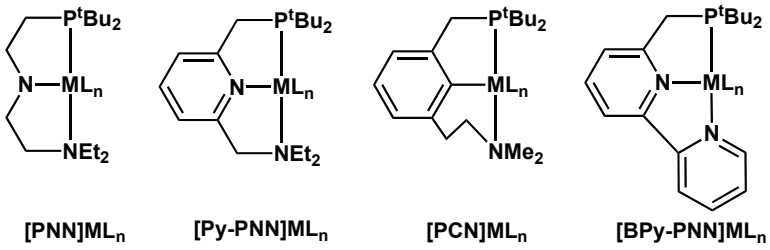

Figure 1-5. Examples of PNN and PCN pincer complexes.

1.5 Stoichiometric and Catalytic Reactivity of PNN Pincer Complexes

1.5.1 Formation of Amides from Amines and Alcohols by [Py-PNN]Ru

[Py-PNN] complexes of ruthenium that feature a central pyridine donor have proven to be among the most reactive mixed donor pincer complexes reported. Treatment of such [Py-PNN]Ru complexes with a strong base leads to dearomatization of the central pyridine ring (Scheme 1-2).[24b] This dearomatization step has proven key to the reactivity of such PNN Ru complexes and gives rise to unique metal-ligand cooperativity. The dearomatization process leads to the transformation of the central nitrogen donor from a neutral pyridine to an anionic pyridyl group. The dearomatized complex can be rearomatized by reaction with dihydrogen to form a dihydride complex (Scheme 1-2). This dihydride complex can then reductively eliminate H_2 at room temperature followed by a hydride transfer from the benzylic ligand backbone to reform the dearomatized species.

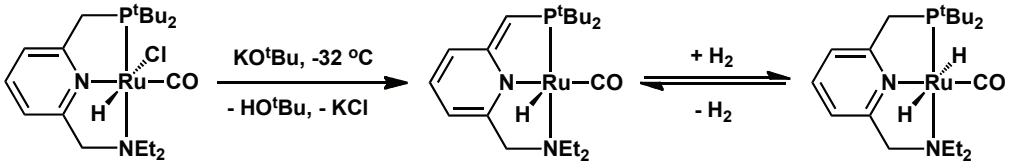

Scheme 1-2. Dearomatization of a [Py-PNN]Ru complex and subsequent rearomatization.

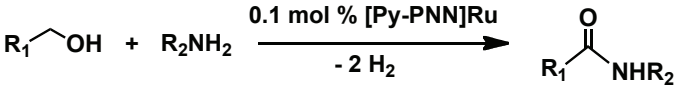

Scheme 1-3. Catalytic formation of amides from alcohols and amines.

The process of dehydrogenative dearomatization of the [Py-PNN] pincer complex renders such Ru species as effective H_2 shuttles that are active as catalysts in dehydrogenative coupling reactions.[24a, b, 26] One particularly noteworthy example of this chemistry is the dehydrogenative coupling of alcohols and amines to form amides using a

dearomatized [Py-PNN]Ru catalyst (Scheme 1-3).[26c] This reaction is highly desirable because of the biological and pharmaceutical relevance of amides. In the past, harsher reaction conditions including stoichiometric equivalents of coupling reagents such as dicyclohexyl carbodiimide (DCC) as well as strong acids and bases have been required to form amide bonds.[27] In the Ru-catalyzed reaction reported by Milstein and co-workers, the only byproduct is H_2, which in turn is also a useful commodity. The proposed catalytic cycle for this reaction features dissociation of the hemilabile amine ligand arm as a key step (Scheme 1-4). Initial dissociation of the amine arm from the dearomatized hydrido carbonyl complex A results in the formation of a coordinatively unsaturated species which can then coordinate the alcohol substrate and undergo subsequent chemistry to form the rearomatized complex B. β-hydride elimination from B leads to the formation of an aldehyde and the dihydride complex D, which can then reductively eliminate H_2, followed by dearomatization of the pyridine ring and recoordination of the amine arm to reform the catalytically active complex A. The aldehyde formed undergoes a reaction with the amine to form a hemiaminal that is subsequently dehydrogenated by complex A to form the desired amide. Amide yields ranged from 58-99%, and were obtained from a variety of primary amines and primary alcohols in relatively short reaction times utilizing 0.1 mol % of catalyst under reflux conditions. Reactions of secondary amines and alcohols did not result in the formation of amides at the reaction conditions.

The coordination of a substrate to complex A is greatly aided by the presence of a hemilabile amine donor (Scheme 1-4). Dissociation of the amine arm allows for facile coordination of the substrate to the metal center *trans* to the phosphine ligand. Without

dissociation of the hemilabile donor, the substrate would be forced to coordinate to the metal center *trans* to a hydride ligand, which is likely to be a much slower process due to the highly *trans*-labilizing nature of hydride ligands. Therefore, if an analogous (PNP)Ru complex was used, a strongly coordinated phosphine arm would be less likely to dissociate from the metal center, which would force the substrates to coordinate *trans* to the hydride ligand. This would be anticipated to result in a much slower reaction than that observed in the case of the analogous [Py-PNN] system, which would result in decreased catalytic activity of the PNP-ligated species versus that of the highly reactive [Py-PNN] complex.

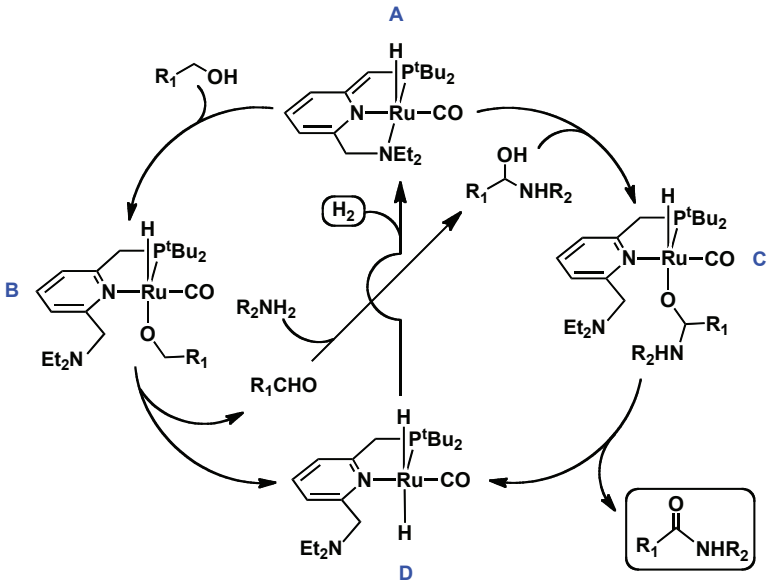

Scheme 1-4. Proposed catalytic cycle for the dehydrogenative formation of amides.

1.5.2 Hydrogenation of Amides by [BPy-PNN]Ru to form Alcohols and Amines

In 2010, Milstein and co-workers reported the reverse reaction to that discussed in section 1.5.1, the catalytic formation of alcohols and amines from amides and hydrogen (Scheme 1-5).[24d] The previously unreported complex [BPy-PNN]Ru(H)Cl(CO) proved

to be the most efficient and selective pre-catalyst for this reaction. The new complex [BPy-PNN]Ru(H)Cl(CO) is similar in structure to the [Py-PNN]Ru analogue previously discussed (*vide supra*) and was synthesized by reacting the [BPy-PNN] pro-ligand with 1 equiv. of $Ru(H)Cl(PPh_3)_3(CO)$. Subsequent dehydrochlorination with KO^tBu led to dearomatization of the ligand backbone, as previously reported for [Py-PNN]Ru(H)Cl(CO) (Scheme 1-6). The dearomatized complex was effective at performing the amide hydrogenation reaction with 17 different amides at a catalyst loading of 1 mol % at 110 °C. Modest to excellent yields of 58-98 % were reported for the primary alcohols, primary amines, and secondary amines formed.

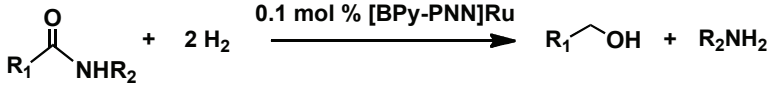

Scheme 1-5. Catalytic hydrogenative formation of amines and alcohols from amides.

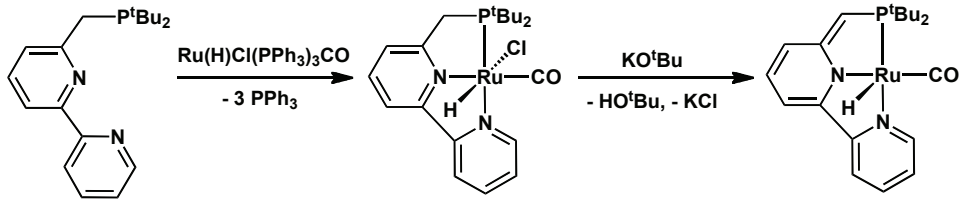

Scheme 1-6. Synthesis of dearomatized [BPy-PNN]Ru(H)CO.

The mechanism proposed for this reaction involves the initial hydrogenation of the dearomatized complex A (Scheme 1-7) to form a $[BPy\text{-}PNN]Ru(H)_2(CO)$ intermediate (B). Coordination of the amide leads to the formation of intermediate C. A subsequent carbonyl insertion into one of the Ru-H bonds leads to the formation of intermediate D. The benzylic arm of the pincer backbone is then deprotonated by the NH group of the coordinated hemiaminoxy group, which liberates the free amine and leaves a coordinated aldehyde on the Ru center (intermediate E). Intermediate E is then

hydrogenated by H_2 to form the rearomatized dihydride complex F, which undergoes a hydride transfer to the coordinated aldehyde to obtain the alkoxide complex G. The benzylic arm of the pincer backbone is then deprotonated by the alkoxide ligand, resulting in the liberation of an alcohol as well as reformation of the catalytically active species A. Once again, the presence of a hemilabile donor in the pincer architecture proved to be a key component of the reaction. Complex B in the proposed catalytic cycle is a coordinatively and electronically saturated 6-coordinate, 18-electron Ru complex; in order to coordinate the amide substrate, the flanking pyridine donor must dissociate from the metal centre in B, leaving a coordination site open for the substrate to bind. If this was the mechanism operating for this reaction, one would expect that related PNP complexes that do not feature a hemilabile donor should not perform this reaction at all due to the formation of a saturated 6-coordinate, 18-electron complex early in the catalytic cycle. In accordance with this mechanistic proposal, the dearomatized complex [Py-PNP]Ru(H)CO, which does not feature a hemilabile amine donor, showed no catalytic activity for this reaction. The analogous dearomatized complex [Py-PNN]Ru(H)CO was catalytically active, but less efficient.

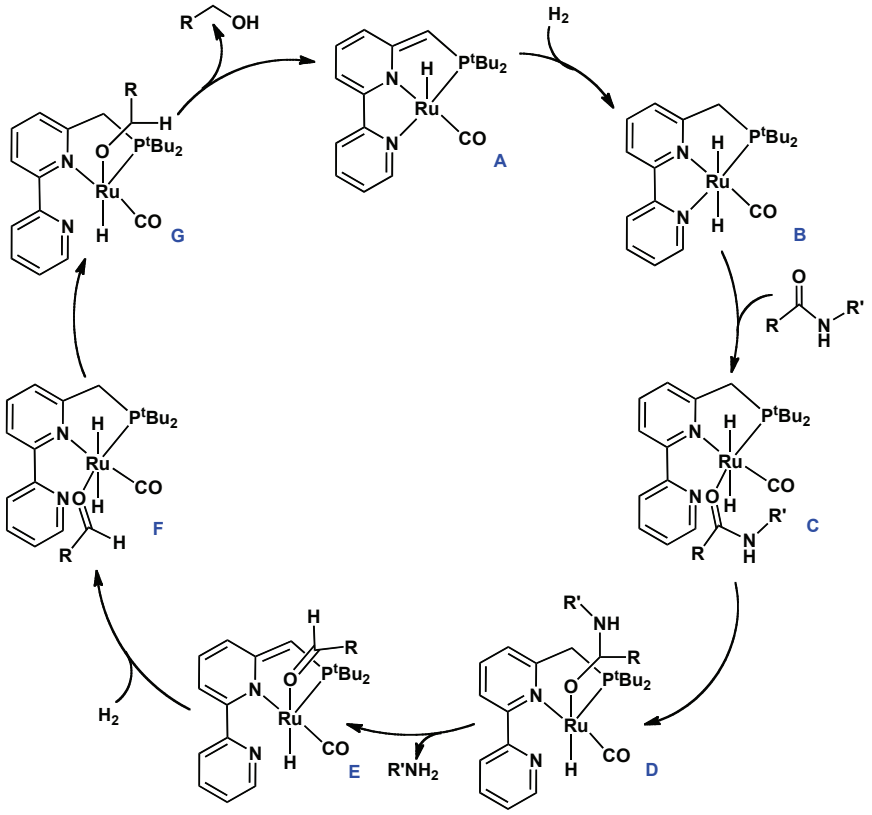

Scheme 1-7. Proposed mechanism for the Ru-catalyzed hydrogenation of amides.

1.5.3 Splitting of H_2O into H_2 and O_2 by [Py-PNN]Ru

Another important example of reactivity featuring PNN-ligated Ru complexes is in the splitting of water to form H_2 and O_2.[28] This reaction is potentially very important because of its relevance to energy research, as H_2 has been proposed as a clean, sustainable fuel source. However, the production of H_2 typically requires the use of sacrificial oxidants or reductants, which is undesirable due to the amount of waste produced.[29] There is a large need to develop a catalytic system capable of producing H_2 efficiently from cheap, readily available sources such as H_2O. Up until this point, much progress had been made in this area, specifically in the reduction of H_2O to H_2.[30] The oxidation half of this cycle, the production of O_2 from H_2O, is much less understood. The

catalytic formation of O-O bonds at a metal center is proposed to involve a bimolecular mechanism involving metal-oxo complexes.[29,31] However, there is insufficient experimental evidence to provide a clear reaction mechanism.

As shown in Scheme 1-8, the dearomatized [Py-PNN]Ru(H)CO is able to activate water to form the trans hydrido-hydroxo complex [Py-PNN]Ru(CO)(H)(OH). This process is thought to occur via coordination of H_2O to the empty coordination site on the Ru center followed by proton migration to the dearomatized ligand backbone. A labeling experiment using D_2O confirmed this hypothesis, as ^2H incorporation into the ligand backbone was observed, supporting the proposed water coordination/proton migration mechanism. Additionally, when $H_2{}^{17}O$ was used as the source of water, ^{17}O incorporation into the hydroxyl ligand was observed.

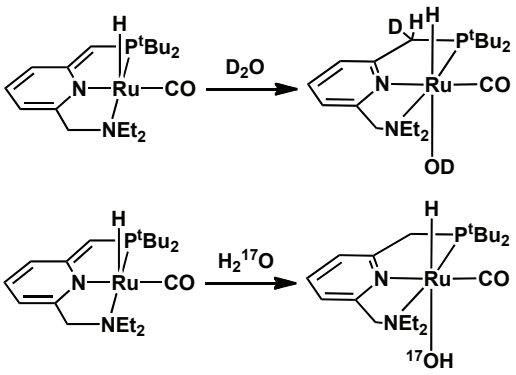

Scheme 1-8. Formation of a *trans* hydrido-hydroxo ruthenium complex.

Heating of [Py-PNN]Ru(CO)(H)(OH) with one equivalent of water for three days led to the formation of the *cis*-dihydroxo complex [Py-PNN]Ru(CO)$(OH)_2$, as well as the evolution of H_2 gas (Scheme 1-9). Subsequent irradiation of [Py-PNN]Ru(CO)$(OH)_2$ led to the evolution of O_2 gas and reformation of [Py-PNN]Ru(H)CO (Scheme 1-9). Isotopic labeling studies were used to confirm that the O_2 formed results from the dihydroxo complex, and not a bimetallic mechanism. It is proposed that O_2 is formed by reductive

elimination of H_2O_2 from [Py-PNN]Ru(CO)$(OH)_2$ followed by disproportionation into O_2 and H_2O. Attempts to trap hydroxyl radicals were unsuccessful, suggesting that O_2 is likely formed by a 2-electron oxidation of H_2O_2. This keeps the O-O bond from the reductive elimination of H_2O_2 intact, which is supported by isotopic labeling experiments. The observation that H_2 and O_2 are generated without the presence of dinuclear or metal-oxo complexes advances the current understanding of transition metal mediated water splitting. This observation is inconsistent with the generally accepted proposed mechanisms of water splitting, and may aid in the future understanding of water splitting by transition metals. Of note, the analogous dearomatized complex [Py-PNP]Ru(H)CO does not exhibit similar reactivity with water, suggesting that the mixed donor PNN ligand framework is necessary for the reactivity observed.

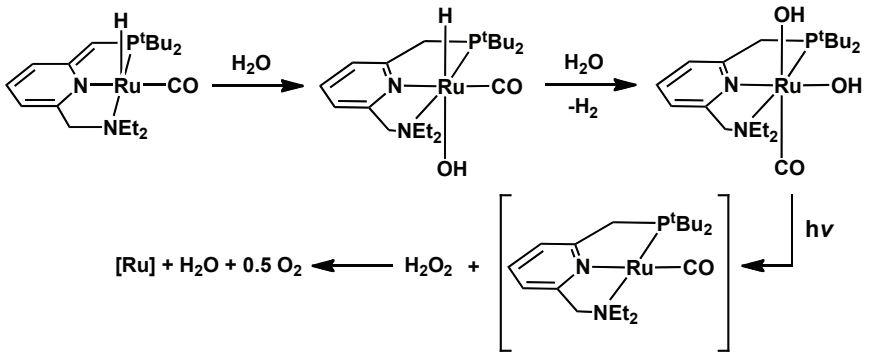

Scheme 1-9. Proposed mechanism for the Ru-mediated formation of H_2 and O_2 from H_2O.

1.5.4 Transfer Hydrogenation of Ketones Using a [PNN]Ir Complex

Relatively few examples have been reported involving the chemistry of Group 9 mixed neutral donor pincer complexes. One example comes from Gusev and co-workers, who reported a series of [PNN]Ir hydride complexes and investigated their catalytic activity in the transfer hydrogenation of ketones.[24e] The synthesis of [PNN]Ir

polyhydride complexes was achieved by reacting the neutral [PNHN] pro-ligand with half an equivalent of $Ir[Cl(COE)_2]_2$ (COE = cyclooctene), followed by treatment with H_2 to provide [R-PNHN]$Ir(H)_2Cl$ (Scheme 1-10). To form Ir complexes with a central amido donor, [PNHN]$Ir(H)_2Cl$ was treated with one equiv. of KO^{t}Bu, which resulted in dehydrochlorination and the formation of [PNN]$Ir(H)_2$. Subsequent hydrogenation of [PNN]$Ir(H)_2$ with one equiv. of H_2 led to the synthesis of [PNHN]$Ir(H)_3$ (Scheme 1-10).

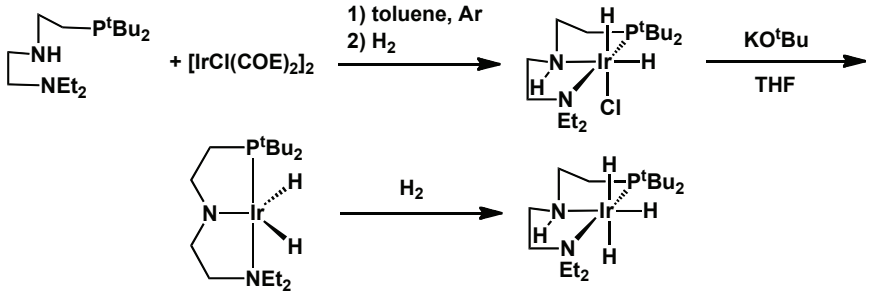

Scheme 1-10. Formation of [PNHN]$Ir(H)_2Cl$, [PNN]$Ir(H)_2$, and [PNHN]$Ir(H)_3$.

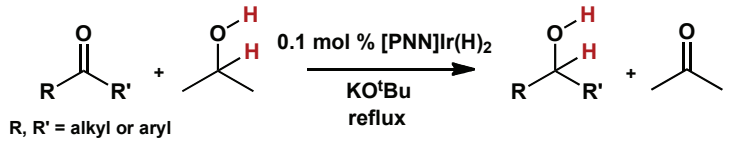

Scheme 1-11. [PNN]$Ir(H)_2$ catalyzed transfer hydrogenation of ketones.

Gusev and co-workers then tested the activity of [PNN]$Ir(H)_2$ as a catalyst for the transfer hydrogenation of ketones in basic isopropanol (Scheme 1-11). [PNN]$Ir(H)_2$ was found to be a competent catalyst for this reaction, and its activity was found to be comparable to the analogous [PNP]$Ir(H)_2$ complex, suggesting that the hemilabile character of the amine donor in [PNN]$Ir(H)_2$ likely does not play a prominent role in the mechanism of catalysis. A bifunctional mechanism involving metal-ligand cooperativity was proposed for this reaction (Scheme 1-12). It is proposed that [PNN]$Ir(H)_2$ is hydrogenated by 2-propanol to form [R-PNHN]$Ir(H)_3$ with loss of acetone. The trihydride complex in turn transfers an equiv. of H_2 to the ketone substrate to form the

alcohol product, with the Ir-H furnishing an equiv. of H^-, while the Ir-NH furnishes an equiv. of H^+ to the ketone. Although the catalytic activity of [PNN]Ir$(H)_2$ is not improved over [PNP]Ir$(H)_2$, it is encouraging that the catalytic activity of [PNN]Ir$(H)_2$ is comparable to the more traditional [PNP]Ir$(H)_2$. This result shows that even without demonstrating hemilabile activity, mixed donor pincer complexes can be competent catalysts for catalytic transformations.

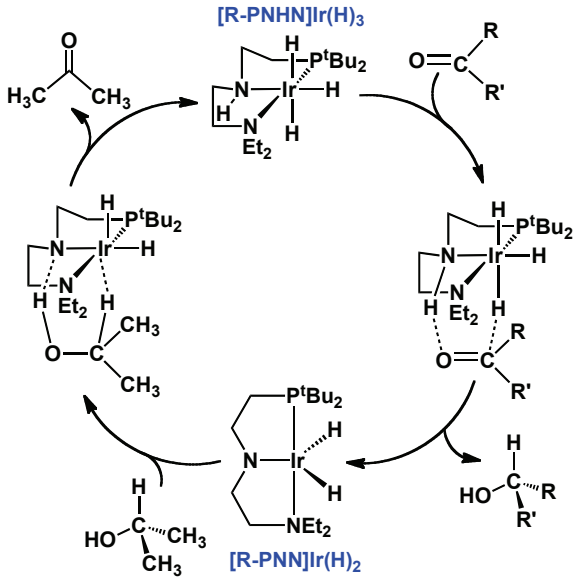

Scheme 1-12. Mechanism for transfer hydrogenation of ketones using [PNN]Ir$(H)_2$.

1.6 Synthesis and Reactivity of a PCN Pt-oxo Complex

The chemistry of [PCN] ligated metal complexes is not nearly as established as that of species supported by [PNN] ligation. In one particularly prominent example of reactivity involving [PCN]-ligated complexes, Milstein and co-workers reported the synthesis and reactivity of a highly unusual terminal Pt^{IV}-oxo complex.[32] Until this example, very few late metal complexes featuring terminal oxo ligands had been isolated.[33] Oxo ligands are highly π-donating and thus do not typically form stable

complexes with electron rich late metals like platinum. The few examples that did previously exist featured highly π-withdrawing ligands to help stabilize the unstable Pt=O moiety.[34] Furthermore, oxo complexes are particularly interesting to study because of their potential to engage in oxygen transfer reactions.

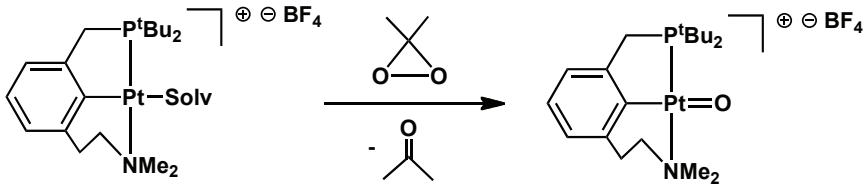

Scheme 1-13. Synthesis of a cationic Pt-oxo complex.

Milstein and co-workers found that the reaction of $\{[PCN]Pt(Solv)^+\}[BF_4]^-$ (Solv = acetone) with one equivalent of dioxirane resulted in the elimination of acetone and the formation of the novel cationic Pt^{IV}-oxo complex $\{[PCN]Pt{=}O^+\}[BF_4]^-$ (Scheme 1-13). This complex was characterized using a combination of X-ray diffraction, ESI-MS, DFT studies, and heteronuclear NMR experiments, which all supported the formation of this unusual complex. DFT calculations suggest that late metal oxo complexes are highly unstable due to occupation of high energy Pt-O π* molecular orbitals. The optimized structure of $\{[PCN]Pt{=}O^+\}$ features a distorted square planar geometry, with the O atom lying 35.3° out of the P-Pt-N plane. It is believed that the non planarity of this complex decreases the occupation of the Pt-O π* molecular orbitals, which results in the increased stability observed for $\{[PCN]Pt{=}O^+\}$.

The reactivity of this unusual Pt-oxo complex was investigated, including its ability to act as an oxygen transfer agent (Scheme 1-14). Complete transfer of the oxygen atom from platinum to phosphorus was observed in the reaction of $\{[PCN]Pt{=}O^+\}$ with PPh_3, demonstrating the effectiveness of the Pt-oxo complex as an

oxygen transfer reagent. Oxygen atom transfer was also observed in the reaction of the Pt-oxo complex with 4 equiv. of CO to yield {[PCN]Pt(CO)$^+$} as well as CO_2. In the presence of H_2, {[PCN]Pt=O$^+$} reacted to form the cationic solvate complex {[PCN]Pt(Solv)$^+$} (Solv = acetone) as well as H_2O. The reaction of {[PCN]Pt=O$^+$} with KH yielded the neutral Pt hydroxide complex, [PCN]Pt(OH), which demonstrated that the oxo ligand is susceptible to nucleophillic attack. Upon reaction with H_2O, water activation yielded a Pt^{IV} dihydroxo complex, where one H_2O molecule is also coordinated to the metal center. This result is particularly interesting because Pt^{IV}-oxo complexes have been proposed as intermediates in water oxidation catalysis.[29a, 35] Furthermore, Pt^{IV} dihydroxo complexes are of great interest as they have been proposed as intermediates in the oxidation of alkanes with O_2 to form alcohols.[36]

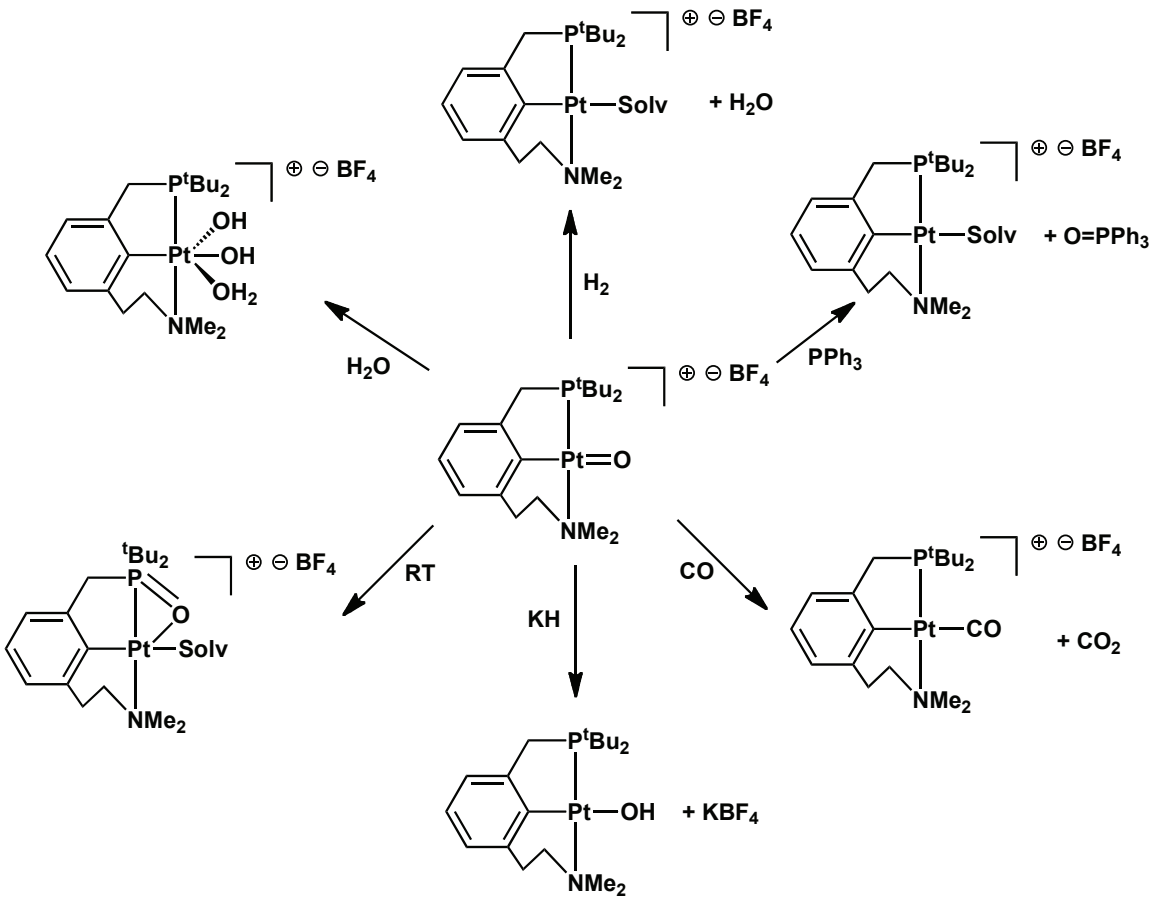

Scheme 1-14. Reactivity of {[PCN]Pt=O$^+$}[BF$_4$]$^-$.

In summary, Milstein and co-workers have shown that the [PCN] pincer framework is able to support an unprecedented cationic Pt^{IV}-oxo complex that exhibits interesting and potentially useful reactivity, such as water activation. This work demonstrates the ability of mixed donor pincer ligands to form reactive metal complexes that feature unusual reactivity.

1.7 Alternative Pincer Designs – Silyl Pincer Complexes

Research in the Turculet group is focused on the structure, synthesis, and reactivity of late transition metal silyl pincer complexes. As previously discussed, variability of the central anionic donor in pincer ligands has been vastly underexplored in

the past.[37] In this context, pincer ligands that feature alternative elements as central anionic donors are of interest. It is believed that by changing the nature of the central donor the reactivity of the resulting metal complexes will also be altered. In this context, the introduction of a silyl central donor could lead to new highly reactive pincer metal complexes. Since Si is more electropositive than C or N, silyl ligands are stronger σ electron donors than alkyl, aryl, or amido groups. This increase in electron donating ability should result in a more electron rich metal center, which in turn is more likely to undergo challenging oxidative addition reactions. Another desirable feature of silyl ligands is their highly *trans*-labilizing nature.[38] This *trans*-labilization promotes coordinative unsaturation at the metal center, which is a characteristic of highly reactive metal complexes.

There is literature precedent for the inclusion of silyl donors in polydentate ligands. In the late 1980's, Stobart and co-workers reported the synthesis of bi-[39], tri-[40], and tetradentate[41] (phosphino)silyl ligands and their coordination to platinum group metals (Figure 1-6).[39-42] However, Stobart and co-workers did not fully explore the organometallic reactivity of these complexes.

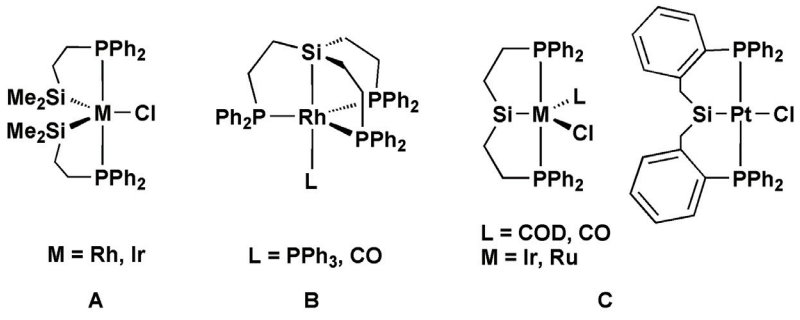

Figure 1-6. Polydentate ligands featuring silyl donors.

A more recent example of silyl pincer ligation comes from Tilley and co-workers, who have reported the synthesis of NSiN pincer complexes based on a bis(8-

quinolyl)silyl framework (Figure 1-7).[43] Although a series of Rh, Ir, and Pt [NSiN] complexes were synthesized, they proved to be relatively unreactive.[43a,43c,43d] The reactivity of [NSiN]Ir complexes was limited to Si-H bond cleavage in tertiary alkyl and aryl hydrosilanes.[43b] [NSiN]Ir complexes were also shown to catalyze arylsilane redistribution of a variety of primary and secondary aryl silanes, as well as dehydrogenative arene silylation of various arenes with a primary silane.[43b] However, these [NSiN]Ir catalysts were not very active and gave poor product yields. This lack of reactivity could potentially be attributed to the quinolyl donors, which are relatively poor electron donors to late transition metals in comparison to phosphines. The less electron rich metal center is less likely to undergo oxidative addition reactions, a key step in numerous organometallic bond cleavage processes. Additionally, the bis(8-quinolyl)silyl framework lacks the modularity of other pincer designs, making it difficult to readily alter the steric and electronic features of the ligand.

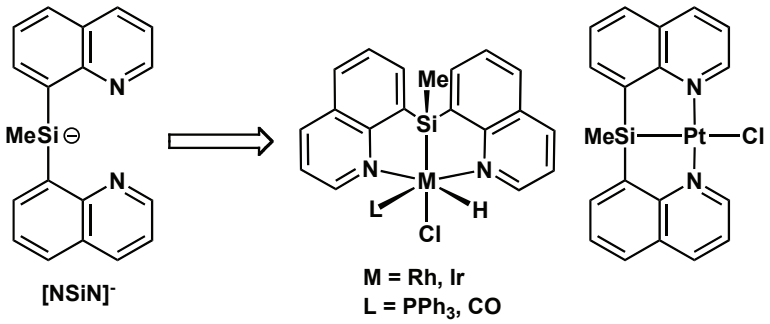

Figure 1-7. Rh, Ir, and Pt complexes featuring NSiN pincer ligands.

Research in the Turculet group has focused on the synthesis of late metal complexes featuring bis(phosphino)silyl pincer ligands of the type [k^3-(2-$R_2PC_6H_4)_2Si$Me]$^-$ ([R-PSiP], R = alkyl or aryl; Figure 1-8).[44] It is proposed that complexes featuring this type of [R-PSiP] ligation are good candidates for performing challenging bond cleavage reactions that could lead to the development of new metal-

mediated reactions. The *ortho*-phenylene backbone of these ligands is rigid and contains no β-hydrogens, which should aid the stability of the resulting metal complexes. Additionally, these ligands contain two neutral phosphine donors, which are compatible with electron rich late transition metal centers. Furthermore, these ligands are highly modular as the R groups on the phosphine donors can easily be altered to achieve the desired steric and electronic effects in the resulting metal complexes. In previous work reported by the Turculet group, the [R-PSiP] ligand framework has been shown to support very unusual and reactive late metal complexes. Examples of these complexes include formally 14-electron Ru complexes,[44f] Ir complexes that undergo oxidative addition of ammonia,[44e] and Ni complexes that undergo unprecedented reversible sp^2-sp^3 and sp^3-sp^3 C-Si bond cleavage.[44d] The extension of this chemistry into the investigation of the synthesis and reactivity of cobalt complexes featuring PSiP ligation will be described in Chapter 4 of this document.

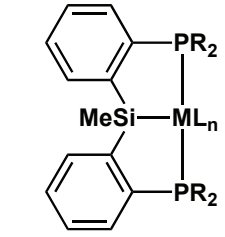

[R-PSiP]ML_n
M = late transition metal
R = alkyl, aryl

Figure 1-8. Bis(phosphino)silyl pincer complexes investigated in the Turculet group.

The research described in Chapters 2 and 3 builds on knowledge gained by the Turculet group on the synthesis and reactivity of silyl pincer ligands and complexes to access new types of pincer species that feature two different neutral donors within the silyl ligand architecture. The synthesis of mixed donor pincer ligands of the type [R-

PSiN-R'] (R, R' = alkyl, aryl) and their corresponding platinum group metal complexes are detailed (Figure 1-9). It was anticipated that these new [R-PSiN-R'] ligated complexes could be more electron rich than related PCN and PNN complexes due to the presence of a central silyl donor, and may therefore exhibit unique reactivity. Thus, the structure and reactivity of PSiN ligated complexes will be compared to that of related PCN and PNN complexes. The structure and reactivity of these new PSiN complexes will also be compared to related PSiP complexes previously reported in the Turculet group in order to investigate the effects of introducing a potentially hemilabile amine donor.

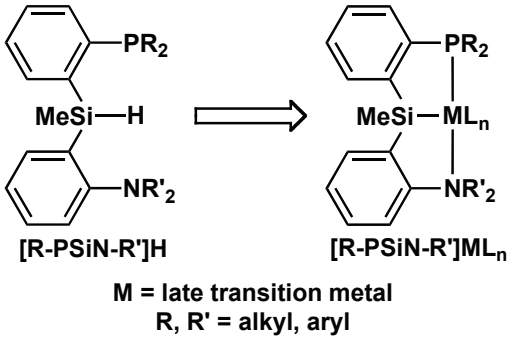

Figure 1-9. New PSiN-ligated transition metal complexes.

1.8 P,N Ligands In Organometallic Chemistry and Catalysis

As described in section 1.4, the reactivity exhibited by PHOX ligated complexes in an assortment of catalytic reactions demonstrated that P,N ligands featuring a mixed set of neutral donors can outperform catalytic systems featuring more traditional P,P or N,N bidentate ligation.[23] This discovery led to a rapid development of bidentate P,N ligands for the use as ancillary ligands in a wide range of catalytic applications (Figure 1-10).[23] The improved reactivity of P,N ligated systems versus P,P and N,N ligated

systems can been attributed to multiple factors. As discussed in section 1.4, the hemilability of the N donor in such ligands could potentially lead to the formation of highly reactive species not accessible via P,P or N,N ligation. Alternatively, one can explain the increased reactivity of P,N ligands without invoking hemilability. Soft phosphine donors are good σ-donors and π-acceptors, which makes them ideal for stabilizing low oxidation state species (through the π-accepting nature of phosphorus). The N donors in such ligands are often strong σ-donors, which can promote the formation of complexes in high oxidation states. Thusly, the combination of P and N donors in a bidentate ligand may provide an ideal hybrid that is capable of stabilizing intermediate oxidation states that often form during a catalytic cycle, making them highly effective ancillary ligands for catalysis.

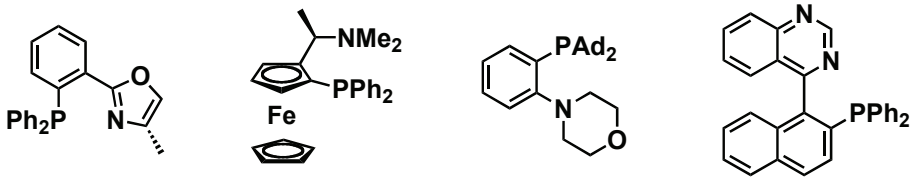

Figure 1-10. Examples of P,N ligands in catalysis.

Despite the plethora of neutral, bidentate P,N ligands in the literature there has been very little investigation into the synthesis of monoanionic P,N ligands and their corresponding transition metal complexes. One monoanionic P,N motif that has been explored are P,N ligands containing a pendant NH (or NH_2) moiety (NHP ligation, Figure 1-11). Such protonated amines are proposed to be deprotonated during certain steps of catalytic reactions, often as part of a bifunctional metal-ligand type process.[45] Due to the in situ formation of these monoanionic ligands, there are limited examples of isolated transition metal complexes featuring monoanionic P,N ligation (Figure 1-11).[46] Comparatively, the isolation of transition metal complexes featuring monoanionic N,N

ligation are extremely common, with β-diketiminate (commonly known as 'nacnac') ligands representing one of the most ubiquitous ligand classes in organometallic chemistry.[47]

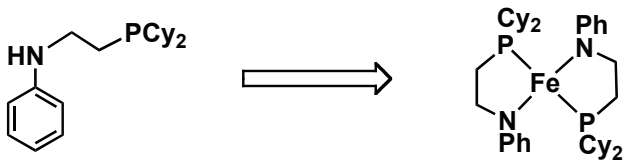

Figure 1-11. Neutral NHP pro-ligand (left) and an iron complex containing two monoanionic P,N ligands.

1.9 *N*-Phosphinoamidine Ligands - Towards Monoanionic P,N ligation

Inspired by the dearth of reports detailing monoanionic P,N ligation in the literature, the synthesis of transition metal complexes containing monoanionic P,N ligands became a target of inquiry. In a collaboration with Chevron Phillips Chemical Company (CPChem), the investigation of *N*-phosphinoamidine ligation was undertaken (Figure 1-12). This ligand class was previously disclosed by CPChem, and it was reported that chromium complexes featuring *N*-phosphinoamidine ligation are highly effective ethylene oligimerization catalysts.[48] This ligand class is extremely modular, with four sites (R^1 - R^4) where the ligand substituents can be easily modified. Of particular interest is the R^4 position, where one can envision that if R^4 = H, the resulting phosphinoamidine could be deprotonated, thereby providing a monoanionic phosphinoamidinate (Figure 1-12). Chapter 5 will detail the synthesis and characterization of *N*-phosphinoamidine pro-ligands and the corresponding low-coordinate phosphinoamidinate base metal complexes. The application of such

complexes in the catalytic hydrosilylation and hydroboration of unsaturated substrates will be detailed in Chapters 6 and 7.

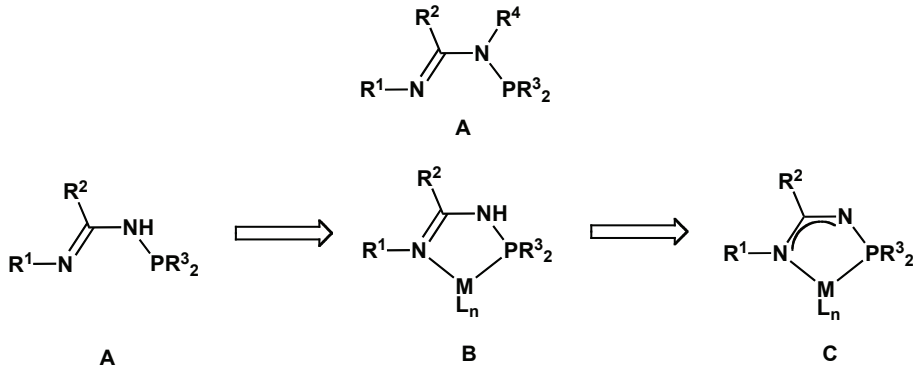

Figure 1-12. *N*-phosphinoamidine pro-ligands (A), neutral *N*-phosphinoamidine complex (B) and monoanionic *N*-phosphinoamidinate complex (C).

CHAPTER 2: Synthesis, Characterization and Reactivity of Ru, Rh, and Ir Complexes Featuring the [^{t}Bu-PSiN-Me]H Pro-Ligand

2.1 Introduction

As highlighted in Chapter 1, transition metal complexes featuring mixed donor pincer ligation have demonstrated the ability to perform a number of challenging stoichiometric and catalytic reactions. These reactions can be described as breakthroughs for the area of pincer chemistry, however there is still much to be explored. In this context, one component of my thesis research focused on the synthesis, characterization, and reactivity of the [^{t}Bu-PSiN-Me]H pro-ligand and [^{t}Bu-PSiN-Me]-ligated transition metal complexes (Figure 2-1). Progress to date will be discussed in this chapter.

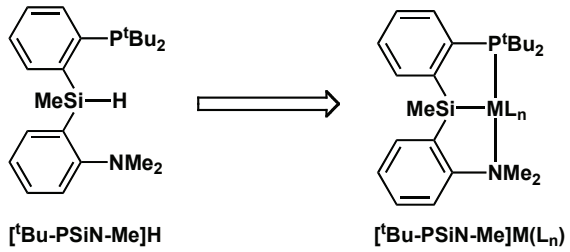

Figure 2-1. The [^{t}Bu-PSiN-Me]H pro-ligand (left) and a [^{t}Bu-PSiN-Me]M(L$_n$) complex (right).

2.2 Results and Discussion

2.2.1 Synthesis and Characterization of the [^{t}Bu-PSiN-Me]H Pro-Ligand

Previous work in the Turculet group has shown that tertiary bis(phosphino)silanes are effective as pro-ligands for the synthesis of bis(phosphino)silyl pincer complexes.[43] Such tertiary silanes feature a Si-H bond that can readily undergo oxidative addition to electron rich late metal centers to form metalated pincer complexes. This process is facilitated by the two phosphine donors that can coordinate to the metal, in turn bringing

the Si-H bond in close proximity to the metal center, thus enabling the oxidative addition reaction. The synthesis of such pro-ligands is a facile three-step process (Scheme 2-1). The phosphine donor is installed by reaction of a secondary phosphine with 2-bromoiodobenzene using a Pd catalyst in the presence of base to form a 2-bromo(phosphino)benzene derivative.[49] In the second step, the 2-bromo(phosphino)benzene derivative is lithiated using ^{n}BuLi, followed by quenching of the lithiated species formed *in situ* with 0.5 equiv. Cl_2SiMeH to form the desired bis(phosphino)silane.

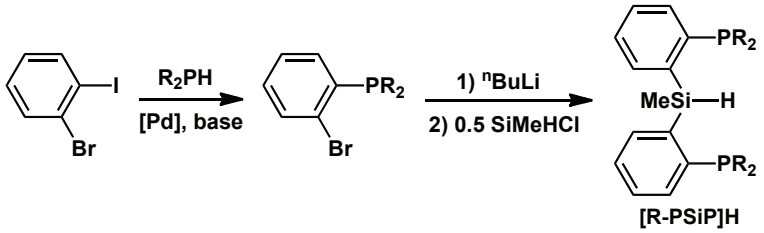

Scheme 2-1. Synthesis of [R-PSiP]H pro-ligands.

In a similar fashion, it was hypothesized that analogous tertiary (phosphinoamino)silanes would function as pro-ligands for the synthesis of (phosphinoamino)silyl pincer complexes. However, (phosphinoamino)silanes cannot be prepared by the same synthetic route due to the non-symmetrical nature of the target molecules. A new step-wise synthetic route was therefore devised. The phosphino ligand arm was synthesized by use of a Pd coupling reaction of $^{t}Bu_2PH$ with 2-bromoiodobenzene in the presence of Cs_2CO_3. The resulting aryl phosphine (**2-1**) was isolated as a beige solid in 89% yield (Scheme 2-2).[49] Subsequent lithiation of **2-1** using ^{n}BuLi at -78 °C resulted in the formation of **2-2**, which was isolated as a pale brown solid in 98% yield (Scheme 2-2).

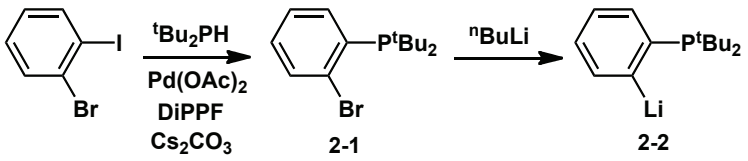

Scheme 2-2. Synthesis of lithiated aryl phosphine **2-2**.

The commercially available 2-bromo-N,N-dimethylaniline was chosen as the starting point for the installation of the amino donor. A Grignard reagent was prepared by reaction of 2-bromo-N,N-dimethylaniline with Mg in THF. This Grignard reagent was then added dropwise to a THF solution of excess Cl_2SiMeH to afford the aryl silane **2-3** (Scheme 2-3). An excess of Cl_2SiMeH was used in an attempt to minimize the formation of the undesired diarylsilane. In this vein, we also considered that the Grignard reagent might discourage the formation of the diarylsilane over an analogous reaction with a more aggressive aryllithium species. Crude **2-3** was isolated as a red oil and subsequent vacuum distillation (0.01 mm Hg) furnished the desired product (bp = 39 ^{o}C) as a colorless oil in 47% yield.

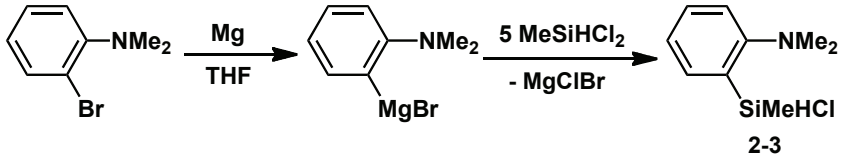

Scheme 2-3. Synthesis of (aminoaryl)chlorosilane **2-3**.

The (phosphinoamino)silyl pro-ligand ([^{t}Bu-PSiN-Me]H, **2-4**) was synthesized by reaction of **2-2** and **2-3** at -35 °C (Scheme 2-4) and was isolated in 78% yield as a brown oil. The $^{31}P\{^{1}H\}$ NMR spectrum of **2-4** displays a single resonance at 23.2 ppm indicating the presence of a single phosphine environment. The ^{1}H NMR spectrum of **2-4** (benzene-d_6) features a resonance at 5.87 ppm (m), which is in the range expected for a Si-*H*. In addition, the ^{1}H NMR spectrum of **2-4** also contains two sets of doublets

corresponding to the P(^{t}*Bu*)$_2$ protons at 1.16 ppm (d, 9 H, $^3J_{PH}$ = 11 Hz) and 1.10 ppm (d, 9 H, $^3J_{PH}$ = 11 Hz), respectively. A singlet resonance is observed for the N(*Me*)$_2$ protons at 2.34 ppm. IR analysis of **2-4** (thin film) revealed a broad stretch of medium intensity at 2128 cm^{-1}, consistent with an Si-*H* stretch. The ^{29}Si NMR spectrum of **2-4** revealed a resonance at -24.4 ppm ($^1J_{SiH}$ = 205 Hz), consistent with the formation of a tertiary silane. In comparison, ^{29}Si resonances for the [Ph-PSiP]H and [Cy-PSiP]H pro-ligands were observed to be -23.2 ppm and -24.2 ppm respectively.[43a,b]

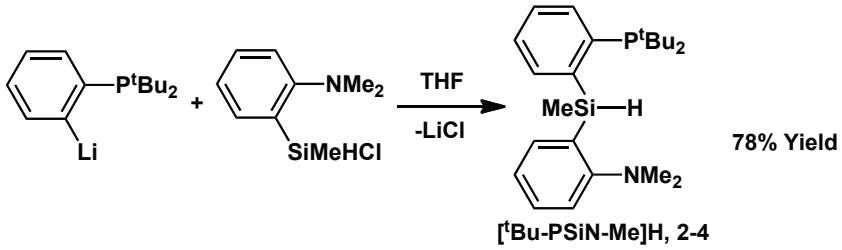

Scheme 2-4. Synthesis of [^{t}Bu-PSiN-Me]H pro-ligand **2-4**.

2.2.2 Coordination Chemistry of [^{t}Bu-PSiN-Me]H with Ru

As outlined in Chapter 1, Ru complexes featuring mixed donor pincer ligation have demonstrated the ability to perform a large number of challenging stoichiometric and catalytic transformations, including numerous examples of hydrogenative and dehydrogenative chemistry. In this context, Ru was chosen as an ideal candidate for initial coordination chemistry studies involving [^{t}Bu-PSiN-Me].

Multiple attempts were made to ligate **2-4** to a large number of readily available and commonly used Ru staring materials including $(PPh_3)_3RuCl_2$, $[(p\text{-cymene})RuCl_2]_2$, $(PPh_3)_3Ru(CO)(H)Cl$, $(PPh_3)_3Ru(H)Cl$, $[(\eta^6\text{-}C_6H_6)RuCl_2]_2$, and Cp*Ru(PPh$_3$)Cl. Unfortunately, these reactions were largely unsuccessful. In most cases, quantitative reaction of **2-4** was observed by $^{31}P\{^1H\}$ NMR spectroscopy, indicating that the pro-

ligand underwent a complete reaction with the Ru starting materials. In such cases, several new resonances were observed in the $^{31}P\{^{1}H\}$ NMR spectra indicating the formation of multiple phosphorus containing products. However, the isolation of single products from these reaction mixtures proved difficult. By comparison, the reaction of **2-4** with (1,5-COD)Ru(2-methylallyl)$_2$ (COD = cyclooctadiene) resulted in the quantitative formation of a single phosphorus containing product (^{31}P NMR). Upon further analysis, the formation of a unique Ru carbene complex resulting from C–H bond activation of an NMe group in the [^{t}Bu-PSiN-Me] ligand and of the 1,5-cyclooctadiene, respectively, was observed (**2-5**, Scheme 2-5). The synthesis, characterization, and reactivity of **2-5** and a related complex are described herein.

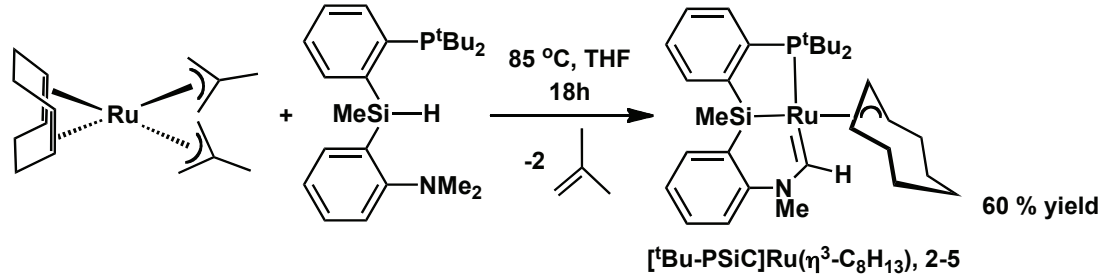

Scheme 2-5. Synthesis of the Ru carbene complex [^{t}Bu-PSiC]Ru(η^3-C_8H_{13}) (**2-5**).

2.2.3 Synthesis and Characterization of a Ru Carbene Complex

The Fischer carbene complex **2-5** was synthesized by heating [^{t}Bu-PSiN-Me]H (**2-4**) with one equiv. of (1,5-COD)Ru(2-methylallyl)$_2$ in THF solution for 18 hours at 85 °C (Scheme 2-5). NMR analysis of the reaction mixture revealed quantitative conversion of [^{t}Bu-PSiN-Me]H (^{31}P NMR: 23.2 ppm) to a new product featuring a single ^{31}P NMR resonance at 105.7 ppm. After removal of solvent and purification, **2-5** was isolated as a brown solid in 60% yield. The NMR features of **2-5** are very diagnostic for

the formation of a late metal carbene complex. The carbenic carbon and hydrogen give rise to $^{13}C\{^{1}H\}$ and ^{1}H NMR resonances (benzene-d_6) of 250.8 and 13.11 ppm, respectively. The extreme downfield location of these resonances is very common for Ru carbene complexes.[50] ^{1}H NMR characterization also revealed the presence of only one methyl group on the amine donor (2.82 ppm, s, 3 H), which is consistent with the proposed formulation. The presence of the newly formed cyclooctenyl ligand can also be easily observed in the ^{1}H NMR spectrum; the allylic protons give rise to three diagnostic resonances at 4.81, 4.13, and 3.61 ppm respectively.

The X-ray crystal structure of **2-5** confirmed the formation of a C_1 symmetric ruthenium carbene complex (Figure 2-2, Table 2-1). The Ru=C bond length was observed to be 1.902(2) Å, a value consistent with other Ru Fischer carbene complexes. For example, a comparable 16-electron Fischer carbene complex reported by Stradiotto and co-workers features a Ru=C bond length of 1.941(2) Å.[50] A short N-C bond distance of 1.353(2) Å was observed for the bond between nitrogen and the carbenic carbon (C(41)), consistent with π-donation form nitrogen to carbon.[50] Comparatively, the N-C bond distance between nitrogen and the methyl carbon was observed to be 1.468(2) Å, an expected value for a C-N σ-bond.[50] The sum of the bond angles around nitrogen is 359.9°, which is also consistent with π-donation. The geometry around Ru is best described as distorted square-pyramidal with Si at the apical site, while the remaining ligands occupy basal sites. A P-Ru-C(41) bond angle of 97.47(5)° indicates the P-Si-C fragment binds to Ru in a geometry closer to facial (expected angle = 90°) than meridional (expected angle = 180°). The allylic fragment of the cyclooctenyl group features Ru-C bond lengths of 2.275(2), 2.174(2), and 2.212(2) Å respectively. These

bond lengths are consistent with those of comparable Ru complexes featuring allyl groups, and are consistent with the cyclooctenyl ligand binding to the metal in a η^3 fashion.[51]

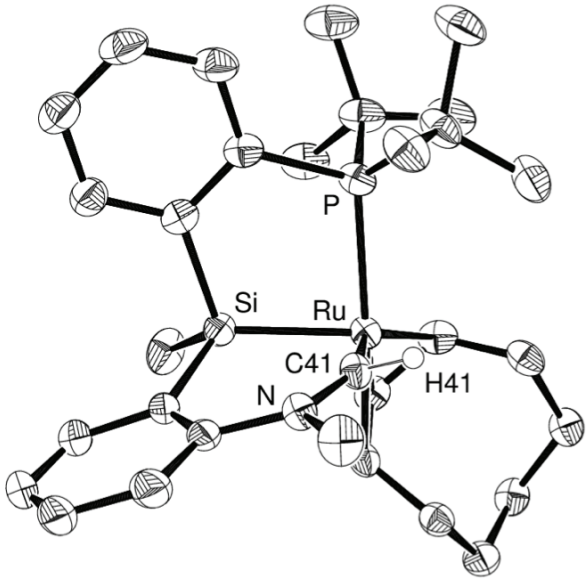

Figure 2-2. The crystallographically determined structure of **2-5**, shown with 50% displacement ellipsoids. All non-carbenic H atoms have been omitted for clarity.

Although the mechanism for the formation of **2-5** is not known, a proposed mechanism is shown in Scheme 2-6. Since the (1,5-COD)Ru(methylallyl)$_2$ starting material is an 18-electron complex, the first step of this proposed mechanism involves dissociation of one of the alkene fragments of the cyclooctadiene group followed by coordination of the phosphine arm of **2-4**. The next proposed step involves a η^3-η^1 interconversion of one of the methylallyl ligands in order to form an electronically and coordinatively unsaturated intermediate capable of oxidative addition of the Si-H bond. The oxidative addition of the Si-H bond is followed by a C-H reductive elimination to liberate an equivalent of 2-butene, which is then followed by another η^3-η^1 methylallyl conversion and amine coordination. Coordination of the amine ligand arm delivers one

of the amine methyl substituents into close proximity of the metal center, facilitating an oxidative addition of one of the methyl C-H bonds. This oxidative addition is followed by another reductive elimination of 2-butene to yield a Ru alkyl intermediate, which is proposed to undergo an α-H migration from the alkyl group to the metal center to form the carbene group. Following the formation of the carbene, it is proposed that the an alkene fragment of the bound cyclooctadiene group inserts into the newly formed Ru-H bond. The insertion step is followed by C-H oxidative addition of one of the C-H bonds that is in an α position relative to the previously coordinated alkene, followed by a C-H reductive elimination. The final step of this proposed mechanism involves a η^1-η^3 interconversion of the newly formed cyclooctenyl fragment to form the final product, **2-5**.

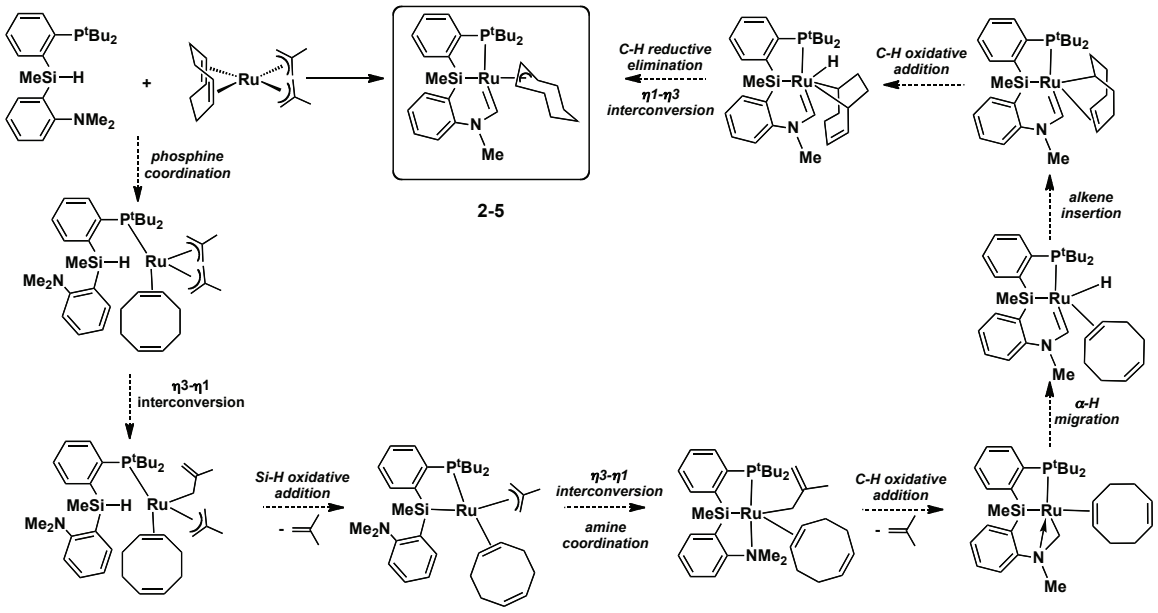

Scheme 2-6. Proposed mechanism for the formation of **2-5**.

2.2.4 Reactivity Studies of a [PSiC]Ru Carbene Complex

It was initially proposed that **2-5** may be an ideal candidate for the activation of E-H (E = main group element, e.g. H, Si, B, C) bonds, as one can envision the addition of an E-H bond across the Ru=C bond. Upon performing reactions with primary, secondary, and tertiary silanes no reactivity was observed, even at high temperatures (80-100 °C). However, upon treatment of **2-5** with H_2 (ca. 1 atm) in benzene at 110 °C, quantitative conversion to a new product was observed by $^{31}P\{^1H\}$ NMR spectroscopy over the course of four days. Upon isolation (53% yield), the product of this hydrogenation reaction was determined to be a Ru η^6-benzene complex in which the carbene moiety has been reduced to an alkyl ligand, **2-6** (Scheme 2-7). Alternatively, is was found that **2-6** can also be synthesized by simply heating **2-5** in benzene solution at 110 °C, however the reaction takes roughly 4 times as long using this preparative route.

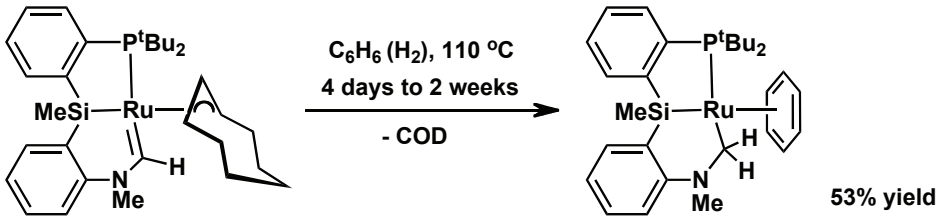

Scheme 2-7. Synthesis of [PSiC]Ru(η^6-C_6H_6) (**2-6**).

Complex **2-6** features a single peak in the $^{31}P\{^1H\}$ NMR spectrum at 108.4 ppm. The features of the ^1H NMR spectrum for **2-6** are consistent with the formation of a Ru alkyl complex containing benzene coordinated to the metal center in an η^6-fashion. The resonance for the η^6-benzene hydrogens is observed as a singlet at 4.90 ppm (benzene-d_6), a value consistent with other η^6-benzene coordinated Ru complexes.[52] Two resonances are observed for the diasterotopic methylene hydrogens adjacent to the Ru

center (4.58 ppm, m, 1 H; 1.92 ppm, m, 1 H). The diastereotopic relationship between these hydrogens was confirmed by the presence of a crosspeak between these two resonances in the 2D-COSY NMR spectrum.

The solid-state structure of **2-6** was confirmed using X-ray diffraction techniques (Figure 2-3, Table 2-1). A Ru-C(41) bond length of 2.156(1) Å is observed, consistent with a value expected for a Ru-C single bond.[50] The N-C(41) bond length was determined to be 1.465(2) Å, indicative of a N-C single bond with little π-donation from N to C.[49] The P-Ru-C(41) bond angle was observed to be 88.42(4)°, a value very close to the 90° that would be expected for a facial binding mode of a tridentate ligand. Notably, this angle is much more acute than the 97.47(5)° observed in complex **2-5**. The P-Ru-Si and C41-Ru-Si bond angles of 83.00(1)° and 74.14(6)° are quite acute compared to the 90° expected for an octahedral d^6, 18-electron complex, suggesting a distortion due to the presence of the η^6-benzene ligand. This type of distortion is well documented for transition metal complexes containing a single η^5 or η^6 bound arene.[52] The geometry of these complexes is commonly described as a "half sandwich" or "piano stool" geometry, where the η^6-C_6H_6 can be thought of as being the seat of the piano stool and the P-Si-C(41) ligands can be described as being the legs of the piano stool.

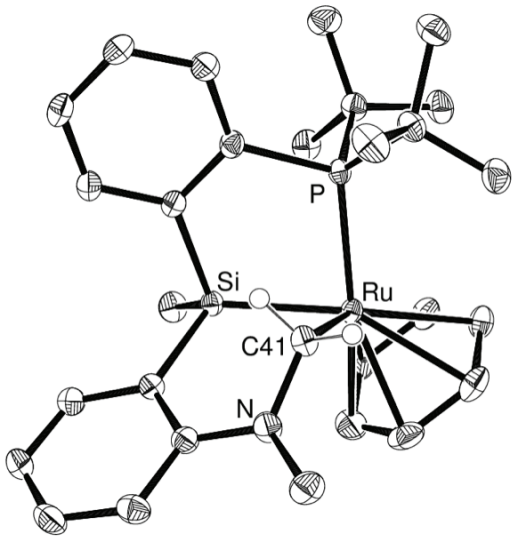

Figure 2-3. The crystallographically determined structure of **2-6**, shown with 50% displacement ellipsoids. All non-diastereotopic H atoms have been omitted for clarity.

Bond Lengths (Å)				
2-5	Ru-P	2.3698(4)	Ru-C(41)	1.9101(15)
	Ru-Si	2.2461(5)		
2-6	Ru-P	2.3458(4)	Ru-C(41)	2.1558(13)
	Ru-Si	2.3322(4)		
Bond Angles (°)				
2-5	P-Ru-C(41)	97.47(5)	Si-Ru-C(41)	83.34(5)
	P-Ru-Si	85.223(16)		
2-6	P-Ru-C(41)	88.42(4)	Si-Ru-C(41)	74.14(6)
	P-Ru-Si	83.001(16)		

Table 2-1. Selected interatomic distances (Å) and angles (°) for **2-5** and **2-6**.

A proposed mechanism for the formation of **2-6** with or without the presence of H_2 is shown in Scheme 2-8. For both mechanisms, the first proposed step involves an η^3-η^1 interconversion of the cyclooctenyl ligand. In the presence of H_2, coordination of H_2 is proposed to occur in a side-on fashion followed by a σ-bond metathesis step, which results in the formation a new Ru-H bond as well as a cyclooctene (COE) ligand. This process is then followed by dissociation of the COE ligand and coordination of benzene,

potentially in an η^2-fashion. The final step of this mechanism involves an α-H migration from Ru to the carbenic carbon and coordination of benzene to Ru in a η^6-fashion. Without the presence of H_2, the η^3- η^1 interconversion of the cyclooctenyl ligand is followed by a β-H elimination from the cyclooctenyl group. This β-H elimination results in the formation of 1,3-COD, which can simply dissociate from the metal center. Upon dissociation of COD, benzene can coordinate to Ru in a η^2-fashion. Benzene coordination is followed by α-H migration from Ru to the carbenic carbon and η^6-coordination of the benzene ligand to the metal.

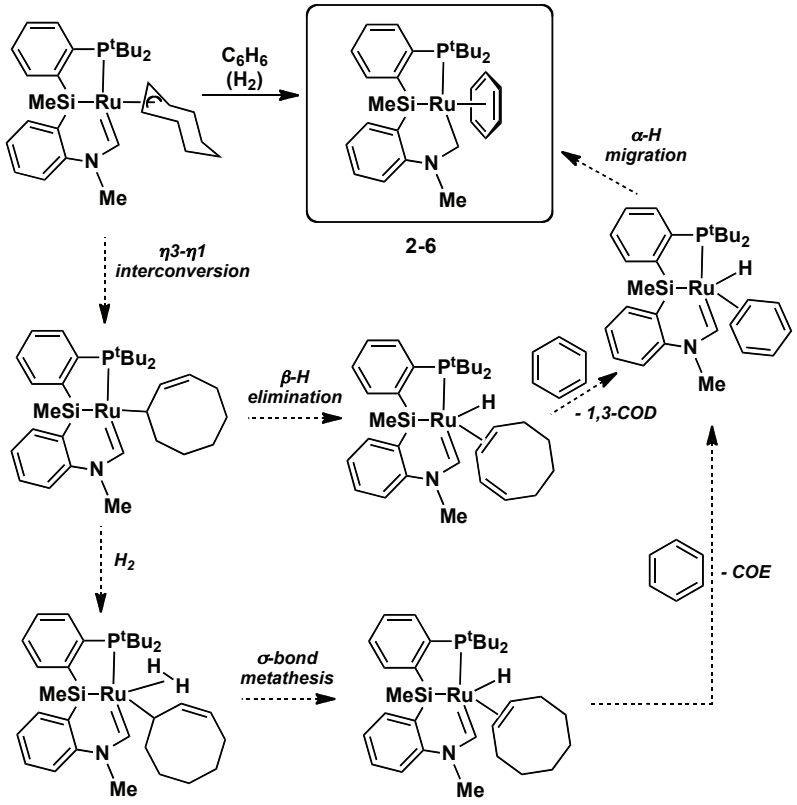

Scheme 2-8. Proposed mechanism for the formation of **2-6**.

In reactivity studies complex **2-6** was found to be unreactive with a variety of hydrosilanes as well as H_2, even with heating for multiple days at high temperatures (80 - 100 °C). This result is not surprising as **2-6** is an 18-electron complex that is

coordinatively and electronically saturated.

2.2.5 Coordination Chemistry of [^{t}Bu-PSiN-Me]H with Rh and Ir

A rich history of chemistry involving pincer complexes of Rh and Ir exists in the literature.[4] Of particular note, Ir complexes containing cyclometalated pincer ligands have demonstrated an exceptional ability to perform bond activations of inert E-H bonds, including the N-H bonds in ammonia.[53] Such bond activation processes are generally thought to occur via oxidative addition of the E-H bond to an extremely reactive 14-electron, coordinatively unsaturated M^I (M = Rh or Ir) intermediate. Generation of such 14 electron, M^I intermediates generally occurs by reductive elimination from a 16-electron, M^{III} complex. Previous work from the Turculet group has demonstrated that silyl pincer complexes of Ir have the ability to perform such challenging reactions, activating both sp^2-CH bonds[43b] and N-H bonds in ammonia (Scheme 2-9).[43e] The upcoming sections will detail the synthesis, characterization, and reactivity studies of Group 9 complexes featuring [^{t}Bu-PSiN-Me] ligation.

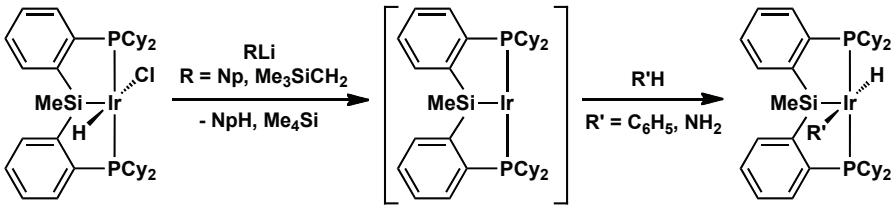

Scheme 2-9. Oxidative addition of C_6H_6 and NH_3 to a [Cy-PSiP]Ir^I intermediate.

2.2.6 Synthesis and Characterization of [^{t}Bu-PSiN-Me]M(H)Cl Complexes

As discussed above, Rh and Ir complexes containing silyl pincer ligation have been reported in the literature by the Turculet group.[43b, 43e] Complexes of the type [Cy-

PSiP]M(H)Cl (M = Rh or Ir) can be synthesized by reaction of the [Cy-PSiP]H pro-ligand with readily available $[(COE)_2MCl]_2$ (COE = cyclooctene) starting materials. To synthesize analogous [^{t}Bu-PSiN-Me]M(H)Cl complexes, a similar synthetic route was chosen. However, no reaction was observed upon treatment of [^{t}Bu-PSiN-Me]H with either $[(COE)_2RhCl]_2$ or $[(COE)_2IrCl]_2$ at room temperature. Alternatively, when the closely related $[(COD)MCl]_2$ dimers were used as the metal starting materials, the formation of the hydrido chloride complexes [^{t}Bu-PSiN-Me]Rh(H)Cl (**2-7**) and [^{t}Bu-PSiN-Me]Ir(H)Cl (**2-8**) was observed at room temperature (Scheme 2-10). In both cases quantitative formation of **2-7** and **2-8** was observed by $^{31}P\{^1H\}$ NMR spectroscopy (**2-7**: 101.0 ppm, d, $^1J_{PRh}$ = 164 Hz; **2-8**: 62.6 ppm, s) within an hour of performing the reaction. Surprisingly, the room temperature conditions required for the formation of **2-7** and **2-8** are much milder than those required to synthesize analogous [Cy-PSiP]M(H)Cl complexes (3 days at 75 °C). After purification, **2-7** and **2-8** were isolated as yellow solids in yields of 94% and 99%, respectively. The ^1H NMR spectra of **2-7** and **2-8** (benzene-d_6) support the formation of the desired C_1 symmetric hydrido chloride complexes. One particularly diagnostic set of resonances are those for the Me groups on the neutral amino donor. One would expect that for a C_1 symmetric κ^3-PSiN complex there would be two different methyl resonances observed for the metal bound NMe_2 group due to the lack of symmetry of the molecule. Indeed, two N*Me* resonances are observed in the ^1H NMR spectra of **2-7** and **2-8** (**2-7**: 3.06 ppm, s, 3 H; 2.96 ppm, s, 3 H; **2-8**: 3.17 ppm, s, 3 H; 2.94 ppm, s, 3 H), confirming the κ^3-PSiN coordination. In addition, the ^1H NMR spectra of **2-7** and **2-8** also feature hydride resonances at -20.18

ppm (dd, 1 H, $^{1}J_{RhH}$ = 30 Hz, $^{2}J_{PH}$ = 21 Hz) and -25.00 ppm d, 1 H, $^{2}J_{PH}$ = 20 Hz), respectively.

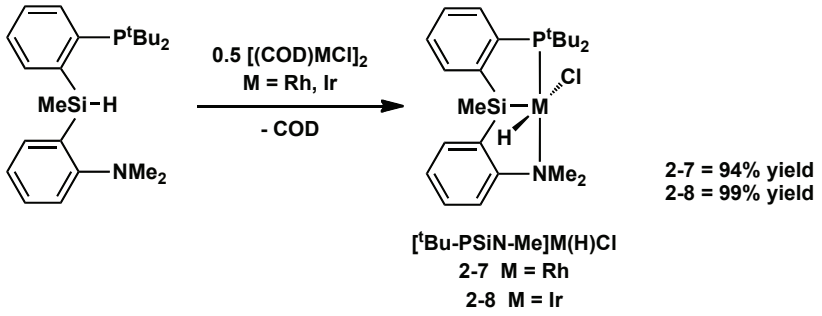

Scheme 2-10. Synthesis of [^{t}Bu-PSiN-Me]M(H)Cl complexes **2-7** and **2-8**.

The X-ray crystal structures of **2-7** and **2-8** confirm the formation of five-coordinate hydrido chloride complexes with similar geometries in the solid state (Figure 2-4, Table 2-2). For both **2-7** and **2-8**, the five-coordinate structures exhibit distorted square-based pyramidal coordination geometry at the metal center, with Si occupying the apical coordination site. The P-M-N bond angles of 163.70(3)° and 164.84(5)° for **2-7** and **2-8**, respectively, indicate a meridional binding of the PSiN ligand. Interestingly, the structures feature acute Si–M–H(1) angles (**2-7**, 67.4°; **2-8**, 71.0°). As such, the geometry at the metal center can also be described as "Y-shaped", in which the chloride ligand is positioned opposite to the acute angle of the "Y". Such Y-shaped coordination geometry is also adopted by analogous PSiP-ligated Rh and Ir species and is not uncommon for five-coordinate d^6 complexes that feature a weak π-donor such as Cl; this phenomenon has been attributed to electronic effects.[54] The structures for **2-7** and **2-8** also feature relatively short Si···H(1) distances of 2.13 (**2-7**) and 2.24 (**2-8**) Å, respectively, falling within the range indicative of an Si-H interaction (typically 1.7 – 2.4 Å;[55] sum of van der Waals radii = 3.4 Å). Such close Si···H contacts were also noted in the solid state structures of the related [Cy-PSiP]M(H)Cl (M = Rh, Ir) complexes.[43b, 43e]

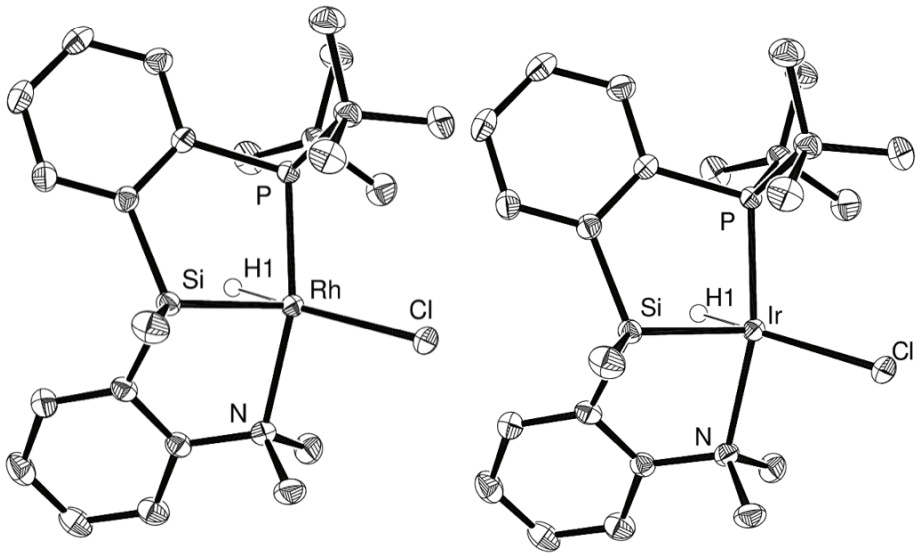

Figure 2-4. The crystallographically determined structure of **2-7** (left) and **2-8** (right), shown with 50% displacement ellipsoids. All non-hydrido H atoms have been omitted for clarity.

Bond Lengths (Å)				
2-7	Rh-P	2.2421(4)	Rh-H(1)	1.46(2)
	Rh-N	2.2349(12)	Rh-Cl	2.4365(5)
	Rh-Si	2.2175(4)		
2-8	Ir-P	2.2380(5)	Ir-H(1)	1.46(3)
	Ir-N	2.2318(18)	Ir-Cl	2.4261(6)
	Ir-Si	2.2355(6)		
Bond Angles (°)				
2-7	P-Rh-N	163.70(5)	Si-Rh-H(1)	67.4(9)
	Si-Rh-Cl	132.103(14)	Cl-Rh-H(1)	160.2(9)
2-8	P-Ir-N	164.84(5)	Si-Ir-H(1)	71.0(12)
	Si-Ir-Cl	131.38(2)	Cl-Ir-H(1)	156.3(12)

Table 2-2. Selected interatomic distances (Å) and angles (°) for **2-7** and **2-8**.

2.2.7 Synthesis and Characterization of a PMe_3 adduct of [^{t}Bu-PSiN-Me]Rh(H)Cl

As outlined in Chapter 1, the design of this new class of PSiN ligands is such that they feature a potentially hemilabile amine donor capable of reversible coordination to the metal center. To this effect, it was proposed that introduction of a donor ligand to

complexes **2-7** and **2-8** may result in the formation of adducts where the neutral amine donor has been displaced from the metal center. In this context, reaction of **2-7** with one equiv. of PMe_3 resulted in the formation of the adduct **2-9**, where the neutral amine donor had indeed been displaced from the metal coordination sphere by PMe_3 (Scheme 2-11).

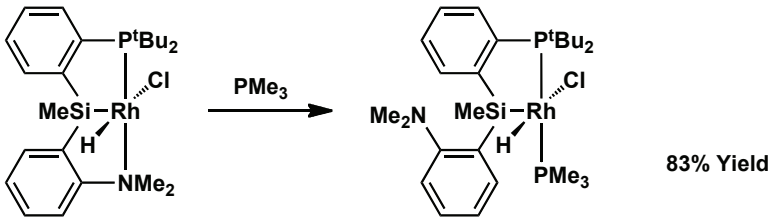

[^{t}Bu-PSiN-Me]Rh(H)Cl(PMe_3), 2-9

Scheme 2-11. Synthesis of PMe_3 adduct [^{t}Bu-PSiN-Me]Rh(H)Cl(PMe_3) (**2-9**).

The formation of **2-9** was corroborated by the observation of a new set of resonances in the $^{31}P\{^1H\}$ NMR spectrum of the reaction mixture (88.4 ppm, dd, $^2J_{PP}$ = 356 Hz, $^1J_{PRh}$ = 123 Hz; 4.88, dd, $^2J_{PP}$ = 356 Hz, $^1J_{PRh}$ = 123 Hz). The large coupling constant of 356 Hz observed for $^2J_{PP}$ is indicative of *trans* coupling between the two phosphines, a result expected if PMe_3 simply displaces the amine donor. In addition, the amino methyl groups are observed to be equivalent in the ^1H NMR spectrum for **2-9** (benzene-d_6), giving rise to a single resonance at 1.97 ppm (s, 6 H), which is consistent with dechelation of the amino ligand arm such that the NMe_2 group can undergo rapid rotation and inversion on the NMR timescale rendering the methyl groups chemically equivalent. Furthermore, the hydride resonance in **2-9** is highly coupled compared to that in **2-7**, indicative of additional coupling due to the presence of coordinated PMe_3 (-16.8 ppm, m, 1 H).

The X-ray crystal structure of **2-9** confirmed the formation of a five-coordinate hydrido chloride PMe_3 adduct, where the amine donor is indeed not coordinated to the metal center (Figure 2-5, Table 2-3). By examining the bond angles and distances, one

can see that **2-9** adopts a very similar geometry to **2-7** and **2-8** in the solid state. For **2-9**, The P(1)-Rh-P(2) bond angle of 169.68(1)° indicates that the PMe_3 coordinates to the metal centre *trans* to the phosphorus of the PSiN ligand, which is consistent with the structure in solution. Complex **2-9** exhibits distorted square-based pyramidal coordination geometry at the metal center, with Si occupying the apical coordination site. In a similar fashion to **2-7** and **2-8**, the structure of **2-9** features an acute Si–Rh–H(1) angle of 67.1(8)°. As such, the geometry at the metal center can also be described as "Y-shaped", in which the chloride ligand is positioned opposite to the acute angle of the "Y". The analogous PMe_3 adduct of **2-8** has not been isolated, although NMR data for the reaction mixture indicates that the PMe_3 displaces the amino donor from the metal center in a similar fashion to **2-9**. Attempts to isolate this complex are ongoing.

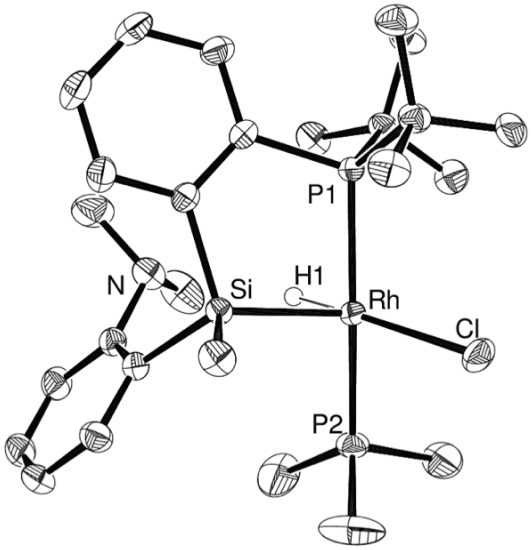

Figure 2-5. The crystallographically determined structure of **2-9** shown with 50% displacement ellipsoids. All non-hydrido H atoms have been omitted for clarity.

Bond Lengths (Å)				
2-9	Rh-P(1)	2.3463(4)	Rh-H(1)	1.46(2)
	Rh-P(2)	2.3031(4)	Rh-Cl	2.4300(4)
	Rh-Si	2.2584(4)		
Bond Angles (°)				
2-9	P(1)-Rh-P(2)	169.676(15)	Si-Rh-H(1)	67.1(8)
	Si-Rh-Cl	125.470(17)	Cl-Rh-H(1)	166.0(8)

Table 2-3. Selected interatomic distances (Å) and angles (°) for **2-9**.

The formation of complex **2-9** was encouraging for the future reactivity of [^{t}Bu-PSiN-Me] ligated transition metal complexes. The facile displacement of the potentially hemilabile amine donor demonstrates that this ligand arm is capable of dissociating from the metal center, which is a necessary component of a hemilabile ligand. The hemilabile nature of the [^{t}Bu-PSiN-Me] ligand was further corroborated by the synthesis of Pd and Pt complexes featuring [^{t}Bu-PSiN-Me]-ligation. The amino donor in such complexes was shown to reversibly dissociate from the metal center at room temperature, which demonstrates the truly hemilabile nature of the ligand.[57]

2.2.8 Reactivity Studies of [^{t}Bu-PSiN-Me] Ligated Rh and Ir Complexes

Complexes **2-7** and **2-8** are attractive targets for the study of E-H bond activation chemistry via a putative [^{t}Bu-PSiN-Me]M^{I} (M = Rh, Ir) reactive intermediate. Unfortunately, attempts to dehydrohalogenate **2-7** and **2-8** in order to access 14 electron species of the type [^{t}Bu-PSiN-Me]M^{I} proved largely unsuccessful. The synthetic routes described in Scheme 2-12 were used in the attempts to form these M^{I} intermediates. It was found that upon alkylation of **2-7** or **2-8** with either Me_3CCH_2Li or Me_3SiCH_2Li in either benzene or cyclohexane solvent, very short-lived (seconds to minutes) deep red

solutions formed, followed by the rapid formation of a grey metallic precipitate and brown solution. These short-lived red species exhibited extremely broad $^{31}P\{^{1}H\}$ and ^{1}H NMR features which were difficult to interpret in a meaningful fashion. The ^{1}H NMR spectra of the reaction mixtures did not feature resonances attributable to hydride ligands. Attempts were made to trap [^{t}Bu-PSiN-Me]M^{I} species using donor ligands such as ethylene (1 atm) and PMe_3, however no products from these reactions could be isolated. The inability to successfully trap a [^{t}Bu-PSiN-Me]M^{I} intermediate is suggestive of the extreme instability of these intermediates. Comparatively, the trapping of M^{I} intermediates from [Cy-PSiP]M(H)Cl is relatively facile, indicating that such PSiP-ligated M^{I} species are somewhat longer lived.[58]

Despite the apparent instability of [^{t}Bu-PSiN-Me]M^{I} species, attempts were made to generate such reactive intermediates *in situ* (benzene and cyclohexane) in order to activate Si-H and sp^2-CH bonds in the presence of either hydrosilanes ($PhSiH_3$ and Ph_2SiH_2; 1 or 5 equiv.) or benzene (large excess), respectively. Unfortunately, no clean reactivity was observed for these reactions. In all cases, extremely broad $^{31}P\{^{1}H\}$ and ^{1}H NMR spectra were observed for the reaction mixtures with no decoalescence apparent at lower temperatures.

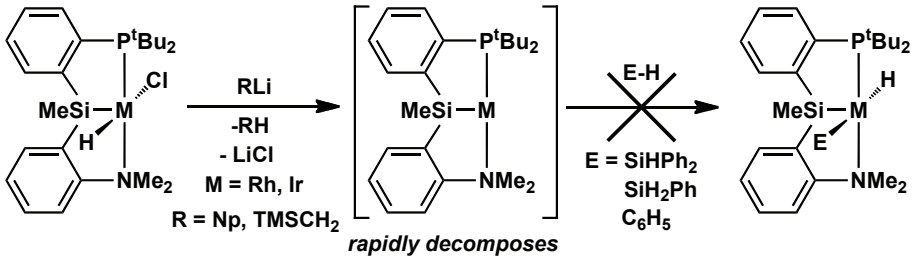

Scheme 2-12. Attempts to activate E-H bonds via 14-electron M^{I} complexes.

2.2.9 Synthesis and Characterization of [^{t}Bu-PSiN-Me] Ligated Cationic Group 9 Complexes

In an effort to access Rh and Ir complexes that could undergo E-H bond activation chemistry, the synthesis of potentially cationic complexes featuring [^{t}Bu-PSiN-Me] ligation was undertaken (Scheme 2-13). Significant precedent exists for E-H bond activation reactions mediated by cationic M^{III} (M = Rh or Ir) complexes, including examples of alkane C-H bond cleavage.[59] Of note, cationic Ir^{III} complexes developed by Bergman and co-workers have shown the ability to activate sp^3-CH bonds in substrates such as cyclohexane and methane.[59a]

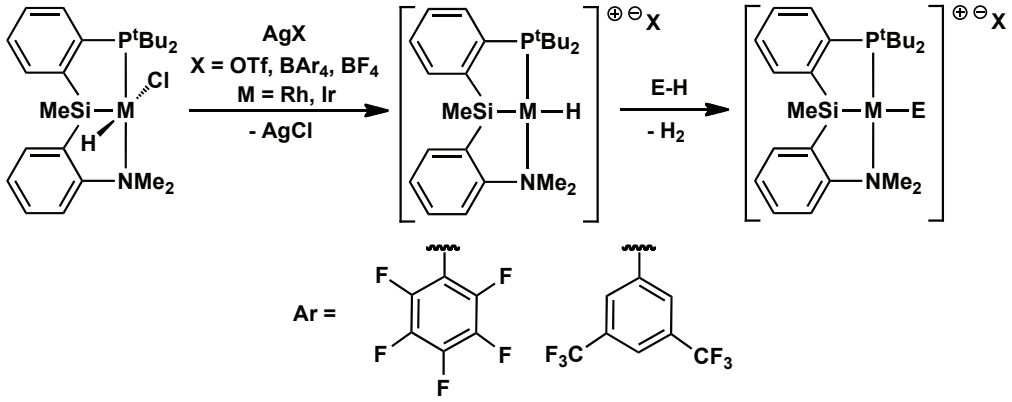

Scheme 2-13. Proposed synthesis and reactivity of cationic [^{t}Bu-PSiN-Me]M^{III} complexes.

In this context, the reaction of either **2-7** or **2-8** with 1 equiv. of AgOTf in fluorobenzene resulted in the formation of [^{t}Bu-PSiN-Me]M(H)OTf complexes (**2-10**, M = Rh and **2-11**, M = Ir) in high yield (Scheme 2-14). These reactions appeared to occur almost instantaneously, as a significant amount of solid (presumably AgCl) immediately precipitated from solution, coupled with an immediate color change of the solutions from yellow to amber. The ^{31}P NMR resonances for **2-10** and **2-11** (benzene-d_6; **2-10**: 95.5 ppm, d; **2-11**: 59.8 ppm, s) are shifted slightly upfield from those of complexes **2-7** and **2-8** (*cf.* 101.0 and 62.6 ppm for **2-7** and **2-8**, respectively) and were observed to be

significantly broader. The ^{1}H and ^{13}C NMR data for **2-10** and **2-11** largely mirror those of **2-7** and **2-8**.

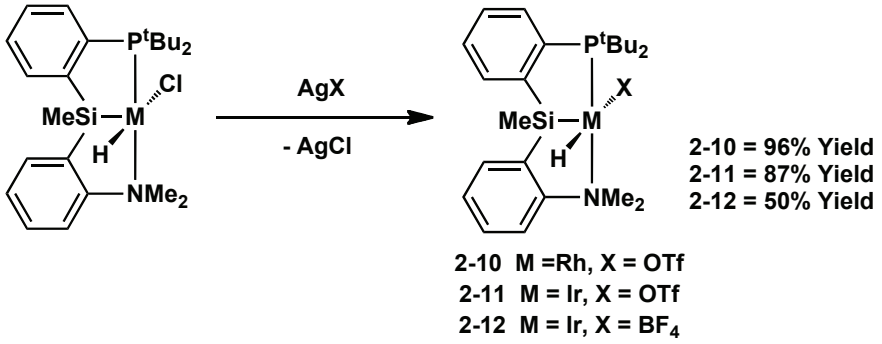

Scheme 2-14. Synthesis of 'cationic' [^{t}Bu-PSiN-Me]M^{III} complexes **2-10** - **2-12**.

The synthesis of BF_4 analogues of **2-10** and **2-11** was undertaken by the reaction of complexes **2-7** and **2-8** with 1 equiv. of $AgBF_4$. These reactions were met with significantly less success than the synthesis of the related triflate species, and in the case of Rh the product of the reaction appears to be highly unstable. Upon treatment of **2-7** with 1 equiv. of $AgBF_4$ in fluorobenzene, a metallic grey precipitate was observed in the reaction vial within minutes of mixing. Resonances similar to those of **2-10** could be observed in the ^{31}P and ^{1}H NMR spectra of the reaction mixture, however these resonances were accompanied by several other broad resonances. Due to the apparent lack of stability of this complex, its isolation was not pursued further. Comparatively, upon mixing **2-8** with $AgBF_4$, it was found that [^{t}Bu-PSiN-Me]Ir(H)BF_4 (**2-12**) could be isolated in 50% yield as a yellow-brown solid. Multiple small impurities were observed in the $^{31}P\{^{1}H\}$ NMR of the crude reaction mixture, however after a thorough pentane wash, **2-12** could be isolated cleanly. The NMR features of **2-12** mirror those of **2-11**, and the incorporation of the BF_4 ligand can be readily observed in the ^{11}B (0.6 ppm) and ^{19}F (-158.1 ppm) NMR spectra.

The attempted synthesis of potentially cationic complexes featuring bulky, non-coordinating counteranions such as $B(C_6F_5)_4^-$ was also pursued. The reaction of either **2-7** or **2-8** with 1 equiv. of either $Ag[B(C_6F_5)_4]$ or $Na[B(3,5\text{-}(CF_3)_2C_6H_3)_4]$ proceeded quickly in fluorobenzene, however the formation of grey metallic precipitate could be observed within minutes and no clean products could be isolated from these mixtures. Performing the reactions at low temperature (-35 °C) did not appear to aid in the isolation of clean products. Due to the extreme instability of such complexes, their synthesis and isolation were not further pursued.

The ability to isolate complexes **2-10**, **2-11**, and **2-12** and not analogues featuring $[B(C_6F_5)_4]^-$ or $[B(3,5\text{-}(CF_3)_2C_6H_3)_4]^-$ counteranions can be rationalized by considering the coordinating ability of the respective counteranions. Triflate counteranions have the ability to remain coordinated inner-sphere, thereby maintaining a close contact with the metal center by binding through the negatively charged oxygen atom of the triflate moiety. BF_4^- counteranions also have a similar ability to coordinate the metal center through one of the fluorine atoms. The ability of such counteranions to coordinate to the metal center is facilitated by their relatively small size. To this effect, it is likely that in **2-10** and **2-**11, the counteranions are bound directly to the metal center, thereby helping to stabilize the resulting complexes. Alternatively, the $[B(C_6F_5)_4]^-$ and $[B(3,5\text{-}(CF_3)_2C_6H_3)_4]^-$ counteranions are the least likely to coordinate to the metal center, as their negative charge is distributed over many electronegative atoms, which would render the resulting complexes truly cationic and may lead to their apparent instability. Interestingly, when **2-11** and **2-12** were dissolved in THF, the THF appeared to polymerize quite rapidly, forming an insoluble solid. It is well established that THF is

polymerized by highly electrophilic cationic initiators,[60] suggesting that **2-11** and **2-12** may have some appreciable cationic character in polar solvent. Notably, a series of complexes of the type {[Cy-PSiP]M(H)}X (M = Ir; X = OTf^-, BF_4^-, $[B(C_6F_5)_4]^-$, or $[B(3,5\text{-}(CF_3)_2C_6H_3)_4]^-$) have been isolated in the Turculet group and have proven to be relatively stable,[58] suggesting that PSiP ligation may be better suited for the stabilization of cationic group 9 complexes than PSiN ligation.

Single crystals of **2-10** and **2-11** were obtained from concentrated benzene solutions and the solid state structures of these complexes were determined by use of X-ray diffraction techniques (Figure 2-6, Table 2-4). Both complexes are five-coordinate in the solid state and exhibit distorted square-based pyramidal coordination geometries with Si occupying the apical coordination sites and an inner-sphere triflate ligand coordinated trans to hydride. Similarly to the hydrido chloride complexes **2-7**, **2-8**, and **2-9**, the structures of **2-10** and **2-11** feature acute Si–M–H1 angles (**2-10**: 74.4°; **2-11**: 74.1°) such that the geometry can also be described as "Y-shaped", with the triflate ligand positioned opposite to the acute angle of the "Y". The structures also feature relatively short Si···H1 distances (**2-10**: 2.3 Å; **2-11**: 2.4 Å) that fall within the range indicative of an Si-H interaction (typically 1.7 – 2.4 Å;[55] sum of van der Waals radii = 3.4 Å).

Although the triflate ligand in **2-10** and **2-11** appears to be bound to the metal in the solid state, it may be somewhat labile in solution. This was probed by attempting the reaction of **2-10** and **2-11** with 2-electron donors such as PMe_3 and DMAP to see how readily these donors could displace the triflate ligand. Unfortunately, such reactions resulted in the displacement of the weakly bound amino ligand arm and not the triflate, making the lability of the triflate group difficult to probe. The displacement of the amino

arm can be observed in the NMe_2 resonances in the ^1H NMR spectrum for such reactions, as such NMe_2 resonances were rendered equivalent, suggesting displacement of NMe_2 from the metal center.

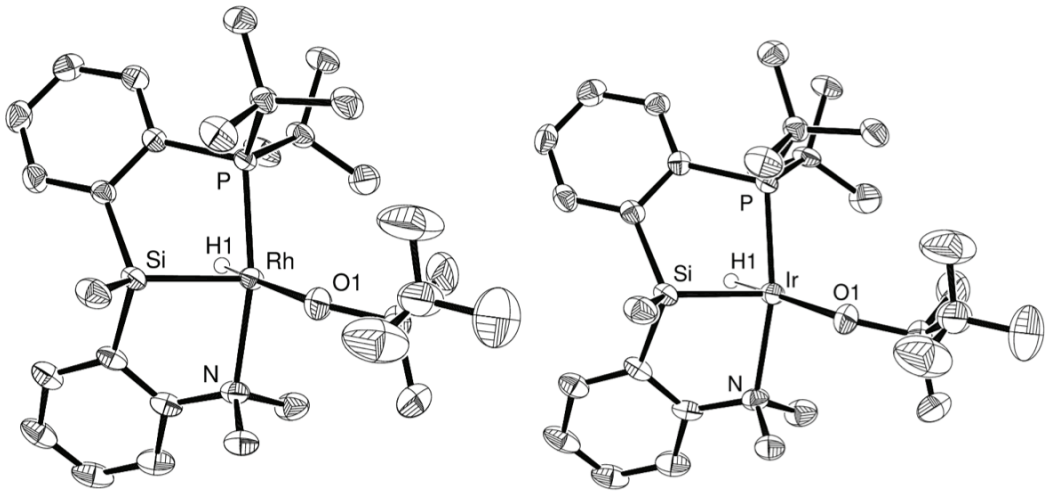

Figure 2-6. The crystallographically determined structures of **2-10** (left) and **2-11** (right) shown with 50% displacement ellipsoids. All non-hydrido H atoms have been omitted for clarity.

Bond Lengths (Å)				
2-10	Rh-P	2.2573(6)	Rh-H1	1.44(3)
	Rh-N	2.219(2)	Rh-Ol	2.2325(18)
	Rh-Si	2.2246(7)		
2-11	Ir-P	2.2528(13)	Ir-H1	1.549(10)
	Ir-N	2.215(4)	Ir-Ol	2.241(4)
	Ir-Si	2.2397(14)		
Bond Angles (°)				
2-10	P-Rh-N	162.75(6)	Si-Rh-H1	74.4(11)
	Si-Rh-O1	114.51(5)	Cl-Rh-H1	170.8(11)
2-11	P-Ir-N	164.34(11)	Si-Ir-H1	74.1(17)
	Si-Ir-Ol	111.84(10)	Cl-Ir-H1	173.3(18)

Table 2-4. Selected interatomic distances (Å) and angles (°) for **2-10** and **2-11**.

2.2.10 Potential C-H Activation by [^{t}Bu-PSiN-Me]-Ligated Ir Complexes

Upon obtaining ^{1}H NMR data for complexes **2-11** and **2-12** (benzene-d_6), it was observed that the hydride resonances were quite broad, had no apparent ^{31}P coupling, and integrated to slightly less than one proton (typically 0.8 - 0.9 protons) when the spectra were recorded 10 minutes after dissolving the sample. When the ^{1}H NMR spectrum was recorded 8 hours after dissolving the sample, the hydride resonances observed for both **2-11** and **2-12** were further diminished, integrating to approximately 0.1 protons. Furthermore, a broadening and slight decrease in the intensity of the ^{1}H resonance corresponding to one of the P^{t}Bu$_2$ substituents could be observed over the same time period, accompanied by an increase in the intensity of the resonance corresponding to C_6H_6. Comparatively, the ^{1}H NMR spectrum of the Rh complex **2-10** (benzene-d_6) did not exhibit this behavior over the same time period. A possible explanation for the changes observed in the spectra of **2-11** and **2-12** is that the complexes are undergoing reaction with the benzene-d_6 solvent, potentially by a σ-bond metathesis process, and slowly incorporating ^{2}H into the hydride position and one of the PSiN ligand P^{t}Bu substituents (Scheme 2-15). As outlined in Scheme 2-15, an equivalent of C_6D_6 could undergo a σ-bond metathesis step with the Ir-H resulting in the formation of C_6D_5H and Ir-D. The resulting Ir-D could then undergo a similar intramolecular σ-bond metathesis process with a C-H group of one of the P^{t}Bu substituents, thereby incorporating deuterium into the P^{t}Bu$_2$ moiety. Notably, full deuteration of the P^{t}Bu substituent was not observed within 8 hours at room temperature (^{1}H NMR). Allowing **2-11** and **2-12** to sit in solution longer resulted in decomposition of the complexes. Attempts to promote the full deuteration of the P^{t}Bu substituent by heating were unsuccessful. Heating the

samples to or above 60 °C resulted in the rapid decomposition of **2-11** and **2-12**, as indicated by the rapid appearance of a grey metallic precipitate.

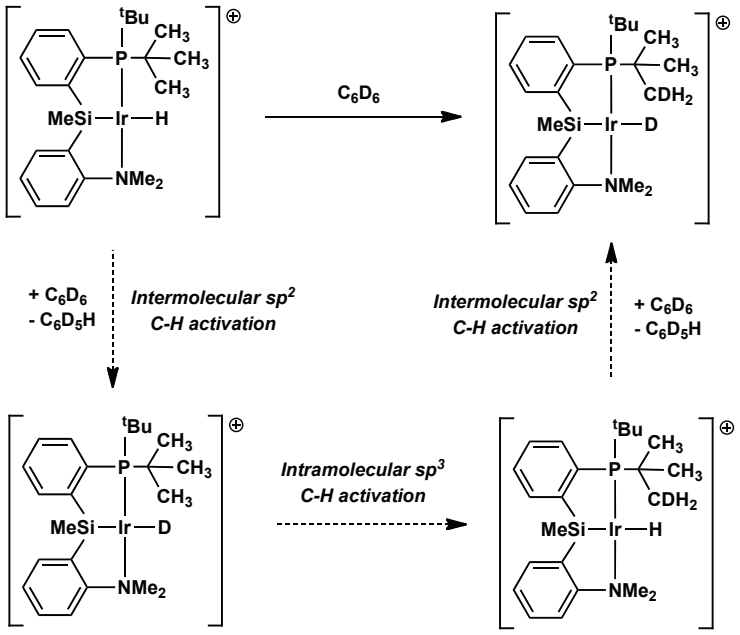

Scheme 2-15. Potential C-H activation by [^{t}Bu-PSiN-Me]Ir complexes.

The potential incorporation of ^{2}H into only one of the P^{t}Bu groups can be rationalized by the proximity of one of the ^{t}Bu groups to the hydride position. By analyzing the X-ray crystal structure of **2-11** (Figure 2-5), it appears that one of the P^{t}Bu substituents is in closer proximity to the hydride ligand while the other is positioned closer to the triflate group. Thus, the ^{t}Bu group closer to the hydride position would at first glance be expected to preferentially undergo a σ-bond metathesis-like process with the hydride ligand. Attempts to observe ^{2}H incorporation into **2-11** and **2-12** by use of ^{2}H NMR spectroscopy were unsuccessful. A potential explanation for the lack of ^{2}H signals observed could be due to the dynamic nature of the H/D exchange process, as the ^{2}H signals would be expected to be broadened by this process. Furthermore, attempts to observe such a process by use of solution IR spectroscopy were also unsuccessful, as a

broad stretch was observed in the range (2100 - 2200 cm^{-1}) expected for the Ir-H/Ir-D stretches, rendering the results of the experiment ambiguous.

Encouraged by the proposed reactivity of **2-11** and **2-12** with sp^2-CH bonds it was hypothesized that such complexes might be quite reactive with weaker E-H bonds such as Si-H bonds. The reaction of **2-11** and **2-12** with 5 equiv. of $PhSiH_3$ or Ph_2SiH_2 resulted in the rapid evolution of gas (presumably H_2) and the rapid formation of a metallic grey precipitate. Analysis of the $^{31}P\{^1H\}$ NMR spectra of the reaction mixtures revealed several small resonances containing a poor signal-to-noise ratio. The ^1H NMR spectra of the reaction mixtures were quite convoluted, however new resonances could be observed around 5.0 ppm, potentially corresponding to the products of silane dehydrocoupling.[61] No organometallic products could be isolated from such reaction mixtures. Similar results were obtained for the reaction of the Rh complex **2-10** with hydrosilanes. These results indicated that the [^{t}Bu-PSiN-Me] ligand framework may not be ideal for the study of E-H bond activation at Ir^{III}, as organometallic products could not be isolated. To this effect, it was hypothesized that altering the donor properties of the ancillary PSiN ligand may aid in the synthesis of thermally robust, reactive PSiN-ligated metal complexes that exhibit facile reactivity with E-H bonds.

2.3 Conclusions

Attempts to cyclometalate [^{t}Bu-PSiN-Me]H to Ru led to the isolation of a Ru Fischer carbene complex resulting from CH bond activation of an N*Me* group in the pincer ligand. Conversely, complexes of the type [^{t}Bu-PSiN-Me]M(H)Cl (M = Rh, Ir) that feature κ^3-PSiN coordination proved readily accessible. The reaction of [^{t}Bu-PSiN-

Me]Rh(H)Cl with PMe_3 lead to the displacement of the NMe_2 ligand arm from the metal coordination sphere, which demonstrated the ability of the amino ligand arm to dissociate from the metal center. However, attempts to generate a [^{t}Bu-PSiN-Me]M^I species capable of oxidatively adding E-H bonds proved unsuccessful. It was found that potentially cationic [^{t}Bu-PSiN-Me]Ir(H)X (X = OTf, BF_4) complexes appeared to be reactive towards sp^2-CH bonds in benzene. Unfortunately, the instability of such complexes made it difficult to truly probe their reactivity towards E-H bonds. Modification of the [^{t}Bu-PSiN-Me] ligand may provide a means to circumvent these problems and facilitate the isolation of thermally stable organometallic species capable of performing challenging E-H bond activations. The investigation of alternative PSiN ligation will be the subject of Chapter 3 of this thesis.

2.4 Experimental Section

2.4.1 General Considerations

All experiments were conducted under argon or nitrogen in an MBraun glovebox or using standard Schlenk techniques. Tetrahydrofuran and diethyl ether were distilled from Na/benzophenone ketyl; while benzene, toluene, and pentane were purified over one activated alumina column and one column packed with activated Q-5. All purified solvents were stored over 4 Å molecular sieves. Benzene-d_6 was degassed via three freeze-pump-thaw cycles and stored over 4 Å molecular sieves. All other reagents were purchased from Strem or Aldrich and used without further purification. Unless otherwise stated, ^{1}H, ^{13}C, ^{31}P NMR, ^{15}N, and ^{29}Si characterization data were collected at 300K on a Bruker AV-500 spectrometer operating at 500.1, 125.8, 202.5, 50.7 and 99.4 MHz

(respectively) with chemical shifts reported in parts per million downfield of $SiMe_4$ (for ^1H, ^{13}C, and ^{29}Si), or 85% H_3PO_4 in D_2O (for ^{31}P). ^1H and ^{13}C NMR chemical shift assignments are based on data obtained from ^{13}C-DEPTQ, ^1H-^1H COSY, ^1H-^{13}C HSQC, and ^1H-^{13}C HMBC NMR experiments. ^{29}Si NMR assignments are based on ^1H-^{29}Si HMBC and ^1H-^{29}Si HMQC experiments. Despite prolonged acquisition times, less than expected unique resonances were observed for **2-11** and **2-12**. Elemental analyses were performed by Canadian Microanalytical Service Ltd. of Delta, British Columbia, Canada and by Columbia Analytical Services of Tucson, Arizona. Infrared spectra were recorded as thin films between NaCl plates using a Bruker VECTOR 22 FT-IR spectrometer at a resolution of 4 cm^{-1}. X-ray data collection, solution, and refinement were carried out by Drs. Robert MacDonald and Michael J. Ferguson at the University of Alberta X-ray Crystallography Laboratory, Edmonton, Alberta.

2.4.2 Synthetic Procedures and Characterization Data

$(2\text{-}BrC_6H_4)P^tBu_2$ (2-1). Cs_2CO_3 (7.51 g, 25.0 mmol), DiPPF (0.29 g, 0.70 mmol), and $Pd(OAc)_2$ (0.14 g, 0.83 mmol) were allowed to stir using a magnetic stirbar in ca. 20 mL of 1,4-dioxane for 20 minutes. A color change from orange to dark brown was observed. HP^tBu_2 (2.80 g, 19.2 mmol) and 2-bromoiodobenzene (5.42 g, 19.2 mmol) were added to the reaction mixture and the resulting solution was allowed to stir at 110 °C for 18 hours. The reaction mixture was subsequently allowed to cool to room temperature and the volatile components were removed *in vacuo*. The residue was extracted with benzene (ca. 20 mL) and CH_2Cl_2 (ca. 3 mL). The collected extracts were filtered through silica and Celite and dried under vacuum to yield **2-1** as a pale brown

solid (5.1 g, 89%). ^{1}H NMR (500 MHz, benzene-d_6): δ 7.62 (d, 1 H, J = 7 Hz, H_{arom}), 7.53 (m, 1 H, H_{arom}), 6.91 (app t, 1 H, J = 7 Hz, H_{arom}), 6.74 (m, 1 H, J = 7 Hz, H_{arom}), 1.15 (d, 9 H, PCMe_3, $^{3}J_{PH}$ = 12 Hz. ^{13}C{^{1}H} NMR (125.8 MHz, benzene-d_6): δ 139.4 (d, $C_{arom,}$ $^{3}J_{CP}$ = 31 Hz), 136.6 (CH$_{arom}$), 135.8 (d, $C_{arom,}$ $^{2}J_{CP}$ = 38 Hz), 134.3 (CH$_{arom}$), 130.8 (CH$_{arom}$), 126.4 (CH$_{arom}$), 33.4 (d, J = 28 Hz, PCMe$_3$), 30.8 (d, J = 18 Hz, PCMe_3). ^{31}P{^{1}H} NMR (202.5 MHz, benzene-d_6): δ 32.6 (s).

(2-LiC$_6$H$_4$)P^{t}Bu$_2$ (2-2). A solution of ^{n}BuLi (1.6 M in hexanes, 2.9 mL, 4.7 mmol) was added to a solution of **2-1** (1.4 g, 4.7 mmol) in ca. 5 mL of pentane at -78° C. A color change from light brown to pale yellow was observed. The reaction mixture was allowed to warm to room temperature, and after 2 hours the volatile components were removed *in vacuo*. The residue was triturated with pentane (ca. 2 mL) and dried under vacuum to yield **2-2** as a pale beige solid (1.1 g, 98%). ^{1}H NMR (500 MHz, THF-d_8): δ 7.55 (d, 1 H, J = 7 Hz, H_{arom}), 7.37 (m, 1 H, H_{arom}), 6.72 (m, 1 H, H_{arom}), 6.68 (m, 1 H, H_{arom}), 1.18 (d, 9 H, $^{3}J_{PH}$ = 10 Hz, PCMe_3). ^{13}C{^{1}H} NMR (125.8 MHz, THF-d_8): δ 149.3 (C_{arom}), 141.3 (d, $^{2}J_{CP}$ = 40 Hz, CH$_{arom}$), 130.9 (CH$_{arom}$), 128.1 (C_{arom}), 124.7 (CH$_{arom}$), 32.6 (d, J = 26 Hz, PCMe$_3$), 33.4 (d, J = 13 Hz, PCMe_3). ^{31}P{^{1}H} NMR (202.5 MHz, THF-d_8): δ 39.6 (s).

(2-NMe$_2$C$_6$H$_4$)SiMeHCl (2-3). A solution of 2-bromo-N,N-dimethylaniline (5.00 g, 25.0 mmol) in ca. 75 mL THF was added dropwise to flask containing Mg turnings (0.91 g, 37.5 mmol). The reaction mixture was heated for 18 h at 75° C. The resulting brown solution was allowed to cool to room temperature, and was then added dropwise to a solution of Cl_2SiMeH (14.3 g, 125 mmol) in in ca. 50 mL of THF at -78° C. A color change to orange was observed. After stirring for 18 h the volatile

components were removed *in vacuo*, and the residue was extracted with benzene (ca. 30 mL). The benzene extract was filtered through Celite to yield a red oil. This oil was then distilled under vacuum (<0.1 mm Hg) to afford a colorless oil (bp = 39° C, <0.1 mm Hg) that was identified as **2-3** (2.34 g, 47%). ^{1}H NMR (500 MHz, benzene-d_6): δ 7.89 (m, 1 H, H_{arom}), 7.15 (m, 1 H, H_{arom}), 7.06 (m, 1 H, H_{arom}), 6.84 (m, 1 H, H_{arom}), 5.55 (m, 1 H, Si-*H*), 2.20 (s, 6H, NMe_2), 0.60 (d, 3 H, J = 3 Hz, Si*Me*). ^{13}C{^{1}H} NMR (125.8 MHz, benzene-d_6): δ 160.65 (C_{arom}), 136.6 (CH_{arom}), 133.9 (C_{arom}) 132.9 (CH_{arom}), 127.3 (CH_{arom}), 121.4 (CH_{arom}), 46.6 (NMe_2), 2.4 (Si*Me*). ^{29}Si NMR (300 K, 99.4 MHz, benzene-d_6): δ -21.0.

[^{t}Bu-PSiN-Me]H (2-4). A precooled (-35° C) solution of **2-2** (0.25 g, 1.1 mmol) in ca. 3 mL of THF was added to a precooled (-35° C) solution of **2-3** (0.22 g, 1.1 mmol) in ca. 3 mL of THF. A color change to dark brown was observed. After standing for 2 hours at room temperature the volatile components of the reaction mixture were removed *in vacuo*, and the residue was extracted with benzene (ca. 10 mL). The benzene extract was filtered through Celite and dried under vacuum to yield **2-1** as a brown oil (0.41 g, 78%). ^{1}H NMR (500 MHz, benzene-d_6): δ 7.81 (m, 1 H, H_{arom}), 7.70 (m, 1 H, H_{arom}), 7.65 (m, 1 H, H_{arom}), 7.22 (m, 1 H, H_{arom}), 7.15 – 7.13 (overlapping resonances, 2 H, H_{arom}), 7.08 (m, 1 H, H_{arom}), 6.99 (m, 1 H, H_{arom}), 5.87 (m, 1 H, $^{1}J_{SiH}$ = 14 Hz, Si-*H*), 2.34 (s, 6 H, NMe_2), 1.16 (d, 9 H, $^{3}J_{PH}$ = 11 Hz, PCMe_3), 1.10 (d, 9 H, $^{3}J_{PH}$ = 11 Hz, PCMe_3), 0.83 (m, 3 H, Si*Me*). ^{13}C{^{1}H} NMR (125.8 MHz, benzene-d_6): δ 161.6 (C_{arom}), 149.1 (d, $^{1}J_{CP}$ = 51 Hz, C_{arom}), 144.7 (d, $^{2}J_{CP}$ = 21 Hz, C_{arom}), 138.7 (CH_{arom}), 137.2 (d, CH_{arom}), 136.6 (C_{arom}), 135.1 (CH_{arom}), 131.5 (CH_{arom}), 128.9 (CH_{arom}), 128.6 (CH_{arom}), 125.3 (CH_{arom}), 121.5 (CH_{arom}), 46.6 (NMe_2), 33.6 (d, J = 8 Hz, PCMe_3), 33.4 (d, J = 8 Hz,

P*C*Me$_3$), 31.5 - 31.3 (overlapping resonances, 2 *CMe*$_3$), -1.6 (Si*Me*). ^{31}P{^{1}H} NMR (202.5 MHz, benzene-d_6): δ 23.2 (s). ^{29}Si NMR (300 K, 99.4 MHz, benzene-d_6): δ -24.4 ppm ($^1J_{SiH}$ = 205 Hz). IR (Thin film, cm^{-1}): 2128 (br, m, Si-H). Anal. Calcd for $C_{23}H_{36}NPSi$: C, 71.64; H, 9.41; N, 3.63. Found: C, 71.23; H, 9.18; N, 3.50.

[^{t}Bu-PSiCH=]Ru(η^3-C$_8$H$_{13}$) (2-5). A solution of **2-4** (0.40 g, 1.0 mmol) in ca. 5 mL of THF was added to a solution of (1,5-COD)Ru(methylallyl)$_2$ (0.33 g, 1.0 mmol) in ca. 5 mL of THF. The reaction mixture was heated at 85 ^{o}C for 18 h. A color change from pale yellow to dark brown was observed. The volatile components were removed *in vacuo*, and the residue was triturated with pentane (5 × 3 mL) and dried under vacuum to yield **2-5** as a brown solid (0.37 g, 60%). ^{1}H NMR (500 MHz, benzene-d_6): δ 13.11 (s, 1 H, R=C*H*), 7.96 (d, 1 H, *J* = 7 Hz, *H*$_{arom}$), 7.67 (m, 1 H, *H*$_{arom}$), 7.55 (d, 1 H, *J* = 7 Hz, *H*$_{arom}$), 7.27 (m, 1 H, *H*$_{arom}$), 7.21 (m, 1 H, *H*$_{arom}$), 6.93 – 6.90 (overlapping resonances, 2 H, *H*$_{arom}$), 6.72 (d, 1 H, *J* = 8 Hz, *H*$_{arom}$), 4.81 (m, 1 H, *H*$_{C8H13}$), 4.13 (m, 1 H, *H*$_{C8H13}$), 3.61 (m, 1 H, *H*$_{C8H13}$), 2.82 (s, 3 H, N*Me*), 2.26 - 2.41 (overlapping resonances, 2 H, *H*$_{C8H13}$), 1.94 (m, 1 H, *H*$_{C8H13}$), 1.68 (m, 1 H, *H*$_{C8H13}$), 1.56 (m, 2 H, *H*$_{C8H13}$) 1.47 (d, 9 H, $^3J_{PH}$ = 12 Hz, P*CMe$_3$*), 1.30 - 1.40 (overlapping resonances, 4 H, *H*$_{C8H13}$), 1.07 – 1.25 (overlapping resonances, 9 H, P*CMe$_3$*), 0.51 (s, 3 H, Si*Me*). ^{13}C{^{1}H} NMR (300 K, 125.8 MHz, benzene-d_6): δ 250.8 (Ru=*C*), 162.2 (d, $^1J_{CP}$ = 49 Hz, *C*$_{arom}$), 151.0 (*C*$_{arom}$), 145.1 (d, $^2J_{CP}$ = 37 Hz, *C*$_{arom}$), 134.2 (*C*H$_{arom}$), 132.8 (d, $^2J_{CP}$ = 18 Hz, *C*H$_{arom}$), 132.4 (*C*$_{arom}$), 131.9 (*C*H$_{arom}$), 129.3 (*C*H$_{arom}$), 128.9 (*C*H$_{arom}$), 125.1 (*C*H$_{arom}$), 123.7 (*C*H$_{arom}$), 116.7 (*C*H$_{arom}$), 101.3 (*C*H$_{C8H13}$), 71.9 (*C*H$_{C8H13}$), 56.0 (*C*H$_{C8H13}$), 48.9 (N*Me*), 37.7 (*C*H$_{2\ C8H13}$), 36.7 (d, $^1J_{CP}$ = 10 Hz, P*C*Me$_3$), 35.4 (d, $^1J_{CP}$ = 6 Hz, P*C*Me$_3$), 33.1 (*C*H$_{2\ C8H13}$), 31.9 - 32.2 (overlapping resonances, 2 PC*Me$_3$*), 30.9 (*C*H$_{2\ C8H13}$), 30.8 (*C*H$_{2\ C8H13}$), 23.8 (*C*H$_{2\ C8H13}$),

2.4 (Si*Me*). $^{31}P\{^{1}H\}$ NMR (300 K, 202.5 MHz, benzene-d_6): δ 105.7 (s). ^{29}Si NMR (300 K, 99.4 MHz, benzene-d_6): δ 44.3. Anal. Calcd for $C_{31}H_{46}NPRuSi$: C, 62.81; H, 7.82; N, 2.36. Found: C, 62.75; H, 7.49; N, 2.33. A single crystal of **2-5** suitable for X-ray diffraction analysis was grown from benzene solution at room temperature.

[^{t}Bu-PSiCH$_2$-]Ru(η^6-C$_6$H$_6$) (2-6). A thick walled Schlenk tube fitted with a resealable Teflon stopcock was charged with a solution of **2-5** (0.13 g, 0.22 mmol) in ca. 5 mL of benzene. The reaction mixture was degassed via three freeze-pump-thaw cycles and H_2 (ca. 1atm) was introduced. The reaction mixture was allowed to stir at 75 ^{o}C for 72 h. A color change to dark brown was observed. The volatile components of the reaction mixture were removed *in vacuo*, and the residue was triturated with pentane (5 × 3 mL) and dried under vacuum to yield **2-6** as a brown solid (0.066 g, 53%). ^{1}H NMR (500 MHz, benzene-d_6): δ 8.25 (apparent d, 1 H, J = 7 Hz, H_{arom}), 8.06 (d, 1 H, J = 7 Hz, H_{arom}), 7.52 (m, 1 H, H_{arom}), 7.39 (m, 1 H, H_{arom}), 7.08 (m, 1 H, H_{arom}), 7.01 – 6.90 (overlapping resonances, 2 H, H_{arom}), 6.48 (d, 1 H, J = 8 Hz, H_{arom}), 4.90 (s, 6 H, H_{C6H6}), 4.58 (m, 1 H, RuCH_2), 2.65 (s, 3 H, N*Me*), 1.92 (m, 1 H, RuCH_2), 1.24 (d, 9 H, P*CMe$_3$*, $^{3}J_{PH}$ = 12 Hz), 1.19 (s, 3 H, Si*Me*), 0.92 (d, 9 H, P*CMe$_3$*, $^{3}J_{PH}$ = 12 Hz). $^{13}C\{^{1}H\}$ NMR (300 K, 125.8 MHz, benzene-d_6): δ 160.3 (d, $^{1}J_{CP}$ = 42 Hz, C_{arom}), 154.0 (C_{arom}), 139.7 (d, $^{2}J_{CP}$ = 40 Hz, C_{arom}), 136.0 (CH$_{arom}$), 135.5 (d, $^{2}J_{CP}$ = 18 Hz, CH$_{arom}$), 133.1 (CH$_{arom}$), 129.5 (CH$_{arom}$), 129.2 (CH$_{arom}$), 127.6 (C_{arom}), 126.0 (CH$_{arom}$), 114.2 (CH$_{arom}$), 110.4 (CH$_{arom}$), 88.9 (CH$_{C6H6}$), 42.5 (N*Me*), 38.9 (d, $^{1}J_{CP}$ = 18 Hz, PCMe$_3$), 37.4 (d, $^{1}J_{CP}$ = 9 Hz, PCMe$_3$), 35.8 (d, $^{2}J_{CP}$ = 11 Hz, RuCH$_2$), 33.7 (C*Me$_3$*), 30.8 (C*Me$_3$*), 8.3 (Si*Me*). $^{31}P\{^{1}H\}$ NMR (300 K, 202.5 MHz, benzene-d_6): δ 108.4 (s). ^{29}Si NMR (300 K, 99.4 MHz, benzene-d_6): δ 33.4. Anal. Calcd for $C_{29}H_{40}NPRuSi$: C, 61.89; H, 7.16; N, 2.49. Found:

C, 61.56; H, 6.94; N, 2.40. A single crystal of **2-6** suitable for X-ray diffraction analysis was grown from benzene solution at room temperature.

[^{t}Bu-PSiN-Me]Rh(H)Cl (2-7). A solution of **2-4** (0.28 g, 0.73 mmol) in ca. 5 mL of benzene was added to a solution of $[(1,5\text{-COD})RhCl]_2$ (0.18 g, 0.37 mmol) in ca. 5 mL of benzene. An immediate color change from orange to yellow was observed. The reaction mixture was allowed to stir at room temperature for 18 h, and the volatile components were subsequently removed *in vacuo*. The residue was triturated with pentane (2 × 2 mL) and dried *in vacuo* to yield **2-7** as a yellow solid (0.36 g, 94%). ^{1}H NMR (300 K, benzene-d_6): δ 7.75 (d, 1 H, J = 7 Hz, H_{arom}), 7.62 (m, 1 H, H_{arom}), 7.46 (m, 1 H, H_{arom}), 7.15 (m, 1 H, H_{arom}), 7.02 – 6.98 (overlapping resonances, 3 H, H_{arom}), 6.92 (m, 1 H, H_{arom}), 3.06 (s, 3 H, N*Me*), 2.96 (s, 3 H, N*Me*), 1.48 (d, 9 H, $^3J_{PH}$ = 12 Hz, P*CMe*$_3$), 1.29 (d, 9 H, $^3J_{PH}$ = 12 Hz, P*CMe*$_3$), 0.93 (s, 3 H, Si*Me*), -20.18 (dd, 1 H, Rh*H*, $^1J_{RhH}$ = 30 Hz, $^2J_{PH}$ = 21 Hz). ^{13}C{^{1}H} NMR (300 K, 125.8 MHz, benzene-d_6): δ 165.3 (C_{arom}), 155.4 (d, $^2J_{CP}$ = 40 Hz, C_{arom}), 146.3 (d, $^1J_{CP}$ = 49 Hz, C_{arom}), 144.8 (C_{arom}), 132.5 (CH$_{arom}$), 132.3 (CH$_{arom}$), 131.8 (CH$_{arom}$), 129.3 - 129.6 (overlapping resonances, CH$_{arom}$), 127.2 (CH$_{arom}$), 127.0 (CH$_{arom}$), 119.5 (CH$_{arom}$), 54.9 (N*Me*), 47.7 (N*Me*), 37.0 (d, J = 14 Hz, P*C*Me$_3$), 36.8 (d, J = 20 Hz, P*C*Me$_3$), 32.1 (C*Me*$_3$), 30.1 (C*Me*$_3$), 7.1 (Si*Me*). ^{31}P{^{1}H} NMR (300 K, 202.5 MHz, benzene-d_6): δ 101.0 (d, $^1J_{PRh}$ = 164 Hz). ^{29}Si NMR (300 K, 99.4 MHz, benzene-d_6): δ 45.8. IR (Thin film, cm^{-1}): 2115 (br, m, Rh-H). Anal. Calcd for $C_{23}H_{36}ClNPRhSi$: C, 52.82; H, 6.93; N, 2.67. Found: C, 52.52; H, 6.73; N, 2.59. A single crystal of **2-7** suitable for X-ray diffraction analysis was grown from benzene solution at room temperature.

[^{t}Bu-PSiN-Me]Ir(H)Cl (2-8). A solution of **2-4** (0.26 g, 0.67 mmol) in ca. 5 mL of benzene was added to a solution of $[(1,5\text{-COD})IrCl]_2$ (0.23 g, 0.34 mmol) in ca. 5 mL of benzene. An immediate color change from orange to yellow was observed. The reaction mixture was allowed to stir at room temperature for 18 h, and the volatile components were subsequently removed *in vacuo*. The residue was triturated with pentane (2 × 2 mL) and dried *in vacuo* to yield **2-8** as a yellow solid (0.41 g, 99%). ^{1}H NMR (500 MHz, benzene-d_6): δ 7.83 (d, 1 H, J = 7 Hz, H_{arom}), 7.68 (m, 1 H, H_{arom}), 7.54 (m, 1 H, H_{arom}), 7.12 (m, 1 H, H_{arom}), 6.99 – 6.94 (overlapping resonances, 3H, H_{arom}), 6.90 (m, 1 H, H_{arom}), 3.17 (s, 3 H, N*Me*), 2.94 (s, 3 H, N*Me*), 1.47 (d, 9 H, $^3J_{PH}$ = 14 Hz, P*CMe*$_3$), 1.30 (d, 9 H, $^3J_{PH}$ = 14 Hz, P*CMe*$_3$), 0.79 (s, 3 H, Si*Me*), -25.00 (d, 1 H, Ir*H*, $^2J_{PH}$ = 20 Hz). ^{13}C{^{1}H} NMR (300 K, 125.8 MHz, benzene-d_6): δ 166.5 (C_{arom}), 156.0 (d, $^2J_{CP}$ = 29 Hz, C_{arom}), 148.5 (d, C_{arom}, $^1J_{CP}$ = 55 Hz), 145.9 (C_{arom}), 132.3 (CH$_{arom}$), 132.0 (CH$_{arom}$), 131.7 (CH$_{arom}$), 129.2 (CH$_{arom}$), 129.0 (CH$_{arom}$), 126.8 - 127.0 (overlapping resonances, CH$_{arom}$), 118.9 (CH$_{arom}$), 54.9 (N*Me*), 47.7 (N*Me*), 37.0 (d, J = 14 Hz, P*C*Me$_3$), 36.8 (d, J = 20 Hz, P*C*Me$_3$), 32.1 (*CMe*$_3$), 30.1 (*CMe*$_3$), 7.1 (Si*Me*). ^{31}P{^{1}H} NMR (300 K, 202.5 MHz, benzene-d_6): δ 62.6 (s). ^{29}Si NMR (300 K, 99.4 MHz, benzene-d_6): δ 3.0. IR (Thin film, cm^{-1}): 2229 (br, m, Ir-H). Anal. Calcd for $C_{23}H_{36}ClNPIrSi$: C, 45.04; H, 5.92; N, 2.28. Found: C, 45.32; H, 6.12, N, 2.44. A single crystal of **2-8** suitable for X-ray diffraction analysis was grown from benzene solution at room temperature.

[^{t}Bu-PSiN-Me]Rh(H)Cl(PMe$_3$) (2-9). A solution of **2-7** (0.14 g, 0.27 mmol) in ca. 5 mL of benzene was treated with PMe_3 (0.028 mL, 0.27 mmol). The reaction mixture was allowed to stand at room temperature for 20 minutes. The volatile

components of the reaction mixture were subsequently removed *in vacuo*. The residue was triturated with pentane (3 × 2 mL) and dried *in vacuo* to yield to yield **2-9** as a pale yellow solid (0.13 g, 80%). ^{1}H NMR (300 K, benzene-d_6): δ 7.72 (d, 1 H, J = 7 Hz, H_{arom}), 7.60 (m, 1 H, H_{arom}), 7.23 (m, 1 H, H_{arom}), 7.15 (m, 1 H, H_{arom}), 7.11 – 7.03 (overlapping resonances, 2 H, H_{arom}), 6.92 – 6.99 (overlapping resonances, 2 H, H_{arom}), 1.97 (s, 6 H, NMe_2), 1.54 (app t, 18 H, $^{3}J_{PH}$ = 13 Hz, 2 PCMe_3), 1.29 (s, 3 H, SiMe), 0.95 (d, 9 H, $^{3}J_{PH}$ = 8 Hz, PMe_3), -16.8 (m, 1 H, RhH). ^{13}C{^{1}H} NMR (300 K, 125.8 MHz, benzene-d_6): δ 160.7 (C_{arom}), 152.5 (C_{arom}), 142.5 (C_{arom}), 139.9 (C_{arom}), 136.8 (CH_{arom}), 134.0 (CH_{arom}), 132.8 (CH_{arom}), 131.5 (CH_{arom}), 129.5 (CH_{arom}), 126.7 (CH_{arom}), 126.1 (CH_{arom}), 124.2 (CH_{arom}), 45.9 (NMe_2), 37.0 (PCMe$_3$), 36.3 (PCMe$_3$), 31.8 (PCMe_3), 31.4 (PCMe_3), 15.6 (d, $^{1}J_{PC}$ = 28 Hz, PMe_3) 5.0 (SiMe). ^{31}P{^{1}H} NMR (300 K, 202.5 MHz, benzene-d_6): δ 88.4 (dd, 1 P, $^{2}J_{PP}$ = 356 Hz, $^{1}J_{PRh}$ = 123 Hz), -4.88 (dd, 1 P, $^{2}J_{PP}$ = 356 Hz, $^{1}J_{PRh}$ = 123 Hz). ^{29}Si NMR (300 K, 99.4 MHz, benzene-d_6): δ 30.0. IR (Thin film, cm^{-1}): 2091 (br, m, Rh-H). Anal. Calcd for $C_{26}H_{45}ClNP_2RhSi$: C, 52.04; H, 7.56; N, 2.33. Found: C, 52.47; H, 7.37; N, 2.06. A single crystal of **2-9** suitable for X-ray diffraction analysis was grown from benzene solution at room temperature.

[^{t}Bu-PSiN-Me]Rh(H)OTf (2-10). A solution of AgOTf (0.044 g, 0.17 mmol) in ca. 3 mL of fluorobenzene was added to a solution of **2-7** (0.091 g, 0.17 mmol) in ca. 3 mL of fluorobenzene. An immediate color change from yellow to amber was observed. The volatile components of the reaction mixture were subsequently removed *in vacuo*. The residue was extracted with ca. 5 mL of benzene and the extract was filtered through Celite. The benzene solution was subsequently dried *in vacuo* and the remaining residue was triturated with pentane (2 × 2 mL) and dried under vacuum to yield **2-10** as a brown-

yellow solid (0.11 g, 96%). ^{1}H NMR (300 K, benzene-d_6): δ 7.62 (d, 1 H, J = 7 Hz, H_{arom}), 7.47 (m, 1 H, H_{arom}), 7.28 (m, 1 H, H_{arom}), 7.09 (m, 1 H, H_{arom}), 6.97 – 6.90 (overlapping resonances, 3 H, H_{arom}), 6.80 (m, 1 H, H_{arom}), 3.03 (s, 3 H, N*Me*), 3.00 (s, 3 H, N*Me*), 1.27 (d, 9 H, $^{3}J_{PH}$ = 14 Hz, P*CMe*$_3$), 1.19 (d, 9 H, $^{3}J_{PH}$ = 14 Hz, P*CMe*$_3$), 0.84 (s, 3 H, Si*Me*), -24.46 (m, 1 H, Rh*H*). ^{13}C{^{1}H} NMR (300 K, 125.8 MHz, benzene-d_6): δ 164.5 (C_{arom}), 152.2 (C_{arom}) 142.8 (d, C_{arom}), 144.8 (C_{arom}), 132.5 (CH$_{arom}$), 132.4 (CH$_{arom}$), 131.8 (CH$_{arom}$), 130.3 (CH$_{arom}$), 129.9 (CH$_{arom}$), 127.8 (CH$_{arom}$), 127.4 (CH$_{arom}$), 119.3 (CH$_{arom}$), 55.0 (N*Me*), 47.0 (N*Me*), 37.2 (d, J = 22 Hz, P*C*Me$_3$), 35.8 (d, J = 14 Hz, P*C*Me$_3$), 31.6 (C*Me*$_3$), 29.6 (C*Me*$_3$), 5.8 (Si*Me*). ^{31}P{^{1}H} NMR (300 K, 202.5 MHz, benzene-d_6): δ 96.5 (d, $^{1}J_{PRh}$ = 164 Hz). ^{29}Si NMR (300 K, 99.4 MHz, benzene-d_6): δ 49.4. ^{19}F{^{1}H} NMR (300 K, 282.4 MHz, benzene-d_6): -78.6. IR (Thin film, cm^{-1}): 2148 (br, m, Rh-H). A single crystal of **2-10** suitable for X-ray diffraction analysis was grown from slow evaporation benzene at room temperature.

[^{t}Bu-PSiN-Me]Ir(H)OTf (2-11). A solution of AgOTf (0.042 g, 0.16 mmol) in ca. 3 mL of fluorobenzene was added to a solution of **2-8** (0.098 g, 0.16 mmol) in ca. 3 mL of fluorobenzene. An immediate color change from yellow to amber was observed. The volatile components of the reaction mixture were subsequently removed *in vacuo*. The residue was extracted with ca. 5 mL of benzene and the extract was filtered through Celite. The benzene solution was subsequently dried *in vacuo* and the remaining residue was triturated with pentane (2 × 2 mL) and dried under vacuum to yield **2-11** as a yellow solid (0.10 g, 87%). ^{1}H NMR (500 MHz, benzene-d_6): δ 7.71 (d, 1 H, J = 7 Hz, H_{arom}), 7.54 (d, 1 H, J = 7 Hz, H_{arom}), 7.37 (m, 1 H, H_{arom}), 7.06 (m, 1 H, H_{arom}), 6.95 – 6.88 (overlapping resonances, 3 H, H_{arom}), 6.79 (m, 1 H, H_{arom}), 3.17 (s, 3 H, N*Me*), 3.04 (s, 3

H, N*Me*), 1.31 (d, 9 H, $^{3}J_{PH}$ = 14 Hz, P*CMe*$_3$), 1.23 (d, 9 H, $^{3}J_{PH}$ = 14 Hz, P*CMe*$_3$), 0.69 (s, 3 H, Si*Me*), -31.7 (broad s, 1 H, Ir*H*). $^{13}C\{^{1}H\}$ NMR (300 K, 125.8 MHz, benzene-d_6): δ 132.4 (*C*H$_{arom}$), 131.9 (*C*H$_{arom}$), 131.6 (*C*H$_{arom}$), 129.9 (*C*H$_{arom}$), 129.6 (*C*H$_{arom}$), 127.5 (*C*H$_{arom}$), 127.3 (*C*H$_{arom}$) 118.8 (*C*H$_{arom}$), 55.5 (N*Me*), 48.2 (N*Me*), 31.8 (C*Me*$_3$), 29.6 (C*Me*$_3$),. $^{31}P\{^{1}H\}$ NMR (300 K, 202.5 MHz, benzene-d_6): δ 59.8 (s). ^{29}Si NMR (300 K, 99.4 MHz, benzene-d_6): δ 4.6. $^{19}F\{^{1}H\}$ NMR (300 K, 282.4 MHz, benzene-d_6): -78.3. IR (Thin film, cm^{-1}): 2267 (br, m, Ir-H). A single crystal of **2-11** suitable for X-ray diffraction analysis was grown from slow evaporation of benzene at room temperature.

[^{t}Bu-PSiN-Me]Ir(H)BF$_4$ (2-12). A solution of $AgBF_4$ (0.048 g, 0.25 mmol) in ca. 3 mL of fluorobenzene was added to a solution of **2-8** (0.15 g, 0.25 mmol) in ca. 3 mL of fluorobenzene. An immediate color change from yellow to brown was observed. The volatile components of the reaction mixture were subsequently removed *in vacuo*. The residue was extracted with ca. 5 mL of benzene and the extract was filtered through Celite. The benzene solution was subsequently dried *in vacuo* and the remaining residue was triturated with pentane (3 × 2 mL) and dried under vacuum to yield **2-12** as a yellow solid (0.94 g, 50%). ^{1}H NMR (500 MHz, benzene-d_6): δ 7.75 (m, 1 H, *H*$_{arom}$), 7.59 (m, 1 H, *H*$_{arom}$), 7.44 (m, 1 H, *H*$_{arom}$), 7.10 (m, 1 H, *H*$_{arom}$), 6.98 – 6.92 (overlapping resonances, 3 H, *H*$_{arom}$), 6.85 (m, 1 H, *H*$_{arom}$), 3.14 (s, 3 H, N*Me*), 3.07 (s, 3 H, N*Me*), 1.35 (d, 9 H, $^{3}J_{PH}$ = 14 Hz, P*CMe*$_3$), 1.23 (d, 9 H, $^{3}J_{PH}$ = 14 Hz, P*CMe*$_3$), 0.67 (s, 3 H, Si*Me*), -25.0 (broad s, 1 H, Ir*H*). $^{13}C\{^{1}H\}$ NMR (300 K, 125.8 MHz, benzene-d_6): δ 132.7 (*C*H$_{arom}$), 132.2 (*C*H$_{arom}$), 131.8 (*C*H$_{arom}$), 129.7 (*C*H$_{arom}$), 128.9 – 129.9 (overlapping resonances with C_6H_6, 2C, *C*H$_{arom}$), 127.4 (*C*H$_{arom}$), 119.1 (*C*H$_{arom}$), 55.1 (N*Me*), 48.8 (N*Me*), 31.9

(C*Me*$_3$), 30.0 (C*Me*$_3$). ^{31}P{^{1}H} NMR (300 K, 202.5 MHz, benzene-d_6): δ 60.0 (broad s). ^{29}Si NMR (300 K, 99.4 MHz, benzene-d_6): δ 78.2. ^{19}F{^{1}H} NMR (300 K, 282.4 MHz, benzene-d_6): δ -158.1. ^{11}B NMR (300 K, 96.3 MHz, benzene-d_6): δ 0.6. IR (Thin film, cm^{-1}): 2147 (br, m, Ir-H).

2.4.3 Crystallographic Solution, Refinement and Structural Details for 2-5 - 2-11

Crystallographic data for each of **2-5**, **2-6**, **2-7**, **2-8**, **2-9, 2-10** and **2-11** were obtained at 193(±2)K on a Bruker D8/APEX II CCD diffractometer using a graphite-monochromated Mo Kα (λ = 0.71073 Å) radiation, employing a sample that was mounted in inert oil and transferred to a cold gas stream on the diffractometer. Programs for diffractometer operation, data collection, and data reduction (including SAINT) were supplied by Bruker. Gaussian integration (face-indexed) was employed as the absorption correction method in each case. All structures were solved by use of the Patterson search/structure expansion and were refined by use of full-matrix least-squares procedures (on F^2) with R_1 based on $F_o^2 \geq 2\sigma(F_o^2)$ and wR_2 based on $F_o^2 \geq -3\sigma(F_o^2)$. Anisotropic displacement parameters were employed throughout for the non-hydrogen atoms. The atomic coordinates and isotropic displacement parameter for the hydrido ligands in **2-7**, **2-8**, **2-9**, and **2-10** were freely refined. The Ir–H1 distance for **2-11** was fixed at 1.55(1) Å during refinement. Otherwise, all hydrogen atoms were added at calculated positions and refined by use of a riding model employing isotropic displacement parameters based on the isotropic displacement parameter of the attached atom. Additional crystallographic information is provided in Appendix A.

CHAPTER 3: Synthesis and Characterization of Late Transition Metal Complexes Featuring Alternative PSiN Ligation

3.1 Introduction

As was discussed in Chapter 2, the exploration of the synthesis and reactivity of transition metal complexes featuring the mixed donor PSiN tridentate ligand [^{t}Bu-PSiN-Me] (**2-4**) was pursued (Figure 3-1). It was found that despite being able to synthesize late transition metal complexes supported by [^{t}Bu-PSiN-Me] ligation, such complexes lacked the high stability that has previously been demonstrated by other late transition metal pincer species.[4] In an effort to further explore PSiN ligation to late metal centers, the study of late metal complexes supported by alternative PSiN ligation was undertaken. These investigations will be described in this chapter.

3.2 Results and Discussion

3.2.1 Synthesis and Characterization of Alternative PSiN Pro-Ligands

In order to access PSiN-ligated complexes that feature more robust metal-nitrogen interactions, the synthesis of the new PSiN ligand [^{t}Bu-PSiN-Et]H (**3-2**) was pursued (Figure 3-1). It was proposed that the introduction of an extra methylene linker between the phenylene ring of the pincer backbone and the amino donor in [^{t}Bu-PSiN-Et]H should result in a greater localization of electron density on the amine, resulting in an increase of electron donation from the amine to the metal center, and thus the formation of more robust metal complexes. Notably, reports of related ligands in the literature suggest that the electron donating ability of [^{t}Bu-PSiN-Et]H should be greater that that of [^{t}Bu-PSiN-Me]H.[62] In an effort to further investigate the effects of altering of the PSiN ligand

architecture, another PSiN pro-ligand [^{t}Bu-PSiNPy]H (**3-3**) containing a pyridyl nitrogen donor was designed (Figure 3-1). Due to the ability of a pyridyl group to act as both a σ-donor and π-acceptor, it was proposed that incorporation of a pyridyl group may result in the formation of a PSiN ligand that is more compatible with electron-rich late metal centers. Lastly, a third PSiN pro-ligand [^{t}Bu-PSi=N]H (**3-4**) that contains a Schiff base as the nitrogen donor was also pursued (Figure 3-1). The incorporation of a Schiff base into the PSiN ligand architecture was desirable due to the significant precedent for Schiff base ligands to be highly effective ancillary ligands for a large variety of transition metal complexes.[63] Furthermore, Schiff base ligands have been previously demonstrated to be redox active ligands in certain situations, potentially opening up new reactivity pathways.

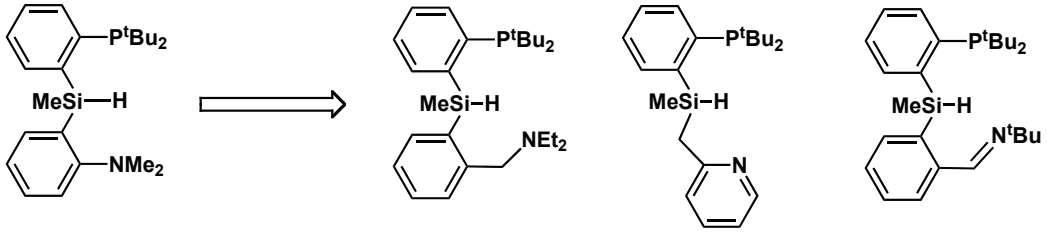

Figure 3-1. Proposed PSiN pro-ligands [^{t}Bu-PSiN-Et]H (**3-2**), [^{t}Bu-PSiNPy]H (**3-3**), and [^{t}Bu-PSi=N]H (**3-4**).

The new PSiN pro-ligands **3-2 - 3-4** were synthesized by an alternative route to that employed for the synthesis of **2-4** (Scheme 3-1). Initial attempts to synthesize **3-2** via the same route that was used for **2-4**, involving the reaction of Cl_2SiMeH and the Grignard reagent derived from 2-bromo-N,N-diethylbenzylamine, proved difficult. As such, a new synthetic route involving the formation of a (phosphinoaryl)chlorosilane was devised (Scheme 3-1). Such a synthetic route is ideal for the synthesis of a variety of PSiN ligand precursors, as the chlorosilane can be readily functionalized to introduce

different amino donors (Scheme 3-2). It was found that the (phosphinoaryl)chlorosilane species **3-1** could be synthesized by initial lithiation of the 2-bromoaryl phosphine **2-1** with one equiv. of ^{n}BuLi in cold (-78 °C) pentane, followed by treatment of the resulting lithium salt (**2-2**) with one equiv. of Cl_2SiMeH. Notably, the addition of Cl_2SiMeH must be conducted slowly and at low temperature (-78 °C), as the formation of another product is observed if the Cl_2SiMeH is added too quickly or at higher temperatures. This alternative product is proposed to be the bis(phosphino)silane [^{t}Bu-PSiP]H, where two equiv. of **2-2** have reacted with Cl_2SiMeH. Fortunately, the formation of [^{t}Bu-PSiP]H can be avoided when the addition of Cl_2SiMeH is conducted slowly at low temperature. The desired chlorosilane **3-1** was isolated as a brown oil in 94% yield. The ^{31}P NMR spectrum of **3-1** displays a single resonance at 23.9 ppm indicating the presence of a single phosphine environment. The ^{1}H NMR spectrum of **3-1** (benzene-d_6) reveals a resonance at 6.12 ppm (m), which is in the range expected for a Si-*H*. Notably, the Si-H resonance integrates to 1 proton relative to the protons on the phenylene backbone of the ligand, confirming the formation of the (phosphinoaryl)chlorosilane **3-1** and not the potential product [^{t}Bu-PSiP]H. IR analysis of **2-4** (thin film) revealed a broad stretch of medium intensity at 2190 cm^{-1}, consistent with an Si-*H* stretch. Furthermore, the ^{29}Si NMR spectrum of **3-1** revealed a resonance at -10.5 ppm, entirely consistent with the formation of a silane species of this type.[44,57]

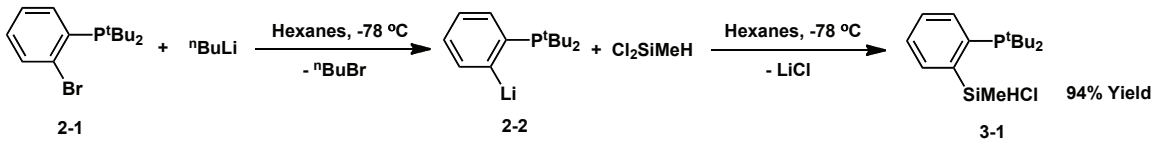

Scheme 3-1. Synthesis of (phosphinoaryl)chlorosilane **3-1**.

The PSiN pro-ligands **3-2** - **3-4** were subsequently synthesized by the reaction of **3-1** with one equiv. of either 2-lithio-N,N-diethlybenzylamine, 2-picolyllithium, or N-(2-lithiobenzylidene)*tert*-butylamine, respectively (Scheme 3-2). Compounds **3-2** - **3-4** were isolated as highly viscous oils in 71 – 97% yields after workup, and were characterized primarily by the use of multinuclear NMR methods. The three silanes exhibited similar NMR features. For example, the ^{31}P NMR resonances observed for **3-2** - **3-4** were very similar in chemical shift (**3-2**: 23.5 ppm; **3-3**: 24.1; **3-4**: 23.8 ppm), which suggests that the electronic properties of the phosphine are not significantly altered when different amines are incorporated into the PSiN ligand architecture. Furthermore, each of **3-2** - **3-4** exhibits a ^{29}Si resonance that is characteristic of a tertiary silane and compares favorably to related pro-ligands in the literature (**3-2**: -26.8 ppm; **3-3**: -15.5 ppm; **3-4**: -23.6 ppm).[44,57]

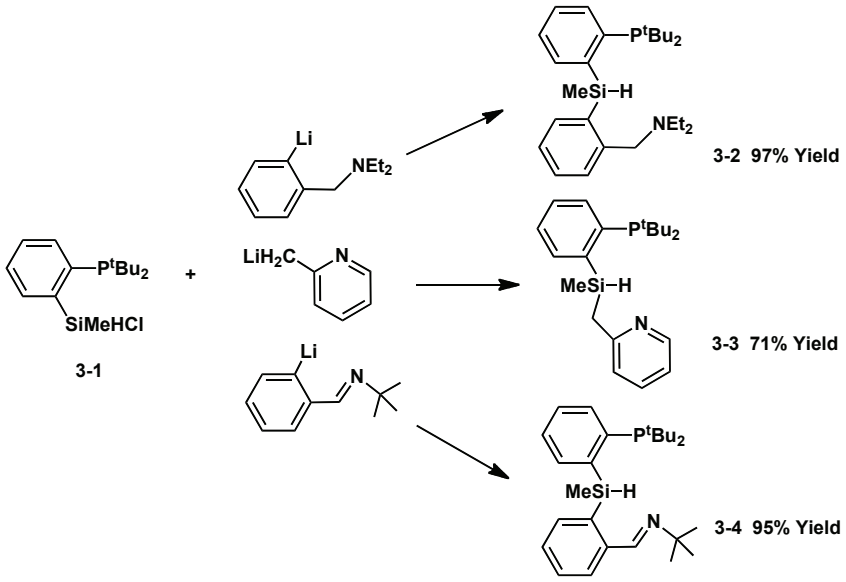

Scheme 3-2. Synthesis of PSiN pro-ligands **3-2** - **3-4**.

3.2.2 Synthesis and Characterization of Rh, Ir, and Pd Complexes Featuring the [^{t}Bu-PSiN-Et]H Pro-Ligand

Initial attempts to cyclometalate **3-2** focused on reactions with Ru starting materials including $(PPh_3)_3RuCl_2$, $[(p\text{-cymene})RuCl_2]_2$, $(PPh_3)_3Ru(CO)(H)Cl$, $(PPh_3)_3Ru(H)Cl$, $[(\eta^6\text{-}C_6H_6)RuCl_2]_2$, Cp*Ru($PPh_3$)Cl, and (1,5-COD)Ru(2-methylallyl)$_2$ (COD = cyclooctadiene). Unfortunately, these reactions were largely unsuccessful, leading to the formation of multiple unidentified products (^{31}P NMR). The isolation of single products from these reaction mixtures proved difficult. These observations suggest that PSiN ligation to Ru is not favorable, as no cyclometalated (PSiN)Ru complexes could be isolated from reactions of either the [^{t}Bu-PSiN-Me]H or [^{t}Bu-PSiN-Et]H pro-ligands.

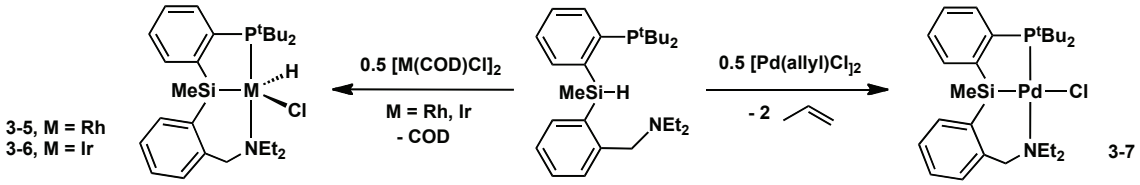

Scheme 3-3. Synthesis of [^{t}Bu-PSiN-Et] ligated Rh, Ir, and Pd complexes **3-5** - **3-7**.

In an effort to promote [^{t}Bu-PSiN-Et] coordination to group 9 metal centers, **3-2** was reacted with $[(COD)MCl]_2$ (M = Rh, Ir) dimers. The formation of the hydrido-chloride complexes [^{t}Bu-PSiN-Et]Rh(H)Cl (**3-5**) and [^{t}Bu-PSiN-Et]Ir(H)Cl (**3-6**) proved to be facile at room temperature (Scheme 3-3). In both cases, within an hour of performing the reaction, quantitative formation of **3-5** and **3-6** was observed by ^{31}P NMR spectroscopy (**3-5**: 97.3 ppm, d, $^1J_{PRh}$ = 151 Hz; **3-6**: 59.9 ppm, s). After purification, **3-5** and **3-6** were isolated as yellow solids in 89% and 91% yields, respectively. The ^{1}H NMR spectra of **3-5** and **3-6** (benzene-d_6) support the formation of C_1 symmetric hydrido-chloride complexes analogous to **2-7** and **2-8**. The coordination of the neutral

amino donor to the metal center is supported by the observation of diastereotopic benzylic protons and two inequivalent sets of N*Et* resonances in the ^{1}H NMR spectra of **3-5** and **3-6**. For example, the NEt_2 donor gives rise to two independent methyl resonances at 1.36 (apparent t, J = 7 Hz; 3 H) and 0.62 ppm (apparent t, J = 7 Hz, 3 H) in the ^{1}H NMR spectrum of **3-5** and 1.32 (apparent t, J = 7 Hz, 3 H) and 0.52 ppm (apparent t, J = 7 Hz, 3 H) in the spectrum of **3-6**.

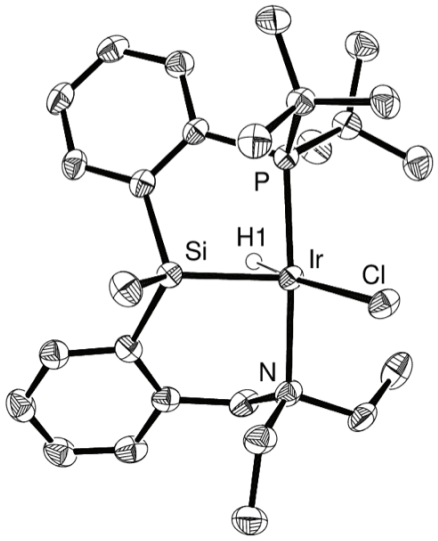

Figure 3-2. The crystallographically determined structure of **3-6** shown with 50% displacement ellipsoids. All non-hydrido H atoms have been omitted for clarity.

X-ray crystallographic analysis confirmed the formation of the five-coordinate hydrido chloride complex **3-6** (Figure 3-2, Table 3-1). Notably, **3-6** exhibits a geometry in the solid state very similar to that of the related PSiN ligated complexes **2-7** and **2-8**. The five-coordinate structure is best described as having distorted square-based pyramidal coordination geometry at the metal center, with Si occupying the apical coordination site. The P-Ir-N bond angle of 168.52(8)° indicates a meridional geometry for the metalated PSiN ligand. As in the case of **2-7** and **2-8**, as well as other analogous PSiP Rh and Ir complexes, the geometry at the metal center can also be described as "Y-

shaped", in which the chloride ligand is positioned opposite to the acute angle of the "Y". Furthermore, **3-6** features a relatively short Si···H1 distance of 2.23 Å, falling within the range indicative of an Si-H interaction (typically 1.7 – 2.4 Å;[55] sum of van der Waals radii = 3.4 Å).

Bond Lengths (Å)			
Ir-P	2.246(1)	Ir-H1	1.58(3)
Ir-N	2.207(3)	Ir-Cl	2.453(1)
Ir-Si	2.256(1)		
Bond Angles (°)			
P-Ir-N	168.52(8)	Si-Ir-H1	68.4(13)
Si-Ir-Cl	127.22(3)	Cl-Ir-H1	164.4(13)

Table 3-1. Selected interatomic distances (Å) and angles (°) for [^{t}Bu-PSiN-Et[Ir(H)Cl (**3-6**).

The dehydrohalogenation of **3-5** and **3-6** was pursued with the hope of accessing 14-electron [^{t}Bu-PSiN-Et]M^{I} (M = Rh, Ir) species that may be capable of activating E-H (E = main group element) bonds. Synthetic routes analogous to those outlined in Scheme 2-12 were used in the attempts to form these M^{I} intermediates. It was found that upon alkylation of **3-5** and **3-6** with either NpLi or $TMSCH_2Li$ in either benzene of cycclohexane, the formation of very short-lived orange-red species was observed in solution, followed by the formation of a grey metallic precipitate and brown/black solutions. These short-lived species exhibited extremely broad $^{31}P\{^{1}H\}$ and ^{1}H NMR spectra which were difficult to interpret in a meaningful fashion, similar to the observations discussed in Chapter 2 where similar reactions were attempted with [^{t}Bu-PSiN-Me]M^{I} complexes. These observations suggest that the introduction of the extra methylene linker into the PSiN ligand framework does not result in the formation of significantly more stable PSiN-ligated group 9 complexes.

In an effort to investigate the coordination chemistry of **3-2** at group 10 metal centers, attempts were made to cyclometalate **3-2** to Pd containing starting materials such as $[Pd(allyl)Cl]_2$, $(MeCN)_2PdCl_2$, and $PdCl_2$. All reactions led to the full consumption of **3-2**, with the same product being formed in all cases (by ^{31}P NMR). Reaction of **3-2** with half an equiv. of $[Pd(allyl)Cl]_2$ resulted in the immediate formation of a brown solution that gave rise to a ^{31}P NMR resonance at 101.1 ppm. Upon standing in solution for longer than 2 hours at room temperature significant decomposition of this product was observed, with palladium black precipitating in the reaction vial. Despite instability of this product in solution, full multinuclear NMR characterization was obtained and these data are consistent with the formation of [^{t}Bu-PSiN-Et]PdCl (**3-7**, Scheme 3-3). The downfield chemical shift observed in the ^{31}P NMR spectrum for **3-7** (101.1 ppm) suggests that the phosphino arm of the PSiN ligand has been metalated. Furthermore, a Si-H resonance was not observed in the ^1H NMR spectrum of **3-7**, which indicates that the Si-H bond in **3-2** was cleaved in the metalation of the ligand. Lastly, the ^1H NMR spectrum of **3-7** features diastereotopic benzylic protons and inequivalent N*Et* groups, similar to **3-5** and **3-6**, which is consistent with coordination of the amino donor to the metal center. This observation is in contract to the analogous [^{t}Bu-PSiN-Me]PdCl species, where the amino donor was demonstrated to be hemilabile at room temperature.[6] Notably, **3-7** was also not stable in the solid state. Storage of solid brown **3-7** at -35 °C overnight resulted in the formation of a grey solid, presumably containing Pd metal. ^{31}P NMR analysis of this grey solid revealed a resonance at 101.1 ppm corresponding to **3-7**, however the signal to noise ratio was extremely poor, which is consistent with degradation of this material in the solid state.

3.2.3 Synthesis and Characterization of Group 10 Complexes Featuring the [^{t}Bu-PSiNPy]H Pro-Ligand

Initial attempts at the cyclometalation of **3-3** focused on reactions with a wide variety of Ru staring materials. In a similar fashion to PSiN pro-ligands **2-4** and **3-2** these reactions were largely unsuccessful. In all cases, quantitative consumption of **3-2** was observed by ^{31}P NMR spectroscopy, however multiple unidentified phosphorus containing products were formed. Additionally, in reactions with Ru complexes containing PPh_3, formation of free PPh_3 was often observed, indicating the displacement of PPh_3 from the metal center. Isolation of single products from these reaction mixtures has remained elusive.

In order to promote [^{t}Bu-PSiNPy] ligation to group 9 metal centers, **3-3** was reacted with $[(COD)MCl]_2$ (M = Rh, Ir) dimers. Unlike the previously discussed PSiN ligands **2-4** and **3-2**, **3-3** does not cleanly cyclometalate to form the corresponding [^{t}Bu-PSiNPy]M(H)Cl complexes. Rather, the formation of several unidentified products was observed (^{31}P NMR), with two species appearing to be major products (δ = 61.3 and 100.4 for reaction with Ir). The ^{1}H NMR spectra of these reaction mixtures indicated multiple hydride resonances, however these products could not be unambiguously assigned. The use of $[(COE)_2MCl]_2$ starting materials or heating of the reaction mixtures did not result in the formation of a clean product. A potential reason for the product distribution observed in such reactions could be β-hydride elimination in the ligand backbone, which may lead to decomposition and the generation of new hydride-containing products. Attempts to separate the major products from the rest of the reaction mixture have proved difficult, as recrystallizations or selective extractions have not furnished any clean product.

In an effort promote the ligation of [^{t}Bu-PSiNPy] to other late metal centers, reactions with group 10 metals were targeted. Towards this end, **3-3** was reacted with one equiv. of $NiBr_2$ in the presence of NEt_3, resulting in the formation of a new major product **3-8** (by ^{31}P NMR) upon heating at 65 °C for 18 h in THF (Scheme 3-4). A downfield ^{31}P NMR shift of 90.4 ppm was observed for this complex, which is significantly downfield of the corresponding shift for **3-3** (24.1 ppm), indicating phosphine coordination to the metal center. The ^{1}H NMR spectrum of **3-8** no longer contains a signal at 5.30 ppm corresponding to the Si-H proton of the free ligand, indicating that oxidative addition of the Si-H bond has occurred. Additionally, the proton corresponding to the α-position of the pyridyl ring has shifted significantly downfield (10.24 ppm) compared with the signal of the same proton on the free ligand (8.49 ppm). This observation supports the conclusion that the pyridine donor is coordinating to the metal center. However, it should be noted that several broad resonances can be observed in both upfield (< 0 ppm) and downfield (>10 ppm) regions of the ^{1}H NMR spectrum of the reaction mixture, suggesting that paramagnetic species are also likely present. The identity of these paramagnetic species is unknown, however their formation is not completely unanticipated as Ni compounds can readily adopt Ni^{I} and Ni^{III} oxidation states.[64] The isolation of **3-8** from the reaction mixture has thus far remained elusive, as recrystallizations and selective extractions have yet to furnish any clean product.

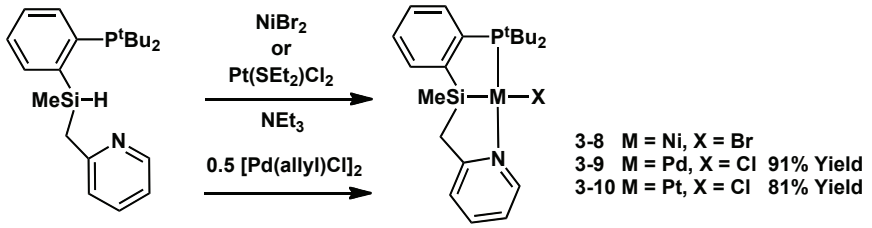

Scheme 3-4. Synthesis of [^{t}Bu-PSiNPy] ligated Ni, Pd, and Pt complexes **3-8** - **3-10**.

In an effort to synthesize Pd complexes featuring [^{t}Bu-PSiNPy] ligation **3-3** was reacted with a variety of Pd starting materials. The reaction of **3-3** with $Pd_2(DBA)_3$ in THF at room temperature led to the formation of a complex mixture of unidentified products (^{31}P NMR) within minutes. The compounds $PdBr_2$, $PdCl_2$ and $(MeCN)_2PdCl_2$ were each allowed to react with one equivalent of **3-3** in the presence of NEt_3 in THF. These reactions each resulted in the quantitative (by ^{31}P NMR) formation of a new product that is consistent with a metalated species, as indicated by downfield ^{31}P NMR shifts observed (δ 98.3 ppm, 96.8 ppm, and 97.2 ppm, respectively). Similarly, the reaction of **3-3** with half an equiv. of $[Pd(allyl)Cl]_2$ afforded a new product that gives rise to a ^{31}P NMR resonance at 96.4 ppm. Based on ^{31}P NMR data, it is likely that the $PdCl_2$, $(MeCN)_2PdCl_2$ and $[Pd(allyl)Cl]_2$ starting materials all lead to the same product, which is tentatively formulated as [^{t}Bu-PSiNPy]PdCl (**3-9**, Scheme 3-4). A preparative scale reaction of **3-2** with one equivalent of $PdBr_2$ in the presence of NEt_3 in THF was subsequently carried out. After several hours at room temperature the reaction mixture produced a palladium mirror within the vial indicating product decomposition. Alternatively, a preparative scale reaction of **3-3** with half an equivalent of $[Pd(allyl)Cl]_2$ resulted in the clean formation of **3-9**, which was isolated as a pale grey solid in 91% yield. As with **3-8**, the ^{1}H NMR spectrum of **3-9** no longer contains the Si-H signal of the ligand at 5.30 ppm, indicative of Si-H bond cleavage. Additionally, the proton corresponding to the α-position of the pyridyl ring has shifted significantly downfield (10.18 ppm) compared with the signal of the same proton on the free ligand (8.49 ppm). This observation supports the conclusion that the pyridine donor is coordinating to the Pd center. Notably, storage of the pale grey **3-9** at -35 °C over the period of days results in

the formation of a deep grey solid, presumably containing Pd metal. ^{31}P NMR analysis of this deep grey solid revealed an absence of any discernable resonances, indicative of product decomposition.

In an effort to synthesize Pt complexes featuring [^{t}Bu-PSiNPy] ligation, **3-3** was reacted with each of $Pt(PhCN)_2Cl_2$, $(COD)PtCl_2$ (COD = 1,5-cyclooctadiene), and $Pt(SEt_2)_2Cl_2$ in the presence of an equiv. of Et_3N and subsequently heated at 65 ºC for 24 h. The reactions of $Pt(PhCN)_2Cl_2$ and $(COD)PtCl_2$ were carried out in THF and the reaction of $Pt(SEt_2)_2Cl_2$ was carried out in toluene. Compound **3-3** was also reacted with one equivalent of $Pt(PPh_3)_4$ and subsequently heated at 65 ºC for 24 h in THF solution. The reactions of **3-3** with $(COD)PtCl_2$ and $Pt(SEt_2)_2Cl_2$ each resulted in the quantitative (by ^{31}P NMR) formation of a new product, as indicated by a downfield ^{31}P NMR resonance observed at 75.0 ($^{1}J_{PPt}$ = 4729 Hz) and 74.2 ppm ($^{1}J_{PPt}$ = 4720 Hz), respectively. It is highly likely that these two reactions both led to the formation of the same product, tentatively formulated as [^{t}Bu-PSiNPy]PtCl (**3-10**, Scheme 3-4). ^{31}P NMR analysis of the $Pt(PhCN)_2Cl_2$ and $Pt(PPh_3)_4$ reactions indicated the formation of complex reaction mixtures featuring multiple unidentified products. In a preparative scale reaction, **3-3** was treated with one equivalent of $Pt(SEt_2)_2Cl_2$ in the presence of NEt_3. Upon heating at 65 °C for 18 h in benzene solution **3-10** was isolated as a yellow solid in 81% yield. Complex **3-10** was characterized by multinuclear NMR methods. A ^{31}P NMR signal at 74.2 ppm ($^{1}J_{PPt}$ = 4720 Hz) was observed for **3-10**. The presence of ^{195}Pt satellites indicates that the phosphino arm of the PSiN ligand has successfully coordinated to the metal. The coupling constant of 4720 Hz is comparable to related PSiN-ligated Pt^{II} complexes previously reported.[57] As with both **3-8** and **3-9**, the proton

corresponding to the α-position of the pyridyl ring has shifted significantly downfield (10.19 ppm) compared with the signal of the same proton on the free ligand (8.49 ppm). This again supports the conclusion that the pyridine donor is coordinating to the Pt center.

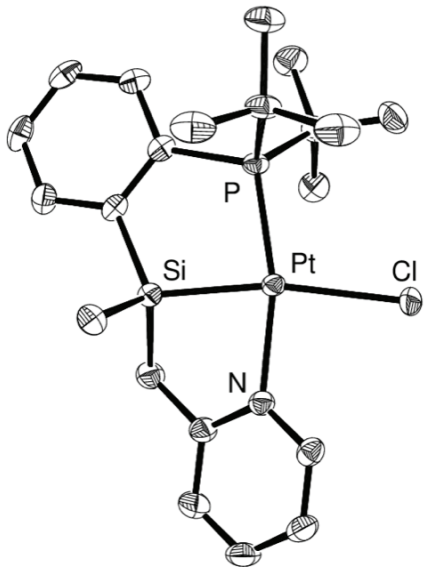

Figure 3-3. The crystallographically determined structure of **3-10** shown with 50% displacement ellipsoids. All non-hydrido H atoms have been omitted for clarity.

The solid state structure of **3-10** was confirmed by single-crystal X-ray diffraction analysis (Figure 3-3, Table 3-2) and indicates approximate square planar coordination geometry at Pt, with *trans*-disposed phosphino and pyridyl donors. The distorted square planar geometry is confirmed by the P-Pt-N and Si-Pt-Cl bond angles of 164.47(6)° and 168.47(2)°, respectively, as well as the P-Pt-Si and N-Pt-Si bond angles of 85.96(2) and 79.68(6)°, respectively. Notably, the Pt-Si distance of 2.2470(4) Å is somewhat short and falls just outside the range characteristic of Pt-Si bond distances (2.255 - 2.444 Å).[65] The short Pt-Si interatomic distance observed is likely due to the chelating nature of the tridentate PSiN ligand. Notably, **3-10** is quite stable both in solution and in the solid state, with no apparent decomposition observed over the course of weeks at room

temperature. Thus it appears that of the group 10 triad, **3-10** is the most suited for further reactivity studies.

Bond Lengths (Å)			
Pt-P	2.2365(6)	Pt-Si	2.2470(7)
Pt-N	2.138(2)	Pt-Cl	2.4840(6)
Bond Angles (°)			
P-Pt-N	164.47(6)	P-Pt-Si	85.96(2)
Si-Pt-Cl	168.47(2)	N-Pt-Si	79.68(6)

Table 3-2. Selected interatomic distances (Å) and angles (°) for [^{t}Bu-PSiN-Py]Pt-Cl (**3-10**).

3.3 Conclusions

In an effort to synthesize more robust late transition metal complexes featuring PSiN ligation, the synthesis of alternative PSiN pro-ligands and their corresponding late metal complexes was pursued. In order to establish a method for the facile modification of the PSiN ligand architecture, an alternative synthesis of PSiN pro-ligands was devised involving the formation of a (phosphinoaryl)chlorosilane (**3-1**), followed by installation of the amino donor arm. This synthetic route was found to be highly versatile, allowing for the successful synthesis of [^{t}Bu-PSiN-Et]H (**3-2**), [^{t}Bu-PSiNPy]H (**3-3**), and [^{t}Bu-PSi=N]H (**3-4**) in good yields. It was found that **3-2** and **3-3** could be cyclometalated to late transition metals such as Rh, Ir, Ni, Pd, and Pt resulting in the formation of hydrido-chloride complexes **3-5** and **3-6** and group 10 metal-halide complexes **3-8** - **3-10**. Unfortunately, with the exception of the Pt complex **3-10**, such late metal complexes proved to be largely unstable both in solution and in the solid state. The PSiN ligand [^{t}Bu-PSi=N]H (**3-4**), containing a Schiff base as the nitrogen donor was also synthesized, however it has yet to be successfully metalated to a transition metal center. The

observations made throughout the course of the work described in Chapters 2 and 3 lead to the conclusion that PSiN late transition metal complexes supported by such pincer ligands are relatively unstable species.

3.4 Experimental Section

3.4.1 General Considerations

Unless otherwise stated all experiments were performed under atmospheres of nitrogen or argon in an MBraun glovebox or using standard Schlenk techniques. All solvents used were dry and oxygen free unless otherwise noted. THF was distilled from Na/benzophenone ketyl, while benzene, toluene, and pentane were purified over one activated alumina column and one column packed with activated Q-5. All purified solvents were stored over 4 Å molecular sieves. Benzene-d_6 was degassed via three freeze-pump-thaw cycles and stored over 4 Å molecular sieves. 2-lithio-N,N-diethlylbenzylamine[9a] and 2-picolyllithium[9b] were prepared according to literature procedures. The compound N-(2-lithiobenzylidene)*tert*-butylamine was prepared by the reaction of N-(2-bromobenzylidene)*tert*-butylamine with ^{n}BuLi at -35 °C in hexanes. All other reagents used were purchased from Aldrich or Strem and used without further purification. All NMR characterization data were collected at 300 K on a Bruker AV-500 NMR spectrometer operating at 500.1, 125.8, 202.5 and 99.4 MHz for ^{1}H, ^{13}C, ^{31}P and ^{29}Si nuclei, respectively. Chemical shifts are reported in parts per million downfield of $SiMe_4$ (for ^{1}H, ^{13}C and ^{29}Si), or 85 % H_3PO_4 in D_2O (for ^{31}P). ^{1}H and ^{13}C NMR chemical shift assignments are based on data obtained from ^{13}C-DEPTQ, ^{1}H-^{1}H COSY, ^{1}H-^{13}C HSQC, and ^{1}H-^{13}C HMBC NMR experiments. Despite prolonged acquisition

times, not all carbon resonances are observed in complexes **3-8** - **3-10**. ^{29}Si NMR assignments are based on ^{1}H-^{29}Si HMBC experiments. The infrared spectra were recorded as thin films between NaCl plates using a Bruker Vector 22 FT-IR spectrometer at a resolution of 4 cm^{-1}. Elemental analyses were performed by Canadian Microanalytical Service Ltd. of Delta, British Columbia, Canada. X-ray data collection, solution, and refinement were carried out by Drs. Robert MacDonald and Michael J. Ferguson at the University of Alberta X-ray Crystallography Laboratory, Edmonton, Alberta.

3.4.2 Synthetic Procedures and Characterization Data

(2-P^{t}Bu$_2$C$_6$H$_4$)SiMeHCl (3-1). A solution of **2-1** (0.87 g, 2.9 mmol) in ca. 25 mL of hexane was cooled to -78 ºC. ^{n}BuLi (2.86 M in hexanes, 1.00 mL, 2.86 mmol) was added to the flask *via* syringe and a color change from pale brown to pale orange was observed. The reaction mixture was allowed to warm to room temperature and stir for 24 h. The mixture was then cooled again to -78 ºC and Cl_2SiMeH (0.30 mL, 2.9 mmol) was added dropwise to the flask *via* syringe. The mixture was allowed to warm to room temperature and stir for 1 h. The solvent was then removed *in vacuo* and the residue was extracted with ca. 10 mL hexane. The hexane extract was filtered through Celite and subsequently dried *in vacuo* to yield **3-1** as a brown oil (0.81 g, 94%). ^{1}H NMR (500 MHz, benzene-d_6): δ 8.21 (d, 1 H, J = 7 Hz, H_{arom}), 7.57 (apparent d, 1 H, J = 8 Hz, H_{arom}), 7.10 - 7.21 (overlapping resonances, 2 H, H_{arom}), 6.12 (m, 1 H, Si-*H*), 1.06 (d, 9 H, $^{3}J_{PH}$ = 12 Hz, PCMe_3), 1.04 (d, 9 H, $^{3}J_{PH}$ = 12 Hz, PCMe_3), 0.89 (m, 3 H, Si*Me*). ^{13}C{^{1}H} NMR (125.8 MHz, benzene-d_6): δ 145.6 (d, $^{1}J_{CP}$ = 53 Hz, C_{arom}), 143.2 (d, $^{2}J_{CP}$

= 13 Hz, C_{arom}), 136.6 (d, J = 20 Hz, CH_{arom}), 134.3 (CH_{arom}), 129.9 - 130.0 (overlapping resonances, CH_{arom}), 34.0 (d, PCMe$_3$, $^1J_{CP}$ = 20 Hz), 33.2 (d, $^1J_{CP}$ = 20 Hz, PCMe$_3$), 31.3 (d, $^2J_{CP}$ = 20 Hz, PCMe_3), 30.6 (d, $^2J_{CP}$ = 20 Hz, PCMe_3), 4.8 (d, $^4J_{CP}$ = 13 Hz, SiMe). $^{31}P\{^1H\}$ NMR (202.5 MHz, benzene-d_6): δ 23.9. ^{29}Si NMR (300 K, 99.4 MHz, benzene-d_6): δ -10.5. IR (Thin film, cm^{-1}): 2190 (br, s, Si-H).

[^{t}Bu-PSiN-Et]H (3-2). A solution of **3-1** (0.94 g, 3.1 mmol) in ca. 5 mL of precooled benzene (ca. 6 ºC) was added to a solution of 2-lithio-N,N-diethylbenzylamine (0.53 g, 3.1 mmol) in ca. 3 mL of benzene. A color change from light to dark brown was immediately observed. After standing at room temperature for 1 h the reaction mixture was filtered through Celite and the volatile components were removed *in vacuo* to yield **3-2** as a yellow-brown oil (1.3 g, 97%). ^{1}H NMR (500 MHz, benzene-d_6): δ 7.65-7.71 (overlapping resonances, 2 H, H_{arom}), 7.63 (d, 1 H, J = 7 Hz, H_{arom}), 7.58 (m, 1 H, H_{arom}), 7.25 (m, 1 H, H_{arom}), 7.16 - 7.13 (overlapping resonances, 2 H, H_{arom}), 7.10 (m, 1 H, H_{arom}), 5.86 (m, 1 H, Si-H), 4.04 (m, 1 H, Ar-CH_2N), 3.61 (m, 1 H, Ar-CH_2N), 2.49 (m, 4 H, NCH_2CH$_3$), 1.15 (d, 9 H, $^3J_{PH}$ = 11 Hz, PCMe_3), 1.10 (d, 9 H, $^3J_{PH}$ = 11 Hz PCMe_3), 0.91 (t, 6 H, J = 7 Hz, NCH$_2$CH_3), 0.80 (d, 3 H, J = 4 Hz, SiMe). $^{13}C\{^1H\}$ NMR (125.8 MHz, benzene-d_6): δ 148.5 (d, $^1J_{CP}$ = 49 Hz, C_{arom}), 147.2 (C_{arom}), 144.7 (d, $^2J_{CP}$ = 21 Hz, C_{arom}), 138.0 (d, J = 4 Hz, C_{arom}), 137.0 (CH_{arom}), 136.8 (d, $^2J_{CP}$ = 18 Hz, CH_{arom}), 135.2 (CH_{arom}), 129.6 (CH_{arom}), 129.0 (CH_{arom}), 128.9 (CH_{arom}), 128.8 (CH_{arom}), 126.6 (CH_{arom}), 59.3 (Ar-CH_2N), 46.8 (NCH_2CH$_3$), 35.1 - 35.5 (overlapping resonances, PCMe$_3$), 31.2 (d, $^2J_{CP}$ = 14 Hz, PCMe_3), 11.9 (NCH$_2$$CH_3$), -1.4 (d, $^4J_{CP}$ = 8 Hz, SiMe). $^{31}P\{^1H\}$ NMR (202.5 MHz, benzene-d_6): δ 23.5. ^{29}Si NMR (300 K, 99.4 MHz, benzene-d_6): δ -26.8. IR (Thin film, cm^{-1}): 2164 (br, m, Si-H).

[^{t}Bu-PSiNPy]H (3-3). Compound **3-1** (0.81 g, 2.7 mmol) and 2-lithiomethylpyridine (0.27 g, 2.7 mmol) were each dissolved in ca. 4 mL THF and placed in the freezer at -35 ºC for 30 min. The two solutions were subsequently combined and the reaction mixture was allowed to stand at room temperature for 24 h. The solvent was then removed *in vacuo* and the residue was extracted with ca. 15 mL of benzene. The benzene extarct was filtered through Celite and subsequently dried *in vacuo* to yield **3-3** as a red-brown oil (0.69 g, 71%). ^{1}H NMR (500 MHz, benzene-d_6): δ 8.49 (m, 1 H, H_{arom}), 7.75 - 7.73 (overlapping resonances, 2 H, H_{arom}), 7.20 - 7.13 (overlapping resonances, 2 H, H_{arom}), 7.01 (m, 1 H, H_{arom}), 6.87 (d, 1 H, J = 8 Hz, H_{arom}), 6.55 (m, 1 H, H_{arom}), 5.30 (m, 1 H, Si-*H*), 3.02 (m, 2 H, CH_2), 1.19 (d, 9 H, $^3J_{PH}$ = 12 Hz, PCMe_3), 1.18 (d, 9 H, $^3J_{PH}$ = 12 Hz, PCMe_3), 0.57 (m, 3 H, Si*Me*). ^{13}C{^{1}H} NMR (125.8 MHz, benzene-d_6): δ 162.3 (C_{arom}), 150.0 (CH$_{arom}$), 147.5 (d, $^1J_{CP}$ = 50 Hz, C_{arom}), 144.6 (d, $^2J_{CP}$ = 20 Hz, C_{arom}), 136.7 (d, $^2J_{CP}$ = 18 Hz, CH$_{arom}$), 136.0 (CH$_{arom}$), 135.2 (CH$_{arom}$), 129.2 (CH$_{arom}$), 128.8 (CH$_{arom}$), 123.2 (CH$_{arom}$), 119.9 (CH$_{arom}$), 28.9 (d, J = 10 Hz, CH$_2$), 33.4 (d, $^1J_{CP}$ = 4 Hz, PCMe$_3$), 33.2 (d, $^1J_{CP}$ = 4 Hz, PCMe$_3$), 31.4 - 31.2 (overlapping resonances, CMe_3), -2.6 (d, $^4J_{CP}$ = 10 Hz, Si*Me*). ^{31}P{^{1}H} NMR (202.5 MHz, benzene-d_6): δ 24.1. ^{29}Si NMR (99.4 MHz, benzene-d_6): δ -15.5. IR (Thin film, cm^{-1}): 2149 (br, m, Si-H).

[^{t}Bu-PSi=N]H (3-4). A solution of **3-1** (0.33 g, 1.1 mmol) in ca. 2 mL of precooled benzene (ca. 6 ºC) was added to a solution of 2-lithio-N,N-diethlybenzylamine (0.18 g, 1.1 mmol) in ca. 2 mL of benzene. A color change from light to dark brown was observed immediately. After standing at room temperature for 1 h the reaction mixture was filtered through Celite and the volatile components were removed *in vacuo* to yield

3-4 as a brown oil (0.44 g, 95%). ^{1}H NMR (500 MHz, benzene-d_6): δ 8.77 (s, 1 H, H_{imine}), 8.38 (d, 1 H, J = 8 Hz, H_{arom}), 7.74 (m, 1 H, H_{arom}), 7.65-7.68 (overlapping resonances, 2 H, H_{arom}), 7.25 (m, 1 H, H_{arom}), 7.15 (overlapping with benzene-d_6, 1 H, H_{arom}), 7.11 (overlapping resonances, 2 H, H_{arom}), 5.86 (m, 1 H, Si-*H*), 1.22 (s, 9 H, N-C*Me*$_3$), 1.18 (d, 9 H, P*CMe*$_3$, $^{3}J_{PH}$ = 12 Hz), 1.13 (d, 9 H, P*CMe*$_3$, $^{3}J_{PH}$ = 12 Hz), 0.81 (m, 3 H, Si*Me*). ^{13}C{^{1}H} NMR (125.8 MHz, benzene-d_6): δ 156.6 (N=*C*H), 147.9 (d, C_{arom}, $^{1}J_{CP}$ = 52 Hz), 144.9 (d, $^{2}J_{CP}$ = 20 Hz, C_{arom}), 143.5 (C_{arom}), 139.6 (d, J = 5 Hz, C_{arom}), 137.9 (*C*H$_{arom}$), 137.4 (d, $^{2}J_{CP}$ = 22 Hz, *C*H$_{arom}$), 135.5 (*C*H$_{arom}$), 130.2 (*C*H$_{arom}$), 130.0 (*C*H$_{arom}$), 129.4 (*C*H$_{arom}$), 129.2 (*C*H$_{arom}$), 127.7 (*C*H$_{arom}$), 58.3 (N=C-*C*Me$_3$), 33.6 (apparent t, J = 30 Hz, P*C*Me$_3$), 31.0 -31.5 (overlapping resonances, *CMe*$_3$), -0.6 (d, $^{4}J_{CP}$ = 8 Hz, Si*Me*). ^{31}P{^{1}H} NMR (202.5 MHz, benzene-d_6): δ 23.8. ^{29}Si NMR (300 K, 99.4 MHz, benzene-d_6): δ -23.6. IR (Thin film, cm^{-1}): 2152 (br, m, Si-H).

[^{t}Bu-PSiN-Et]Rh(H)Cl (3-5). A solution of **3-2** (0.40 g, 0.94 mmol) in ca. 5 mL of benzene was added to a solution of [(1,5-COD)RhCl]$_2$ (0.23 g, 0.47 mmol) in ca. 5 mL of benzene. An immediate color change from orange to yellow was observed. The volatile components of the reaction mixture were removed *in vacuo*, and the residue was triturated with pentane (2 × 2 mL) and dried under vacuum to yield **3-5** as a yellow solid (0.53 g, 89%). ^{1}H NMR (300 K, benzene-d_6): δ 7.99 (d, 2 H, J = 7 Hz, H_{arom}), 7.62 (t, J = 6 Hz, 1 H, H_{arom}), 7.23 (d, J = 6 Hz, 1 H, H_{arom}), 7.15 – 7.09 (overlapping resonances, 2 H, H_{arom}), 6.97 (t, 1 H, J = 7 Hz, H_{arom}), 6.83 (d, J = 8 Hz, 1 H, H_{arom}), 4.40 (m, 1 H, $H_{benzylic}$), 3.84 (m, 1 H, N-CH_{alkyl}), 3.63 (m, 1 H, N-CH_{alkyl}), 3.48 (m, 1 H, $H_{benzylic}$) 3.23 (m, 1 H, N-CH_{alkyl}), 2.43 (m, 1 H, N-CH_{alkyl}), 1.53 (d, 9 H, $^{3}J_{PH}$ = 14 Hz, PC*Me*$_3$), 1.43 (d, 9 H, $^{3}J_{PH}$ = 14 Hz, PC*Me*$_3$,), 1.36 (t, 3 H, NCH$_2$C*H*$_3$, J = 7 Hz), 1.20 (s, 3 H, Si*Me*),

0.62 (t, 3 H, NCH_2CH_3, J = 7 Hz), -19.21 (dd, 1 H, $^1J_{RhH}$ = 29 Hz, $^2J_{PH}$ = 21 Hz, Rh*H*). $^{13}C\{^1H\}$ NMR (300 K, 125.8 MHz, benzene-d_6): δ 156.8 (C_{arom}), 146.3 (d, $^1J_{CP}$ = 49 Hz, C_{arom}), 142.6 (C_{arom}), 141.6 (C_{arom}), 134.0 (CH_{arom}), 132.7 (d, CH_{arom}, $^2J_{CP}$ = 18 Hz), 132.2 (CH_{arom}), 131.3 (CH_{arom}), 129.6 (CH_{arom}), 129.1 (CH_{arom}), 127.8 (CH_{arom}), 126.8 (CH_{arom}), 65.7 ($CH_{2benzylic}$), 52.5 (NCH_2CH_3), 51.1 (NCH_2CH_3), 37.6 (d, J = 15 Hz, $PCMe_3$), 37.3 (d, J = 20 Hz, $PCMe_3$), 30.9 - 31.4 (overlapping resonances, CMe_3), 14.6 (NCH_2CH_3), 12.7 (NCH_2CH_3), 9.4 (Si*Me*). $^{31}P\{^1H\}$ NMR (300 K, 202.5 MHz, benzene-d_6): δ 97.3 (d, $^1J_{PRh}$ = 152 Hz). ^{29}Si NMR (300 K, 99.4 MHz, benzene-d_6): δ 36.2. IR (Thin film, cm^{-1}): 2089 (br, m, Rh-H).

[^{t}Bu-PSiN-Et]Ir(H)Cl (3-6). A solution of **3-2** (0.34 g, 0.80 mmol) in ca. 5 mL of benzene was added to a solution of $[(1,5\text{-COD})IrCl]_2$ (0.27 g, 0.40 mmol) in ca. 5 mL of benzene. An immediate color change from orange to orange-brown was observed. The volatile components of the reaction mixture were removed *in vacuo*, and the residue was triturated with pentane (2 × 2 mL) and dried under vacuum to yield **3-6** as a yellow solid (0.48 g, 91%). ^{1}H NMR (300 K, benzene-d_6): δ 8.06 (apparent t, 2 H, J = 8 Hz, H_{arom}), 7.60 (t, 1 H, J = 7 Hz, H_{arom}), 7.23 (d, 1 H, J = 6 Hz, H_{arom}), 7.15 (overlapping with C_6H_6, 1 H, H_{arom}), 7.08 (apparent t, 1 H, J = 7 Hz, H_{arom}), 6.96 (m, 1 H, H_{arom}), 6.80 (d, 1 H, J = 8 Hz, H_{arom}), 4.78 (m, 1 H, $H_{benzylic}$), 3.99 (m, 1 H, N-CH_{alkyl}), 3.75 - 3.78 (overlapping resonances, 2 H, N-CH_{alkyl} + $H_{benzylic}$), 3.30 (m, 1 H, N-CH_{alkyl}), 2.66 (m, 1 H, N-CH_{alkyl}), 1.51 (d, 9 H, $^3J_{PH}$ = 14 Hz, PCMe_3), 1.43 (d, 9 H, $^3J_{PH}$ = 13 Hz, PCMe_3), 1.32 (t, J = 6 Hz, 3 H, NCH_2CH_3), 1.07 (s, 3 H, Si*Me*), 0.52 (t, J = 6 Hz, 3 H, NCH_2CH_3), -23.2 (d, 1 H, Ir*H*, $^2J_{PH}$ = 18 Hz). $^{13}C\{^1H\}$ NMR (300 K, 125.8 MHz, benzene-d_6): δ 157.5 (C_{arom}), 146.3 (d, $^1J_{CP}$ = 53 Hz, C_{arom},), 142.4 (C_{arom}), 141.2 (C_{arom}), 134.6 (CH_{arom}),

132.5 (d, $^{2}J_{CP}$ = 18 Hz, *C*H_{arom}), 132.1 (*C*H_{arom}), 131.4 (*C*H_{arom}), 129.5 (*C*H_{arom}), 129.0 (*C*H_{arom}), 128.0 (*C*H_{arom}), 126.7 (*C*H_{arom}), 67.7 (*C*$H_{2benzylic}$), 54.9 (N*C*H_2CH$_3$), 51.7 (N*C*H_2CH$_3$), 36.8 (d, *J* = 28 Hz, P*C*Me$_3$), 37.3 (d, *J* = 21 Hz, P*C*Me$_3$), 32.1 (C*Me*$_3$), 30.9 (C*Me*$_3$), 15.5 (NCH$_2$*C*H$_3$), 7.9 (NCH$_2$*C*H$_3$), 6.3 (Si*Me*). ^{31}P{^{1}H} NMR (300 K, 202.5 MHz, benzene-d_6): δ 59.9. ^{29}Si NMR (300 K, 99.4 MHz, benzene-d_6): δ -5.2. IR (Thin film, cm^{-1}): 2212 (br, m, Ir-H). A single crystal of **3-6** suitable for X-ray crystallographic analysis was grown from a concentrated benzene solution

[^{t}Bu-PSiN-Et]PdCl (3-7). A solution of [Pd(allyl)Cl]$_2$ (0.034 g, 0.094 mmol) in ca. 2 mL of THF was added to a solution of **3-2** (0.080 g, 0.19 mmol) in ca. 2 mL of THF to furnish a clear brown solution. After standing at room temperature for 1 hour the volatile components of the reaction mixture were removed *in vacuo* and the solid residue was washed with pentane (2 × 1 mL) and subsequently dried under vacuum to yield **3-7** as a brown solid (0.056 g, 52%). ^{1}H NMR (300 K, benzene-d_6): δ 7.64 - 7.67 (overlapping resonances, 2 H, *H*$_{arom}$), 7.54 (m, 1 H, *H*$_{arom}$), 7.22 (m, 1 H, *H*$_{arom}$), 7.07 - 7.11 (overlapping resonances, 3 H, *H*$_{arom}$), 6.99 (d, *J* = 7 Hz, 1 H, *H*$_{arom}$), 4.56 (m, 1 H, N-C*H*$_{alkyl}$), 4.07 (apparent d, 1 H, *J* = 7 Hz, *H*$_{benzylic}$), 4.00 (m, 1 H, N-C*H*$_{alkyl}$), 2.94 (m, 1 H, *H*$_{benzylic}$), 2.86 (m, 1 H, N-C*H*$_{alkyl}$), 2.20 (m, 1 H, N-C*H*$_{alkyl}$), 1.55 (t, 3 H, *J* = 7 Hz, NCH$_2$C*H*$_3$), 1.48 (d, 9 H, PC*Me*$_3$, $^{3}J_{PH}$ = 15 Hz), 1.37 (d, 9 H, PC*Me*$_3$, $^{3}J_{PH}$ = 15 Hz), 0.73 (t, *J* = 7 Hz, 3 H, NCH$_2$C*H*$_3$), 0.68 (s, 3 H, Si*Me*). ^{13}C{^{1}H} NMR (300 K, 125.8 MHz, benzene-d_6): δ 153.4 (d, $^{1}J_{CP}$ = 47 Hz, *C*$_{arom}$), 143.6 (*C*$_{arom}$), 142.6 (d, $^{2}J_{CP}$ = 41 Hz, *C*$_{arom}$), 133.3 (*C*H_{arom}), 132.9 (*C*H_{arom}), 132.4 (*C*H_{arom}), 131.5 (*C*H_{arom}), 129.8 (*C*H_{arom}), 129.3 (*C*H_{arom}), 128.0 (*C*H_{arom}), 127.0 (*C*H_{arom}), 58.8 (*C*$H_{2benzylic}$), 53.2 (N*C*H_2CH$_3$), 51.9 (N*C*H_2CH$_3$), 37.1 - 37.3 (overlapping resonances, P*C*Me$_3$), 31.6 - 31.8 (overlapping

resonances P*C*Me$_3$, J = 20 Hz), 15.6 (NCH$_2$*C*H$_3$), 9.0 (NCH$_2$*C*H$_3$), 4.4 (Si*Me*). ^{31}P{^{1}H} NMR (300 K, 202.5 MHz, benzene-d_6): δ 101.1. ^{29}Si NMR (300 K, 99.4 MHz, benzene-d_6): δ 37.7.

[^{t}Bu-PSiNPy]NiBr (3-8). NEt$_3$ (0.041 mL, 0.30 mmol) was added to a solution of **3-3** (0.11 g, 0.30 mmol) in ca. 4 mL of THF. This mixture was subsequently added to a solution of NiBr$_2$ (0.065 g, 0.30 mmol) in ca. 4 mL of THF to produce a tan colored solution. The reaction mixture was transferred to a Schlenk tube and heated at 65 ºC for 18 h. A color change from tan to dark green was observed. The solvent was removed *in vacuo* and the solid residue was extracted with ca. 5 mL of benzene. The benzene extract was filtered through Celite and dried under vacuum. The remaining residue was washed with pentane (3 × 1 mL) to yield crude **3-8** (contaminated with an unidentified paramagnetic side product) as a pale green-grey solid (0.14 g). NMR characterization data are provided for the diamagnetic product **3-8**. ^{1}H NMR (500 MHz, benzene-d_6): δ 10.24 (m, 1 H, H_{arom}), 7.60 (dd, 1 H, J = 8 Hz, H_{arom}), 7.35 (d, 1 H, J = 7 Hz, H_{arom}), 7.15 – 7.11 (overlap with C$_6$H$_6$, 1 H, H_{arom}), 7.03 (m, 1 H, H_{arom}), 6.72 (t, 1 H, J = 7 Hz, H_{arom}), 6.61 (d, 1 H, J = 8 Hz, H_{arom}), 6.37 (t, 1 H, J = 7 Hz, H_{arom}), 2.92 (d, 1 H, J = 15 Hz, C*H*$_2$), 1.95 (d, 1 H, J = 15 Hz, C*H*$_2$), 1.63 (d, 9 H, $^3J_{PH}$ = 14 Hz, PC*Me*$_3$), 1.48 (d, 9 H, $^3J_{PH}$ = 14 Hz, PC*Me*$_3$), 0.10 (s, 3 H, Si*Me*). ^{13}C{^{1}H} NMR (125.8 MHz, benzene-d_6): δ 155.3 (*C*H$_{arom}$), 137.6 (*C*H$_{arom}$), 134.5 (*C*H$_{arom}$), 132.3 (d, $^2J_{CP}$ = 19 Hz, *C*H$_{arom}$), 130.1 (*C*H$_{arom}$), 128.7 (*C*H$_{arom}$), 123.8 (*C*H$_{arom}$), 121.2 (*C*H$_{arom}$), 32.3 (*C*H$_2$), 32.0 (C*Me*$_3$), 31.4 (C*Me*$_3$), 0.05 (Si*Me*). ^{31}P{^{1}H} NMR (202.5 MHz, benzene-d_6): δ 90.4. ^{29}Si NMR (99.4 MHz, benzene-d_6): δ 56.2.

[^{t}Bu-PSiNPy]PdCl (3-9). A solution of $[Pd(allyl)Cl]_2$ (0.053 g, 0.14 mmol) in ca. 4 mL of THF was added to a solution of **3-3** (0.10 g, 0.29 mmol) in ca. 4 mL of THF to produce a dark green-brown solution. The reaction mixture was placed in the freezer at -35 ºC and allowed to stand at this temperature for 36 h. The volatile components of the reaction mixture were then removed *in vacuo* and the remaining solid was washed with pentane (3 × 1 mL) and dried under vacuum to yield **3-3** as a pale grey solid (0.13 g, 91%). ^{1}H NMR (500 MHz, benzene-d_6): δ 10.18 (m, 1 H, H_{arom}), 7.58 (m, 1 H, H_{arom}), 7.36 (d, 1 H, J = 7 Hz, H_{arom}), 7.18 – 7.15 (overlap with C_6H_6, 1 H, H_{arom}), 7.05 (m, 1 H, H_{arom}), 6.83 (m, 1 H, H_{arom}), 6.76 (d, 1 H, J = 8 Hz, H_{arom}), 6.48 (t, 1 H, J = 6 Hz, H_{arom}), 2.82 (d, 1 H, J = 15 Hz, CH_2), 2.25 (d, 1 H, J = 15 Hz, CH_2), 1.52 (d, 9 H, $^3J_{PH}$ = 14 Hz, PCMe_3), 1.39 (d, 9 H, $^3J_{PH}$ = 15 Hz, PCMe_3), 0.24 (s, 3 H, SiMe). ^{13}C{^{1}H} NMR (125.8 MHz, benzene-d_6): δ 164.5 (C_{arom}), 153.6 (CH$_{arom}$), 138.1 (CH$_{arom}$), 133.9 (CH$_{arom}$), 132.9 (d, $^2J_{CP}$ = 24 Hz, CH$_{arom}$), 130.5 (CH$_{arom}$), 129.0 (CH$_{arom}$), 124.0 (CH$_{arom}$), 121.5 (CH$_{arom}$), 32.9 (CH$_2$), 31.4 (d, $^2J_{CP}$ = 6 Hz, CMe_3), 31.0 (d, $^2J_{CP}$ = 6 Hz, CMe_3), 2.6 (SiMe). ^{31}P{^{1}H} NMR (202.5 MHz, benzene-d_6): δ 96.4. ^{29}Si NMR (99.4 MHz, benzene-d_6): δ 57.6.

[^{t}Bu-PSiNPy]PtCl (3-10). NEt_3 (0.040 mL, 0.29 mmol) was added to a solution of **3-3** (0.10 g, 0.29 mmol) in ca. 4 mL of benzene. This mixture was subsequently added to a solution of $Pt(SEt_2)_2Cl_2$ (0.13 g, 0.29 mmol) in ca. 4 mL of benzene to produce a yellow solution. The reaction mixture was transferred to a Schlenk tube and heated at 65 ºC for 18 h. The solution was cooled to room temperature and filtered through Celite. The volatile components of the reaction mixture were removed *in vacuo* and the remaining residue was washed with pentane (3 × 1 mL) and dried under vacuum to yield

3-10 as a yellow solid (0.14 g, 81%). ^{1}H NMR (500 MHz, benzene-d_6): δ 10.29 (m, 1 H, H_{arom}), 7.66 (m, 1 H, H_{arom}), 7.52 (m, 1 H, H_{arom}), 7.16 – 7.13 (overlap with C_6H_6, 1 H, H_{arom}), 7.04 (m, 1 H, H_{arom}), 6.82 (m, 1 H, H_{arom}), 6.73 (d, 1 H, J = 8 Hz, H_{arom}), 6.46 (m, 1 H, H_{arom}), 2.72 (d, 1 H, J = 15 Hz, CH_2), 2.22 (d, 1 H, J = 15 Hz, CH_2), 1.59 (d, 9 H, $^{3}J_{PH}$ = 14 Hz, PCMe_3), 1.39 (d, 9 H, $^{3}J_{PH}$ = 15 Hz, PCMe_3), 0.21 (s, 3 H, SiMe). ^{13}C{^{1}H} NMR (125.8 MHz, benzene-d_6): δ 152.3 (CH$_{arom}$), 151.2 (C_{arom}), 138.2 (CH$_{arom}$), 134.0 (CH$_{arom}$), 133.3 (d, $^{2}J_{CP}$ = 18 Hz, CH$_{arom}$), 130.5 (CH$_{arom}$), 128.4 (CH$_{arom}$), 124.9 (CH$_{arom}$), 122.0 (CH$_{arom}$), 32.8 (CH$_2$), 31.6 (d, $^{2}J_{CP}$ = 4 Hz, CMe_3), 30.9 (d, $^{2}J_{CP}$ = 5 Hz, CMe_3), 1.1 (SiMe). ^{31}P{^{1}H} NMR (202.5 MHz, benzene-d_6): δ 74.2 (s with Pt satellites, $^{1}J_{PPt}$ = 4720 Hz). ^{29}Si NMR (99.4 MHz, benzene-d_6): δ 31.5. A single crystal of **3-10** suitable for X-ray crystallographic analysis was grown from a concentrated benzene solution.

3.4.3 Crystallographic Solution, Refinement and Structural Details for 3-6 and 3-10

Crystallographic data for **3-6** were obtained at 173(±2)K on a Bruker PLATFORM/APEX II CCD diffractometer and for **3-10** data were obtained at 173(±2)K on a Bruker D8/APEX II CCD diffractometer. For both structures data were obtained using graphite-monochromated Mo Kα (λ = 0.71073 Å) radiation, employing a sample that was mounted in inert oil and transferred to a cold gas stream on the diffractometer. Programs for diffractometer operation, data collection, and data reduction (including SAINT) were supplied by Bruker. Gaussian integration (face-indexed) was employed as the absorption correction method in each case. Both structures were solved by use of the Patterson search/structure expansion and were refined by use of full-matrix least-squares procedures (on F^2) with R_1 based on $F_o^2 \geq 2\sigma(F_o^2)$ and wR_2 based on $F_o^2 \geq -3\sigma(F_o^2)$.

Anisotropic displacement parameters were employed throughout for the non-hydrogen atoms. The atomic coordinates and isotropic displacement parameter for the hydrido ligand in **3-6** was freely refined. Otherwise, all hydrogen atoms were added at calculated positions and refined by use of a riding model employing isotropic displacement parameters based on the isotropic displacement parameter of the attached atom. Additional crystallographic information is provided in Appendix A.

CHAPTER 4: Synthesis, Reactivity and Characterization of Cobalt Complexes Featuring the Bis(phosphino)silyl Ligand [Cy-PSiP]

4.1 Introduction

Over recent years there has been increasing interest in replacing platinum group metals with first-row transition metals in catalytic applications due to their high abundance, reduced toxicity, and significantly lower cost.[67] However, replacing platinum group metals with first-row transition metals has remained a significant challenge due to the divergent reactivity trends between first row (3d) and second/third row (4d/5d) transition metals. One predominant factor for the divergent reactivity of the first row transition metals is the oxidation states available to these metals. First row transition metals favor oxidation states one oxidation state apart, primarily as a result of their low ionization potentials. For example, the Co^{I}, Co^{II} and Co^{III} oxidation states are readily accessible, which often results in Co complexes undergoing one-electron redox reactions.[68] Thus, while a two-electron oxidation of Co^{I} to Co^{III} is possible, examples of such processes are limited.[69] By comparison, two-electron redox processes such as oxidative addition and reductive elimination feature prominently in almost all platinum group metal catalytic systems.[70] Thus, obtaining two-electron redox chemistry at Co centers represents one goal in developing new organometallic Co species, as such reactivity may be of importance in generating complexes that mimic the reactivity of platinum group metal catalysts. Alternatively, highly reactive Co complexes might mediate catalytic processes by entirely different mechanisms that do not rely on the traditional two-electron redox steps so commonly associated with their heavier transition metal congeners.

The design of suitable ancillary ligands that can support reactive first row metal complexes plays a key role in the development of new first row metal species that may have applications in catalysis. In this context, there has been increased recent interest in developing the chemistry of Co pincer complexes. A report from Caulton on the reducing potential of [^{tBu}PNP]Co^{I} suggested that this complex is potentially more reducing than [^{tBu}PNP]Rh^{I} on the basis of the carbonyl stretching frequencies of analogous [^{tBu}PNP]Co(CO) and [^{tBu}PNP]Rh(CO) species.[71] The carbonyl IR stretching frequency observed for the Co complex was 1885 cm^{-1} whereas the carbonyl IR stretching frequency observed for the Rh analogue was 1932 cm^{-1}. The lower stretching frequency observed for the Co complex suggests that the metal center donates more electron density into the π^* orbitals of the carbonyl ligand, thereby elongating the C-O bond. This result was surprising as conventional wisdom suggests that π-basicity increases down a periodic group.[72] At the time it was suggested that this apparent strong π-basicity from Co may result in a facile two electron oxidation of Co^{I} to Co^{III}.

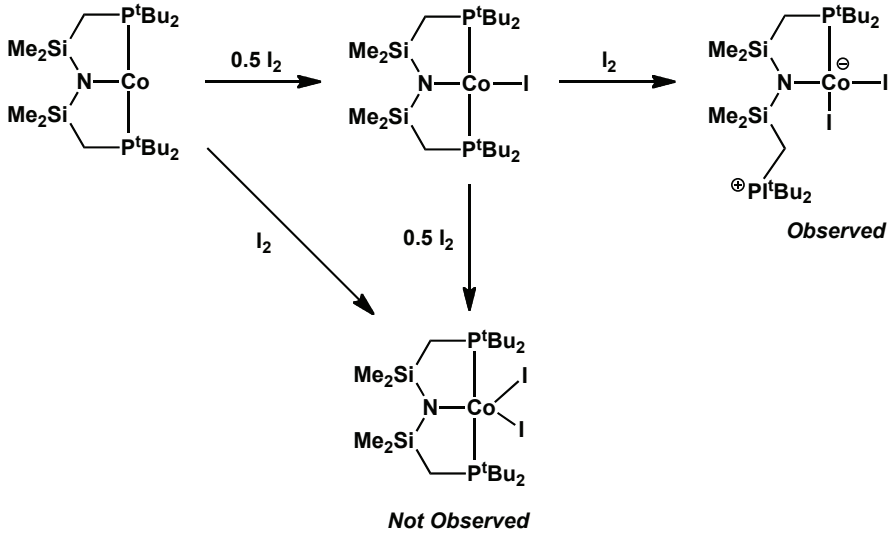

Scheme 4-1. Reaction of [^{tBu}PNP]Co with I_2.

To probe the potential of [^{tBu}PNP]Co^{I} to mediate two-electron oxidative addition reactions, [^{tBu}PNP]Co was allowed to react with I_2, a substrate that contains a relatively weak covalent bond. This reaction resulted in the formation of the divalent iodide complex [^{tBu}PNP]Co-I, with none of the desired oxidative addition product [^{tBu}PNP]Co-$(I)_2$ observed. The addition of excess I_2 to the reaction mixture did not result in the formation the desired trivalent diiodide complex, rather the oxidation of one of the phosphine arms of the pincer ligand was attained, resulting in the formation of an iodophosphonium group (Scheme 4-1). This observation suggests that the π-basicity of the metal center is not the only factor that governs whether a two-electron process occurs at the metal center. Notably, a subsequent report from Caulton on the reactivity of the same [^{tBu}PNP]Co system with H_2 indicated the formation of [^{tBu}PNP]Co^{III} dihydride complexes, where the proposed oxidative addition was shown to be reversible.[69d] Such a result indicated that despite the high spin nature of [^{tBu}PNP]Co^{I} complexes, they are capable of mediating two-electron processes with certain substrates.

Heinekey and co-workers have reported on the synthesis of [^{tBu}POCOP]Co pincers. While [^{tBu}POCOP]Ir complexes have garnered much attention in the catalytic dehydrogenation of alkanes and ammonia borane,[73] Ir is too expensive for most industrial applications. To this effect, Heinekey and co-workers identified the analogous cobalt complex [^{tBu}POCOP]Co as a desirable target for dehydrogenative reactions.[74] At the outset of the study, no simple dihydrogen complexes of Co had been reported; therefore it was of great interest to further investigate the nature of cobalt-hydrogen interactions.

The reaction of [^{tBu}POCOP]Co with H_2 at 195K immediately led to the formation of a new complex which was identified as a non-classical H_2 complex, where the H_2 ligand is bound in a side-on fashion (Scheme 4-2). This species decomposes above 220K and is only stable under a H_2 atmosphere. The identity of the side on bound ligand was corroborated with Density Functional Theory (DFT) calculations as well as on the basis of a large H-D coupling constant in the [^{tBu}POCOP]Co(HD) complex ($^1J_{HD}$ = 28 Hz). The oxidative addition product, a [^{tBu}POCOP]Co^{III} dihydride complex, was not observed in this reaction. However, when [^{tBu}POCOP]Co was exposed to a higher pressure of H_2 the formation of [^{tBu}POCOP]Co(H_2)(H)(H) was observed (Scheme 4-2). The short T_1(min) value observed for this complex was deemed most consistent with a Co(III) dihydrogen-dihydride complex, an observation corroborated by DFT calculations. Like the previously discussed [POCOP]Co(H_2) species, [^{tBu}POCOP]Co(H_2)(H)(H) could only be observed at low temperature under a H_2 atmosphere, which limits the potential application of these complexes. Modification of such complexes so as to facilitate their stability at room temperature would be highly desirable, as it would allow for a more robust study of the interaction of Co complexes with H_2.

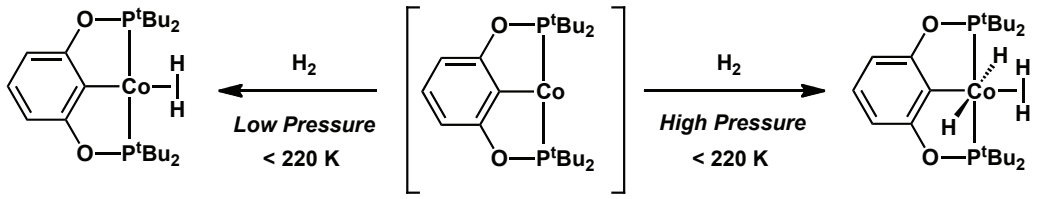

Scheme 4-2. Reaction of [POCOP]Co with H_2 at different pressures.

In an effort to further explore the chemistry of Co pincer species, the synthesis and reactivity of complexes featuring bis(phosphino)silyl (PSiP) ligation was targeted. Despite the apparent interest in first row metal pincer species, little attention has been given to Co pincer complexes featuring central anionic donors other than C or N. It was anticipated that the incorporation of a highly electron donating silyl donor into the ligand framework may generate electron-rich Co complexes whose reactivity is divergent from that of [^{tBu}POCOP]Co and [^{tBu}PNP]Co species. In this regard, the synthesis and reactivity of Co^{I} and Co^{II} complexes featuring sterically demanding [Cy-PSiP] ligation are discussed in this chapter.[75]

4.2 Results and Discussion

4.2.1 Synthesis and Reactivity of [Cy-PSiP]Co-X (X = Cl, I) Complexes

As an entry point into [Cy-PSiP]Co chemistry, the simple CoX_2 salts (X = Cl, I) were identified as ideal starting materials due to their inexpensive nature as well as the potential formation of highly desirable [Cy-PSiP]Co-X complexes upon the expected Si-H oxidative addition of the [Cy-PSiP] ligand, followed by dehydrohalogenation of the resulting Co complex (Scheme 4-3). Such [Cy-PSiP]Co-X complexes may be easily functionalized by reaction with reagents such as lithium salts and Grignard reagents, and are also an ideal starting point for reduction to Co^{I} species.

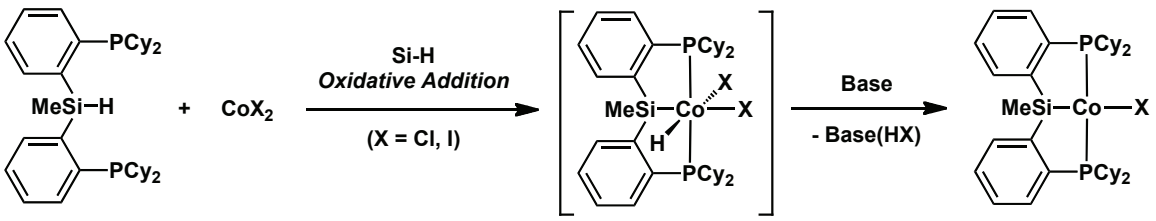

Scheme 4-3. Proposed synthesis of [PSiP]Co-X complexes.

The reaction of [Cy-PSiP]H with $CoCl_2$ was met with limited success. Reaction of [Cy-PSiP]H with $CoCl_2$ in the presence of 10 equiv. NEt_3 at room temperature produced a deep brown solution that appeared to contain multiple products by $^{31}P\{^1H\}$ and ^1H NMR spectroscopy, as well as unreacted $CoCl_2$. A minute amount (ca. 5% yield) of X-ray quality crystals were grown from a concentrated toluene solution of this reaction mixture and were crystallographically characterized as [Cy-PSiP]Co-Cl (**4-1**, Table 4-1, Figure 4-1).

The reaction of [Cy-PSiP]H with CoI_2 proved to be far more successful. Mixing of the reactants in THF in the presence of 10 equiv. of NEt_3 at room temperature resulted in the immediate color change from deep green-blue to deep red. Washing of the crude reaction product with pentane after removal of solvent and NEt_3HI resulted in the isolation of [Cy-PSiP]Co-I (**4-2**) as an analytically pure orange solid in 95% yield (Scheme 4-4). The use of only 1 equiv. of NEt_3 resulted in lower yields of isolated **4-2**. The difference in the yield of product between **4-1** and **4-2** may be attributed to the significantly increased solubility of CoI_2 over $CoCl_2$. The more soluble CoI_2 may promote phosphine coordination to the metal center and thus a more facile oxidative addition of the Si-H bond to furnish the metalated product.

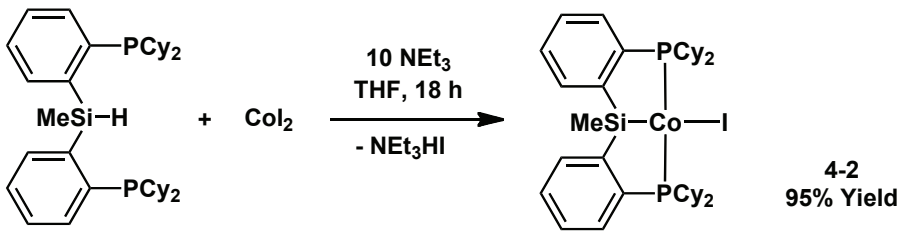

Scheme 4-4. Synthesis of [Cy-PSiP]Co-I (**4-2**).

X-ray quality crystals of **4-2** were obtained from a concentrated toluene solution and crystallographic analysis confirmed the formulation of this complex as [Cy-PSiP]Co-I (Table 4-1, Figure 4-1). ^{1}H NMR data obtained for **4-2** was difficult to interpret in a meaningful fashion due to the paramagnetic nature of the 15-electron complex. The ^{1}H NMR spectrum of **4-2** (benzene-d_6) revealed a number of broad resonances between -11.7 and 14.5 ppm, indicating a paramagnetic compound is likely present. Attempts were made to obtain ^{31}P and ^{29}Si NMR data, however no signals were observed for either nucleus, presumably due to their proximity to the paramagnetic metal center. Solution magnetic moment measurements resulted in a calculated μ_{eff} value of 1.86 B.M (S = ½). This measurement indicates that **4-2** is a low spin d^7 complex containing one unpaired electron instead of a potential high spin d^7 complex containing three unpaired electrons. A similar electronic structure was observed in [^{tBu}POCOP]Co-I reported by Heinekey.[73] Alternatively, comparable [PNP]Co-Cl and [PNP]Co-Br complexes were found to have high spin electronic structures.[69c,69d,71,76] These observations demonstrate a potential difference between PSiP and PNP ligation for Co complexes, as PSiP ligation appears to promote the formation of low-spin Co^{II} complexes, whereas PNP ligation appears to promote the formation of high-spin Co^{II} complexes.

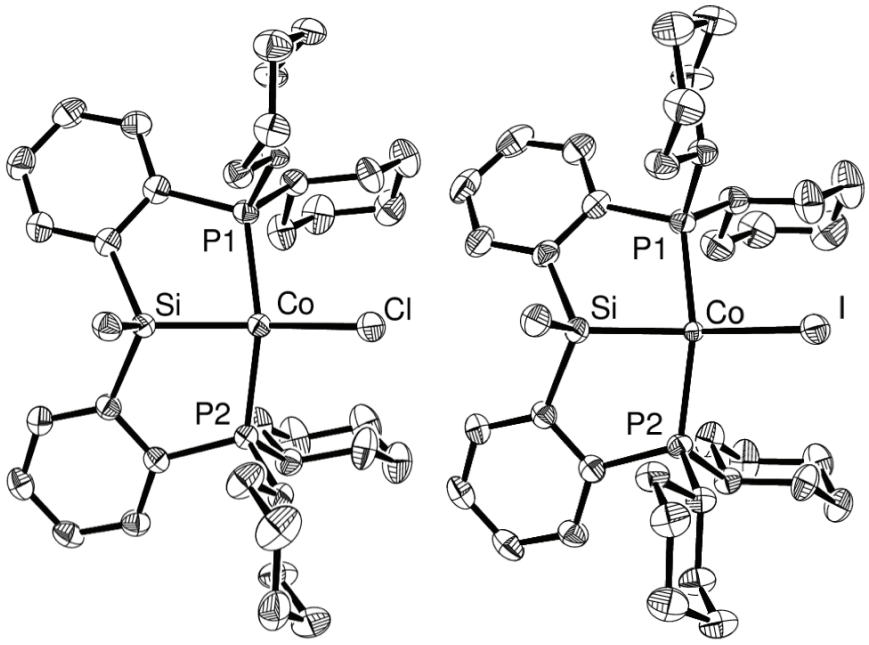

Figure 4-1. The crystallographically determined structures of **4-1**•C_7H_8 (left) and **4-2**•C_7H_8 (right), shown with 50% displacement ellipsoids. All H atoms have been omitted for clarity.

Complexes **4-1** and **4-2** exhibit very similar structures in the solid state (Table 4-1, Figure 4-1). Both complexes feature distorted square planar coordination geometry at the Co center. The deviation from square planarity can be observed in **4-2** by examining P(1)-Co-P(2) and Si-Co-I bond angles of 158.45(3)° and 149.35(2)°, respectively. A similar type of deviation can be seen in **4-1** where P(1)-Co-P(2) and Si-Co-Cl bond angles of 160.30(2)° and 152.63(2)° are observed. The deviation from a more idealized geometry can be rationalized by considering the tridentate, chelating nature of the [Cy-PSiP] ligand. Comparatively, [^{tBu}POCOP]Co-I also exhibits a distorted square planar geometry in the solid state, however the geometry is much closer to the idealized square planar geometry, with P-Co-P and C-Co-I angles of 162.81(4)° and 179.60(11)°, respectively. The moderate differences in geometry observed between the POCOP- and PSiP-ligated complexes can potentially be attributed to the presence of an sp^2-C central

donor in [^{tBu}POCOP]Co-I that allows the tridentate ligand to adopt a planar structure at the central donor site in contrast to the sp^3-Si donor in **4-2**, where the Si atom is tetrahedral at the central donor site. Alternatively, [PNP]Co-Cl and [PNP]Co-Br complexes have been shown to adopt distorted tetrahedral structures in the solid state,[69c,69d,71,76] again highlighting the differences between PSiP and PNP ligation.

Bond Lengths (Å)				
4-1•C_7H_8	Co-P(1)	2.2077(6)	Co-P(2)	2.2156(5)
	Co-Si	2.2340(6)	Co-Cl	2.2710(6)
4-2•C_7H_8	Co-P(1)	2.2292(8)	Co-P(2)	2.2275(7)
	Co-Si	2.2381(8)	Co-I	2.5879(4)
Bond Angles (°)				
4-1•C_7H_8	P1-Co-P(2)	160.30(2)	P(1)-Co-Cl	98.64(2)
	Si-Co-Cl	152.63(2)	P(2)-Co-Cl	99.02(2)
	P(1)-Co-Si	83.90(2)	P(2)-Co-Si	84.44(2)
4-2•C_7H_8	P(1)-Co-P(2)	158.45(3)	P(1)-Co-I	101.35(6)
	Si-Co-I	149.35(2)	P(2)-Co-I	97.86(2)
	P(1)-Co-Si	84.52(3)	P(2)-Co-Si	83.92(3)

Table 4-1. Selected Interatomic Distances (Å) and Angles (º) for **4-1•C_7H_8** and **4-2•C_7H_8**.

Several attempts were made to reduce **4-2** to a potential [Cy-PSiP]Co^I species. Reducing agents such as Na/Hg (0.5 and 1%), sodium naphthalenide, and Mg were used with little success. In every case, **4-2** reacted with the reducing agent within minutes at room temperature (or -35 °C) to afford a deep brown solution. These brown solutions persisted even after stirring for several hours at room temperature. Upon removal of the solvent *in vacuo*, an oily brown material was obtained in each case. Despite multiple attempts to recrystallize/purify this product, no pure material was successfully isolated from these attempted reduction reactions.

4.2.2 Synthesis and Reactivity of [Cy-PSiP]Co(PMe_3)X (X = Cl, I) Complexes

In an attempt to stabilize a reactive [Cy-PSiP]Co^{I} species, the introduction of an additional phosphine donor was attempted. Treatment of **4-2** with one equiv. of PMe_3 in THF resulted in the immediate formation of the 17-electron species [Cy-PSiP]Co(PMe_3)I (**4-3**, Scheme 4-5), which was isolated as a red solid in 77% yield. Similarly to **4-2**, paramagnetic **4-3** proved to be difficult to characterize by NMR methods. A ^{1}H NMR spectrum was observed, however no structural information could be interpreted from the data due to paramagnetic shifting and broadening of the resonances observed. Similarly to **4-2**, no ^{31}P or ^{29}Si NMR resonances were observed for **4-3** due to the proximity of the P and Si atoms to the paramagnetic Co center. Solution magnetic moment measurements resulted in a calculated μ_{eff} value of 1.65 B.M. This value indicates the presence of one unpaired electron in **4-3**, a low-spin configuration similar to **4-2**. It was found that the related complex [Cy-PSiP]Co(PMe_3)Cl (**4-4**) could be synthesized by a method involving the *in situ* generation of [Cy-PSiP]Co-Cl (**4-1**) and subsequent reaction with PMe_3. Mixing of [Cy-PSiP]H and $CoCl_2$ in the presence of 10 equiv. of NEt_3 for 2 hours in THF followed by addition of PMe_3 resulted in a color change of the solution from deep brown to deep red. Removal of solvent and NEt_3HCl, followed by washing with pentane resulted in the isolation of **4-4** as a red solid in 29% yield (Scheme 4-5). Complex **4-4** features a ^{1}H NMR spectrum similar to that of **4-3** and a μ_{eff} value of 1.89 B.M. (S = ½) was calculated for this complex.

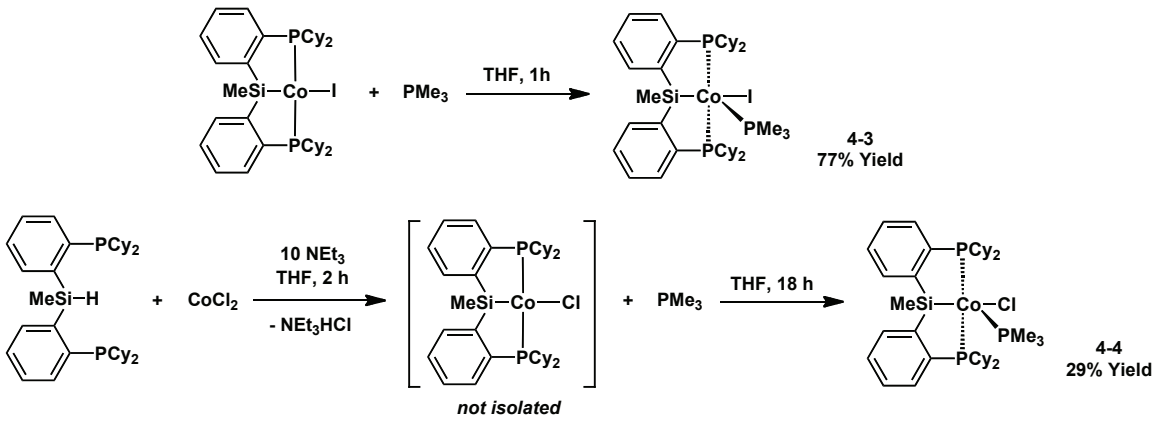

Scheme 4-5. Synthesis of [Cy-PSiP]Co(PMe_3)I (**4-3**) and [Cy-PSiP]Co(PMe_3)Cl (**4-4**).

X-ray quality crystals of **4-4** were obtained from a concentrated Et_2O/THF solution (ca. 9:1) at -35 °C. While single crystals of **4-3** suitable for X-ray diffraction analysis were not isolated, it is anticipated that the solid state structure of **4-3** is likely very similar to that of **4-4**. Crystallographic characterization revealed that **4-4** adopts distorted trigonal bipyramidal geometry at the Co center in the solid state, with Si and Cl in the axial positions (Table 4-2, Figure 4-2). The trigonal bipyramidal geometry is highlighted by the observed Si-Co-Cl bond angle of 172.61(3)° and the sum of the bond angles between the Co center and the three phosphines comprising the trigonal plane of 357.8°. Interestingly, the solid state structures of **4-1** and **4-2** reveal that the Cy-PSiP ligand is flexible enough upon complexation to Co to adopt structures where the phosphine donors are either *trans*- (as in **4-1**; P(1)-Co-P(2) bond angle of 160.30(2)°) or *cis*-disposed (as in **4-4**; P(1)-Co-P(2) bond angle of 132.80(3)°). A similar trigonal bipyramidal geometry was also reported by Peters and co-workers for related Co complexes supported by tetradentate P_3Si ligands.[77]

Bond Lengths (Å)				
4-4	Co-P(1)	2.2634(7)	Co-P(2)	2.2906(7)
	Co-P(3)	2.2174(8)	Co-Cl	2.2957(7)
	Co-Si	2.2597(7)		
Bond Angles (°)				
4-4	P(1)-Co-P(2)	132.80(3)	P(1)-Co-P(3)	105.46(3)
	P(1)-Co-Si	84.95(3)	Si-Co-P(3)	90.42(3)
	Si-Co-Cl	172.61(3)		

Table 4-2. Selected Interatomic Distances (Å) and Angles (°) for **4-4**. Only one of the two crystallographically independent molecules of **4-4** is described.

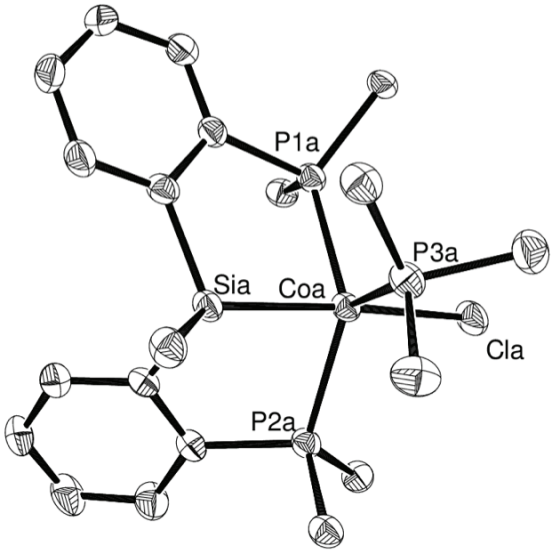

Figure 4-2. The crystallographically determined structure of **4-4** shown with 50% displacement ellipsoids. Cyclohexyl substituents and all H atoms have been omitted for clarity. Only one of the two crystallographically independent molecules of **4-4** is shown.

The reduction of **4-3** to the corresponding Co^{I} species was pursued. Reaction of **4-3** with Na/Hg (0.5 and 1%) and sodium naphthalenide in THF resulted in a color change of the solution from deep red to deep brown over the course of a minutes. A new diamagnetic product could be observed in the reaction mixture by $^{31}P\{^{1}H\}$ NMR spectroscopy, however the ^{1}H NMR spectrum indicated the presence of multiple species in the reaction mixture. Alternatively, reaction of **4-3** with the milder reducing agent Mg

was met with considerable success. Mixing of **4-3** with 10 equiv. of Mg in THF for 18 hours resulted in a color change of the solution from deep red to brown to orange over the course of the reaction. Upon work-up, the 18-electron Co^{I} dinitrogen adduct [Cy-PSiP]Co(PMe_3)(N_2) (**4-5**) was isolated in 97% yield (Scheme 4-6). Notably, it was found that **4-5** could also be synthesized by generating **4-3** *in situ*, followed by reaction with Mg.

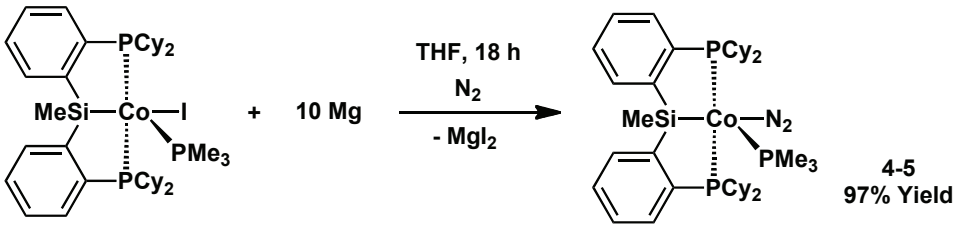

Scheme 4-6. Synthesis of [Cy-PSiP]Co(PMe_3)(N_2) (**4-5**).

Thus, it appears that under a N_2 atmosphere the 16-electron Co(I) species [Cy-PSiP]Co(PMe_3) prefers to coordinate N_2 to form the 18-electron complex **4-5**. Notably, the same observation was reported by Peters for related [P_3Si]Co complexes.[77a] Due to its diamagnetic nature, **4-5** was fully characterized by multinuclear NMR methods. The $^{31}P\{^{1}H\}$ NMR spectrum of **4-5** features two resonances at 66.4 (d, 2 P, $^{2}J_{PP}$ = 83 Hz, *P*Si*P*) and -14.8 ppm (t, 1 H, $^{2}J_{PP}$ = 83 Hz, *P*Me_3), which is consistent with the formation of a C_s symmetric complex where both phosphine donors of the PSiP ligand are rendered equivalent. In addition, the relatively small $^{2}J_{PP}$ coupling constant of 83 Hz is consistent with cis orientation of the pincer phosphino donors relative to the PMe_3 ligand. Unfortunately, single crystals of **4-5** suitable for X-Ray diffraction analysis have remained elusive. Efforts to crystallographically characterize **4-5** are ongoing.

The presence of the N_2 ligand in **4-5** was corroborated by the use of IR spectroscopy. A stretching frequency of 2065 cm^{-1} was observed for the bound N_2, which

is well within the expected range for a transition metal N_2 complex (1920 – 2150 cm^{-1}).[70] In an effort to examine the degree of activation in the N_2 ligand, the stretching frequency was compared to similar complexes found in the literature (Table 4-3); the N_2 stretching frequency observed for **4-5** appears to be comparable to related Co complexes. The N_2 stretching frequency of 2065 cm^{-1} observed for **4-5** is very close to the 2063 cm^{-1} value reported by Peters for the related $[P^{iPr}{}_3Si]Co(N_2)$ complex,[77a] indicating that the reducing ability of such complexes is comparable. Notably, a related $[P^{iPr}{}_3Si]Fe$ complex also reported by Peters exhibits a significantly decreased N_2 stretching frequency of 2008 cm^{-1}, indicating a N_2 ligand that is much more strongly activated than the N_2 ligand in **4-5**.[77a] Therefore, the degree of activation of the N_2 ligand in **4-5** is best described as moderate, indicating that the N_2 ligand may be labile enough to facilitate reactions at this 18-electron complex. Furthermore, it should also be noted that number of cobalt complexes featuring bridging N_2 ligands have also been isolated, with the degree of N_2 activation being much greater. For example, stretching frequencies of ca. 1600 cm^{-1} have been observed for (β-diketiminate)Co-N_2 complexes, indicative of the reduction of the N-N bond order from 3 to 2.[78]

Entry	Complex	ν_{NN} (cm^{-1})	Reference
1	[Cy-PSiP]Co(PMe_3)(N_2)	2065	This work
2	$[P^{Ph}{}_3Si]Co(N_2)$	2095	12a
3	$[P^{iPr}{}_3Si]Co(N_2)$	2063	12a
5	$[P^{iPr}{}_3Si]Fe(N_2)$	2008	12a

Table 4-3. Comparison of Co(N_2) IR stretching frequencies.

4.2.3 Investigation of Oxidative Addition to [Cy-PSiP]Co(PMe$_3$)(N$_2$)

As previously discussed, the degree of N_2 activation in **4-5** was determined to be fairly moderate. While this complex may not be ideal for the investigation of nitrogen fixation, the N_2 ligand may be able to act as a labile ligand that will allow access to the 16-electron Co^I species [Cy-PSiP]Co(PMe$_3$). [Cy-PSiP]Co(PMe$_3$) is a promising species for Co mediated bond activation chemistry, as oxidative addition at the Co^I center would lead to the formation of a 6-coordinate 18-electron Co^{III} complex that is anticipated to be quite stable (Scheme 4-7).

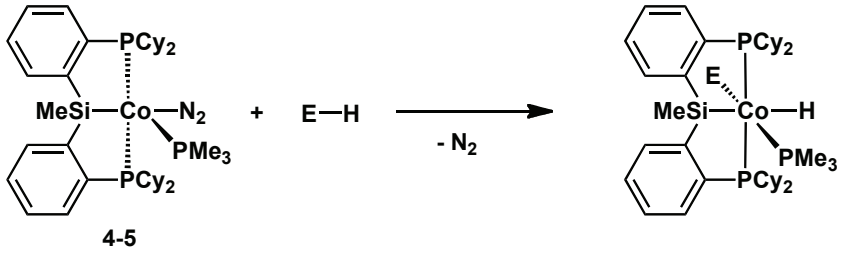

Scheme 4-7. Potential E-H bond activation by [Cy-PSiP]Co(PMe$_3$)(N$_2$) (**4-5**).

The potential of **4-5** to undergo oxidative addition of I_2 and iodobenzene was investigated initially. These substrates contain relatively weak I-I and C-I bonds, respectively, that should be highly reactive in oxidative addition reactions. Treatment of **4-5** with either 1 or 10 equiv. of I_2 resulted in an extremely exothermic reaction. Unfortunately, no clean Co containing product could be isolated from these reaction mixtures. A significant amount of what appeared to be free [Cy-PSiP]H ligand was observed in the reaction mixtures by $^{31}P\{^1H\}$ NMR spectroscopy (-7.8 ppm). As well, a significant amount of a brown precipitate was observed, presumably containing Co metal. The apparent decomposition can potentially be attributed to the highly exothermic nature of this reaction. Alternatively, reaction of **4-5** with either 1 or 10 equiv. of iodobenzene resulted in an immediate color change of the solution from orange to deep red. ^1H NMR

spectroscopy indicated the disappearance of **4-5** as well as the formation of new paramagnetic products. Attempts to isolate the product of this reaction have not been successful thus far, as single crystals have yet to be obtained from the reaction mixture. Characterization of the crude material by use of NMR techinques has not been fruitful due to the paramagnetic nature of the product. It is proposed that **4-5** undergoes a one electron oxidation in the course of this reaction to form paramagnetic Co^{II} species (Scheme 4-8). Such products could be formed by the Co center reacting with iodobenzene to give [Cy-PSiP]Co(PMe_3)(I) (**4-3**).[79] Such a reaction would also produce a phenyl radical that could potentially undergo reaction with [Cy-PSiP]Co(PMe_3) to form [Cy-PSiP]Co(PMe_3)(C_6H_5). Notably, no biphenyl was observed in the reaction mixture by ^1H NMR spectroscopy, suggesting that the phenyl radical may indeed be trapped by Co. Similar reactivity has been previously observed in one electron oxidations of [^{Ph}PNP]Co^{II} complexes to [^{Ph}PNP]Co^{III}.[76] The attempted separation and crystallographic characterization of the products of this reaction are ongoing.

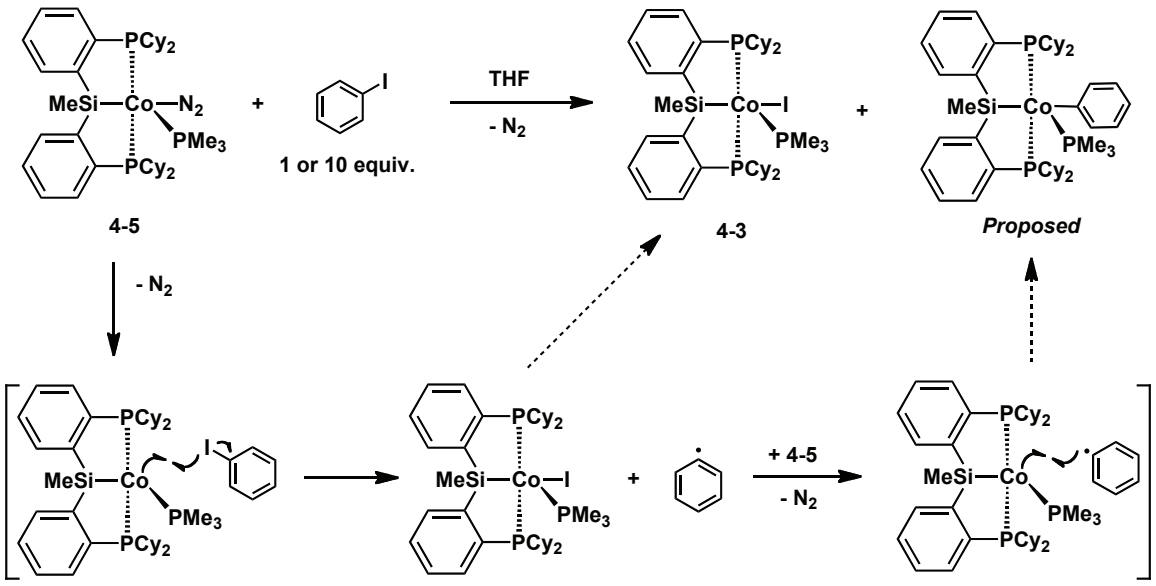

Scheme 4-8. Potential reaction between [Cy-PSiP]Co(PMe_3)(N_2) (**4-5**) and iodobenzene.

4.2.4 Investigation of Reactivity of [Cy-PSiP]Co(PMe_3)(N_2) with H_2 and NH_3BH_3

In recent years, Co complexes have become a target of interest for both hydrogenative and dehydrogenative catalysis.[80] Despite the applications of Co species in catalysis, the investigation of how H_2 reacts with Co in a stoichiometric manner is underexplored. Thorough investigation of how H_2 binds to Co could potentially reveal important mechanistic information of relevance to Co catalyzed hydrogenation. In this regard, the development of a robust system capable of H_2 binding to Co would be highly desirable.

In this regard, treatment of a degassed C_6D_6 solution containing **4-5** with H_2 (1 atm) at room temperature resulted in a color change from orange to yellow-brown over the course of two minutes. $^{31}P\{^1H\}$ and ^1H NMR spectroscopy indicated the quantitative formation of a new diamagnetic species, **4-6**, which is tentatively formulated as [Cy-PSiP]Co(PMe_3)H_2 where the hydride ligands may be coordinated in either a nonclassical fashion to afford a Co^I dihydrogen complex or in a classical mode to give a Co^{III} dihydride complex. Two broadened resonances were observed in the $^{31}P\{^1H\}$ NMR spectrum for **4-6** at 91.6 and 0.1 ppm, respectively. Notably, no coupling could be observed between the two ^{31}P resonances due to line broadening. Complex **4-6** was also observed by $^{31}P\{^1H\}$ NMR when **4-5** was allowed to react with 10 equiv. of H_3NBH_3 in THF at room temperature for 18 h. The formation of the same species from the reaction with either H_2 or H_3NBH_3 suggests that the H_3NBH_3 is dehydrogenated, releasing an equivalent of H_2 to react with the Co center. The dehydrogenation of H_3NBH_3 does not appear to be catalytic as only a small amount of dehydrogenated $[BH_2NH_2]_n$ product (relative to unreacted H_3NBH_3) was present after the reaction was complete, as

determined by ^{11}B NMR.[81] Unfortunately, attempts to isolate **4-6** by subjecting the reaction mixture to vacuum resulted in product decomposition, suggesting that H_2 is readily eliminated and **4-6** is stable only under an H_2 atmosphere.

The ^1H NMR spectrum of **4-6** features a diagnostic hydride resonance at -13.51 ppm (benzene-d_6, broad t, J = 38 Hz) (Figure 4-3) that integrates to two hydrogen atoms (relative to the [Cy-PSiP] ligand backbone). In an attempt to obtain more information about the nature of the dihydride/dihydrogen ligand by observing H-D coupling, **4-5** was allowed to react with HD gas (generated by reaction of $LiAlH_4$ with D_2O). Such H-D coupling constants have been used to evaluate whether the complex contains an H-D bond. Unfortunately, the room temperature ^1H NMR spectrum appeared extremely similar to that of the reaction with H_2, with a broad triplet being observed at -13.48 ppm. Cooling of this potential H-D complex to 223K did not result in a significant change in the lineshape of the hydride resonance, rendering the calculation of an H-D coupling constant difficult.

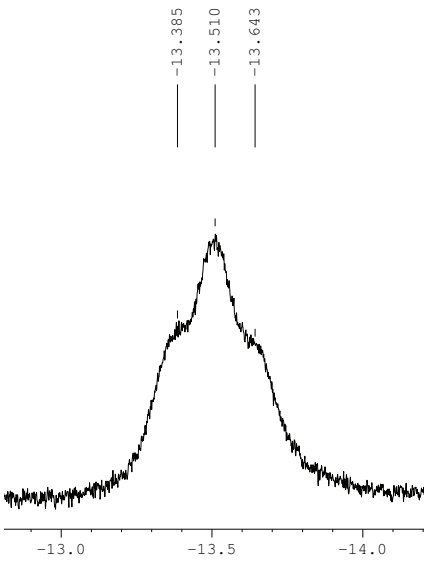

Figure 4-3. Broadened hydride ^1H NMR resonance observed in **4-6** (benzene-d_6).

In order to obtain more information about the nature of the hydride ligands in complex **4-6**, variable temperature NMR experiments were conducted to determine the T_{1min} value for the dihydrogen/dihydride. Such T_1 measurements have previously been demonstrated to be effective at differentiating between classical hydride and nonclassical dihydrogen ligands.[82] In a classical dihydride complex the hydride ligands have been shown to exhibit longer T_{1min} values (on the order of hundreds of milliseconds), whereas non-classically bound dihydrogen ligands typically have much shorter T_{1min} values (on the order of tens of milliseconds). Upon conducting the T_1 measurements it was found that **4-6** exhibits a T_{1min} value of 33 ms (233 K) indicating that the H_2 in **4-6** is coordinated to the metal in a side-on fashion, commonly known as a nonclassical H_2 adduct. Such a coordination of H_2 indicates that the cobalt center in **4-6** is best described as being in the Co^I oxidation state, with no formal oxidative addition of H_2 having occurred (Scheme 4-9).

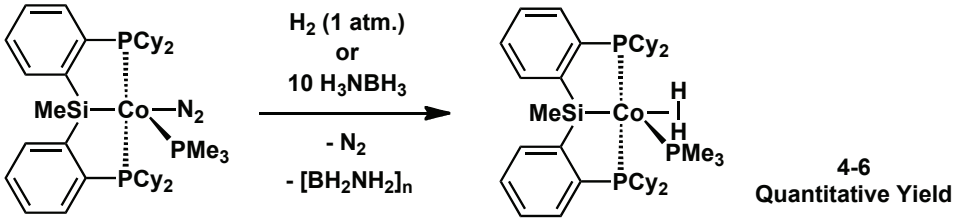

Scheme 4-9. Formation of non-classical $Co(H_2)$ complex **4-6**.

The proposed nonclassical H_2 complex **4-6** was found to be stable at room temperature for multiple days when kept under an atmosphere of H_2. Unfortunately, exposure of **4-6** to vacuum for two hours resulted in significant decomposition, which precluded the isolation of this complex. Furthermore, when a solution containing **4-6** was exposed to an atmosphere of N_2, regeneration of the dinitrogen complex **4-5** was slowly observed over the course of several days by $^{31}P\{^1H\}$ NMR. These results are

similar to those reported for [PNP]Co and [POCOP]Co dihydrogen complexes, which have been shown to be unstable under vacuum. Alternatively, **4-6** does appear to be stable at room temperature, unlike [PNP]Co and [POCOP]Co dihydrogen complexes. The enhanced stability of **4-6** can potentially be attributed to the presence of an additional phosphine ligand relative to [PNP]Co or [POCOP]Co complexes. Notably, a related [^{iPr}P$_3$Si]Co(H$_2$) complex reported by Peters was found to be stable both at room temperature and under vacuum.[77b]

4.3 Conclusions

Cyclometalation of [Cy-PSiP]H to CoI_2 resulted in the formation of the four-coordinate [Cy-PSiP]Co-I complex (**4-2**) in high yield relative to the analogous reaction with $CoCl_2$, which afforded only minute amounts of [Cy-PSiP]Co-Cl. Attempts to reduce **4-2** to a Co^I species were unsuccessful, as mixtures containing multiple products were formed in such reactions. However, coordination of an additional phosphine ligand to the Co center afforded clean reduction to Co^I. In this regard, reaction of **4-2** with PMe_3 resulted in the formation of the corresponding phosphine adduct [Cy-PSiP]Co(PMe_3)I (**4-3**), which was successfully reduced using 10 equiv. of Mg to form the Co^I species [Cy-PSiP]Co(PMe_3)(N_2) (**4-5**) in high yield. Comparison of N_2 stretching frequencies to the literature revealed that the degree of N_2 activation in **4-5** was moderate such that it may provide access to the 16-electron Co^I species [Cy-PSiP]Co(PMe_3).

Attempts to oxidatively add iodobenzene and H_2 to [Cy-PSiP]Co(PMe_3)(N_2) did not result in the expected Co^{III} oxidative addition products. In the case of iodobenzene, the formation of what are postulated to be multiple paramagnetic Co^{II} species was

observed. Treatment of **4-5** with H_2 resulted in the generation of a new species where the N_2 ligand in **4-5** had been displaced by H_2 to provide a nonclassical dihydrogen complex, as confirmed by the use of T_{1min} measurements. Thus it appears that although the electron-rich [Cy-PSiP]Co(PMe_3) species may be accessed in the course of such reactions, it does not readily undergo oxidative addition. Future studies will further explore the coordination chemistry of (PSiP)Co, with the goal of accessing new complexes that may more easily undergo such two-electron redox processes.

4.4 Experimental Section

4.4.1 General Considerations

All experiments were conducted under nitrogen in an MBraun glovebox or using standard Schlenk techniques. Tetrahydrofuran and diethyl ether were distilled from Na/benzophenone ketyl; while benzene, toluene, and pentane were purified by sparging with nitrogen followed by drying in a double column solvent purification system purchased from MBraun with one activated alumina column and one column packed with activated Q-5. All purified solvents were stored over 4 Å molecular sieves. Benzene-d_6 was degassed via three freeze-pump-thaw cycles and stored over 4 Å molecular sieves. Triethylamine was deoxygenated and dried by sparging with nitrogen and subsequent distillation from CaH_2. Silanes were purchased from Gelest, degassed via three freeze-pump-thaw cycles, and stored over 4 Å molecular sieves. All other reagents were purchased from Strem or Aldrich and used without further purification. ^1H characterization data for compounds **4-2** - **4-4** and **4-6** were collected at 300K on a Bruker AV-300 spectrometer operating at 300.1 MHz with chemical shifts reported in parts per

million downfield of $SiMe_4$. ^1H, ^{13}C, ^{31}P, and ^{29}Si characterization data for **4-5** were collected at 300K on a Bruker AV-500 spectrometer operating at 500.1, 125.8, 202.5, and 99.4 MHz (respectively) with chemical shifts reported in parts per million downfield of $SiMe_4$ (for ^1H, ^{13}C, and ^{29}Si), or 85% H_3PO_4 in D_2O (for ^{31}P). ^1H and ^{13}C NMR chemical shift assignments for **4-5** are based on data obtained from ^{13}C-DEPTQ, ^1H-^1H COSY, ^1H-^{13}C HSQC, and ^1H-^{13}C HMBC NMR experiments. ^{29}Si NMR assignments are based on ^1H-^{29}Si HMBC and ^1H-^{29}Si HMQC experiments. Elemental analyses were performed by Canadian Microanalytical Service Ltd. of Delta, British Columbia, Canada. Infrared spectra were recorded as thin films between KBr plates using a Bruker TENSOR 27 FT-IR spectrometer at a resolution of 4 cm^{-1}. X-ray data collection, solution, and refinement were carried out by Drs. Robert MacDonald and Michael J. Ferguson at the University of Alberta X-ray Crystallography Laboratory, Edmonton, Alberta. Magnetic moments (Evans method) were determined according to literature procedures.[83]

4.4.2 Synthetic Details and Characterization Data

[Cy-PSiP]Co-Cl (4-1). A solution of [Cy-PSiP]H (0.11 g, 0.19 mmol) and NEt_3 (0.019 g, 0.19 mmol) in ca. 5 mL of THF was added via pipette to a stirring solution of anhydrous $CoCl_2$ (0.025 g, 0.19 mmol) in ca. 5 mL of THF at room temperature. An immediate color change from pale green to dark brown was observed and the reaction was allowed to stir for 18 h at room temperature. After 18 h the volatile components of the reaction mixture were removed *in vacuo* and the reaction mixture was extracted with ca. 5 mL of C_6H_6. The benzene extract was then filtered through Celite and the filtrate was dried under vacuum. A minute amount of crystalline material of **4-1·C_7H_8** suitable

for X-ray diffraction analysis was grown from toluene at room temperature.

[Cy-PSiP]Co-I (4-2). A solution of [Cy-PSiP]H (0.50 g, 0.85 mmol) and NEt_3 (0.86 g, 8.5 mmol) in ca. 5 mL of THF was added via pipette over 2 minutes to a stirring solution of anhydrous CoI_2 (0.26 g, 0.85 mmol) in ca. 40 mL of THF at room temperature. A color change from blue to brown to deep red was observed over the course of the addition. The reaction mixture was then allowed to stir for 18 h at room temperature. After 18 h, the volatile components of the reaction mixture were removed *in vacuo* and the residue was extracted with ca. 10 mL of benzene. The benzene extract was then filtered through Celite and the filtrate was dried under vacuum. The remaining orange-red solid was washed with 2 × 2 mL of pentane to yield **4-2** as an orange solid (0.63 g, 95%). Melting point = 250-255 °C. ^{1}H NMR (300 MHz, benzene-d_6): δ 14.5, 9.6, 8.0, 7.8, 6.4, 4.4, 3.2, 2.3, 0.2 – 1.9 (overlapping peaks), -0.3, -0.8, -1.6, -3.3, -7.4, -11.7. μ_{eff} (benzene-d_6): 1.86 (S = ½) μ_B. Anal. Calcd. for $C_{37}H_{55}ICoP_2Si$: C, 57.29; H, 7.15. Found: C, 57.20; H, 6.88. Single crystals of **4-2** suitable for X-ray diffraction analysis were grown from a concentrated toluene solution at -35 °C.

[Cy-PSiP]Co(PMe_3)I (4-3). To a solution of **4-2** (0.10 g, 0.13 mmol) in ca. 5 mL of THF was added PMe_3 (0.010 g, 0.13 mmol) via syringe. An immediate color change to deep red was observed and the reaction mixture was allowed to stir for 1 h at room temperature. After 1 h the volatile components of the reaction mixture were removed *in vacuo* and the residue was washed with 2 mL pentane. Upon removal of solvent **4-3** was isolated as a red powder (0.087 g, 77 %). Melting point = 254-258 °C. ^{1}H NMR (300 MHz, benzene-d_6): δ 7.3-7.5 (overlapping peaks), 6.0, 4.2, 4.0, 2.6, 0.7-2.0 (overlapping peaks), 0.3. μ_{eff} (benzene-d_6): 1.65 μ_B (S = ½). Anal. Calcd. for $C_{40}H_{64}ICoP_3Si$: C, 56.40;

H, 7.57. Found: C, 56.35; H, 7.54.

[Cy-PSiP]Co(PMe_3)Cl (4-4). A solution of [Cy-PSiP]H (0.20 g, 0.34 mmol) and NEt_3 (0.34 g, 3.38 mmol) in ca. 5 mL THF was added to a solution of $CoCl_2$ (0.044 g, 0.34 mmol) in ca. 15 mL of THF. The solution was allowed to stir for 2 h, over which time a color change from light blue to dark brown was observed. After 2 hours, PMe_3 (0.026 g, 34 μL, 0.034 mmol) was added to the solution via syringe and the solution immediately turned deep red. The reaction mixture was then allowed to stir for 18 h at room temperature. After 18 h, the volatile components of the reaction mixture were removed *in vacuo* and the residue was extracted with 10 mL of benzene and filtered through Celite. The solvent was again removed *in vacuo* and the deep red residue was then washed with 2 × 2 mL pentane. Upon removal of solvent **4-4** was isolated as a red solid (0.071 g, 29%). Melting point = 164 °C (dec.). ^{1}H NMR (300 MHz, benzene-d_6): δ 7.6, 5.5, 3.2-4.2 (overlapping resonances), 2.4, 0.2-2.2 (overlapping resonances), -4.0, -5.7. μ_{eff} (benzene-d_6): 1.89 μ_B (S = ½). Anal. Calcd. for $C_{40}H_{64}ClCoP_3Si$: C, 63.19; H, 8.48. Found: C, 62.90; H, 8.36. Single crystals suitable for X-ray diffraction analysis were grown from 9:1 Et_2O/THF solution at -35 °C.

[Cy-PSiP]Co(PMe_3)(N_2) (4-5). **Method 1:** Magnesium powder (0.077g, 3.17 mmol) was added as a solid to a stirring solution of **4-4** (0.27, 0.32 mmol) in ca. 10 mL THF at room temperature. The solution was left to stir for 18 h over which time a color change from red to brown to orange-red was observed. After 18 h the solvent was removed *in vacuo* and the residue was extracted with ca. 10 mL of benzene and filtered through Celite. The filtrate was dried in *vacuo* and the resulting orange solid was washed with pentane (2 × 2 mL) to afford **4-5** as an orange solid (0.22 g, 97 %). **Method 2:** To a

solution of **4-2** (0.63 g, 0.81 mmol) in ca. 10 mL of THF was added PMe_3 (0.061 g, 82 μL, 0.81 mmol) via syringe. An immediate color change to deep red was observed and the reaction was allowed to stir for 1 h at room temperature. After 1 h, magnesium powder (0.20 g, 8.06 mmol) was added as a solid and the reaction mixture was stirred for 18 h, over which time a color change from deep red to brown to orange-red was observed. After 18 h, the solvent was removed *in vacuo* and the residue was extracted with ca. 15 mL of benzene. The benzene extract was filtered through Celite and the filtrate was dried under vacuum. The remaining residue was washed with pentane (2 × 2 mL) to afford **4-5** as an orange solid (0.59 g, 96 %). ^{1}H NMR (500 MHz, benzene-d_6): δ 7.72 (d, 2 H, J = 7 Hz, H_{arom}), 7.52 (apparent d, 2 H, J = 7 Hz, H_{arom}), 7.22 – 7.11 (overlapping resonances, 4 H, H_{arom}), 2.46 (m, 2 H, P*Cy*), 2.24 (m, 2 H, P*Cy*), 2.06-2.14 (overlapping resonances, 4 H, P*Cy*), 0.64-1.85 (overlapping resonances, 48 H, P*Cy* + P*Me*$_3$ (1.33 ppm, d, $^2J_{PH}$ = 6 Hz) + Si*Me* (0.75 ppm)). ^{13}C{^{1}H} NMR (125.8 MHz, benzene-d_6): δ 160.3 (apparent d, J = 62 Hz, C_{arom}), 146.3 (apparent t, J = 18 Hz, C_{arom}), 132.5 (apparent t, J = 11 Hz, *C*H_{arom}), 129.2 (*C*H_{arom}), 128.9 (*C*H_{arom}), 127.2 (*C*H_{arom}), 41.1 (apparent t, J = 24 Hz, *C*H_{Cy}), 33.1 (apparent t, J = 4 Hz, *C*H_{Cy}), 30.3 (*C*H_{2Cy}), 29.9 (*C*H_{2Cy}), 29.6 (*C*H_{2Cy}), 28.8 – 28.9 (overlapping resonances, *C*H_{2Cy}), 28.3 (*C*H_{2Cy}), 27.3 (*C*H_{2Cy}), 26.4 (*C*H_{2Cy}), 23.5 (d, $^2J_{PC}$ = 19 Hz, P*Me*$_3$), 8.1 (d, J = 13 Hz, Si*Me*). ^{31}P{^{1}H} NMR (202.5 MHz, benzene-d_6): δ 66.4 (d, 2 P, $^2J_{PP}$ = 83 Hz, Cy*P*Si*P*), -14.8 (t, 1 P, $^2J_{PP}$ = 83 Hz, *P*Me$_3$) . ^{29}Si NMR (99.4 MHz, benzene-d_6): δ 56.2. IR (Thin film, cm^{-1}): 2065 (s, N_2). Anal. Calcd. for $C_{40}H_{64}CoN_2P_3Si$: C, 63.81; H, 8.57, N, 3.72. Found: C, 63.47; H, 8.76; N, 3.55.

[Cy-PSiP]Co(PMe_3)(H_2) (4-6). **Method 1:** A degassed solution of **4-5** (0.010 g, 0.013 mmol) in a J. Young NMR tube was exposed to 1 atm H_2 with vigorous agitating of the solution. The solution changed color from orange to yellow-brown over the course of two minutes. The sample was then analyzed by ^{31}P and ^{1}H NMR indicating quantitative conversion of the starting **4-5** to [Cy-PSiP]Co(PMe_3)(H_2) (**4-6**). The sample was left under an atmosphere of H_2 to prevent decomposition. **Method 2:** To a solution of **4-5** (0.096 g, 0.13 mmol) in ca. 5 mL THF was added H_3NBH_3 (0.061 g, 0.81 mmol) as a solid. A slow color change from orange to yellow-brown was observed and the reaction was allowed to stir for 18 h at room temperature. After 18 h, an aliquot of the reaction mixture was analyzed by $^{31}P\{^{1}H\}$ NMR spectroscopy and the quantitative conversion of **4-5** to **4-6** was observed. ^{1}H NMR (300.1 MHz, benzene-d_6): δ 8.18 (d, 2 H, J = 7 Hz, H_{arom}), 7.22 – 7.32 (overlapping resonances, 4 H, H_{arom}), 7.09 (m, 2 H, H_{arom}), 2.52 (m, 2 H, P*Cy*), 2.00 - 2.20 (overlapping resonances, 6 H, P*Cy*), 1.09-1.81 (overlapping resonances, 42 H, P*Cy* + P*Me*$_3$ (1.33 ppm, d, $^{2}J_{PH}$ = 6 Hz) + Si*Me* (1.22 ppm)), 0.81 (m, 2 H, P*Cy*), 0.50 (m, 2 H, P*Cy*), -13.51 (broad t, 2 H, J = 38 Hz). $^{31}P\{^{1}H\}$ NMR (202.5 MHz, benzene-d_6): δ 91.6 (br s, 2 P, Cy*P*Si*P*), 0.1 (br s, 1 P, *P*Me_3).

4.4.3 Crystallographic Solution, Refinement and Structural Details for 4-1·C_7H_8, 4-2·C_7H_8, and 4-4

Crystallographic data for each of **4-1·C_7H_8**, **4-2·C_7H_8**, and **4-4** were obtained at 173(±2) K on a Bruker D8/APEX II CCD diffractometer using graphite-monochromated Mo Kα (λ = 0.71073 Å) radiation, employing a sample that was mounted in inert oil and transferred to a cold gas stream on the diffractometer. Programs for diffractometer operation, data collection, and data reduction (including SAINT) were supplied by

Bruker. Gaussian integration (face-indexed) was employed as the absorption correction method in each case. Structures for **4-1•C$_7$H$_8$** and **4-4** were solved by direct methods while the structure for **4-2•C$_7$H$_8$** was solved by Patterson search/structure expansion. All structures were refined by use of full-matrix least-squares procedures (on F^2) with R_1 based on $F_o^2 \geq 2\sigma(F_o^2)$ and wR_2 based on $F_o^2 \geq -3\sigma(F_o^2)$. During the structure solution process for each of **4-1•C$_7$H$_8$** and **4-1•C$_7$H$_8$** one equivalent of toluene was located in the asymmetric unit and refined in a satisfactory manner. Anisotropic displacement parameters were employed throughout for all the non-hydrogen atoms. All hydrogen atoms were added at calculated positions and refined by use of a riding model employing isotropic displacement parameters based on the isotropic displacement parameter of the attached atom. Additional crystal data can be found in Appendix A.

CHAPTER 5: Synthesis and Characterization of Low Coordinate (*N*-Phosphinoamidinate)Iron Complexes

5.1 Introduction

Over recent years there has been an increased effort in the isolation of low coordinate transition metal complexes, largely due to their potential to form highly reactive, coordinatively and electronically unsaturated species. Of particular interest is the isolation of first row transition metal complexes featuring a low coordination number (defined as 3 or less for the purposes of this document) due to the presence and exemplary reactivity of species of this type in metalloproteins.[84] In the case of metalloproteins, the low-coordinate environment of the transition metal is typically stabilized by the presence of non-coordinating bulky amino acid residues. In a similar fashion, one can envision mimicking this strategy in an effort to isolate low-coordinate first-row transition metal complexes by the use of an appropriate sterically demanding ancillary ligand. Efforts in this area of research have led to the isolation of a number three-coordinate transition metal complexes of both the early and late transition metals by the groups of Bradley,[85] Wolczanski,[86] and Cummins.[87] The reactivity of such three-coordinate complexes is largely limited to stoichiometric reactivity, due to the propensity of species of this type to form very strong bonds upon reaction, with complexes containing very strong metal-ligand multiple bonds often being formed.[85-87] The formation of strong bonds in such reactions has limited the applicability of species of this type in catalysis, due to the inability of such species to turnover catalytically. Current research in this area has focused on the use of ancillary ligands to support the formation of catalytically active, low-coordinate first-row transition metal complexes.

A series of recent reports from Holland have demonstrated that sterically demanding *β*-diketiminate ligands are effective at stabilizing a series of three-coordinate iron complexes.[88] Unlike analogous three-coordinate systems, three coordinate *β*-diketiminate-ligated iron complexes have demonstrated catalytic activity in C-F activation processes[89] and nitrene transfer reactions.[90] Although the reports of catalytic activity involving three-coordinate iron complexes are few, it is encouraging to observe that catalytic turnover is possible with the use of an appropriate ancillary ligand. In an effort to expand upon the chemistry reported by Holland, the use of alternative ancillary ligands to stabilize three-coordinate iron complexes was targeted. The successful application *β*-diketiminate ligands in this chemistry indicated that sterically demanding, monoanionic ligands are suitable for the stabilization of such three-coordinate complexes. Thusly, it is proposed that *N*-phosphinoamidinate ligation may also be appropriate for this application (Figure 5-1). Previously disclosed by Chevron Phillips Chemical Company, the neutral analogues of such ligands (*N*-phosphinoamidine) have been shown to be effective ancillary ligands in the chromium-catalyzed oligimerization of ethylene.[48] *N*-phosphinoamidinate ligation was targeted due to the highly modular nature of such bidentate ancillary ligands, facilitating the ability to fine-tune the steric profile of the ancillary ligand and therefore the resulting metal complexes. Furthermore, the incorporation of a soft phosphine donor into the ancillary ligand framework may potentially lead to reactivity that is divergent to that of complexes featuring two hard nitrogen donors, such as complexes featuring *β*-diketiminate ligation. In this chapter, the synthesis and characterization of sterically demanding *N*-phosphinoamidine ligands and

their corresponding low-coordinate (*N*-phosphinoamidinate)Iron complexes will be detailed.

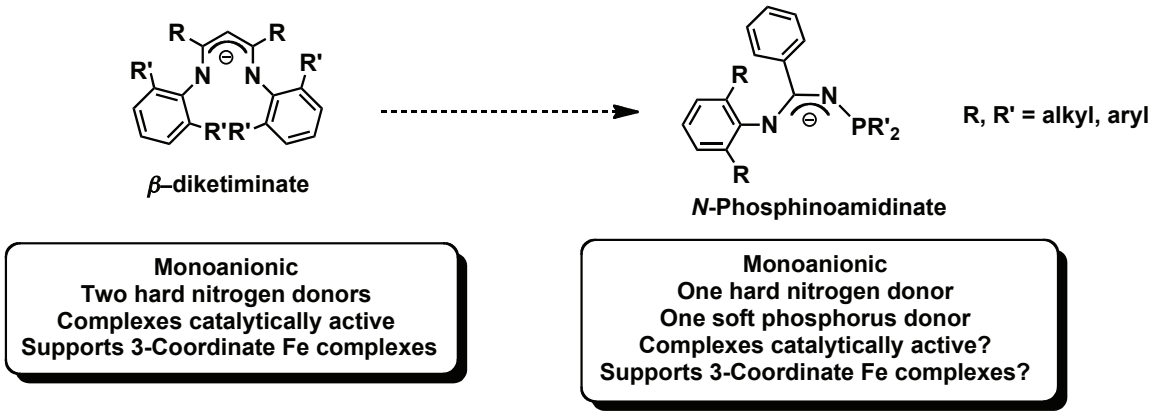

Figure 5-1. Comparison of *β*-diketiminate and *N*-phosphinoamidinate pro-ligands.

5.2 Results and Discussion

5.2.1 Synthesis and Characterization of *N*-Phosphinoamidine Pro-Ligands

Amidines can be prepared conveniently from nitriles and anilines,[48,91] and these amidines can be transformed into the corresponding *N*-phosphinoamidines upon treatment with ^{n}BuLi, followed by quenching with a chlorophosphine.[48] In an effort to access ligand variants featuring significant steric demand at both the nitrogen and phosphorus termini to support low-coordinate iron complexes, the preparation of new *N*-phosphinoamidines pairing bulky *N*-aryl (aryl = 2,6-dimethylphenyl, dmp; 2,6-diisopropylphenyl, dipp) and P^{t}Bu$_2$ functionalities were targeted (Scheme 5-1). Such reactions proceeded smoothly, affording **5-1a** and **5-1b** in 70 and 86% isolated yield, respectively.

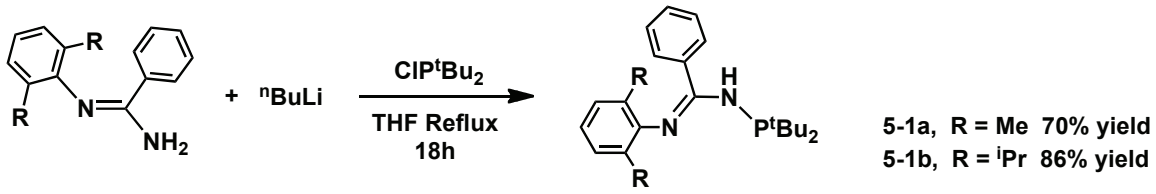

Scheme 5-1. Synthesis of *N*-phosphinoamidine pro-ligands **5-1a** and **5-1b**.

The existence of tautomers has been observed previously in solution for *N*-phosphinoamidines featuring alternative substitution patterns; for example, the previously reported diphenylphosphino analogue of **5-1a** is observed as a 65:35 tautomeric mixture, whereby in the major species the proton resides on the nitrogen that is connected to phosphorus, N(1).[48] However, only a single major isomeric form for each of **5-1a** and **5-1b** was observed at 300 K by use of ^{1}H, ^{13}C and ^{31}P NMR spectroscopy, with any alternative minor isomeric structures contributing much less significantly to the equilibrium mixture. While these phenomena are presently not well understood, it is evident that a single isomeric form of **5-1a** and **5-1b** is preferred due to the steric and/or electronic demands of the P^{t}Bu$_2$ moiety. The apparent phosphorus coupling observed for the N-*H* resonances in the ^{1}H NMR spectra of **5-1a** and **5-1b** supports the connectivity proposed in Scheme 5-1; this was further substantiated via the crystallographic characterization of **5-1b** (Figure 5-2; Table 5-1), whereby the (dipp)N-C distance (1.2807(19) Å) was found to be significantly shorter than the {P^{t}Bu$_2$}N-C distance (1.3679(19) Å).

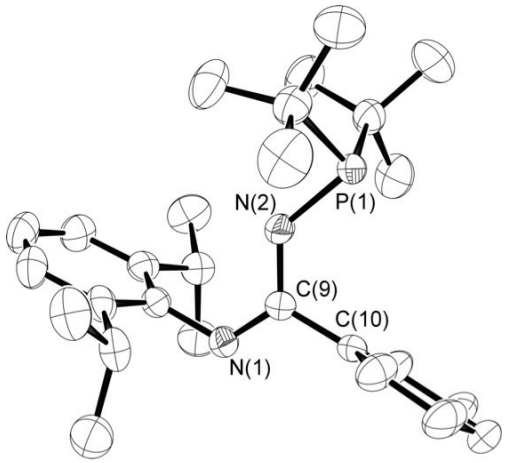

Figure 5-2. Crystallographically determined structure of **5-1b** employing 50% ellipsoids and with hydrogen atoms omitted for clarity.

In an effort to compare the effect of steric bulk of the phosphorus terminus on the resulting transition metal complexes, the diphenylphosphino analogue of **5-1b** (**5-1c**) was also prepared (Scheme 5-2). **5-1c** was synthesized via a similar route as pro-ligands **5-1a** and **5-1b** with a yield of 74% obtained. Unlike **5-1a** and **5-1b**, pro-ligand **5-1c** exists as a 3:1 tautomeric mixture in solution, similar to previously reported $P(Ph)_2$ and P^iPr_2 substituted *N*-phosphinoamidine ligands.[48] The existence of the tautomers can be easily detected in the $^{31}P\{^1H\}$ NMR spectrum, where two distinct resonances (δ= 28.9 and 26.2 ppm) are observed. The integrals of the two resonances in the $^{31}P\{^1H\}$ NMR spectrum integrate in a 3:1 ratio indicating a 3:1 mixture of the tautomers in solution. The ^1H NMR spectrum of the tautomeric mixture is somewhat convoluted due to a large amount of overlap between the resonances of both tautomers, however two very diagnostic N-H resonances can be observed at 4.98 (s) and 5.49 (br d) ppm, indicating a mixture that has protons residing on two different nitrogen atoms. The N-H resonance at 5.49 ppm integrates in a 3:1 ratio to the N-H resonance at 4.98 ppm. Furthermore, the major N-H

resonance at 5.49 ppm appears as a broad doublet, presumably due to ^{31}P coupling indicating that the major tautomer present in solution is likely the tautomer containing the N-H on the nitrogen adjacent to the phosphorus atom.

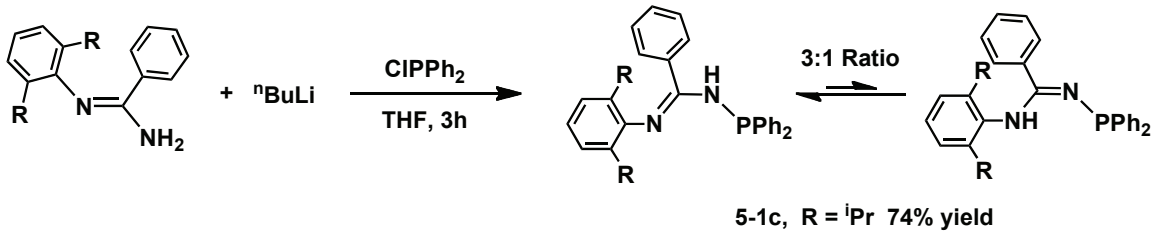

Scheme 5-2. Synthesis of *N*-phosphinoamidine pro-ligand **5-1c**.

5.2.2 Synthesis and Characterization of Low-Coordinate *N*-Phosphinoamidinate Complexes

Upon synthesizing pro-ligands **5-1a** and **5-1b**, initial attempts at the synthesis of low-coordinate iron complexes focused on attempting to ligate neutral *N*-phosphinoamidine pro-ligands **5-1a** and **5-1b** to simple anhydrous iron salts such as $FeCl_2$, $FeBr_2$ and solvates such as $FeCl_2(THF)_2$ and $FeCl_2(THF)_{1.5}$. It was proposed that such ligated FeX_2 (X = Cl, Br) complexes would be ideal precursors for *N*-phosphinoamidinate ligation, as such *N*-phosphinoamidine complexes could potentially undergo a dehydrohalogenation reaction to form *N*-phosphinoamidinate complexes. In all cases, complete consumption of **5-1a** and **5-1b** was observed by ^{31}P NMR spectroscopy regardless of the solvent used (benzene or THF) or the amount of heat applied to the reaction mixture to help facilitate the ligation (up to 85 °C). The difficulty encountered in the attempted ligation of the neutral *N*-phosphinoamidine pro-ligands suggested that another metalation strategy such as deprotometalation or transmetallation may be required in order to achieve optimal (*N*-phosphinoamidinate)iron ligation. To this effect, **5-1a** and **5-1b** were treated with $[Fe\{N(SiMe_3)_2\}_2]$ with the isolation of three-

coordinate *N*-phosphinoamidinate ligated iron-amido complexes being targeted. Upon the apparent loss of $HN(SiMe_3)_2$ via a presumed deprotometalation process, the formation of isolable, crystalline green-yellow solids from pentane solution was observed and were subsequently crystallographically characterized as being the respective (*N*-phosphinoamidinate)iron($N(SiMe_3)_2$) complexes **5-2a** (60 %) and **5-2b** (62 %) (Scheme 5-3). As a point of comparison in reactivity and catalysis, a Co^{II} variant of **5-2b** was also prepared. Under analogous conditions employing $[Co\{N(SiMe_3)_2\}_2]$ and **5-1b**, the (*N*-phosphinoamidinate)cobalt($N(SiMe_3)_2$) complex **5-2c** was obtained as a red crystalline solid in 68 % isolated yield. Elemental analysis data confirmed the absence of additional co-ligands in these paramagnetic complexes, and the measured room temperature solution magnetic moments indicated that the iron complexes **5-2a** and **5-2b** feature $S = 2$ spin centers, while the cobalt complex **5-2c** features an $S = 3/2$ spin center. Three-coordinate *β*-diketiminate-ligated iron complexes reported by Holland also exhibit high spin electronic configurations,[88] suggesting that three-coordinate *β*-diketiminate-ligated and *N*-phosphinoamidinate-ligated iron complexes may exhibit similar electronic properties.

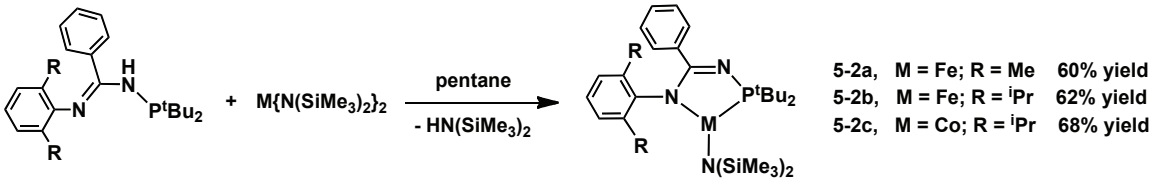

Scheme 5-3. Synthesis of *N*-Phosphinoamidinate-ligated iron and cobalt amido complexes **5-2a** - **5-2c**.

The crystallographic characterization of **5-2a** - **5-2c** (Figure 5-3; Table 5-1) confirms the three-coordinate, trigonal planar nature of these species. Significant differences in the interatomic distances are observed between the neutral (protonated)

pro-ligand **5-1b** and the resultant monoanionic P,N ligands featured in **5-2a** - **5-2c**. Notably, the P-N(1) and N(1)-C(9) distances are shorter in the complexes relative to **5-1b**, while conversely the N(2)-C(9) distances in **5-2a** - **5-2c** are significantly longer than that found in **5-1b**. These structural data suggest that the complexes are best viewed as featuring phosphine-amido ligands, with the formal negative ligand charge residing on N(2), as represented in Scheme 5-2. The sum of the bond angles at the metal confirmed a trigonal planar geometry in each complex (**5-2a**, 358.1º; **5-2b**, 360.0º; **5-2c**, 360.0º), and no significant variation in the P-Fe-N(2) bond angle (i.e., chelating ligand bite angle) was observed between the structurally related complexes **5-2a** and **5-2b**, which feature dmp and dipp substituents at nitrogen, respectively. Within each of **5-2a** - **5-2c**, the ligands are not symmetrically distributed within the trigonal plane, displaying the following progression: P-M-N(2) (ca. 81º) < P-M-N(3) (ca. 132º) < N(2)-M-N(3) (ca. 145º). The overall metrical parameters in **5-2a** and **5-2b** mirror those found in related three-coordinate (N~N)FeX complexes supported by bis(phosphinimino)methanide[92] or *β*-diketiminate ligands,[88,93] with the exception of the chelating ligand bite angle (112º[92] and 95º [88,93] respectively; *cf* 81º in **5-2a** and **5-2b**). Although the identification of three-coordinate iron(II) complexes featuring chelating phosphine-amido ligation in the chemical literature was unsuccessful, the Fe-P and Fe-N distances in recently reported four-coordinate complexes of this type are comparable to those involving the chelating ligands within **5-2a** and **5-2b**.[94]

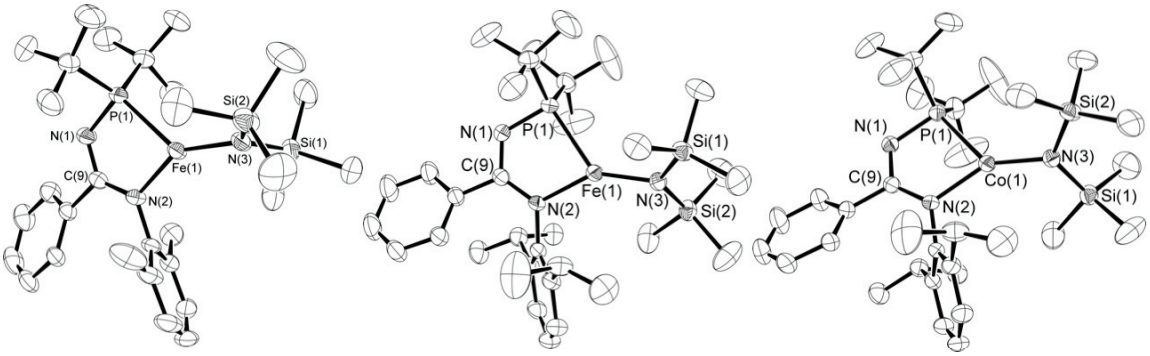

Figure 5-3. Crystallographically determined structures of **5-1a** (left), **5-2b** (center), and **5-2c (**right**)** employing 50% ellipsoids and with hydrogen atoms omitted for clarity.

	5-1b[a]	**5-2a**	**5-2b**[a]	**5-2c**[a]
M-P	--	2.4313(6)	2.4434(6)	2.3873(7)
M-N(2)	--	1.9978(18)	2.0013(15)	1.9762(18)
M-N(3)	--	1.9111(19)	1.9106(16)	1.8939(19)
P-N(1)	1.7174(14)	1.6862(19)	1.6804(17)	1.674(2)
N(1)-C(9)	1.3679(19)	1.309(3)	1.316(2)	1.316(3)
(aryl)N(2)-C(9)	1.2807(19)	1.363(3)	1.353(2)	1.351(3)
P-M-N(3)	--	132.86(6)	132.59(5)	132.04(6)
P-M-N(2)	--	81.10(6)	81.12(5)	81.56(6)
N(2)-M-N(3)	--	144.15(9)	145.84(7)	146.39(8)
Σ angles at M	--	358.1	360.0	360.0

Table 5-1. Selected interatomic distances (Å) and angles (º) for **5-1b**, **5-2a**, **5-2b**, and **5-2c**. [a]Representative data for only one of the two crystallographically independent molecules.

Encouraged by the successful synthesis of three-coordinate amido complexes **5-2a** - **5-2c**, the synthesis of *N*-phosphinoamidine/amidinate ligated, low-coordinate iron complexes featuring alternative substitutions (eg. alkyl, halide) were targeted. In an effort to isolate a three-coordinate (*N*-phosphinoamidate)iron(alkyl) complex, pro-ligand **5-1b** was allowed to react with one equiv. $Fe(Py)_2(CH_2SiMe_3)_2$ in benzene at room temperature for 18 hours. $Fe(Py)_2(CH_2SiMe_3)_2$ was chosen as a starting material due to the presence of the CH_2SiMe_3 groups, which could potentially facilitate *N*-phosphinoamidine/amidinate ligation by liberating an equivalent of $Si(CH_3)_4$ upon

reaction via deprotonation of **5-1b**, potentially resulting in the isolation of a (*N*-phosphinoamidinate)Fe(CH_2SiMe_3) complex. Upon extraction of the crude reaction mixture with pentane, a small amount of the four-coordinate (*N*-phosphinoamidinate)Fe(CH_2SiMe_3)(Py) complex **5-3** was recrystallized from pentane extract and crystallographically characterized as an orange, four-coordinate pyridine adduct (Scheme 5-3). Despite crystallographically characterizing **5-3** from this reaction muxture, the ^{1}H NMR of the reaction mixture suggests there are multiple products (both paramagnetic and diamagnetic) present in solution. Attempts to isolate an analytically pure sample of **5-3** as well as identifying the other products of this reaction are ongoing.

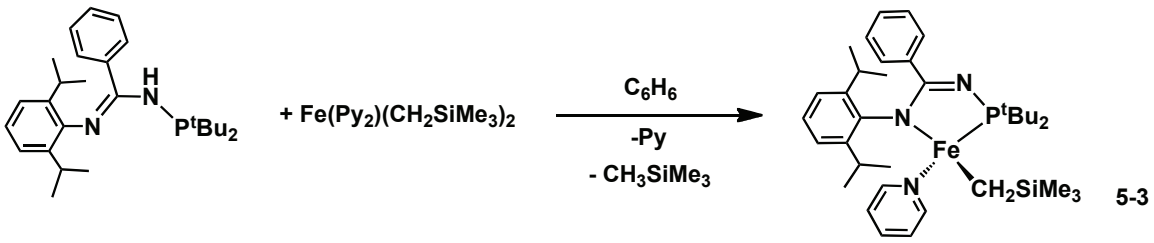

5-3

Scheme 5-4. Synthesis of (*N*-Phosphinoamidinate)iron(alkyl) complex **5-3**.

The crystallographic characterization of **5-3** (Figure 5-5; Table 5-2) confirmed the four-coordinate nature of this species. In a similar fashion to complexes **5-2a** - **5-2c**, distortions in the bond lengths of the P,N ligand are observed relative to the neutral (protonated) species **5-1b**, suggesting that the ligation in these complexes is best described as being *N*-phosphinoamidate ligation, or alternatively as phosphine-amido ligation (Table 5-2). The bond angles at the metal centre range from 79.3º (P-Fe-N(1)) - 132.8º (N(1)-Fe-C(28))º, suggesting **5-3** exhibits a geometry that is significantly distorted from the idealized tetrahedral geometry in the solid state. Such large distortions from an idealized tetrahedral geometry is likely due to the rigid, chelating nature of the P,N ligand as well as the steric bulk of the ligand. Furthermore, a small variation in the chelating

ligand bite angle was observed between the structurally related complexes **5-3** and **5-2b** (79.3º vs. 81.1º). The Fe-P and Fe-N distances in recently reported four-coordinate complexes of this type are comparable to those involving the chelating ligands within **5-3**.[94]

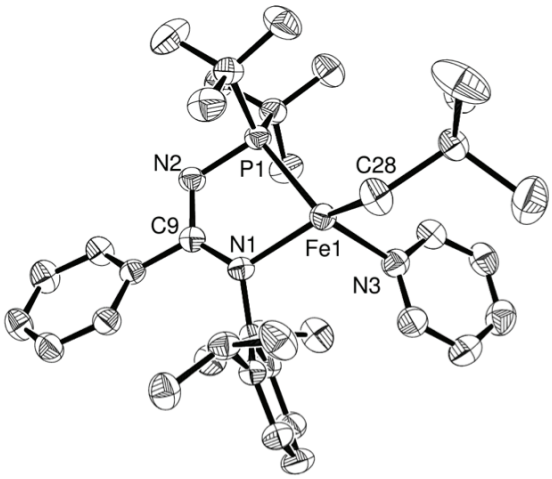

Figure 5-4. Crystallographically determined structure of **5-3** employing 50% ellipsoids and with hydrogen atoms omitted for clarity.

5.2.3 Attempted Synthesis and Characterization of *N*-Phosphinoamidinate Iron Chloride Complexes

Upon the synthesis of complexes **5-2a** - **5-2c** and **5-3**, an alternative pathway to (*N*-phosphinoamidinate)iron complexes was sought, due to the time and cost associated in preparing the $[Fe\{N(SiMe_3)_2\}_2]$[95] and $[Fe(Py)_2(CH_2SiMe_3)_2]$[96] starting materials. A synthesis involving non pre-functionalized iron starting materials such as $FeCl_2$ would be ideal, as the anticipated ligated iron-halide products would provide an optimal route to alternatively functionalized (*N*-phosphinoamidinate)Iron complexes via the use of lithium salts, reducing agents, Grignard reagents, etc. Reaction of **5-1b** and $FeCl_2$ in THF or pyridine appeared to afford no reaction upon heating as a large amount unreacted **5-1b** could be observed in the reaction mixtures via $^{31}P\{^1H\}$ NMR spectroscopy.

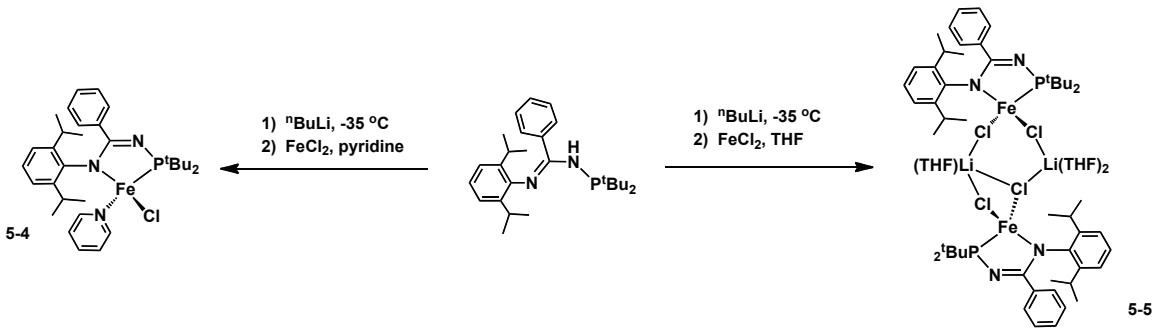

Scheme 5-5. Synthesis of (*N*-phosphinoamidinate)iron(chloride) complexes **5-4** and **5-5**.

In an effort to promote the ligation of **5-1b** to $FeCl_2$, **5-1b** was treated with ^{n}BuLi in pentane at -35 ºC, to presumably form a *N*-phosphinoamidinate lithium salt (Scheme 5-5). After decantation of the pentane supernatant, the lithium salt was dissolved in a more polar solvent (pyridine or THF) and was then allowed to react with $FeCl_2$ at room temperature, resulting in the formation of a deep brown solution. When the reaction was conducted in pyridine solvent, a small amount (ca. 10% yield) of the yellow (*N*-phosphinoamidinate)Fe(Cl)(Py) complex **5-4** was isolated as a crystalline solid after recrystallization of the crude reaction mixture from toluene (Scheme 5-5, Figure 5-5). Unfortunately, attempts at reproducing this synthesis and recrystallization several times has proved unsuccessful, with a mixture of **5-4** (yellow) and an unidentified red compound being isolated. It is proposed that the unidentified red compound may be a $(P,N)_2Fe$ complex where two equiv. of the lithium salt generated from **5-1b** underwent reaction with $FeCl_2$. Alternatively, when conducting the reaction in THF, a small amount of yellow crystals (ca. 10 % yield) were recrystallized from the pentane extract of the crude reaction mixture. The crystals were determined to be compound **5-5** by X-Ray diffraction, where both LiCl and THF have been retained in the crystal lattice (Scheme 5-4, Figure 5-5). The retention of LiCl and THF in the crystal lattice **5-5** is not desired, as the presence of LiCl and THF in **5-5** could potentially result in reactivity alternative to

that of an idealized (*N*-phosphinoamidinate)Fe(Cl) complex. Attempts at reproducibly isolating a (*N*-phosphinoamidinate)Fe(halide) complex are ongoing, with current efforts focusing on using alternative iron sources. Such reactions appear to be producing products in higher yields, however full characterization of the products of these reactions has yet to be conducted.

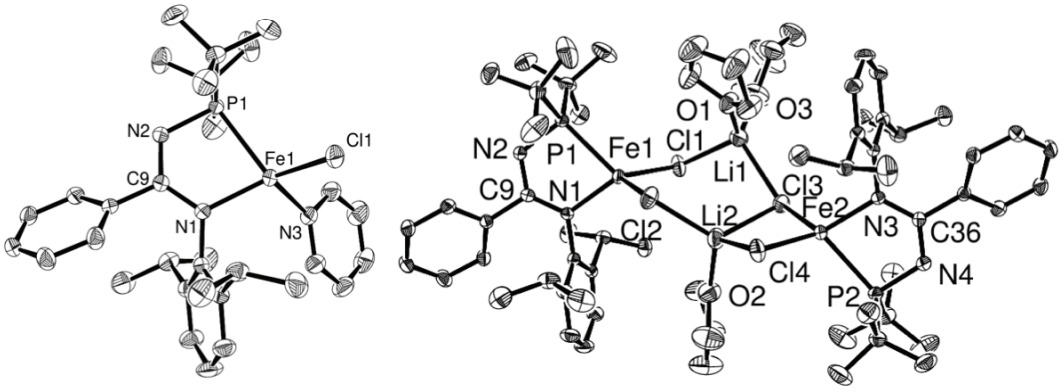

Figure 5-5. Crystallographically determined structure of **5-4•0.5C$_7$H$_8$** and **5-5** employing 50% ellipsoids with solvent molecules and hydrogen atoms omitted for clarity.

The crystallographic characterization of **5-4** and **5-5** (Figure 5-5; Table 5-2) confirmed the four-coordinate nature of these species. In a similar fashion to complexes **5-2a** - **5-2c** and **5-3**, distortions in the bond lengths of the P,N ligands in **5-4** and **5-5** are observed relative to the neutral (protonated) species **5-1b**, suggesting that the ligation in these complexes is best described as being *N*-phosphinoamidate ligation. Complexes **5-4** and **5-5** adopt a distorted tetrahedral geometry similar to that of **5-3**, as the bond angles and distances around the metal are comparable to complex **5-3**. Furthermore, the Fe-P and Fe-N distances in recently reported four-coordinate complexes of this type are comparable to those involving the chelating ligands within **5-4** and **5-5**.[94] Unfortunately, due to the small amount of **5-4** and **5-5** obtained, as well as the difficulty in reproducing these reactions full characterization of **5-4** and **5-5** is incomplete.

	5-1b[a]	**5-3**	**5-4•0.5C_7H_8**	**5-5**
Fe-P	--	2.4324(8)	2.4372(5)	2.4392(5)
Fe-N(1)	--	2.0144(13)	2.0013(15)	2.0219(15)
Fe-C(28)/Fe-Cl	--	2.045(3)	2.2460(5)	--
P-N(2)	1.7174(14)	1.683(3)	1.6912(13)	1.6841(17)
(aryl)N(1)-C(9)	1.3679(19)	1.353(3)	1.353(2)	1.348(2)
N(2)-C(9)	1.2807(19)	1.321(3)	1.315(2)	1.324(2)
P-Fe-N(1)	--	79.25(6)	80.23(4)	79.82(4)

Table 5-2. Selected interatomic distances (Å) and angles (º) for **5-3**, **5-4**, and **5-5**. [a]Representative data for only one of the two crystallographically independent molecules.

5.2.3 Synthesis and Characterization of a (*N*-Phosphinoamidinate)Iron Complex Featuring Two *N*-Phosphinoamidinate Ligands

In an effort to compare the effect of steric bulk of the phosphorus terminus on the structure and reactivity of (*N*-phosphinoamidinate)iron complexes, the synthesis of an analogue of **5-2b** featuring $P(Ph)_2$ substitution was pursued. Reaction of the $P(Ph)_2$ substituted pro-ligand **5-1c** with one equiv. $[Fe\{N(SiMe_3)_2\}_2]$ at room temperature in C_6H_6 resulted in an immediate color of change of the reaction mixture from green to red. Upon recrystallization of the reaction mixture from Et_2O, the (*N*-phosphinoamidinate)iron complex **5-6**, featuring the ligation of two P,N ligands to the metal center was isolated in 30% yield. Repeating the synthesis using 2 equiv. **5-1c** relative to $[Fe\{N(SiMe_3)_2\}_2]$ resulted in the isolation of **5-6** in a slightly higher yield of 45% (Scheme 5-5). Elemental analysis data confirmed the absence of additional co-ligands in **5-6**, and the measured room temperature solution magnetic moments indicated that **5-6** features a $S = 2$ spin center, a high spin electronic configuration similar to iron complexes **5-2a** and **5-2b**.

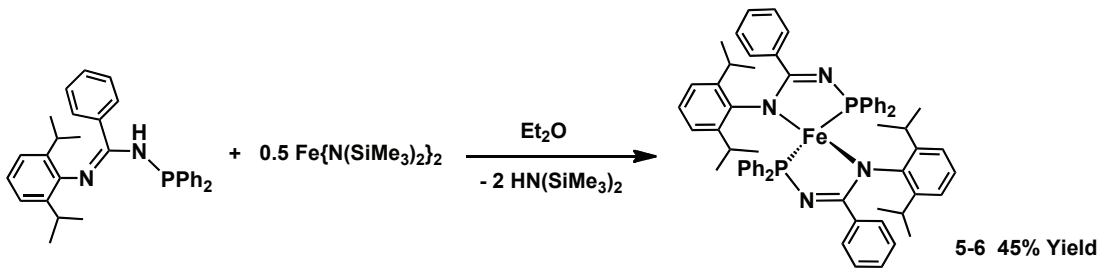

Scheme 5-6. Synthesis of Iron(*N*-phosphinoamidinate)$_2$ complex **5-6**.

The crystallographic characterization of **5-6•Et$_2$O** (Figure 5-6; Table 5-3) confirms the four-coordinate nature of this species, indicating that the formation of three-coordinate iron-amido complexes is not favourable when the less sterically demanding P(Ph)$_2$ substitution is employed. Notably, the bond lengths and angles within the two P,N ligands of **5-6** are very comparable to each other, with no notable deviations. Furthermore, the bond lengths within the P,N ligand in **5-6** mirror those of **5-2b** that features P^{t}Bu$_2$ substitution. For example, the N(2)-C(13) and N(4)-C(44) interatomic distances in **5-6** were determined to be 1.3222(19) and 1.3194(19) Å, comparable to the analogous N(1)-C(9) interatomic distance of 1.316(2) Å in **5-2b**, which was determined to be shorter than the same bond in pro-ligand **5-1b** (1.3679(19) Å). This structural data suggests that **5-6** is best viewed as featuring two *N*-phosphinoamidinate ligands. The geometry around the metal center is best described as a distorted tetrahedral geometry, with the distortions likely being caused by the rigid, chelating nature of the P,N ligand. Bond angles around the metal center range from ca. 79º (P(1)-Fe-N(1)) to 144º (N(1)-Fe-N(3))º, demonstrating the distortions from an optimized tetrahedral geometry. The P-Fe-N bond angles (i.e., chelating ligand bite angle) in **5-6** were observed to be ca. 79º and 81º, extremely similar to the bite angle of 81º observed in the structurally related complex **5-2b**, suggesting that alternative substitution at phosphorus does not result in a significant

deviation of the bite angle of the chelating ligand. Futhermore, the Fe-P and Fe-N interatomic distances in **5-6** are comparable to four-coordinate complexes of this type featuring phosphine-amido ligation.[94]

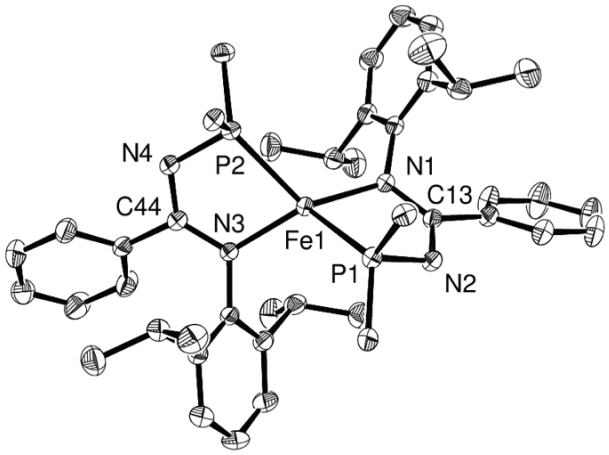

Figure 5-6. Crystallographically determined structure of **5-6·Et$_2$O** employing 50% ellipsoids. Phenyl substituents, Et_2O and hydrogen atoms omitted for clarity.

	5-1b[a]	**5-2b**	**5-6·Et$_2$O**
Fe-P(1)	--	2.4313(6)	2.4463(4)
Fe-N(1)/Fe-N(2)	--	1.9978(18)	2.0156(15)
N(1)-C(9)/ N(2)-C(13)	1.3679(19)	1.309(3)	1.316(2)
(aryl)N(2)-C(9)/(aryl)N(1)-C(13)	1.2807(19)	1.363(3)	1.3629(17)
P-Fe-N	--	81.10(6)	79.47(3)

Table 5-3. Selected Interatomic Distances (Å) and Angles (º) for **5-1b**, **5-2b**, and **5-6·Et$_2$O**. [a]Representative data for only one of the two crystallographically independent molecules.

5.3 Conclusions

N-phosphinoamidine pro-ligands **5-1a** - **5-1c** were found to be readily accessible through the lithiation of amidines and subsequent quenching with a chlorophosphine. The ligation of such pro-ligands as neutral *N*-phosphinoamidines to iron centers was

found to be unsuccessful, typically resulting in no reaction or an incomplete reaction. Alternatively, attempts at monoanionic *N*-phosphinoamidinate ligation were met with considerable success. Ligation of P^tBu_2 substituted *N*-phosphinoamidine pro-ligand **5-1b** via deprotometalation reactions resulted in the formation of three-coordinate, high spin iron-amido complexes **5-2a** - **5-2c** in moderate yields as crystalline solids.

Attempts at isolating (*N*-phosphinoamidinate)Iron(alkyl) and (*N*-phosphinoamidinate)Iron(chloride) complexes were met with less success as the reproducible synthesis and isolation of alkyl and chloride complexes **5-3** - **5-5** has remained elusive. Current efforts towards the isolation of a (*N*-phosphinoamidinate)iron(halide) complex are focused on using alternative iron sources. Attempted synthesis of an analogue of **5-2b** featuring less bulky $P(Ph)_2$ substitution resulted in the formation of four-coordinate complex **5-6**, where two P,N ligands underwent ligation to the metal center. This observation suggests that bulky substitution at phosphorus is required for the isolation of three-coordinate complexes featuring *N*-phosphinoamidinate ligation. The reactivity of complexes **5-2a** - **5-2c** in catalytic applications will be described in subsequent chapters.

5.4 Experimental Section

5.4.1 General Considerations

Unless otherwise noted, all experiments were conducted under nitrogen in a glovebox apparatus or using standard Schlenk techniques. Dry, deoxygenated solvents were used unless otherwise indicated. Pentane and benzene were deoxygenated and dried by sparging with nitrogen and subsequent passage through a double-column solvent

purification system with one column packed with activated alumina and one column packed with activated Q5. Tetrahydrofuran and diethyl ether were dried over Na/benzophenone and distilled under nitrogen. Benzene-d_6 (Cambridge Isotopes) was degassed via three repeated freeze-pump-thaw cycles. ^{1}H, ^{13}C, and ^{31}P NMR characterization data for compounds **5-1a** - **5-1c** were collected at 300K on a spectrometer operating at 500.1, 125.8, and 202.5 MHz (respectively) with chemical shifts reported in parts per million downfield of $SiMe_4$ (for ^{1}H, ^{13}C), and 85% H_3PO_4 in D_2O (for ^{31}P). ^{1}H and ^{13}C NMR chemical shift assignments are based on data obtained from ^{13}C-DEPTQ, ^{1}H-^{1}H COSY, ^{1}H-^{13}C HSQC, and ^{1}H-^{13}C HMBC NMR experiments. ^{1}H characterization data for compounds **5-2a** - **5-2c** and **5-6** were collected at 300K on a spectrometer operating at 300.1 MHz with chemical shifts reported in parts per million downfield of $SiMe_4$. [M{N($SiMe_3$)$_2$}$_2$] (M = Fe, Co)[95,97] and amidines[48] were prepared according to literature procedures. Infrared spectra were recorded as thin films between NaCl plates using a Bruker TENSOR 27 FT-IR spectrometer at a resolution of 4 cm^{-1}. X-Ray data collection was carried out by Dr. Robert MacDonald and Dr. Michael J. Ferguson at the University of Alberta X-ray Crystallography Laboratory, Edmonton, Alberta. Magnetic moments (Evans method) were determined according to literature procedures.[83]

5.4.2 Synthetic Procedures and Characterization Data

Synthesis of 5-1a. N^1-(2,6-dimethylphenyl)benzamidine (2.00 g, 7.13 mmol) was added to an oven-dried round bottom flask with a reflux condenser attached and placed under vacuum. After 20 minutes, the white solid was dissolved in ca. 150 mL THF and

cooled to -78 °C. ^{n}BuLi (2.85 mL, 2.5 M in hexanes, 7.13 mmol) was added to the cooled solution dropwise over 10 minutes. Upon complete addition of ^{n}BuLi, the white suspension was allowed to warm to room temperature over two hours. After two hours, ClP(^{t}Bu)$_2$ (1.36 mL, 7.13 mmol) was added to the suspension dropwise at room temperature over 10 minutes. The reaction mixture was then allowed to stir at reflux temperature for 18 hours. The resulting clear yellow reaction mixture was cooled to room temperature and the volatile components were removed *in vacuo*. The residue was extracted with 20 mL benzene and filtered through celite and the filtrate was concentrated *in vacuo*. The sample was then triturated with pentane (3 × 2 mL) and dried *in vacuo* to yield **5-1a** as an off-white amorphous solid (1.85 g, 70%). Melting point = 96-98 °C. ^{1}H NMR (500 MHz, benzene-d_6): δ 7.92 (d, 2 H, J = 8 Hz, H_{arom}), 7.24 (apparent t, 2 H, J = 8 Hz, H_{arom}), 7.18 (apparent d, 1 H, J = 8 Hz, H_{arom}), 7.11 (apparent d, 2 H, J = 8 Hz, H_{arom}), 6.95 (apparent t, 1 H, J = 8 Hz, H_{arom}), 5.15 (br d, 1H, N*H*), 2.36 (s, 6 H, Ar*Me*$_2$), 0.81 (d, 18 H, $^{3}J_{PH}$ = 12 Hz, P*CMe*$_3$). ^{13}C{^{1}H} NMR (300 K, 125.8 MHz, benzene-d_6): δ 157.9 (d, $C_{arom,}$ J = 15 Hz), 147.4 (C_{arom}) 137.7 (sp$^2C_{amidine}$), 130.7 (CH$_{arom}$), 129.9 (CH$_{arom}$), 129.4 (CH$_{arom}$), 129.2 (C_{arom}), 128.2 (overlapped with C_6D_6, CH$_{arom}$) 123.9 (CH$_{arom}$), 34.7 (d, J = 24 Hz, P*C*Me$_3$), 28.4 (d, J = 15 Hz, P*CMe*$_3$), 19.0 (Ar*Me*$_2$). ^{31}P{^{1}H} NMR (300 K, 202.5 MHz, benzene-d_6): δ 61.9. IR (Thin film, cm^{-1}): 3315 (m, N-*H*), 1623 (s, N=C). HRMS (ESI/[M+H]$^+$ calcd. for $C_{23}H_{34}N_2P$: 369.2454. Found: 369.2465.

Synthesis of 5-1b. N^1-(2,6-diisopropylphenyl)benzamidine (6.20 g, 22.1 mmol) was added to an oven-dried round bottom flask with a reflux condenser attached and placed under vacuum. After 20 minutes, the white solid was dissolved in ca. 250 mL THF and cooled to -78 °C. ^{n}BuLi (8.84 mL, 2.5 M in hexanes, 22.1 mmol) was added to

the cooled solution dropwise over 10 minutes. Upon complete addition of ^{n}BuLi, the white suspension was allowed to warm to room temperature over two hours. After two hours, $ClP(^{t}Bu)_2$ (4.20 mL, 22.1 mmol) was added to the suspension dropwise at room temperature over 5 minutes. The reaction mixture was then allowed to stir at reflux temperature for 18 hours. The resulting clear yellow reaction mixture was cooled to room temperature and the volatile components were removed *in vacuo*. The residue was extracted with 20 mL benzene and filtered through Celite and the filtrate was concentrated *in vacuo*. The sample was then washed with pentane (3 × 2 mL) and dried *in vacuo* to yield **5-1b** as an off-white amorphous solid (8.10 g, 86%). Melting point = 97-99 °C. ^{1}H NMR (500 MHz, benzene-d_6): δ 7.92 (d, 2 H, J = 8 Hz, H_{arom}), 7.21-7.26 (m, overlapping resonances, 4 H, H_{arom}), 7.12-7.15 (m, 2 H, H_{arom}), 5.15 (d, 1 H, N*H*, J = 9 Hz), 3.34 (m, 2 H, C$H_{isopropyl}$), 1.38 (d, 6 H, ^{3}J = 7 Hz, C$H_{3isopropyl}$), 1.32 (d, 6 H, ^{3}J = 7 Hz, C$H_{3isopropyl}$), 0.84 (d, 18H, $^{3}J_{PH}$ = 12 Hz, PCMe_3). $^{13}C\{^{1}H\}$ NMR (300 K, 125.8 MHz, benzene-d_6): δ 157.2 (d, $C_{arom,}$ J = 16 Hz), 144.8 (C_{arom}), 139.2 (C_{arom}), 137.6 ($sp^2C_{amidine}$), 130.4 (CH_{arom}), 129.6 (CH_{arom}), 128.3 (overlapped with C_6D_6, CH_{arom}), 124.4 (CH_{arom}), 123.9 (CH_{arom}), 34.5 (d, J = 23 Hz, PCMe_3), 29.4 ($CH_{isopropyl}$), 28.3 (d, J = 15 Hz, PCMe_3), 24.8 ($CH_{3isopropyl}$), 22.3 ($CH_{3isopropyl}$). $^{31}P\{^{1}H\}$ NMR (300 K, 202.5 MHz, benzene-d_6): δ 61.4. IR (Thin film, cm^{-1}): 3315 (m, N-*H*), 1625 (s, N=C). HRMS (ESI/$[M+H]^+$ calcd. for $C_{27}H_{42}N_2P$: 425.3100. Found: 425.3080. A single crystal suitable for X-ray diffraction analysis was grown from a concentrated pentane solution at -35 °C.

Synthesis of 5-1c. N^1-(2,6-diisopropylphenyl)benzamidine (2.35 g, 8.4 mmol) was added to an oven-dried round bottom flask with a reflux condenser attached and

placed under vacuum. After 20 minutes, the white solid was dissolved in ca. 100 mL THF and cooled to -78 °C. ^{n}BuLi (3.35 mL, 2.5 M in hexanes, 8.4 mmol) was added to the cooled solution dropwise over 3 minutes. Upon complete addition of ^{n}BuLi, the white suspension was allowed to warm to room temperature over two hours. After two hours, $ClP(Ph)_2$ (1.55 mL g, 8.4 mmol) was added to the suspension dropwise at room temperature over 2 minutes and the reaction mixture was then allowed to stir at room temperature for 3 hours. After 3 hours, the volatile components of the reaction mixture were removed *in vacuo*. The residue was extracted with 20 mL benzene, filtered through Celite, and concentrated *in vacuo*. The sample was suspended in 25 mL pentane and filtered away from the yellow supernatant. The off-white filtrate was then dried *in vacuo* to yield **5-1c** as an off-white amorphous solid (2.86 g, 74%). Melting point = 90-94 °C. ^{1}H NMR (500 MHz, benzene-d_6): δ 7.85-8.01 (overlapping resonances, H_{arom}), 7.83 (d, J = 7 Hz, H_{arom}), 7.26 (d, J = 8 Hz, H_{arom}), 6.90-7.19 (overlapping resonances, H_{arom}) 5.49 (br d, N*H*, J = 9 Hz), 4.98 (s, N*H*), 3.21 (overlapping resonances, C$H_{isopropyl}$), 1.26 (m, C$H_{3isopropyl}$), 1.12 (apparent d, J = 6 Hz, C$H_{3isopropyl}$). ^{13}C{^{1}H} NMR (300 K, 125.8 MHz, benzene-d_6): δ 152.8 (C_{arom}), 146.1 (C_{arom}), 145.1 (C_{arom}), 141.5 (C_{arom}), 141.4 (C_{arom}), 139.8 (C_{arom}), 139.4 (C_{arom}), 136.6-136.8 (overlapping resonances, CH$_{arom}$), 132.3 (CH$_{arom}$), 132.0 (CH$_{arom}$), 131.9 (CH$_{arom}$), 131.7 (CH$_{arom}$), 130.9 (CH$_{arom}$), 130.8 (CH$_{arom}$), 130.4 (CH$_{arom}$), 130.0 (CH$_{arom}$), 129.5 (CH$_{arom}$), 129.2 (CH$_{arom}$), 129.1 (CH$_{arom}$), 129.0 (CH$_{arom}$), 128.3 (overlapped with C_6D_6, CH$_{arom}$), 127.7 (CH$_{arom}$), 124.7 (CH$_{arom}$), 124.4 (CH$_{arom}$), 124.3 (CH$_{arom}$), 123.9 (CH$_{arom}$), 29.6 (CH$_{isopropyl}$), 29.4 (CH$_{isopropyl}$), 24.2-24.5 (overlapping resonances, CH$_{3isopropyl}$), 23.1 (CH$_{3isopropyl}$). ^{31}P{^{1}H} NMR (300 K, 202.5 MHz, benzene-d_6): δ 28.9, 26.3. IR (Thin film, cm^{-1}): 3312 (m, N-*H*), 1636 (s, N=C).

Synthesis of 5-2a. A solution of **5-1a** (0.150 g, 0.42 mmol) in ca. 2 mL of pentane was added via pipette to a solution of [Fe{N(SiMe$_3$)$_2$}$_2$] (0.158 g, 0.42 mmol) in ca. 1 mL of pentane. The reaction mixture was allowed to sit at room temperature and a color change from pale green to amber was observed over 1 hour. The reaction mixture was then filtered through Celite to remove a small amount of a fine white precipitate and concentrated to ca. 0.5 mL *in vacuo*. The concentrated solution was placed in the freezer at -35 °C and was allowed to sit for 1 hour. After 1 hour the brown supernatant was decanted and the green-yellow solid was washed with cold (-35 °C) pentane (2 × 0.5 mL). The volatile components were removed *in vacuo* to yield **5-2a** as a crystalline (paralelipiped) green-yellow solid (0.146 g, 60%). Melting point = 107-109 °C. ^{1}H NMR (300.1 MHz, benzene-d_6): δ 98.7 (1 H), 46.1 (2 H), 31.6 (2 H), 28.8 (18 H), 7.5 (2 H) - 14.2 (6 H), -44.0 (18 H), -65.9 (1 H). μ_{eff} (benzene-d_6): 5.04 μ_B, S = 2. Anal. Calcd. for $C_{29}H_{50}FeN_3PSi_2$: C, 59.67; H, 8.63; N, 7.20. Found: C, 58.61; H, 8.60; N, 7.02. A single crystal suitable for X-ray diffraction analysis was grown from a concentrated pentane solution at -35 °C.

Synthesis of 5-2b. A solution of **5-1b** (0.150 g, 0.35 mmol) in ca. 1 mL of pentane was added via pipette to a solution of [Fe{N(SiMe$_3$)$_2$}$_2$] (0.133 g, 0.35 mmol) in ca. 1 mL of pentane. The reaction mixture was allowed to sit at room temperature and a color change from pale green to amber was observed over 1 hour. The reaction mixture was then filtered through Celite to remove a small amount of a fine white precipitate and concentrated to ca. 0.5 mL *in vacuo*. The concentrated solution was placed in the freezer at -35 °C and was allowed to sit for 1 hour. After 1 hour the brown supernatant was decanted and the green-yellow solid was washed with cold (-35 °C) pentane (2 × 0.5

mL). The volatile components were removed *in vacuo* to yield **5-2b** as a crystalline (paralelipiped) green-yellow solid (0.140 g, 62%). Melting point = 143-145 °C. ^{1}H NMR (300.1 MHz, benzene-d_6): δ 98.8 (1 H), 45.9 (2 H), 31.7 (2 H), 24.1-30.5 (overlapping resonances, 26 H), 8.8 (2 H), -43.2 (18 H), -55.5 - (-57.6) (overlapping resonances, 7 H). μ_{eff} (benzene-d_6): 4.95 μ_B, S = 2. Anal. Calcd. for $C_{33}H_{58}FeN_3PSi_2$: C, 61.95; H, 9.14; N, 6.57. Found: C, 61.29; H, 9.02; N, 6.45. A single crystal suitable for X-ray diffraction analysis was grown from a concentrated pentane solution at -35 °C.

Synthesis of 5-2c. A solution of **5-1b** (0.200 g, 0.47 mmol) in ca. 1 mL of pentane was added via pipette to a solution of $[Co\{N(SiMe_3)_2\}_2]$ (0.180 g, 0.47 mmol) in ca. 1 mL of pentane. A color change from deep green to red was observed immediately upon addition. The reaction mixture was allowed to stir for 1 hour and was then filtered through Celite and concentrated to ca. 0.5 mL *in vacuo*. The concentrated solution was placed in the freezer at -35 °C and was allowed to sit for 1 hour. After 1 hour the deep red supernatant was decanted and the red solid was washed with cold (-35 °C) pentane (2 × 0.5 mL). The volatile components were removed *in vacuo* to yield **5-2c** as a crystalline (paralelipiped) red solid (0.205 g, 68%). Melting point = 144 - 146 °C. ^{1}H NMR (300.1 MHz, benzene-d_6): δ 108.6 (2 H), 46.4 (2 H), 35.0 (1 H), 16.1 (2 H), 13.2 (overlapping resonances, 7 H), 7.2-7.6 (overlapping resonances, 19 H), -44.4 (18 H), -54.9 (1 H), -55.7 (6 H). μ_{eff} (benzene-d_6): 4.08 μ_B, S = 3/2. Anal. Calcd. for $C_{33}H_{58}CoN_3PSi_2$: C, 61.65; H, 9.09; N, 6.54. Found: C, 61.01; H, 9.01; N, 6.31. A single crystal suitable for X-ray diffraction analysis was grown from a concentrated pentane solution at -35 °C.

Synthesis of 5-3. A solution of **5-1b** (0.200 g, 0.47 mmol) in ca. 2 mL of benzene was added via pipette to a solution of $Fe(Py)_2(CH_2SiMe_3)_2$ (0.180 g, 0.47 mmol) in ca. 1

mL of benzene and the maroon reaction mixture was allowed to stir for 18 hours. After 18 hours the red-orange reaction mixture was concentrated to ca. 1 mL *in vacuo* and placed in the freezer at -35 °C. After 24 hours the deep red-orange supernatant was decanted and the solid containing crystalline **5-3** was washed with cold (-35 °C) pentane (2 × 0.5 mL). The volatile components were removed *in vacuo* to yield a mixture of solids including crystalline **5-3** as a crystalline orange solid.

Synthesis of 5-4. ^{n}BuLi (92 μL, 2.5 M in hexanes, 0.23 mmol) was added via syringe to a pre-chilled (-35 °C) solution of **5-1b** (0.098 g, 0.23 mmol) in ca. 2 mL of pentane and the reaction mixture was cooled to -35 °C. After 1 hour the solvent was decanted from the reaction mixture and the off-white lithium salt formed was dissolved in ca. 2 mL pyridine. This solution was then added via pipette to a stirring slurry of $FeCl_2$ (0.029 g, 0.23 mmol) in ca. 2 mL of pyridine. A color change from yellow to deep brown was observed immediately upon addition. The reaction mixture was allowed to stir for 18 hours and then the solvent was removed *in vacuo*. The brown residue was extracted with 5 mL toluene and filtered through Celite to furnish a deep brown solution. The solution was then concentrated to ca. 1 mL *in vacuo* and placed in the freezer at -35 °C. After 72 hours, a small amount of yellow crystals were isolated (*ca*. 10% yield) and sent for X-ray diffraction analysis and determined to be **5-4•0.5C$_7$H$_8$**.

Synthesis of 5-5. ^{n}BuLi (164 μL, 2.5 M in hexanes, 0.41 mmol) was added via syringe to a pre-chilled (-35 °C) solution of **5-1b** (0.173 g, 0.41 mmol) in ca. 2 mL of pentane and the reaction mixture was cooled to -35 °C. After 1 hour the solvent was decanted from the reaction mixture and the lithium salt formed was dissolved in ca. 3 mL THF. This solution was then added via pipette to a stirring slurry of $FeCl_2$ (0.052 g, 0.41

mmol) in ca. 2 mL THF. A color change from yellow to deep brown was observed immediately upon addition. The reaction mixture was allowed to stir for 18 hours and then the solvent was removed *in vacuo*. The brown residue was extracted with 10 mL benzene and filtered through Celite to furnish a brown solution. The solvent was removed *in vacuo* and the brown filtrate was washed with 3 × 2 mL pentane furnishing a deep brown solid and a yellow solution. The pentane extract was then concentrated to ca. 1 mL *in vacuo* and placed in the freezer at -35 °C. After 24 hours, a small amount of yellow crystals were isolated (*ca*. 5% yield) and sent for X-ray diffraction analysis and were crystallographically characterized as **5-5**.

Synthesis of 5-6. A solution of **5-1c** (0.130 g, 0.28 mmol) in ca. 2 mL Et_2O was added via pipette to a solution of $[Fe\{N(SiMe_3)_2\}_2]$ (0.052 g, 0.14 mmol) in ca. 2 mL Et_2O. A color change from green to red was observed immediately and the solution was allowed to stir at room temperature for two hours. The solution was concentrated to ca. 0.5 mL *in vacuo* and the concentrated solution was placed in the freezer at -35 °C and was allowed to sit for 18 hours. After 18 hours the deep red supernatant was decanted and the orange solid was washed with cold (-35 °C) pentane (2 × 0.5 mL). The volatile components were removed *in vacuo* to yield **5-6•Et$_2$O** as a crystalline orange solid (0.062 g, 45%). Melting point = 123 - 127 °C. ^{1}H NMR (300.1 MHz, benzene-d_6): δ 36.0, 29.3, 27.7, 23.1, 18.7, 17.8, 15.6, 15.0, 14.7, 13.1, 6.9, 0.1, -10.9, -11.1 -34.1, -38.9. μ_{eff} (benzene-d_6): 4.73 μ_B, S = 2. Anal. Calcd. for $C_{66}H_{74}FeON_4P_2$: C, 74.99; H, 7.05; N, 5.30. Found: C, 73.46; H, 6.91; N, 6.30. A single crystal of **5-6•Et$_2$O** suitable for X-ray diffraction analysis was grown from a concentrated Et_2O solution at -35 °C

5.4.3 Crystallographic Solution, Refinement and Structural Details for 5-1b, 5-2a - 5-2c, 5-3, 5-4•0.5C_7H_8, 5-5, and 5-6•Et_2O

Crystallographic data for each of **5-1b**, **5-2a - 5-2c**, **5-3**, **5-4•0.5C_7H_8**, **5-5 and 5-6•Et_2O** were obtained on either a Bruker D8/APEX II CCD or a Bruker PLATFORM/APEX II CCD diffractometer using either graphite-monochromated Mo Kα (**5-1b**, **5-2b**, **5-2c**, **5-3**, **5-4•0.5C_7H_8**, **5-5** (λ = 0.71073 Å)) or Cu Kα (**5-2a**, **5-6•Et_2O** (λ = 1.5418 Å)) radiation employing samples that were mounted in inert oil and transferred to a cold gas stream on the diffractometer. Data for **5-1b**, **5-2a - 5-2c**, **5-3**, **5-4•0.5C_7H_8**, and **5-6•Et_2O** were obtained at 173(±2) K whereas data for **5-5** was collected at 296K. Programs for diffractometer operation, data collection, and data reduction (including SAINT) were supplied by Bruker. All structures were refined by use of full-matrix least-squares procedures (on F^2) with R_1 based on $F_o^2 \geq 2\sigma(F_o^2)$ and wR_2 based on $F_o^2 \geq -3\sigma(F_o^2)$. During the structure solution process for **5-4**, half an equivalent of toluene was located in the asymmetric unit and refined in a satisfactory manner. Racemic twinning was observed for **5-5**, however the asymmetric unit was refined in a satisfactory manner (Flack parameter = 0.485(7)). During the structure solution process for **5-6**, an equivalent of Et_2O was located in the asymmetric unit and was also refined in a satisfactory manner. Anisotropic displacement parameters were employed throughout for all the non-hydrogen atoms. All hydrogen atoms were added at calculated positions and refined by use of a riding model employing isotropic displacement parameters based on the isotropic displacement parameter of the attached atom. Additional crystal data can be found in Appendix A.

CHAPTER 6: (*N*-Phosphinoamidinate)Iron Pre-Catalysts for the Room Temperature Hydrosilylation of Carbonyl Compounds with Broad Substrate Scope at Low Loadings

6.1 Introduction

The reduction of carbonyl compounds is among the most widely employed transformations in synthetic organic chemistry.[98] Such protocols are employed broadly on both bench-top and industrial reaction scales, and have been shown to accommodate a diversity of substrate classes and functional groups.[99] Among the myriad reduction protocols that have been established, platinum-group metal-catalyzed reductions have proven to be particularly effective, providing high yields and selectivity under mild conditions at low catalyst loading.[98-100] However, the high cost and toxicity of the platinum-group metals has prompted the development of alternative classes of carbonyl reduction catalysts involving first-row transition metals, most notably iron.[101] Iron is a desirable substitute for this application, as it is both abundant and inexpensive, and is significantly less toxic than the platinum-group metals in pharmaceutical applications. The recent emergence of highly effective iron-based catalysts for carbonyl reductions can be attributed in part to the development and application of suitable supporting multidentate ancillary ligands, including those featuring combinations of phosphorus and nitrogen donors.[102]

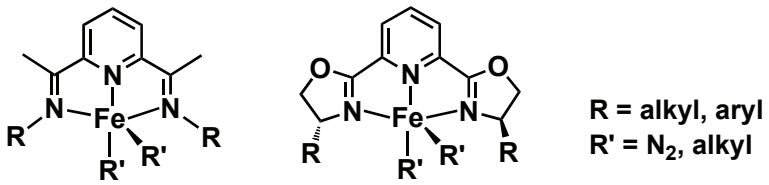

Figure 6-1. PDI (left) and pybox (right) iron complexes developed by Chirik.

Among the various classes of transition-metal catalyzed carbonyl reductions that have been developed, hydrosilylation followed by Si-O bond cleavage upon aqueous workup has emerged as a useful protocol for the synthesis of alcohols that is complementary to reductions employing molecular hydrogen or hydrogen-transfer reagents such as alcohols.[103] Despite the diversity of recent contributions made toward the development of the iron-catalyzed (asymmetric)[104] hydrosilylation of ketones and aldehydes to afford alcohols by the groups of Nishiyama,[105] Beller,[106] Gade,[107] Nikonov,[108] Adolfsson,[109] Darcel and Sortais,[110] Glorius,[111] Guan,[112] Plietker,[113] Royo,[114] Driess,[115] and others,[101-102] reports of such transformations at room temperature and employing low loadings (≤ 1 mol% Fe) are limited to a total of three reports from the groups of Chirik[116] and Tilley.[117] In 2008, Chirik and co-workers[116a] reported on the use of well-defined (bis(imino)pyridine)iron complexes as pre-catalysts for aldehyde (1 example) and ketone (12 examples) hydrosilylation (Figure 6-1). Efficient room temperature carbonyl reductions were observed employing 0.1-1.0 mol% Fe and using two equivalents of either $PhSiH_3$ or Ph_2SiH_2 as the reducing agent, with varying levels of chemoselectivity in carbonyl reductions involving enone substrates. Asymmetric variants of such reactions employing a borane co-catalyst were reported subsequently.[116b] In 2010, Yang and Tilley[117] reported on the use of $[Fe\{N(SiMe_3)_2\}_2]$[95] as a pre-catalyst for the room temperature hydrosilylation of aldehydes (2 examples) and ketones (8 examples) at 0.03-2.7 mol% Fe loading and using 1.6 equivalents of either $PhSiH_3$, Ph_2SiH_2, or $PhMeSiH_2$ as the reducing agent. Importantly, control experiments ruled out the presence of trace platinum group metal impurities as contributing significantly to the observed catalytic activity. Notwithstanding these breakthroughs from the groups of

Chirik and Tilley, the scope of reactivity featured in these reports is limited; notably absent are examples of synthetically relevant substrates such as benzophenones, sterically demanding acyclic dialkyl ketones, and heteroaryl acetophenones. Furthermore, while the first reports of the iron-catalyzed reduction of esters to alcohols appeared only very recently,[118-119] relatively high catalyst loading (5 mol% Fe) and temperature (100 ºC) were required in these systems in order to achieve efficient catalysis.[120] In this context, the identification of new iron-based catalysts for the hydrosilylation of carbonyl compounds to alcohols that operate under mild conditions (room temperature; ≤ 1 mol% Fe; ≤ 1 equiv. silane) and with expanded substrate scope represents an important challenge in current catalysis research.

In seeking to address some of the aforementioned challenges in iron-catalyzed carbonyl reductions, well-defined iron complexes derived from *N*-phosphinoamidines, a new ligand class that was recently utilized for the development of highly active chromium-based ethylene tri-/tetramerization catalysts (discussed in Chapter 5),[48] were targeted. In particular, it was envisioned that three-coordinate (*N*-phosphinoamidinate)iron(amido) species might exhibit some of the desirable reactivity properties of $[Fe\{N(SiMe_3)_2\}_2]$,[117] while at the same time providing a means of enhancing catalyst stability and performance via ancillary ligand modification.[121] This chapter details the successful application of a newly developed three-coordinate (*N*-phosphinoamidinate)iron(amido) pre-catalyst (**5-2b**, synthesis discussed in Chapter 5) in the room temperature hydrosilylation of aldehydes, ketones, and esters to alcohols, at remarkably low loadings (0.01-1.0 mol% Fe), employing only one equivalent of silane

relative to the carbonyl compound, and with the broadest substrate scope reported to date for such iron-catalyzed transformations (Scheme 6-1).

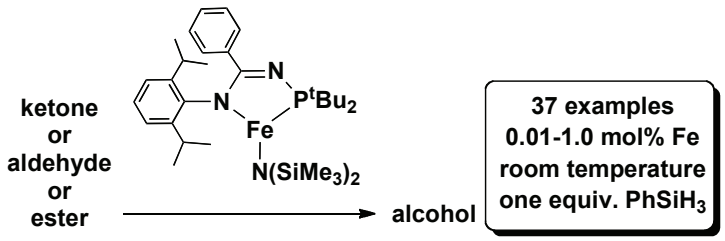

Scheme 6-1. (*N*-Phosphinoamidinate)Iron(amido) catalyst for carbonyl hydrosilylation.

6.2 Results and Discussion

6.2.1 (*N*-Phosphinoamidinate)Iron-Catalyzed Hydrosilylation of Ketones and Aldehydes

Upon synthesizing complexes **5-2a**, **5-2b**, and **5-2c**, their catalytic performance was compared to the diamido complexes [M{N(SiMe$_3$)$_2$}$_2$] (M = Fe, Co) in hydrosilylation chemistry. Acetophenone was selected as a test substrate in combination with 1.6 equiv. phenylsilane, in keeping with the conditions reported by Yang and Tilley.[117] However, in an effort to employ particularly stringent test conditions, only 0.015 mol% Fe was used, measuring the progress of the reaction after four hours. To place these conditions in context, the lowest catalyst loading reported to date for the iron-catalyzed room temperature hydrosilylation of acetophenone involved the use of 0.03 mol% [Fe{N(SiMe$_3$)$_2$}$_2$],[117] whereby 98% conversion was achieved after 18 hours. The results of the preliminary catalyst screen are collected in Table 6-1. Whereas the dmp-functionalized iron complex **5-2a** performed rather poorly under these test conditions (Table 6-1, entry 1), it was encouraging to observe quantitative conversion to the desired 1-phenylethanol (**6-1a**) when using the more sterically hindered dipp-functionalized pre-

catalyst **5-2b** (Table 6-1, entry 2). Interestingly, the use of **5-2c** – the Co^{II} structural analogue of **5-2b** – under analogous conditions afforded no detectable conversion of the acetophenone starting material (Table 6-1, entry 3), thereby supporting the key role of iron in catalyzing the carbonyl reduction chemistry featured herein. Under the challenging test conditions employed, only low conversion was achieved when using $[Fe\{N(SiMe_3)_2\}_2]$ (Table 6-1, entry 4), and negligible conversion was observed when using $[Co\{N(SiMe_3)_2\}_2]$ (Table 6-1, entry 5). While the use of alternative silanes provided some conversion to **6-1a** at higher **5-2b** loadings, under the conditions featured in Table 6-1, the use of Ph_2SiH_2, $PhMeSiH_2$, Et_2SiH_2, or polymethylhydrosiloxane in place of $PhSiH_3$ afforded negligible conversion of the acetophenone starting material. In evaluating the influence of silane stoichiometry on the observed catalysis when using **5-2b**, it was found that the use of 0.6 equivalents of phenylsilane was well tolerated (Table 6-1, entry 6), while a significant drop in conversion was observed when using 0.4 equivalents of phenylsilane (Table 6-1, entry 7). On this basis, and in an effort to circumvent the need for further optimization with respect to the amount of phenylsilane used when exploring other carbonyl substrates, one equivalent of phenylsilane was used as the reductant in all subsequent experiments. Notably, the ability to use only one equivalent of phenylsilane at low catalyst loadings in successful reductions involving the pre-catalyst **5-2b** represents a practical improvement relative to previously reported iron-based catalyst systems for the room temperature hydrosilylation of ketones and aldehydes to alcohols, where larger quantities (1.6 - 2.0 equivalents) of silane are employed.[116-117] Interestingly, the quantitative conversion achieved in the absence of added solvent (Table

6-1, entry 8) suggests that this catalyst system could also be optimized for use under more environmentally benign, solvent-free reaction conditions.

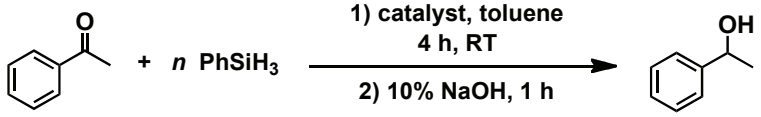

Entry	Fe pre-catalyst (0.015 mol% M)	*n*	**6-1a** (%)[a]
1	**5-2a**	1.6	25
2	**5-2b**	1.6	> 99
3	**5-2c**	1.6	< 5
4	$[Fe\{N(SiMe_3)_2\}_2]$	1.6	19
5	$[Co\{N(SiMe_3)_2\}_2]$	1.6	< 5
6	**5-2b**	0.6	> 99
7	**5-2b**	0.4	27
8	**5-2b**	1.0	> 99

Table 6-1. Preliminary catalytic hydrosilylation screening results. [a]GC conversion.

In monitoring the progress of acetophenone hydrosilylation employing phenylsilane (1.0 equiv.) in combination with pre-catalyst **5-2b** (Table 6-1, entry 8), 59% conversion to **6-1a** was observed over the course of only 10 minutes, which equates to a noteworthy turnover frequency of approximately 23,600 h^{-1}. Preliminary control experiments in which analogous reactions were conducted with the rigorous exclusion of light or in the presence of added mercury resulted in no loss of catalytic performance, thereby suggesting that such transformations are neither photochemically promoted, nor heterogeneous in nature.

Having identified **5-2b** as being a superior catalyst for the hydrosilylation of acetophenone at room temperature, the reaction scope was surveyed with other ketones and aldehydes (Figure 6-3). It was found that a broad range of substrates were successfully accommodated, employing only one equivalent of phenylsilane and ≤ 1 mol% **5-2b**. In building on the successful reduction of acetophenone to afford **6-1a**,

alternative *para*-substituted acetophenones featuring electron-withdrawing or electron-donating substituents were successfully accommodated, as were pyridyl and thiophenyl variants, affording very high conversion to the corresponding secondary alcohols (**6-1b** - **6-1f**). Sterically hindered *ortho*-substituted acetophenones, α-tetralone, as well as branched/benzo-fused variants were also reduced efficiently (**6-1g** - **6-1l**). Structurally diverse dialkyl ketones were suitable substrates when using **5-2b** as a pre-catalyst, resulting in high conversion to both cyclic (**6-1m** - **6-1o**, **6-1q**) and acyclic (**6-1p**, **6-1r** - **6-1t**) secondary alcohols. Benzophenones were also efficiently reduced when using **5-2b** (**6-1u** - **6-1w**), as were benzaldehydes featuring either *ortho*-substitution, or *para*-substitution involving an electron-donating or electron-withdrawing substituent (**6-1x** - **6-1z**). While for some substrates the catalytic abilities of $[Fe\{N(SiMe_3)_2\}_2]$ were found to be comparable to those of **5-2b** under analogous reaction conditions (**6-1j**, **6-1m**, **6-1x**), significantly inferior performance of $[Fe\{N(SiMe_3)_2\}_2]$ was noted in the case of apparently more challenging substrates including 4-chloroacetophenone, α-tetralone, and pivalone (**6-1b**, **6-1i**, **6-1p**). Further comparisons to the published work of Chirik and co-workers[116a] regarding the use of (bis(imino)pyridine)iron complexes for the room temperature hydrosilylation of ketones revealed a similar trend. For example, whereas 82% conversion of α-tetralone was observed over the course of 3 hours at 0.1 mol% Fe is described in a report by Chirik and co-workers,[116a] near quantitative conversion at 0.05 mol% Fe was achieved herein over the course of 4 hours using **5-2b** (**6-1i**, Figure 6-2).

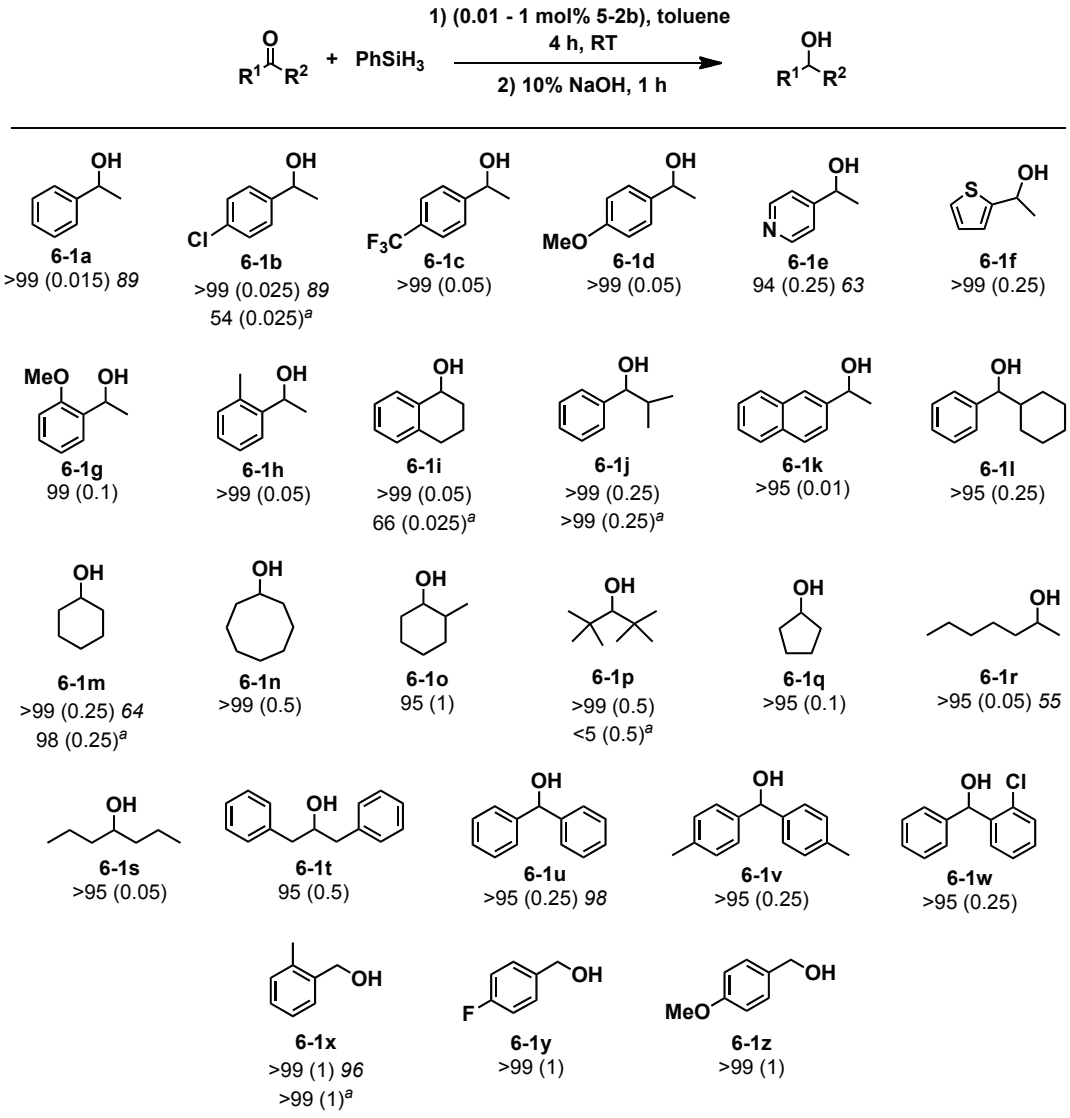

Figure 6-2. (*N*-Phosphinoamidinate)Iron-catalyzed hydrosilylation of ketones and aldehydes; GC conversion (mol% **5-2b**) *isolated yield*. Calibrated GC data confirmed that differences between GC yield and isolated yield can be attributed entirely to losses upon isolation, rather than due to by-product formation. See the experimental section for additional details. [a]GC conversion (mol% [Fe{N(SiMe$_3$)$_2$}$_2$]).

A brief survey regarding chemoselective hydrosilylations confirmed the propensity of **5-2b** to promote the selective reduction of ketones to alcohols in the presence of alkene functionalities (Scheme 6-2). In this regard, both 2-cyclohexenone and 5-hexen-2-one were cleanly transformed into the corresponding secondary alcohols (**6-2a** and **6-2b**) over the course of four hours at room temperature. Notably, the

performance of **5-2b** in the reduction of the latter substrate leading to **6-2b** is more efficient than analogous reactions employing either $[Fe\{N(SiMe_3)_2\}_2]$[117] or (bis(imino)pyridine)iron[116a] catalyst complexes.

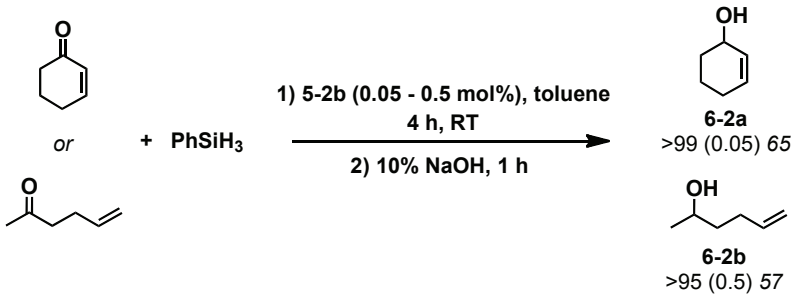

Scheme 6-2. (*N*-Phosphinoamidinate)Iron-catalyzed chemoselective reduction of enones; ^{1}H NMR conversion (mol% **5-2b**) *isolated yield*.

6.2.2 (*N*-Phosphinoamidinate)Iron-Catalyzed Hydrosilylation of Esters

Encouraged by the remarkably broad scope at low catalyst loadings exhibited by **5-2b** in the iron-catalyzed, room temperature hydrosilylation of ketones and aldehydes, attention was turned toward developing the first examples of analogous reductions of esters to alcohols. The iron-catalyzed reduction of esters to alcohols was disclosed by the groups of Darcel[118] and Beller[119] during the course of the studies presented herein; however, both high catalyst loading (5 mol% Fe) and temperature (100 ºC) were employed in these published catalyst systems. The successful application of **5-2b** (≤ 1 mol% Fe) in the first iron-catalyzed room temperature reduction of esters to alcohols is summarized in Figure 6-3. Each of methyl, ethyl and phenethyl phenylacetate were efficiently reduced to 2-phenylethanol (**6-3a**) in the presence of catalytic amounts of **5-2b** (0.25-1.0 mol%). For the hydrosilylation of methyl and ethyl esters, the methanol and ethanol presumably formed was not isolated due to the high volatility of the product.

Furthermore, the crude product from the hydrosilylation of phenethyl phenylacetate contained ca. 2 equiv. of **6-3a** relative to the starting material indicating that the R^2 functionality also forms an alcohol product. The parent methyl benzoate was well-accommodated without significant over-reduction to toluene, as were *para*-substituted variants featuring chloro, methoxy or trifluoromethyl groups, enabling high conversions to the corresponding benzyl alcohol derivatives (**6-3b** - **6-3e**). Further functional group tolerance was demonstrated in the reduction of a pyridine containing ester, affording **6-3f**. Finally, the ability to promote the reduction of esters featuring only aliphatic substitution was achieved in the reduction of ethyl octanoate, which afforded *n*-octanol (**6-3g**) in high isolated yield. The application of $[Fe\{N(SiMe_3)_2\}_2]$ as a pre-catalyst for the reduction of esters has not been reported in the literature previously. However, it is demonstrated herein that while the conversion achieved by use of $[Fe\{N(SiMe_3)_2\}_2]$ can in some cases parallel that obtained when using **5-2b** under similar conditions (e.g. **6-3a** from methyl phenylacetate, Figure 6-3), this simple amide pre-catalyst proved inferior to **5-2b** with alternative substrates, as in the formation of **6-3g**, thereby confirming the key role of the *N*-phosphinoamidine ligand in enhancing catalytic performance. Furthermore, where direct substrate comparisons can be made with the literature, the room temperature catalytic performance of **5-2b** ($\leq$ 1 mol% Fe) using one equivalent of phenylsilane as the reductant was found to be competitive with or superior to that of both $[CpFe(PCy_3)(CO)_2]BF_4$[118] and $Fe(stearate)_2/NH_2CH_2CH_2NH_2$,[119] which operate under much more forcing conditions (5 mol% Fe, 100 ºC, 2-5 equiv. silane).

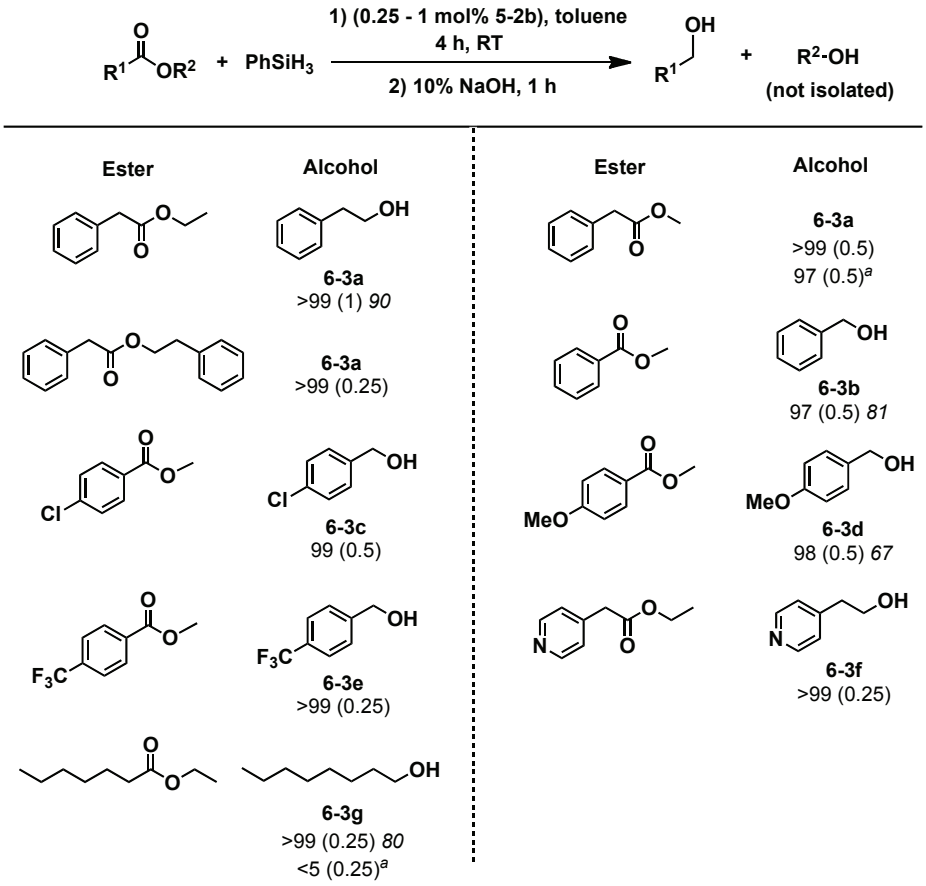

Figure 6-3. (*N*-Phosphinoamidinate)Iron-catalyzed hydrosilylation of esters to alcohols; GC conversion (mol% **5-2b**) *isolated yield*. Calibrated GC data confirmed that differences between GC yield and isolated yield can be attributed entirely to losses upon isolation, rather than due to by-product formation. [a]GC conversion (mol% [Fe{N(SiMe$_3$)$_2$}$_2$]).

6.3 Conclusions

An investigation examining the catalytic utility of new three-coordinate Fe^{II} and Co^{II} *N*-phosphinoamidinate complexes in the challenging room temperature hydrosilylation of carbonyl compounds to alcohols established the superior performance of the well-defined Fe^{II} amido pre-catalyst (**5-2b**), featuring sterically demanding *N*-2,6-diisopropylphenyl and di(*tert*-butyl)phosphino moieties within the *N*-phosphinoamidinate ligand, in such applications. Notably, pre-catalyst **5-2b** operates at very low catalyst

loadings (0.01-1.0 mol% Fe), requires the use of only one equivalent of phenylsilane reductant, and exhibits the broadest scope (37 examples total) of any reported iron pre-catalyst for carbonyl hydrosilylation at room temperature. Included for the first time in the room temperature catalytic survey are examples of iron-catalyzed hydrosilylations of benzophenones, sterically demanding acyclic dialkyl ketones, heteroaryl acetophenones, and esters en route to alcohols. While attempts to better understand the factors that contribute to the desirable catalytic profile exhibited by **5-2b** are ongoing, it is feasible that redox non-innocence involving the *N*-phosphinoamidinate ligand may figure prominently in this regard, as has been implicated in the case of alternative classes of carbonyl reduction catalysts featuring diiminodiphosphine and bis(imino)pyridine co-ligands.[102,104,116]

6.4 Experimental Section

6.4.1 General Considerations

Unless otherwise noted, all experiments were conducted under nitrogen in a MBraun glovebox or using standard Schlenk techniques. Dry, deoxygenated solvents were used unless otherwise indicated. $CDCl_3$ (Cambridge Isotopes) was used as received. Acetophenone and α-tetralone were distilled and then degassed via three repeated freeze-pump-thaw cycles. All other liquid ketones, aldehydes, and esters were degassed via three repeated freeze-pump-thaw cycles. All liquid ketones, aldehydes, and esters were stored over activated 4 Å molecular sieves for a minimum of 12 hours prior to use. Silanes (Gelest) were stored as received over 4 Å molecular sieves. All solid ketones, aldehydes and esters were degassed under vacuum for a minimum of 1 hour and stored

under nitrogen. Flash column chromatography was performed on silica gel (SiliaFlash P60, Silicycle).

^{1}H and ^{13}C characterization data for compounds **6-1a** - **6-1z**, **6-2a** - **6-2g**, and **6-3a** - **6-3g** were collected at 300K on a Bruker AV-300 spectrometer operating at 300.1 and 75.5 MHz (respectively) with chemical shifts reported in parts per million downfield of $SiMe_4$. GC data were obtained on a Shimadzu GC 2014 instrument equipped with a Astec CHIRALDEX B-PH, 30 m, 0.25 mm i.d. column. The following method was used: 90 °C, 5 min; 10 °C/min to 180 °C; and 180 °C, 10 min.

6.4.2 General Procedure for Determining Conversions of Carbonyl Substrates (GP6-1)

In an inert atmosphere glovebox, the carbonyl substrate (0.4 mmol), phenylsilane (49 μL, 0.4 mmol), and a stirbar were added to an oven-dried screw-capped vial. **5-2b** (0.01 - 1 mol%) was then added as a stock solution (0.16 – 16 mM) in toluene (250 μL) and the vial was sealed with a cap containing a PTFE septum and stirred in the glovebox for 4 hours. After 4 hours, the vial was removed from the glovebox and the contents were hydrolyzed with 10% NaOH (1 mL) and left to stir for 1 hour. The organic layer was extracted with Et_2O (3 × 2 mL), dried over $MgSO_4$, and concentrated under reduced pressure. The crude residue was then analyzed by GC or ^{1}H NMR to determine the conversion of the substrate.

6.4.3 General Procedure for Isolation of Carbonyl Substates (0.4 mmol scale) (GP6-2)

In an inert atmosphere glovebox, the carbonyl substrate (0.4 mmol), phenylsilane (49 μL, 0.4 mmol), and a stirbar were added to an oven-dried screw-capped vial. **5-2b** (0.01 - 1 mol%) was then added as a stock solution (0.16 - 16 mM) in toluene (250 μL) and the vial was sealed with a cap containing a PTFE septum and stirred in the glovebox for 4 hours. After 4 hours, the vial was removed from the glovebox and the contents were hydrolyzed with 10% NaOH (1 mL) and left to stir for 1 hour. The organic layer was extracted with Et_2O (3 × 2 mL), dried over $MgSO_4$, and concentrated under reduced pressure. The crude residue was then purified via flash column chromatography.

6.4.4 General Procedure for Isolation of Carbonyl Substates (1 mmol scale) (GP6-3)

In an inert atmosphere glovebox, the carbonyl substrate (1 mmol), phenylsilane (123 μL, 1 mmol), and a stirbar were added to an oven-dried screw-capped vial. **5-2b** (0.01 - 1 mol%) was then added as a stock solution (0.16 - 16 mM) in toluene (625 μL) and the vial was sealed with a cap containing a PTFE septum and stirred in the glovebox for 4 hours. After 4 hours, the vial was removed from the glovebox and the contents were hydrolyzed with 10% NaOH (1 mL) and left to stir for 1 hour. The organic layer was extracted with Et_2O (3 × 3 mL), dried over $MgSO_4$, and concentrated under reduced pressure. The crude residue was purified via flash column chromatography.

6.4.5 Monitoring of Conversions by Use of Gas Chromatography

(6-1a) 1-Phenylethanol. The title compound was synthesized according to **GP6-1** using a 0.24 mM stock solution of **5-2b** (0.015 mol%). The crude product was analyzed by GC. Retention times: 11.226 (ketone), 13.511 (alcohol). >99% conversion of starting material to product was observed.

(6-1b) 1-(4-Chlorophenyl)ethanol. The title compound was synthesized according to **GP6-1** using a 0.4 mM stock solution of **5-2b** (0.025 mol%). The crude product was analyzed by GC. Retention times: 14.609 (ketone), 18.465 (alcohol). 96% conversion of starting material to product was observed.

(6-1c) 1-(4-Trifluoromethylphenyl)ethanol. The title compound was synthesized according to **GP6-1** using a 0.8 mM stock solution of **5-2b** (0.05 mol%). The crude product was analyzed by GC. Retention times: 10.615 (ketone), 14.447 (alcohol). >99% conversion of starting material to product was observed.

(6-1d) 1-(4-Methoxyphenyl)ethanol. The title compound was synthesized according to **GP6-1** using a 0.8 mM stock solution of **5-2b** (0.05 mol%). The crude product was analyzed by GC. Retention times: 18.150 (ketone), 19.709 (alcohol). >99% conversion of starting material to product was observed.

(6-1e) 1-(4-Pyridyl)ethanol. The title compound was synthesized according to **GP6-1** using a 4 mM stock solution of **5-2b** (0.25 mol%). The crude product was analyzed by GC. Retention times: 13.041 (ketone), 18.499 (alcohol). 94% conversion of starting material to product was observed.

(6-1f) 1-(2-Thienyl)ethanol. The title compound was synthesized according to **GP6-1** using a 4 mM stock solution of **5-2b** (0.25 mol%). The crude product was analyzed by

GC. Retention times: 12.601 (ketone), 14.064 (alcohol). >99% conversion of starting material to product was observed.

(6-1g) 1-(2-Methoxyphenyl)ethanol. The title compound was synthesized according to **GP6-1** using a 1.6 mM stock solution of **5-2b** (0.1 mol%). The crude product was analyzed by GC. Retention times: 15.212 (ketone), 16.904 (alcohol). 99% conversion of starting material to product was observed.

(6-1h) 1-(2-Methylphenyl)ethanol. The title compound was synthesized according to **GP6-1** using a 0.8 mM stock solution of **5-2b** (0.05 mol%). The crude product was analyzed by GC. Retention times: 11.619 (ketone), 15.011 (alcohol). >99% conversion of starting material to product was observed.

(6-1i) 1,2,3,4-Tetrahydro-1-naphthol. The title compound was synthesized according to **GP6-1** using a 0.8 mM stock solution of **5-2b** (0.05 mol%). Retention times: 17.497 (ketone), 20.001 (alcohol). 98% conversion of starting material to product was observed.

(6-1j) α-(1-Methylethyl)-benzenemethanol. The title compound was synthesized according to **GP6-1** using a 4 mM stock solution of **5-2b** (0.25 mol%). The crude product was analyzed by GC. Retention times: 12.451 (ketone), 15.185 (alcohol). >99% conversion of starting material to product was observed.

(6-1m) Cyclohexanol. The title compound was synthesized according to **GP6-1** using a 4 mM stock solution of **5-2b** (0.25 mol%). The crude product was analyzed by GC. Retention times: 7.610 (ketone), 9.660 (alcohol). >99% conversion of starting material to product was observed.

(6-1n) Cyclooctanol. The title compound was synthesized according to **GP6-1** using a 8 mM stock solution of **5-2b** (0.5 mol%). The crude product was analyzed by GC.

Retention times: 11.982 (ketone), 14.037 (alcohol). >99% conversion of starting material to product was observed.

(6-1o) 2-Methyl cyclohexanol. The title compound was synthesized according to **GP6-1** using a 16 mM stock solution of **5-2b** (1 mol%). The crude product was analyzed by GC. Retention times: 7.563 (ketone), 9.473 (alcohol). 95% conversion of starting material to product was observed.

(6-1p) 2,2,4,4-Tetramethyl-3-pentanol. The title compound was synthesized according to **GP6-1** using a 8 mM stock solution of **5-2b** (0.5 mol%). The crude product was analyzed by GC. Retention times: 4.531 (ketone), 8.224 (alcohol). 90% conversion of starting material to product was observed.

(6-1x) 2-Methylbenzyl alcohol. The title compound was synthesized according to **GP6-1** using a 16 mM stock solution of **5-2b** (1 mol%). The crude product was analyzed by GC. Retention times: 11.619 (aldehyde), 15.011 (alcohol). >99% conversion of starting material to product was observed.

(6-1y) 4-Fluorobenzyl alcohol. The title compound was synthesized according to **GP6-1** using a 16 mM stock solution of **5-2b** (1 mol%). The crude product was analyzed by GC. Retention times: 9.199 (aldehyde), 14.572 (alcohol). >99% conversion of starting material to product was observed.

(6-1z) 4-Methoxybenzyl alcohol. The title compound was synthesized according to **GP6-1** using a 16 mM stock solution of **5-2b** (1 mol%). The crude product was analyzed by GC. Retention times: 15.212 (aldehyde), 16.904 (alcohol). >99% conversion of starting material to product was observed.

(6-3a) 2-Phenylethanol (from ethyl phenylacetate). The title compound was synthesized according to **GP6-1** using a 16 mM stock solution of **5-2b** (1 mol%). The crude product was analyzed by GC. Retention times: 13.315 (ester), 14.651 (alcohol). >99% conversion of starting material to product was observed.

(6-3a) 2-Phenylethanol (from methyl phenylacetate). The title compound was synthesized according to **GP6-1** using an 8 mM stock solution of **5-2b** (0.5 mol%). The crude product was analyzed by GC. Retention times: 12.286 (ester), 14.651 (alcohol). >99% conversion of starting material to product was observed.

(6-3a) 2-Phenylethanol (from phenethyl phenylacetate). The title compound was synthesized according to **GP6-1** using a 4 mM stock solution of **5-2b** (0.25 mol%). The crude product was analyzed by GC. Retention times: 23.359 (ester), 14.562 (alcohol). >99% conversion of starting material to product was observed.

(6-3b) Benzyl alcohol. The title compound was synthesized according to **GP6-1** using an 8 mM stock solution of **5-2b** (0.5 mol%). The crude product was analyzed by GC. Retention times: 10.793 (ester), 13.974 (alcohol). 97% conversion of starting material to product was observed.

(6-3c) 4-Chlorobenzyl alcohol. The title compound was synthesized according to **GP6-1** using an 8 mM stock solution of **5-2b** (0.5 mol%). The crude product was analyzed by GC. Retention times: 13.895 (ester), 19.460 (alcohol). 99% conversion of the starting material was observed.

(6-3d) 4-Methoxybenzyl alcohol. The title compound was synthesized according to **GP6-1** using an 8 mM stock solution of **5-2b** (0.5 mol%). The crude product was

analyzed by GC. Retention times: 17.160 (ester), 20.584 (alcohol). 98% conversion of starting material to product was observed.

(6-3e) 4-Trifluoromethylbenzyl alcohol. The title compound was synthesized according to **GP6-1** using an 8 mM stock solution of **5-2b** (0.25 mol%). The crude product was analyzed by GC. Retention times: 9.676 (ester), 15.003 (alcohol). 99% conversion of starting material to product was observed.

(6-3f) 2-(4-Pyridyl)ethanol. The title compound was synthesized according to **GP6-1** using a 4 mM stock solution of **5-2b** (0.25 mol%). The crude product was analyzed by GC. Retention times: 16.681 (ester), 21.387 (alcohol). >99% conversion of starting material to product was observed.

(6-3g) 1-Octanol. The title compound was synthesized according to **GP6-1** using a 4 mM stock solution of **5-2b** (0.25 mol%). The crude product was analyzed by GC. Retention times: 9.450 (ester), 11.030 (alcohol). >99% conversion of starting material to product was observed.

6.4.6 Monitoring of Conversions by Use of ^{1}H NMR

(6-1k) 1-Naphthyl ethanol. The title compound was synthesized according to **GP6-1** using a 0.16 mM stock solution of **5-2b** (0.01 mol%). ^{1}H NMR analysis of the crude product showed one compound present as well as residual solvent. The ^{1}H NMR spectrum was compared to literature data to confirm the identity of the alcohol product.[122]

(6-1l) α-(Cyclohexyl)-benzenemethanol. The title compound was synthesized according to **GP6-1** using a 4 mM stock solution of **5-2b** (0.25 mol%). ^{1}H NMR analysis of the crude product showed one compound present as well as residual solvent. The ^{1}H

NMR spectrum was compared to literature data to confirm the identity of the alcohol product.[123]

(6-1q) Cyclopentanol. The title compound was synthesized according to **GP6-1** using a 1.6 mM stock solution of **5-2b** (0.1 mol%). ^{1}H NMR analysis of the crude product showed one compound present as well as residual solvent. The ^{1}H NMR spectrum was compared to literature data to confirm the identity of the alcohol product.[124]

(6-1r) 2-Heptanol. The title compound was synthesized according to **GP6-1** using a 0.8 mM stock solution of **5-2b** (0.05 mol%). ^{1}H NMR analysis of the crude product showed one compound present as well as residual solvent. The ^{1}H NMR spectrum was compared to literature data to confirm the identity of the alcohol product.[125]

(6-1s) 4-Heptanol. The title compound was synthesized according to **GP6-1** using a 0.8 mM stock solution of **5-2b** (0.05 mol%). ^{1}H NMR analysis of the crude product showed one compound present as well as residual solvent. The ^{1}H NMR spectrum was compared to literature data to confirm the identity of the alcohol product.[126]

(6-1t) α-(Phenylmethyl)-benzeneethanol. The title compound was synthesized according to **GP6-1** using a 8 mM stock solution of **5-2b** (0.5 mol%). ^{1}H NMR analysis of the crude product showed one compound present as well as residual solvent. The ^{1}H NMR spectrum was compared to literature data to confirm the identity of the alcohol product.[127]

(6-1u) Diphenylmethanol. The title compound was synthesized according to **GP6-1** using a 4 mM stock solution of **5-2b** (0.25 mol%). ^{1}H NMR analysis of the crude product showed one compound present as well as residual solvent. The ^{1}H NMR spectrum was compared to literature data to confirm the identity of the alcohol product.[128]

(6-1v) 4-Methyl-α-(4-methylphenyl)-benzenemethanol. The title compound was synthesized according to **GP6-1** using a 4 mM stock solution of **5-2b** (0.25 mol%). ^{1}H NMR analysis of the crude product showed one compound present as well as residual solvent. The ^{1}H NMR spectrum was compared to literature data to confirm the identity of the alcohol product.[127]

(6-1w) 2-Chloro-α-phenyl-benzenemethanol. The title compound was synthesized according to **GP6-1** using a 4 mM stock solution of **5-2b** (0.25 mol%). ^{1}H NMR analysis of the crude product showed one compound present as well as residual solvent. The ^{1}H NMR spectrum was compared to literature data to confirm the identity of the alcohol product.[129]

(6-2a) 2-Cyclohexen-1-ol. The title compound was synthesized according to **GP6-1** using a 0.8 mM stock solution of **5-2b** (0.05 mol%). ^{1}H NMR analysis of the crude product showed one compound present as well as residual solvent. The ^{1}H NMR spectrum was compared to literature data to confirm the identity of the alcohol product.[133]

(6-2b) 5-Hexen-2-ol. The title compound was synthesized according to **GP6-1** using an 8 mM stock solution of **5-2b** (0.5 mol%). ^{1}H NMR analysis of the crude product showed one compound present as well as residual solvent. The ^{1}H NMR spectrum was compared to literature data to confirm the identity of the alcohol product.[134]

6.4.7 Control Reactions Involving Acetophenone

TOF measurement. In an inert atmosphere glovebox, acetophenone (47 μL, 0.4 mmol), phenylsilane (49 μL, 0.4 mmol), and a stirbar were added to each of six oven-dried, screw-capped glass vials. Pre-catalyst **5-2b** (0.015 mol%) was then added as a

stock solution (0.24 mM) in toluene (250 μL) to each vial and the vials were sealed with caps containing PTFE septa and magnetic stirring was initiated. After 5 minutes, one vial was removed from the glovebox and the contents were hydrolyzed with 10% NaOH (1 mL) and left to stir for 1 hour. This process was repeated every five minutes until all six reactions had been hydrolyzed. The organic layers were extracted with Et_2O (3 × 2 mL), dried over $MgSO_4$, and concentrated under reduced pressure. The crude residues were then analyzed by GC to determine the conversion of the substrate at different intervals. 59% conversion of acetophenone was observed after 10 minutes resulting in a calculated TOF of 23400 h^{-1}.

Reaction in the absence of light. In an inert atmosphere glovebox, acetophenone (47 μL, 0.4 mmol), phenylsilane (49 μL, 0.4 mmol), and a stirbar were added to an oven-dried screw-capped vial and wrapped in aluminum foil. **5-2b** (0.015 mol%) was then added as a stock solution (0.24 mM) in toluene (250 μL) and the vial was sealed with a cap containing a PTFE septum and stirred in the glovebox for 4 hours. After 4 hours, the vial was removed from the glovebox and was hydrolyzed with 10% NaOH (1 mL) and left to stir for 1 hour. The organic layer was extracted with Et_2O (3 × 2 mL), dried over $MgSO_4$, and concentrated under reduced pressure. The crude residue was then analyzed by GC to determine the conversion of the substrate.

Hg Test for Homogeneity.[130] In an inert atmosphere glovebox, acetophenone (47 μL, 0.4 mmol), phenylsilane (49 μL, 0.4 mmol), Hg (8.0 g, 40 mmol) and a stirbar were added to an oven-dried screw-capped vial. Pre-catalyst **5-2b** (0.015 mol%) was then added as a stock solution (0.24 mM) in toluene (250 μL) and the vial was sealed with a cap containing a PTFE septum and stirred in the glovebox for 4 hours. After 4 hours, the

vial was removed from the glovebox and the contents were hydrolyzed with 10% NaOH (1 mL) and left to stir for 1 hour. The organic layer was extracted with Et_2O (3 × 2 mL), dried over $MgSO_4$, and concentrated under reduced pressure. The crude residue was then analyzed by GC to determine the conversion of the substrate.

Solvent free reaction. In an inert atmosphere glovebox, **5-2b** (0.015 mol%) was added to an oven dried screw-capped vial as a stock solution (0.24 mM) in toluene (250 μL) and the solvent was removed *in vacuo*. Acetophenone (47 μL, 0.4 mmol), phenylsilane (79 μL, 0.4 mmol), and a stirbar were added to the vial and the vial was sealed with a cap containing a PTFE septum and stirred in the glovebox for 4 hours. After 4 hours, the vial was removed from the glovebox and the contents were hydrolyzed with 10% NaOH (1 mL) and left to stir for 1 hour. The organic layer was extracted with Et_2O (3 × 2 mL), dried over $MgSO_4$, and concentrated under reduced pressure. The crude residue was then analyzed by GC to determine the conversion of the substrate.

6.4.8 Comparative Catalytic Experiments Employing $[Fe\{N(SiMe_3)_2\}_2]$

In an inert atmosphere glovebox, the carbonyl substrate (0.4 mmol), phenylsilane (49 μL, 0.4 mmol), and a stirbar were added to an oven-dried screw-capped vial. $[Fe\{N(SiMe_3)_2\}_2]$ (0.01 - 1 mol%) was then added as a stock solution (0.16 - 16 mM) in toluene (250 μL) and the vial was sealed with a cap containing a PTFE septum and stirred in the glovebox for 4 hours. After 4 hours, the vial was removed from the glovebox and the contents were hydrolyzed with 10% NaOH (1 mL) and left to stir for 1 hour. The organic layer was extracted with Et_2O (3 × 2 mL), dried over $MgSO_4$, and concentrated

under reduced pressure. The crude residue was then analyzed by GC to determine the conversion of the substrate.

6.4.9 Characterization of Isolated Alcohols

(6-1a) 1-Phenylethanol

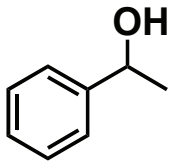

The title compound was synthesized according to **GP6-2** using a 0.24 mM stock solution of **5-2b** (0.015 mol%) and purified by flash column chromatography on silica gel using 95:5 methylene chloride:methanol in a 89% isolated yield (43 mg, 0.36 mmol) as a pale yellow oil. ^{1}H NMR (300.1 MHz, $CDCl_3$): δ 7.25-7.38 (m, 5 H), 4.88 (q, 1 H, J = 7 Hz), 1.94 (br s, 1 H), 1.49 (d, 3 H, J = 7 Hz). $^{13}C\{^{1}H\}$ NMR (75.5 MHz, $CDCl_3$): δ 146.0, 128.7, 127.7, 125.6, 70.6, 25.4. Spectral data are in close agreement with previously reported ^{1}H and ^{13}C NMR characterization data for the title compound.[124]

(6-3b) 1-(4-Chlorophenyl)ethanol

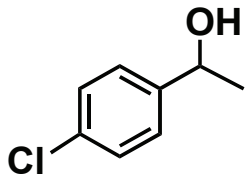

The title compound was synthesized according to **GP6-2** using a 0.4 mM stock solution of **5-2b** (0.025 mol%) and purified by flash column chromatography on silica gel using 25:75 ethyl acetate:hexanes in a 89% isolated yield (56 mg, 0.36 mmol) as a pale yellow oil. ^{1}H NMR (300.1 MHz, $CDCl_3$): δ 7.29 (m, 4 H), 4.86 (q, 1 H, J = 7 Hz), 1.99 (br s, 1 H), 1.46 (d, 3 H, J = 7 Hz). $^{13}C\{^{1}H\}$ NMR (75.5 MHz, $CDCl_3$): δ 144.5, 133.3, 128.8,

127.0, 69.9, 25.5. Spectral data are in close agreement with previously reported ^{1}H and ^{13}C NMR characterization data for the title compound.[131]

(6-1e) 1(4-Pyridyl)ethanol

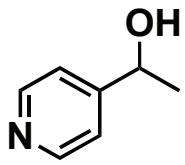

The title compound was synthesized according to **GP6-2** using a 4 mM stock solution of **5-2b** (0.25 mol%) and purified by flash column chromatography on silica gel using 95:5 methylene chloride:methanol in a 63% isolated yield (31 mg, 0.25 mmol) as an off-white solid. ^{1}H NMR (300.1 MHz, $CDCl_3$): δ 8.44 (d, 2 H, J = 5 Hz), 7.30 (d, 2 H, J = 5 Hz), 4.88 (q, 1 H, J = 7 Hz), 3.94 (br s, 1 H), 1.48 (d, 3 H, J = 7 Hz). $^{13}C\{^{1}H\}$ NMR (75.5 MHz, $CDCl_3$): δ 155.8, 149.5, 120.8, 68.7, 25.3. Spectral data are in close agreement with previously reported ^{1}H and ^{13}C NMR characterization data for the title compound.[122]

(6-1m) Cyclohexanol

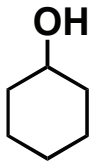

The title compound was synthesized according to **GP6-3** using a 4 mM stock solution of **5-2b** (0.25 mol%) and purified by flash column chromatography on silica gel using 95:5 methylene chloride:methanol in a 64% isolated yield (64 mg, 0.64 mmol) as a pale yellow oil. ^{1}H NMR (300.1 MHz, $CDCl_3$): δ 3.60 - 3.63 (m, 1 H), 1.88-1.89 (m, 2 H), 1.68-1.78 (m, 2 H), 1.10-1.57 (m, 7 H). $^{13}C\{^{1}H\}$ NMR (75.5 MHz, $CDCl_3$): δ 70.5, 35.8, 25.7, 24.3. Spectral data are in close agreement with previously reported ^{1}H and ^{13}C NMR characterization data for the title compound.[124]

(6-1r) 2-Heptanol

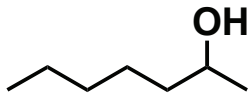

The title compound was synthesized according to **GP6-3** using a 0.8 mM stock solution of **5-2b** (0.05 mol%) and purified by flash column chromatography on silica gel using 95:5 methylene chloride:methanol in a 55% isolated yield (64 mg, 0.55 mmol) as a pale yellow oil. ^{1}H NMR (300.1 MHz, $CDCl_3$): δ 3.80 (sextet, 1 H, J = 5 Hz), 1.29 - 1.44 (m, 9 H), 1.18 (d, 3 H, J = 6 Hz), 0.89 (t, 3 H, J = 7 Hz). ^{13}C{^{1}H} NMR (75.5 MHz, $CDCl_3$): δ 68.2, 39.3, 31.8, 25.5, 23.5, 22.6, 14.0. Spectral data are in close agreement with previously reported ^{1}H and ^{13}C NMR characterization data for the title compound.[125]

(6-1u) Diphenylmethanol

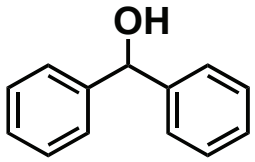

The title compound was synthesized in a procedure similar to **GP6-2** using a 4 mM stock solution of **5-2b** (0.25 mol%) in a 98% isolated yield (73 mg, 0.39 mmol) as a white solid. The crude product did not require column chromatography for purification. ^{1}H NMR (300.1 MHz, $CDCl_3$): δ 7.24 - 7.39 (m, 10 H), 5.84 (s, 1 H), 2.23 (d, 1 H, J = 3 Hz). ^{13}C{^{1}H} NMR (75.5 MHz, $CDCl_3$): δ 143.8, 128.5, 127.6, 126.6, 76.3. Spectral data are in close agreement with previously reported ^{1}H and ^{13}C NMR characterization data for the title compound.[125]

(6-1x) 2-Methylbenzyl alcohol

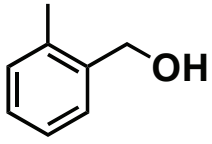

The title compound was synthesized according to **GP6-2** using a 16 mM stock solution of **5-2b** (1 mol%) and purified by flash column chromatography on silica gel using 95:5 methylene chloride:methanol in a 96% isolated yield (47 mg, 0.38 mmol) as a light yellow oil. ^{1}H NMR (300 MHz, $CDCl_3$): δ 7.32 - 7.35 (m, 1 H), 7.16 - 7.21 (m, 3 H), 4.66 (s, 2 H), 2.34 (s, 3 H), 1.81 (br s, 1 H). $^{13}C\{^{1}H\}$ NMR (75.5 MHz, $CDCl_3$): δ 138.9, 136.3, 130.5, 128.0, 127.7, 126.2, 63.7, 18.8. Spectral data are in close agreement with previously reported ^{1}H and ^{13}C NMR characterization data for the title compound.[128]

(6-2b) 2-Cyclohexen-1-ol

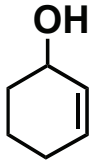

The title compound was synthesized according to **GP6-3** using a 0.8 mM stock solution of **5-2b** (0.05 mol%) and purified by flash column chromatography on silica gel using 95:5 methylene chloride:methanol in a 65% isolated yield (64 mg, 0.65 mmol) as a pale yellow oil. ^{1}H NMR (300 MHz, $CDCl_3$): δ 5.72 - 5.85 (m, 2 H), 4.19 (d, 1 H, J = 3 Hz), 1.58 - 2.02 (m, 7 H). $^{13}C\{^{1}H\}$ NMR (75.5 MHz, $CDCl_3$): δ 130.7, 130.0. 65.7, 32.2, 25.2, 19.1. Spectral data are in close agreement with previously reported ^{1}H and ^{13}C NMR characterization data for the title compound.[133]

(6-2b) 5-Hexen-2-ol

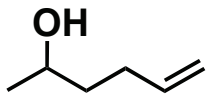

The title compound was synthesized according to **GP6-3** using a 8 mM stock solution of **5-2b** (0.5 mol%) and purified by flash column chromatography on silica gel using 95:5 methylene chloride:methanol in a 57% isolated yield (57 mg, 0.57 mmol) as a pale

yellow oil. ^{1}H NMR (300 MHz, $CDCl_3$): δ 5.77 - 5.89 (m, 1 H), 5.05 (dd, 1 H, *J* = 17, 2 Hz), 4.98 (d, 1 H, *J* = 10 Hz), 3.82 (sextet, 1 H, *J* = 6 Hz), 2.13 - 2.18 (m, 2 H), 1.51 - 1.59 (m, 3 H), 1.20 (d, 3 H, *J* = 6 Hz). ^{13}C{^{1}H} NMR (75.5 MHz, $CDCl_3$): δ 138.7, 115.0. 67.9, 38.5, 30.4, 23.7. Spectral data are in close agreement with previously reported ^{1}H and ^{13}C NMR characterization data for the title compound.[134]

(6-3a) 2-Phenylethanol

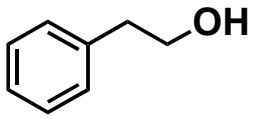

The title compound was synthesized according to **GP6-2** using a 16 mM stock solution of **5-2b** (1 mol%) and purified by flash column chromatography on silica gel using 95:5 methylene chloride:methanol in a 90% isolated yield (44 mg, 0.36 mmol) as a light yellow oil. ^{1}H NMR (300.1 MHz, $CDCl_3$): δ 7.29 - 7.32 (m, 2 H), 7.21-7.25 (m, 3 H), 3.86 (t, 2 H, *J* = 7 Hz), 2.87 (t, 2 H, *J* = 7 Hz), 1.50 (br s, 1 H). ^{13}C{^{1}H} NMR (75.5 MHz, $CDCl_3$): δ 138.7, 129.2, 128.9, 126.7, 63.9, 39.4. Spectral data are in close agreement with previously reported ^{1}H and ^{13}C NMR characterization data for the title compound.[124]

(6-3b) Benzyl alcohol

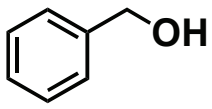

The title compound was synthesized according to **GP6-2** using a 8 mM stock solution of **5-2b** (0.5 mol%) and purified by flash column chromatography on silica gel using 95:5 methylene chloride:methanol in a 81% isolated yield (35 mg, 0.32 mmol) as a light yellow oil. ^{1}H NMR (300.1 MHz, $CDCl_3$): δ 7.28 - 7.36 (m, 5 H), 4.66 (s, 2 H), 1.97 (br

s, 1 H). $^{13}C\{^{1}H\}$ NMR (75.5 MHz, $CDCl_3$): δ 141.1, 128.7, 127.8, 127.2, 65.5. Spectral data are in close agreement with previously reported ^{1}H and ^{13}C NMR characterization data for the title compound.[124]

(6-3d) 4-Methoxybenzyl alcohol

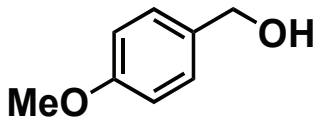

The title compound was synthesized according to **GP6-2** using a 8 mM stock solution of **5-2b** (0.5 mol%) and purified by flash column chromatography on silica gel using 95:5 methylene chloride:methanol in a 67% isolated yield (37 mg, 0.27 mmol) as a colorless oil. ^{1}H NMR (300 MHz, $CDCl_3$): δ 7.27 (d, 2 H, J = 8 Hz), 6.88 (d, 2 H, J = 9 Hz), 4.58 (s, 2 H), 3.79 (s, 3 H) 1.96 (br s, 1 H). $^{13}C\{^{1}H\}$ NMR (75.5 MHz, $CDCl_3$): δ 159.4, 133.3, 128.8, 114.1, 65.1, 55.5. Spectral data are in close agreement with previously reported ^{1}H and ^{13}C NMR characterization data for the title compound.[124]

(6-3g) 1-Octanol

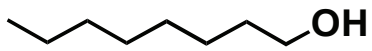

The title compound was synthesized according to **GP6-3** using a 4 mM stock solution of **5-2b** (0.25 mol%) and purified by flash column chromatography on silica gel using 95:5 methylene chloride:methanol in a 80% isolated yield (104 mg, 0.80 mmol) as a colorless oil. ^{1}H NMR (300 MHz, $CDCl_3$): δ 3.62 (t, 2 H, J = 5 Hz), 1.95 (br s, 1 H), 1.54-1.58 (m, 2 H), 1.28 - 1.32 (m, 10 H), 0.86 - 0.90 (m, 3 H). $^{13}C\{^{1}H\}$ NMR (75.5 MHz, $CDCl_3$): δ 62.9, 32.8, 31.8, 29.4, 29.3, 25.7, 22.6, 14.0. Spectral data are in close agreement with previously reported ^{1}H and ^{13}C NMR characterization data for the title compound.[132]

CHAPTER 7: (*N*-Phosphinoamidinate)Cobalt-Catalyzed Hydroboration: Alkene Isomerization Affords Terminal Selectivity

7.1 Introduction

Over the past thirty years, metal-catalyzed alkene hydroboration[135] has evolved into a versatile and atom-economical synthetic methodology for the assembly of alkylboronic ester synthons that in turn can be applied in a range of chemical transformations, including now-ubiquitous Suzuki-Miyaura cross-couplings.[136] Complexes based on the platinum-group metals, in particular rhodium and iridium, are among the most widely explored and broadly effective classes of catalysts for such transformations, offering high levels of selectivity and excellent substrate scope.[137] Notwithstanding the utility of platinum-group metals in this context, their expensive and toxic nature provides motivation for the pursuit of alternative classes of hydroboration catalysts that mimic the desirable behavior of platinum-group metals, and/or provide access to entirely new reactivity manifolds. Catalysts based on comparatively abundant first-row transition metals, including iron and cobalt, represent attractive candidates in this regard.[138]

Some progress has been made as of late with regard to the development of iron catalysts for alkene hydroboration. Notable achievements in this chemistry include the addition of pinacolborane (HBPin) to conjugated dienes,[139] terminal alkenes including unactivated olefins and styrene,[140] as well as cyclic aliphatic alkenes,[140b] where relevant with *anti*-Markovnikov selectivity and including selected examples that proceed at room temperature in the absence of added solvent. The key role of ancillary ligand design in enabling such reactivity is established in these reports, with appropriately substituted

tridentate bis(imino)pyridine[140b] and bipyridylphosphine[140a] ligands, as well as photochemically activated (NHC)$Fe(CO)_4$[140c] pre-catalysts proving effective (Figure 7-1). However, a number of important substrate scope limitations have been encountered to date in iron-catalyzed hydroboration chemistry; efficient transformations involving linear internal aliphatic alkenes have proven to be a considerable challenge, with reports of such reactivity being limited to a small number of examples, whereby high conversion but relatively poor regiochemistry is achieved.[140b,140c]

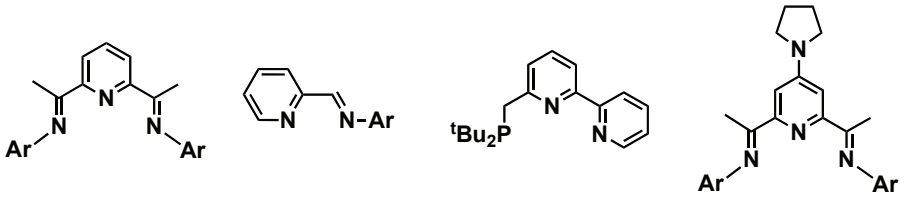

Figure 7-1. Ancillary ligands used in Fe and Co catalyzed alkene hydroboration.

Despite recent progress in the development of iron-catalyzed alkene hydroborations, and the well-established efficacy of the heavier Group 9 metals in such transformations,[135,137] reports of cobalt-catalyzed alkene hydroboration are few. At the time the studies disclosed herein were initiated, reports documenting cobalt-catalyzed alkene hydroboration reactions were limited to a pair of publications by Zaidlewicz and Meller,[141] in which (bisphosphine)$CoCl_2$ complexes were shown to catalyze the hydroboration of 1-octene as well as isoprene in combination with catecholborane, albeit with poor conversion and/or regioselectivity. During the course of conducting this experimental work, the remarkable catalytic efficacy of (bis(imino)pyridine)CoMe[142] and (bipyridylphosphine)$CoCl_2$/$NaBHEt_3$[143] in alkene hydroboration using HBPin was reported. The (bis(imino)pyridine)CoMe (1-5 mol%) system disclosed by Obligacion and Chirik[142] proved capable of catalyzing the addition of HBPin to terminal, geminal,

disubstituted internal, tri- and tetra-substituted alkenes with high activity and *anti*-Markovnikov selectivity, in neat substrate at room temperature, and with selective terminal addition of the BPin moiety. Use of the (bipyridylphosphine)$CoCl_2$/$NaBHEt_3$ catalyst system by Huang and co-workers[143] enabled the room temperature *anti*-Markovnikov hydroboration of vinylarenes and α-olefins with HBPin, at catalyst loadings as low as 0.005 mol%.

It has been shown previously that newly developed *N*-phosphinoamidine/amidinate ligands are effective in supporting first-row transition metal catalysts with applications spanning the chromium-catalyzed selective tri-/tetramerization of ethylene[48] to the iron-catalyzed hydrosilylation of aldehydes, ketones, and esters to alcohols (using **5-2b**, Figure 7-2).[144] Notably, whereas such hydrosilylations proceed under mild conditions (0.01-1.0 mol% Fe; room temperature), and with broadest substrate scope known for such iron-catalyzed transformations, the analogous cobalt complex **5-2c** performed poorly in this chemistry.[144]

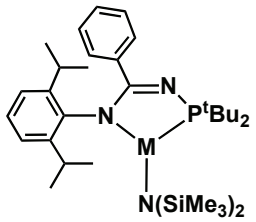

5-2b, M = Fe
5-2c, M = Co

Figure 7-2. Three-coordinate (*N*-phosphinoamidinate)metal(amido) pre-catalysts, **5-2b** and **5-2c**.

Encouraged by the utility of *N*-phosphinoamidines/amidinates in these diverse applications, the identification of first-row transition metal derivatives of such ligands that could be used to address challenges in alkene hydroboration chemistry were pursued.

In particular, it was sought to identify catalysts of this type that are useful in promoting alkene isomerization/hydroboration processes that transform linear internal aliphatic alkenes and related substrates selectively into 1-alkylboronate products - a challenging yet useful reaction class that at the time had only proved feasible with either rhodium or iridium catalysts (Scheme 7-1).[145] Herein the successful application of the three-coordinate (*N*-phosphinoamidinate)cobalt(amido) pre-catalyst (**5-2c**) in the room temperature addition of HBPin to linear and branched mono-substituted terminal alkenes, gem-disubstituted terminal alkenes, linear internal octenes, and cyclic alkenes with or without added solvent and with excellent *anti*-Markovnikov selectivity (where relevant) is reported; the hydroboration of selected ketones using **5-2c** is also presented. The remarkable ability of **5-2c** to promote alkene isomerization/hydroboration processes involving linear internal alkenes, leading to the selective terminal addition of the BPin group, is demonstrated.

7.2 Results and Discussion

Initial investigations focused on the application of **5-2b** (M = Fe) and **5-2c** (M = Co) as pre-catalysts for the addition of HBPin to octene isomers over the course of one hour at room temperature in the absence of additional solvent (Scheme 7-1). In the case of 1-octene (**7-1a**), quantitative formation of the anticipated 1-octylboronic ester (**7-2**) was achieved by use of 1 mol% (unoptimized) of either catalyst. In moving to *cis*-4-octene (**7-1b**), near quantitative formation of the terminal *anti*-Markovnikov hydroboration product (**7-2**) was again observed when using **5-2c** (1 mol%) - a transformation that corresponds to a net alkene isomerization/hydroboration process. The

use of modestly higher loadings of **5-2c** (1.5 mol%) reproducibly enabled the quantitative formation of **7-2**. Such transformations could also be achieved by use of **5-2b**, although consumption of **7-1b** and clean formation of the terminal addition product **7-2** was only achieved at the 2.5 mol% catalyst loading level. Significant differences in reactivity between **5-2b** and **5-2c** were observed when employing the more challenging substrate *trans*-4-octene (**7-1c**); whereas quantitative formation of **7-2** was again observed by use of **5-2c** (2.5 mol%), no conversion was achieved when using **5-2c** as the pre-catalyst, even at the 5 mol% loading level. Efforts to employ lower loadings of **5-2c** in the isomerization/hydroboration of *trans*-4-octene (**7-1c**) by conducting reactions at 65 ºC were unsuccessful, resulting in apparent catalyst decomposition with poor conversions. Notably, the use of $M\{N(SiMe_3)_2\}_2$ (M = Fe or Co)[95,97] as pre-catalysts resulted in negligible conversion of the starting materials for each of the above-mentioned reactions under analogous conditions, thereby underscoring the importance of the ancillary ligand in supporting suitably reactive pre-catalysts in this system. In keeping with the aforementioned results, the hydroboration of an equimolar mixture of **7-1a** - **7-1c** with HBPin in the presence of **5-2c** (2.5 mol%) afforded **7-2** cleanly over the course of one hour at room temperature under neat reaction conditions. It is worthy of mention that while synthetically useful, yet challenging, net alkene isomerization/hydroboration processes of this type catalyzed by rhodium or iridium complexes are known,[145] such processes promoted by cobalt complexes are limited only to a very recent publication by Obligacion and Chirik[142] that appeared while this thesis chapter was in preparation, who employed tridentate (bis(imino)pyridine)CoMe catalysts.

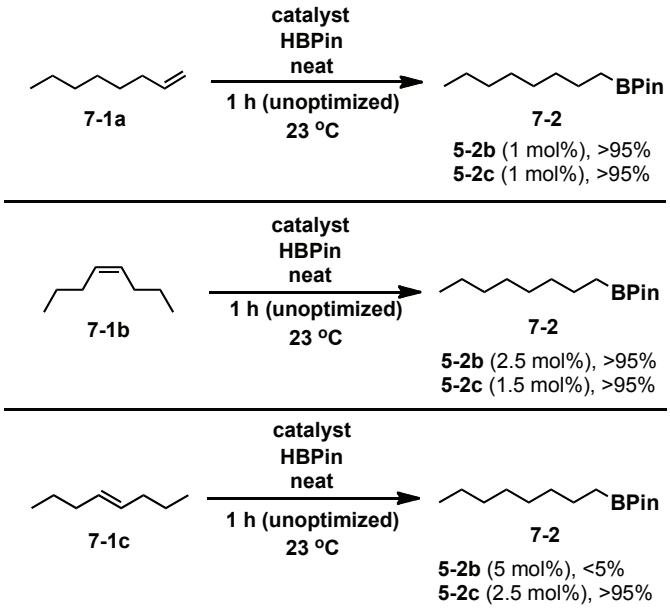

Scheme 7-1. Octene isomerization/hydroboration reactions catalyzed by **5-2b** and **5-2c** employing HBPin (conversions given on the basis of NMR spectroscopic data).

In an effort to learn more about the progress of these alkene isomerization/hydroboration processes involving **5-2c**, it was sought to monitor the fate of trans-4-octene (**7-1c**) under catalytically relevant conditions (neat, room temperature, 2.5 mol% **5-2c**). In probing the reaction by use of ^{1}H NMR methods, the clean consumption of **7-1c** and HBPin along with the formation of **7-2** was observed within 20 minutes, in the absence of detectable intermediates or alternative octene isomers (eg. 1-octene). In reducing the catalyst loading to 1 mol% **5-2c**, again only **7-1c**, HBPin, and **7-2** were observed by use of ^{1}H NMR methods; the reaction did not go to completion under these conditions. In a similar fashion, reactions conducted using 2.5 mol% **5-2c** in the presence of a 2:1 mixture of **7-1c** and HBPin afforded cleanly a 1:1 mixture of unreacted **7-1c** and **7-2**, in the absence of detectable quantities of alternative octene isomers. Collectively, these observations suggest that **5-2c** catalyzed alkene isomerization/hydroboration chemistry employing trans-4-octene (**7-1c**; and presumably

other linear aliphatic internal alkenes by analogy) proceeds via internal L_nCo(octyl) isomeric intermediates that are resistant to reactivity with HBpin until the L_nCo(n-octyl) isomer is accessed. Moreover, the isomerization sequences that are likely to transform internal L_nCo(octyl) isomers into the terminal L_nCo(n-octyl) form that is apparently intercepted by HBPin must proceed in a manner that does not involve facile loss of alkene from putative intermediates of the type L_nCo(octene)(H), given the absence of alternative octene isomers observed during the course of **5-2c** catalyzed transformations involving **7-1c**.

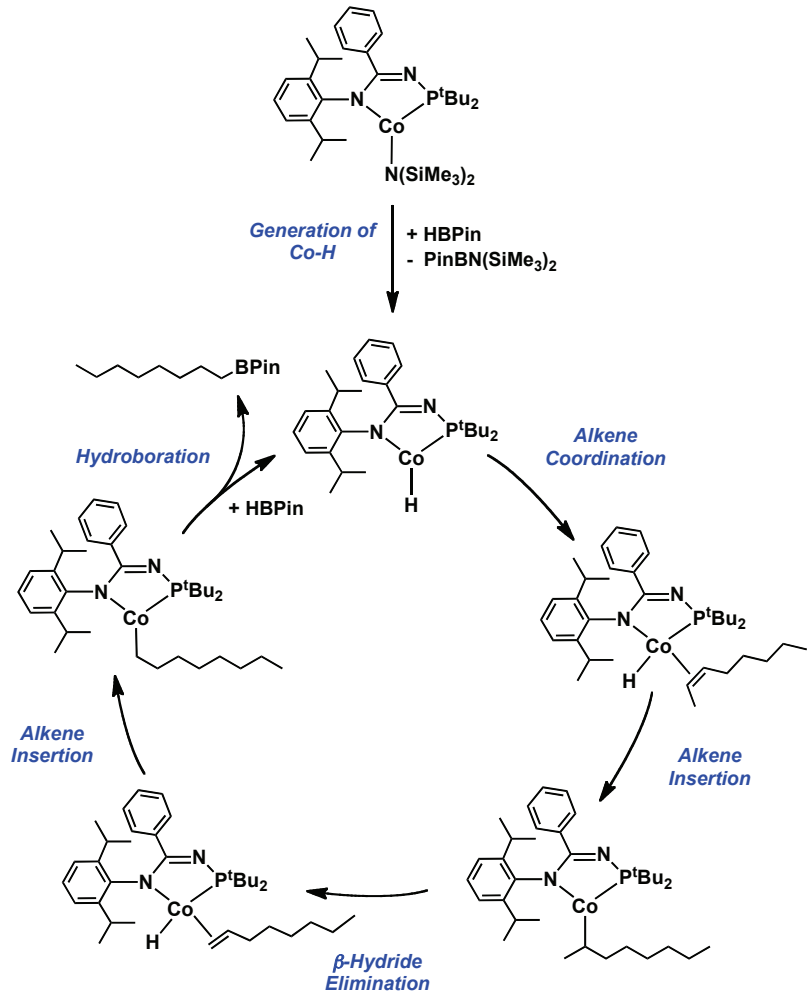

Scheme 7-2. Proposed mechanism for isomerization/hydroboration catalyzed by **5-2c**.

A complete mechanism of this cobalt-catalyzed alkene hydroboration/isomerization process has yet to be elucidated. Literature precedent suggests that there are two potential mechanisms for this process, with one mechanism likely to be operating over the other.[146] The potential mechanism likely to be operating involves a series of fast β-hydride elimination/1,2-insertion sequences mediated by a cobalt-hydride species (known as chain walking), followed by reaction with HBPin (Scheme 7-2 - isomerization of 2-octene to 1-octene shown). Notably, this type of mechanism requires no change in oxidation state at the metal, suggesting that it may be a low energy, facile process. It is proposed that a catalytically active (*N*-phosphinoamidinate)cobalt(hydride) species is formed upon the reaction of the pre-catalyst **5-2c** and HBPin. One possible route to the formation of the cobalt-hydride species could be a metathesis reaction between the H-B bond of HBPin and the Co-N bond of **5-2c** to form new Co-H and B-N containing species. Efforts to isolate and characterize the proposed $PinBN(SiMe_3)_2$ species as well as catalytically active cobalt-hydride species are ongoing. The second potential mechanism for the isomerization/hydroboration reaction involves the formation of π-allyl intermediates generated by C-H oxidative additions of the alkene with a metal center followed by a reductive elimination resulting in an isomerization. This isomerization is then followed by reaction with HBPin to generate the alkylboronate product. Notably, the π-allyl mechanism requires the oxidative addition of a C-H bond, a process that is not favorable at a Co metal center. Deuterium labeling studies conducted by Chirik indicate that the β-hydride elimination/1,2-insertion mechanism (chain walking) is likely to be occurring in the alkene isomerization/hydroboration reaction catalyzed by (bis(imino)pyridine)CoMe.

[142] It is proposed that the alkene isomerization/hydroboration process mediated by **5-2c** is likely to be operating via the same mechanism.

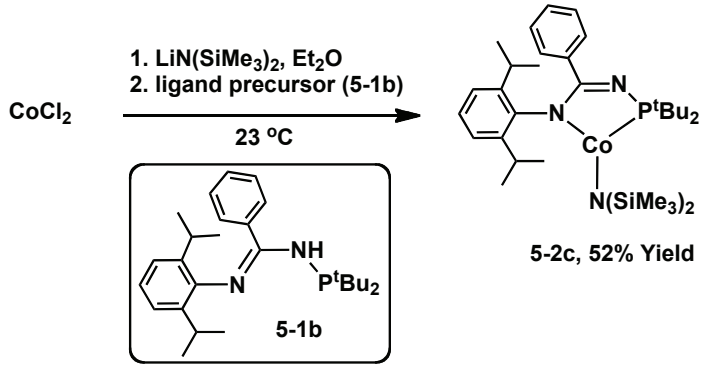

Scheme 7-3. Streamlined synthesis of **5-2c**.

Encouraged by the remarkable catalytic behavior exhibited by **5-2c**, a more streamlined synthetic route to this pre-catalyst was sought (Scheme 7-3). The previously reported synthesis of **5-2c** involves addition of the *N*-phosphinoamidine **5-1b** to the known precursor $Co\{N(SiMe_3)_2\}_2$, followed by recrystallization to give **5-2c** in 68% isolated yield. While apparently simple, the published preparation and subsequent isolation of $Co\{N(SiMe_3)_2\}_2$ from $CoCl_2$ and $NaN(SiMe_3)_2$ is somewhat tedious, involving recrystallization of crude $Co\{N(SiMe_3)_2\}_2$ (reported 53% yield), followed by sublimation;[97] using this protocol pure $Co\{N(SiMe_3)_2\}_2$ is typically obtained in approximately 40% isolated yield, giving an effective yield of **5-2c** of approximately 27% starting from $CoCl_2$. It has been subsequently demonstrated that **5-2c** can be prepared in a much more expedient fashion by sequentially treating $CoCl_2$ with $LiN(SiMe_3)_2$ and **5-1b**, thereby enabling the isolation of pure **5-2c** in 52% isolated yield following recrystallization.

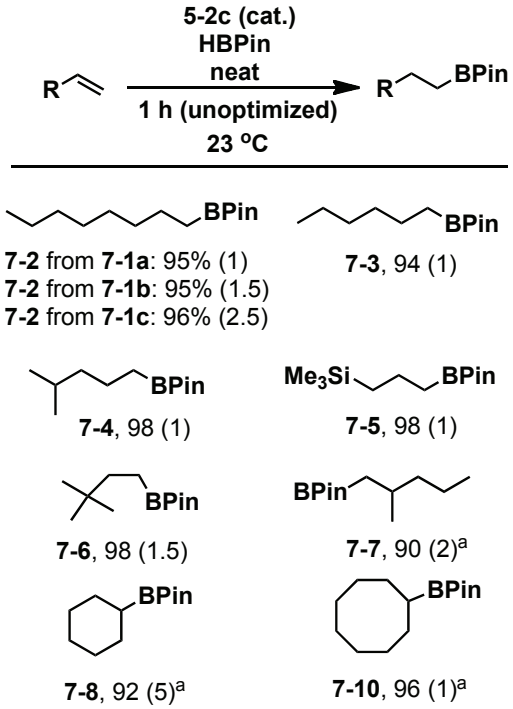

Scheme 7-4. Alkene hydroboration employing **5-2c** as a pre-catalyst. Isolated yields (mol% **5-2c** stated in parentheses) of the *anti*-Markovnikov hydroboration product derived from the corresponding terminal or cyclic alkene, with the exception of hydroborations involving the internal 4-octene isomers **7-1b** and **7-1c**. [a]1.2 equivalents of the alkene employed.

After establishing the hydroboration reactivity of **5-2c** with linear aliphatic alkenes, the hydroboration reactivity of **5-2c** with other olefinic or carbonyl-containing substrates was pursued. The spectroscopically determined conversions of the octenes **7-1a** - **7-1c** and HBPin to **7-2** in the presence of **5-2c** (Scheme 7-1) were authenticated on the basis of the high isolated yields obtained (Scheme 7-4). A selection of other mono-substituted terminal alkenes with varying steric profiles also underwent successful hydroboration with HBPin in the presence of **5-2c**, affording the *anti*-Markovnikov addition products **7-3** - **7-6** in high isolated yields. Similarly excellent results were obtained in the hydroboration of the gem-disubstituted terminal alkene 2-methyl-1-pentene, leading to **7-7**. The ability of **5-2c** to catalyze the hydroboration of cyclic

alkenes was confirmed by the clean transformation of cyclooctene and cyclohexene into the cycloalkylboronate products **7-8** and **7-9** (Scheme 7-4). While the aforementioned transformations were conducted under neat conditions, it was also demonstrated that analogous reactions leading to **7-2** (from **7-1a**) and **7-3** - **7-5** could be conducted in the presence of diethyl ether at the 0.5 mol% level, affording the terminal HBPin addition products (92-97% yield). Further preliminary experimentation with **5-2c** in alkene hydroborations using HBPin under similar conditions revealed some important substrate scope limitations, with styrenes, heteroatom-functionalized alkenes, dienes and enones affording low conversions and/or complex product mixtures. The inability of **5-2c** to catalyze the hydroboration of enones cannot be attributed to the presence of the ketone functionality alone; acetophenone, cyclohexanone, and 2-heptanone were each successfully hydroborated, affording the corresponding secondary alcohols **7-10** - **7-12** cleanly upon workup (Scheme 7-5).

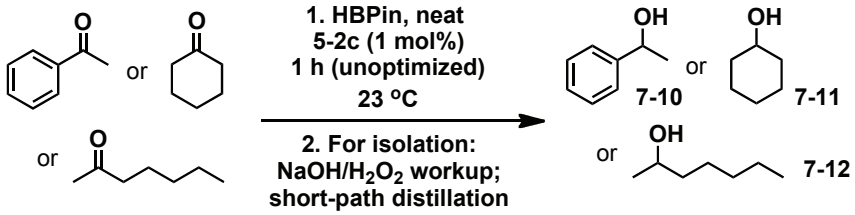

Yield data:
7-10, >95 (NMR); 74 (isolated)
7-11, >95 (NMR); 51 (isolated)
7-12, >95 (NMR); 47 (isolated)

Scheme 7-5. Ketone hydroboration employing **5-2c** as a pre-catalyst. The low isolated yields in the case of **7-11** and **7-12** can be attributed to losses incurred upon distillative workup.

7.3 Conclusions

The results presented in this chapter establish the utility of the easily prepared, three-coordinate (*N*-phosphinoamidinate)cobalt(amido) pre-catalyst (**5-2c**) in challenging room temperature alkene hydroboration reactions that can be conducted in the presence or absence of added solvent. The efficient *anti*-Markovnikov addition of HBPin to linear and branched mono-substituted terminal alkenes, gem-disubstituted terminal alkenes, and linear internal octenes is reported, as is the hydroboration of cyclic alkenes and ketones. Particularly significant is the observation that **5-2c** promotes alkene isomerization/hydroboration processes involving both *cis*- and *trans*-4-octene, leading to the selective terminal addition of the BPin group. With the exception of a recent report that appeared while this chapter was in preparation,[142] such alkene isomerization/hydroboration chemistry is without precedent in base metal hydroboration catalysis, and underscores how appropriately ligated cobalt complexes can provide access to challenging and synthetically useful reactivity manifolds that are normally reserved for the platinum-group metals.

7.4 Experimental Section

7.4.1 General Considerations

Unless otherwise noted, all experiments were conducted under nitrogen in an MBraun glovebox or using standard Schlenk techniques. Dry, deoxygenated solvents were used unless otherwise indicated. Pentane was deoxygenated and dried by sparging with nitrogen and subsequent passage through a double-column solvent purification system purchased from MBraun Inc. with one column packed with activated alumina and one column packed with activated Q5. Diethyl ether and tetrahydrofuran were dried over Na/benzophenone and distilled under nitrogen. $CDCl_3$ (Cambridge Isotopes) was used as received. All alkenes were degassed via three repeated freeze-pump-thaw cycles and were stored over activated 4 Å molecular sieves for a minimum of 12 hours prior to use. Pinacolborane (HBPin, Alfa) was used as received and stored under nitrogen. ^{1}H and ^{13}C NMR characterization data were collected at 300K on a Bruker AV-300 spectrometer operating at 300.1 and 75.5 MHz (respectively) with chemical shifts reported in parts per million downfield of $SiMe_4$. For boron-containing products, a ^{13}C NMR resonance for the carbon attached to the quadrupolar boron center was not observed. ^{11}B NMR characterization data were collected at 300K on a Bruker AV-300 spectrometer operating at 96.3 MHz with chemical shifts reported in parts per million downfield of $BF_3{\cdot}OEt_2$.

7.4.2 General Procedure for Determination of Conversion in Catalytic Hydroboration (GP7-1)

In a nitrogen atmosphere glovebox, an oven-dried screw-capped vial containing a stirbar was charged with pinacolborane (145 μL, 1 mmol) and the alkene (1 or 1.2 mmol) or carbonyl compound (1 mmol). Either **5-2b** or **5-2c** (1 – 5 mol%) was then added as a

solid and the vial was sealed with a cap containing a PTFE septum and stirred in the glovebox for 1 hour. After 1 hour the vial was removed from the glovebox and the catalyst mixture was deactivated by exposure to air. The contents of the vial were extracted with $CDCl_3$ and filtered through silica into a NMR tube. The ^{1}H and/or ^{11}B NMR spectra were analyzed to monitor the progress of the reaction. If no pinacolborane or alkene/carbonyl compound was found to be present in the sample, the reaction was determined to have achieved full conversion. For 4-octene isomers, the ^{13}C DEPT-Q NMR spectrum was also analyzed to aid in determining if an isomerization process involving the starting alkene had occurred.

7.4.3 General Procedure for Determination of NMR Yield in Carbonyl Hydroboration (GP7-2)

In a nitrogen atmosphere glovebox, an oven-dried screw-capped vial containing a stirbar was charged with pinacolborane (145 μL, 1 mmol) and the carbonyl substrate (1 mmol). **5-2c** (1 mol %) was then added as a solid, followed by the addition of a stock solution of Cp_2Fe (internal standard) in C_6D_6 (250 μL of 0.4 M solution, 0.1 mmol) and the vial was sealed with a cap containing a PTFE septum and stirred in the glovebox for 1 hour. After 1 hour an aliquot of the reaction mixture was analyzed by use of ^{1}H NMR spectroscopy. Comparison of the integrals of the methine peaks of the hydroboration products and the cyclopentadienyl peak of Cp_2Fe was used to obtain the NMR yield.

7.4.4 General Procedure for Isolation of Alkene Hydroboration Products (Solvent Free) (GP7-3)

In a nitrogen atmosphere glovebox, an oven-dried screw-capped vial containing a stirbar was charged with pinacolborane (145 μL, 1 mmol) and the alkene substrate (1 or 1.2 mmol). Either **5-2b** or **5-2c** (1 – 5 mol%) was then added as a solid and the vial was sealed with a cap containing a PTFE septum and stirred in the glovebox for 1 hour. After 1 hour the vial was removed from the glovebox and the catalyst mixture was deactivated by exposure to air. The contents were extracted with Et_2O (3 × 2 mL) and the ether extracts were subsequently filtered through silica. The eluent was collected and concentrated under reduced pressure to furnish the hydroboration product. The ^{1}H and ^{13}C NMR spectra of the isolated material were analyzed to determine the purity of the sample.

7.4.5 General Procedure for Isolation of Alkene Hydroboration Products (With Solvent) (GP7-4)

In a nitrogen atmosphere glovebox, an oven-dried screw-capped vial containing a stirbar was charged with pinacolborane (145 μL, 1 mmol) and the alkene substrate (1 mmol). **5-2c** (0.5 mol%) was then added as a stock solution (2 mM) in Et_2O (250 μL) and the vial was sealed with a cap containing a PTFE septum and stirred in the glovebox for 1 hour. After 1 hour the vial was removed from the glovebox and the catalyst mixture was deactivated by exposure to air. The contents were extracted with Et_2O (3 × 2 mL) and filtered through silica. The eluent was collected and concentrated under reduced pressure to furnish the hydroboration product. The ^{1}H and ^{13}C NMR spectra were analyzed to determine the purity of the sample.

7.4.6 General Procedure for Isolation of Alcohols (Ketone Hydroboration Products) (GP7-5)

In a nitrogen atmosphere glovebox, an oven-dried screw-capped vial containing a stirbar was charged with pinacolborane (290 μL, 2 mmol) and the ketone substrate (2 mmol). **5-2c** (0.013 g, 1 mol%) was then added as a solid and the vial was sealed with a cap containing a PTFE septum and stirred in the glovebox for 1 hour. After 1 hour, the vial was removed from the glovebox and the contents were diluted with ca. 10 mL THF. The contents were then hydrolyzed by the addition NaOH (1.0 M in H_2O, 2.0 mL, 2 mmol) and H_2O_2 (30% in H_2O, 1.13 mL, 10 mmol).[7] The organic layer was extracted with Et_2O (3 × 5 mL), washed with $NaHCO_3$ and brine, dried over $MgSO_4$, and concentrated under reduced pressure. The residues obtained were purified by short path distillation under reduced pressure to furnish the alcohol product. The ^1H and ^{13}C NMR spectra were then analyzed to determine the purity of the sample.

7.4.7 Alternative Synthesis of 5-2c.

A solution of $LiN(SiMe_3)_2$ (0.788 g, 4.71 mmol) in Et_2O (10 mL) was added via pipette over 2 minutes to a magnetically stirred slurry of $CoCl_2$ (0.306 g, 2.36 mmol) in Et_2O (5 mL). A color change from pale blue to deep blue green was observed over the course of 5 minutes. The reaction mixture was magnetically stirred for a total of 3 hours, over which time the formation of a white precipitate was observed. Subsequently, **5-1b** (1.00 g, 2.36 mmol) was added to the reaction mixture as a solid and a color change from deep blue green to deep red was observed over the course of 2 minutes. After stirring for an additional 2 hours the reaction mixture was filtered through Celite, the eluent was collected, and the Et_2O was removed under reduced pressure. The deep red residue was

then extracted with pentane (10 mL) and filtered through Celite. The filtrate was then concentrated under reduced pressure to a volume of ca. 3 mL, and the solution was placed in the freezer at -35 °C for 18 hours. After 18 hours the brown supernatant solution was decanted and the red solid crystalline precipitate was washed with cold (-35 °C) pentane (2 × 0.5 mL). The remaining red solid crystalline material (**5-2c**) was dried under reduced pressure (0.786 g, 52%). Spectral data for **5-2c** were in close agreement to samples of **5-2c** synthesized by the route described in Chapter 5.

7.4.8 Monitoring of Conversion/NMR Yield in Catalytic Hydroboration by use of NMR methods.

1-Octene (7-1a), method 1: The conversion of the title compound was determined according to **GP1** using the following amounts of alkene substrate and catalyst: 1-octene (160 μL, 1 mmol), **5-2c** (0.0064 g, 1 mol%). The ^{1}H and ^{11}B NMR spectra obtained indicated full conversion of the starting materials.

1-Octene (7-1a), method 2: The conversion of the title compound was determined according to **GP1** using the following amounts of alkene substrate and catalyst: 1-octene (160 μL, 1 mmol), **5-2b** (0.0064 g, 1 mol%). The ^{1}H and ^{11}B NMR spectra obtained indicated full conversion of the starting materials.

***Cis*-4-Octene (7-1b), method 1:** The conversion of the title compound was determined according to **GP1** using the following amounts of alkene substrate and catalyst: *cis*-4-octene (160 μL, 1 mmol), **5-2c** (0.0096 g, 1.5 mol%). The ^{1}H and ^{11}B NMR spectra obtained indicated full conversion of the starting materials. Data obtained from ^{13}C DEPT-Q NMR experiments confirmed the formation of the terminal hydroboration product, **7-2**.

***Cis*-4-Octene (7-1b), method 2:** The conversion of the title compound was determined according to **GP1** using the following amounts of alkene substrate and catalyst: *cis*-4-octene (160 μL, 1 mmol), **5-2b** (0.0016 g, 2.5 mol%). The ^{1}H and ^{11}B NMR spectra obtained indicated full conversion of the starting materials. Data obtained from ^{13}C DEPT-Q NMR experiments confirmed the formation of the terminal hydroboration product, **7-2**.

***Trans*-4-Octene (7-1c), method 1:** The conversion of the title compound was determined according to **GP1** using the following amounts of alkene substrate and catalyst: *trans*-4-octene (160 μL, 1 mmol), **5-2c** (0.016 g, 2.5 mol%). The ^{1}H and ^{11}B NMR spectra obtained indicated full conversion of the starting materials. Data obtained from ^{13}C DEPT-Q NMR experiments confirmed the formation of the terminal hydroboration product, **7-2**.

***Trans*-4-Octene (7-1c), method 2:** The conversion of the title compound was determined according to **GP1** using the following amounts of alkene substrate and catalyst: *trans*-4-octene (160 μL, 1 mmol), **5-2b** (0.032 g, 5 mol%). The ^{1}H and ^{11}B NMR spectra obtained indicated no conversion of the starting materials.

1-Hexene: The conversion of the title compound was determined according to **GP1** using the following amounts of alkene substrate and catalyst: 1-hexene (128 μL, 1 mmol), **5-2b** (0.0064 g, 1 mol%). The ^{11}B NMR spectrum obtained indicated full conversion of the pinacolborane starting material.

4-Methyl-1-pentene: The conversion of the title compound was determined according to **GP1** using the following amounts of alkene substrate and catalyst: 1-hexene (128 μL,

1 mmol), **5-2b** (0.0064 g, 1 mol%). The ^{11}B NMR spectrum obtained indicated full conversion of the pinacolborane starting material.

Allyltrimethylsilane: The conversion of the title compound was determined according to **GP1** using the following amounts of alkene substrate and catalyst: 1-hexene (164 μL, 1 mmol), **5-2b** (0.0096 g, 1.5 mol%). The ^{11}B NMR spectrum obtained indicated full conversion of the pinacolborane starting material.

***tert*-Butyl ethylene:** The conversion of the title compound was determined according to **GP1** using the following amounts of alkene substrate and catalyst: *tert*-butyl ethylene (129 μL, 1 mmol), **5-2b** (0.0064 g, 1 mol%). The ^{11}B NMR spectrum obtained indicated full conversion of the pinacolborane starting material.

2-Methyl-2-pentene: The conversion of the title compound was determined according to **GP1** using the following amounts of alkene substrate and catalyst: 2-methyl-2-pentene (150 μL, 1.2 mmol), **5-2b** (0.013 g, 2 mol%). The ^{11}B NMR spectrum obtained indicated full conversion of the pinacolborane starting material.

Cyclooctene: The conversion of the title compound was determined according to **GP1** using the following amounts of alkene substrate and catalyst: cyclooctene (164 μL, 1.2 mmol), **5-2b** (0.0064 g, 1 mol%). The ^{11}B NMR spectrum obtained indicated full conversion of the pinacolborane starting material.

Cyclohexene: The conversion of the title compound was determined according to **GP1** using the following amounts of alkene substrate and catalyst: cyclohexene (121 μL, 1.2 mmol), **5-2b** (0.032 g, 5 mol%). The ^{11}B NMR spectrum obtained indicated full conversion of the pinacolborane starting material.

1-Phenylethanol: The NMR yield of the title compound was determined according to **GP2** using the following amounts of carbonyl substrate and catalyst: acetophenone (117 μL, 1 mmol), **5-2b** (0.0064 g, 1 mol%). The ^{1}H NMR spectrum obtained indicated a 96 % NMR yield.

Cyclohexanol: The NMR yield of the title compound was determined according to **GP2** using the following amounts of carbonyl substrate and catalyst: cyclohexanone (104 μL, 1 mmol), **5-2b** (0.0064 g, 1 mol%). The ^{1}H NMR spectra obtained indicated a 98 % NMR yield.

2-Heptanol: The NMR yield of the title compound was determined according to **GP2** using the following amounts of carbonyl substrate and catalyst: 2-heptanone (143 μL, 1 mmol), **5-2b** (0.0064 g, 1 mol%). The ^{1}H NMR spectra obtained indicated a 101 % NMR yield.

7.4.9 Characterization of Isolated Hydroboration Products

(7-2) 2-Octyl-4,4,5,5-tetramethyl-1,3,2-dioxaborolane

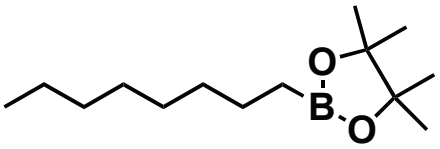

Method 1 (solvent free – from 1-octene, 7-1a): The title compound was synthesized according to **GP3** using the following amounts of alkene substrate and catalyst: 1-octene (160 μL, 1 mmol), **5-2b** (0.0064 g, 1 mol%). After drying *in vacuo* **7-2** was isolated in 95% yield (0.230 g, 0.96 mmol) as a colorless oil. **Method 2 (solvent free – from *cis*-4-octene, 7-1b):** The title compound was synthesized according to **GP3** using the following amounts of alkene substrate and catalyst: *cis*-4-octene (160 μL, 1 mmol), **5-2b** (0.0096 g,

1.5 mol%). After drying *in vacuo* **7-2** was isolated in 95% yield (0.228 g, 0.95 mmol) as a colorless oil. **Method 3 (solvent free – from *trans*-4-octene, 7-1c):** The title compound was synthesized according to **GP3** using the following amounts of alkene substrate and catalyst: trans-4-octene (160 μL, 1 mmol), **5-2b** (0.016 g, 2.5 mol%). After drying *in vacuo* **7-2** was isolated in 96% yield (0.229 g, 0.96 mmol) as a colorless oil. **Method 4 (solvent free - octene mixture, 7-1a-c):** The title compound was synthesized according to **GP2** using the following amounts of alkene substrates and catalyst: 1-octene (53 μL, 0.33 mmol), *cis*-4-octene (53 μL, 0.33 mmol), *trans*-4-octene (54 μL, 0.34 mmol), **5-2b** (0.016 g, 2.5 mol%). After drying *in vacuo* **7-2** was isolated in 95% yield (0.228 g, 0.95 mmol) as a colorless oil. **Method 5 (with solvent – from 1-octene, 7-1a):** The title compound was synthesized according to **GP4** using the following amounts of alkene substrate and catalyst: 1-octene (160 μL, 1 mmol), **5-2b** (0.0032 g, 0.5 mol%). After removal of solvent **7-2** was isolated in 95% yield (0.228 g, 0.96 mmol) as a colorless oil. ^{1}H NMR (300.1 MHz, $CDCl_3$): δ 1.35 (m, 2 H), 1.18-1.22 (overlapping peaks, 22 H), 0.83 (m, 3 H), 0.72 (t, 2 H, J = 8 Hz). $^{13}C\{^{1}H\}$ NMR (75.5 MHz, $CDCl_3$): δ 83.0, 32.6, 32.1, 29.5-29.6 (overlapping peaks), 25.0, 24.2, 22.9, 14.3. ^{11}B NMR (96.3 MHz, $CDCl_3$): δ 34.1. Spectral data are in close agreement with previously reported ^{1}H and ^{13}C NMR characterization data for the title compound.[140b]

(7-3) 2-Hexyl-4,4,5,5-tetramethyl-1,3,2-dioxaborolane

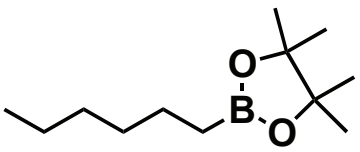

Solvent Free: The title compound was synthesized according to **GP3** using the following amounts of alkene substrate and catalyst: 1-hexene (128 μL, 1 mmol), **5-2b** (0.0064 g, 1

mol%). After drying *in vacuo* **7-3** was isolated in 94% yield (0.200 g, 0.94 mmol) as a colorless oil. **With Solvent:** The title compound was synthesized according to **GP4** using the following amounts of alkene substrate and catalyst: 1-hexene (128 μL, 1 mmol), **5-2b** (0.0032 g, 0.5 mol%). After removal of solvent **7-3** was isolated in 92% yield (0.196 g, 0.92 mmol) as a colorless oil. ^{1}H NMR (300.1 MHz, $CDCl_3$): δ 1.33 (m, 2 H), 1.18-1.24 (overlapping peaks, 18 H), 0.81 (m, 3 H), 0.70 (t, 2 H, J = 8 Hz). $^{13}C\{^{1}H\}$ NMR (75.5 MHz, $CDCl_3$): δ 83.0, 32.3, 31.8, 25.0, 24.1, 22.7, 14.2. ^{11}B NMR (96.3 MHz, $CDCl_3$): δ 34.2. Spectral data are in close agreement with previously reported ^{1}H and ^{13}C NMR characterization data for the title compound.[147]

(7-4) 2-(4-Methylpentyl)-4,4,5,5-tetramethyl-1,3,2-dioxaborolane

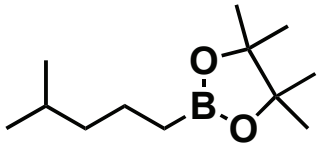

Solvent Free: The title compound was synthesized according to **GP3** using the following amounts of alkene substrate and catalyst: 4-methyl-1-pentene (130 μL, 1 mmol), **5-2b** (0.0064 g, 1 mol%). After drying *in vacuo* **7-4** was isolated in 98% yield (0.208 g, 0.98 mmol) as a colorless oil. **With Solvent:** The title compound was synthesized according to **GP4** using the following amounts of alkene substrate and catalyst: 4-methyl-1-pentene (130 μL, 1 mmol), **5-2b** (0.0032 g, 0.5 mol%). After removal of solvent **6** was isolated in 92% yield (0.193 g, 0.92 mmol) as a colorless oil. ^{1}H NMR (300.1 MHz, $CDCl_3$): δ 1.49 (m, 1 H), 1.35 (m, 2 H), 1.20 (s, 12 H), 1.13 (m, 2 H), 0.82 (d, 6 H, J = 7 Hz), 0.73 (t, 2 H, J = 7 Hz). $^{13}C\{^{1}H\}$ NMR (75.5 MHz, $CDCl_3$): δ 83.0, 42.2, 28.0, 25.0, 22.8, 22.0. ^{11}B NMR (96.3 MHz, $CDCl_3$): δ 34.2. Spectral data are in close agreement with previously reported ^{1}H and ^{13}C NMR characterization data for the title compound.[140b]

(7-5) Trimethyl(3-(4,4,5,5-tetramethyl-1,3,2-dioxaborolan-2-yl)propyl)silane

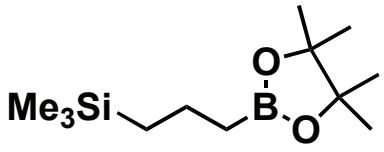

Solvent Free: The title compound was synthesized according to **GP3** using the following amounts of alkene substrate and catalyst: allyltrimethysilane (164 μL, 1 mmol), **5-2b** (0.0064 g, 1 mol%). After drying *in vacuo* **7-5** was isolated in 98% yield (0.238 g, 0.98 mmol) as a colorless oil. **With Solvent:** The title compound was synthesized according to **GP4** using the following amounts of alkene substrate and catalyst: allyltrimethylsilane (164 μL, 1 mmol), **5-2b** (0.0032 g, 0.5 mol%). After removal of solvent **7-5** was isolated in 97% yield (0.236 g, 0.927 mmol) as a colorless oil. ^{1}H NMR (300.1 MHz, $CDCl_3$): δ 1.39 (m, 2 H), 1.20 (s, 12 H), 0.78 (t, 2 H, J = 8 Hz), 0.48 (m, 2 H), -0.08 (s, 9 H). $^{13}C\{^{1}H\}$ NMR (75.5 MHz, $CDCl_3$): δ 83.2, 25.0, 20.3, 18.8, -1.4. ^{11}B NMR (96.3 MHz, $CDCl_3$): δ 34.0. Spectral data are in close agreement with previously reported ^{1}H and ^{13}C NMR characterization data for the title compound.[140b]

(7-6) 2-(3,3-Dimethylbutyl)-4,4,5,5-tetramethyl-1,3,2-dioxaborolane

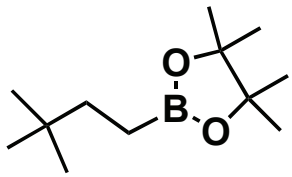

The title compound was synthesized according to **GP3** using the following amounts of alkene substrate and catalyst: *tert*-butylethylene (129 μL, 1 mmol), **5-2b** (0.0096 g, 1.5 mol%). After drying *in vacuo* **7-6** was isolated in 98% yield (0.208 g, 0.98 mmol) as a colorless oil. ^{1}H NMR (300.1 MHz, $CDCl_3$): δ 1.20-1.29 (overlapping peaks, 14 H), 0.81 (s, 9 H), 0.67 (t, 2 H, J = 9 Hz). $^{13}C\{^{1}H\}$ NMR (75.5 MHz, $CDCl_3$): δ 83.0, 37.9, 31.0,

29.0, 25.0. ^{11}B NMR (96.3 MHz, $CDCl_3$): δ 34.4. Spectral data are in close agreement with previously reported ^{1}H and ^{13}C NMR characterization data for the title compound.[140b]

(7-7) 2-(2-Methylpentyl)-4,4,5,5-tetramethyl-1,3,2-dioxaborolane

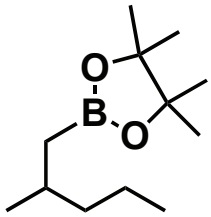

The title compound was synthesized according to **GP3** using the following amounts of alkene substrate and catalyst: 2-methyl-1-pentene (150 μL, 1.2 mmol), **5-2b** (0.013 g, 2 mol%). After drying *in vacuo* **7-7** was isolated in 90% yield (0.191 g, 0.90 mmol) as a colorless oil. ^{1}H NMR (300.1 MHz, $CDCl_3$): δ 1.66 (m, 1 H), 1.13-1.32 (overlapping peaks, 16 H), 0.76-0.88 (overlapping peaks, 7 H), 0.64 (m, 1 H). ^{13}C{^{1}H} NMR (75.5 MHz, $CDCl_3$): δ 83.1, 42.2, 29.4, 25.1, 25.0, 22.8, 20.1, 14.5. ^{11}B NMR (96.3 MHz, $CDCl_3$): δ 34.0. Spectral data are in close agreement with previously reported ^{1}H and ^{13}C NMR characterization data for the title compound.[140b]

(7-8) 2-Cyclohexyl-4,4,5,5-tetramethyl-1,3,2-dioxaborolane

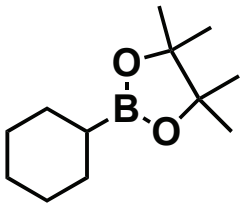

The title compound was synthesized according to **GP3** using the following amounts of alkene substrate and catalyst: cyclohexene (121 μL, 1.2 mmol), **5-2b** (0.032 g, 5 mol%). After drying *in vacuo* **7-8** was isolated in 92% yield (0.194 g, 0.92 mmol) as a pale yellow oil. ^{1}H NMR (300.1 MHz, $CDCl_3$): δ 1.49-1.66 (overlapping peaks, 4 H), 1.25-

1.37 (overlapping peaks, 18 H), 0.95 (m, 1 H). $^{13}C\{^{1}H\}$ NMR (75.5 MHz, $CDCl_3$): δ 82.7, 28.1, 27.3, 27.0, 24.9. ^{11}B NMR (96.3 MHz, $CDCl_3$): δ 33.2. Spectral data are in close agreement with previously reported ^{1}H and ^{13}C NMR characterization data for the title compound.[140b]

(7-9) 2-Cyclooctyl-4,4,5,5-tetramethyl-1,3,2-dioxaborolane

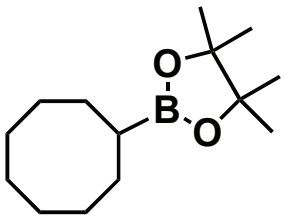

The title compound was synthesized according to **GP3** using the following amounts of alkene substrate and catalyst: cyclooctene (164 μL, 1.2 mmol), **5-2b** (0.0064 g, 1 mol%). After drying *in vacuo* **7-9** was isolated in 96% yield (0.230 g, 0.96 mmol) as a colorless oil. ^{1}H NMR (300.1 MHz, $CDCl_3$): δ 1.49-1.74 (overlapping peaks, 14 H), 1.20 (s, 12 H), 1.08 (m, 1 H). $^{13}C\{^{1}H\}$ NMR (75.5 MHz, $CDCl_3$): δ 82.9, 27.8, 27.2, 27.1, 26.9, 24.9. ^{11}B NMR (96.3 MHz, $CDCl_3$): δ 33.2. Spectral data are in close agreement with previously reported ^{1}H and ^{13}C NMR characterization data for the title compound.[140b]

(7-10) 1-Phenylethanol

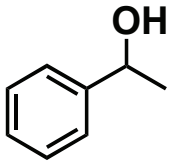

The title compound was synthesized according to **GP5** using the following amounts of ketone substrate and catalyst: acetophenone (234 μL, 2 mmol), **5-2b** (0.013 g, 1 mol%). After distillation (<0.1 mm Hg, bp = 53 °C) **7-10** was isolated in 74% yield (0.181 mg, 1.48 mmol) as a colourless oil. ^{1}H NMR (300.1 MHz, $CDCl_3$): δ 7.27-7.39 (overlapping

peaks, 5 H), 4.89 (q, 1 H, J = 7 Hz), 2.24 (br s, 1 H), 1.51 (d, 3 H, J = 7 Hz). $^{13}C\{^{1}H\}$ NMR (75.5 MHz, $CDCl_3$): δ 145.9, 128.7, 127.7, 125.6, 70.6, 25.4. Spectral data are in close agreement with previously reported ^{1}H and ^{13}C NMR characterization data for the title compound.[148]

(7-11) Cyclohexanol

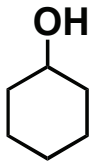

The title compound was synthesized according to **GP5** using the following amounts of ketone substrate and catalyst: cyclohexanone (234 μL, 2 mmol), **1-Co** (0.013 g, 1 mol%). After distillation (<0.1 mm Hg, bp = 30 °C) **13** was isolated in 51% yield (0.102 g, 1.02 mmol) as a pale yellow oil. ^{1}H NMR (300.1 MHz, $CDCl_3$): δ 3.63 (m, 1 H), 1.87-1.96 (m, 2 H), 1.73-1.76 (m, 2 H), 1.09-1.57 (m, 7 H). $^{13}C\{^{1}H\}$ NMR (75.5 MHz, $CDCl_3$): δ 70.4, 35.7, 25.7, 24.3. Spectral data are in close agreement with previously reported ^{1}H and ^{13}C NMR characterization data for the title compound.[148]

(7-12) 2-Heptanol

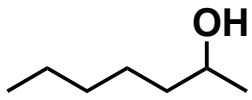

The title compound was synthesized according to **GP5** using the following amounts of ketone substrate and catalyst: 2-heptanone (285 μL, 2 mmol), **5-2b** (0.013 g, 1 mol%). After distillation (<0.1 mm Hg, bp = 29 °C) **7-12** was isolated in 47% yield (0.109 mg, 0.94 mmol) as a pale yellow oil. ^{1}H NMR (300.1 MHz, $CDCl_3$): δ 3.80 (apparent sextet, 1 H, J = 5 Hz), 1.29-1.44 (m, 9 H), 1.18 (d, 3 H, J = 6 Hz), 0.89 (t, 3 H, J = 7 Hz). $^{13}C\{^{1}H\}$ NMR (75.5 MHz, $CDCl_3$): δ 68.2, 39.3, 31.8, 25.4, 23.5, 22.6, 14.0. Spectral

data are in close agreement with previously reported ^{1}H and ^{13}C NMR characterization data for the title compound.[149]

CHAPTER 8: Conclusions and Future Work

8.1 Summary and Conclusions

The synthesis, characterization and reactivity of transition metal complexes supported by heteropolydentate ligation have been detailed in this thesis. In Chapter 2, the synthesis and reactivity of Ru, Rh, and Ir complexes featuring the [^{t}Bu-PSiN-Me]H pro-ligand (**2-4**) were outlined. The cyclometalation of **2-4** to Ru starting materials proved difficult, resulting in either the formation of multiple products or a [^{t}Bu-PSiC]Ru carbene complex (**2-5**), where the PSiN pro-ligand underwent multiple C-H cleavage steps to form a Fischer carbene. The Ru=C bond in **2-5** proved to be fairly unreactive, however the addition of H_2 across this double bond was demonstrated, resulting in the formation of the [PSiC]Ru η^6-benzene complex **2-6**. In an effort to promote the coordination of the amino donor to the metal center, the synthesis of Rh and Ir complexes featuring PSiN ligation was targeted. Complexes of the type [^{t}Bu-PSiN-Me]M(H)Cl (**2-7**, M = Rh; **2-8**, M = Ir) proved to be readily accessible, and coordination the amino donor to the metal center was confirmed for these complexes by X-ray diffraction analysis as well as solution NMR techniques. The amino donor in such complexes proved to be at least somewhat labile, as the NMe_2 group in the Rh complex **2-7** was easily displaced by PMe_3 to form complex **2-9**. Attempts to generate a potentially highly reactive [^{t}Bu-PSiN-Me]M^I species capable of oxidatively adding E-H bonds have proven unsuccessful, with such reactions resulting in decomposition of the metal containing species. Alternatively, it was found that potentially cationic [^{t}Bu-PSiN-Me]Ir(H)X (X = OTf, BF_4) complexes **2-10** and **2-11** appeared to be reactive towards sp^2 (intermolecular)

and sp^3 (intramolecular) C-H bonds. Unfortunately, the instability of such complexes made it difficult to truly probe their stoichiometric reactivity.

In an effort to synthesize more robust late transition metal complexes featuring PSiN ligation, the synthesis of alternative PSiN pro-ligands and their corresponding metal complexes was explored in Chapter 3. In order to establish a method for the facile modification of the PSiN ligand architecture, an alternative modular synthesis of PSiN pro-ligands was devised involving the formation of a (phosphinoaryl)chlorosilane (**3-1**), followed by installation of the amino donor arm. This synthetic route was found to be successful for the synthesis of PSiN pro-ligands [^{t}Bu-PSiN-Me]H (**2-4**), [^{t}Bu-PSiN-Et]H (**3-2**), [^{t}Bu-PSiNPy]H (**3-3**), and [^{t}Bu-PSi=N]H (**3-4**) in good yields. It was found that pro-ligands **3-2** and **3-3** could be metalated to late transition metals such as Rh, Ir, Ni, Pd and Pt. Unfortunately, late metal complexes supported by such alternative PSiN ligands were largely found to be unstable both in solution and in the solid state. These studies led to the conclusion that PSiN ligated late metal species are relatively unstable, and unlike their PSiP analogues, they are therefore not ideally suited for the study of E-H (E = main group element) bond activation processes.

The synthesis and characterization of cobalt complexes featuring bis(phosphino)silyl (PSiP) ligation was the subject of Chapter 4. It was found that the [Cy-PSiP]H pro-ligand could be cyclometalated to the simple cobalt salt CoI_2 to furnish [Cy-PSiP]Co-I (**4-2**) in a high yield, demonstrating the first metalation of a PSiP ligand to a simple cobalt salt. Crystals of the analogous chloride complex **4-1** were isolated, however the reaction proved to be low yielding and inconsistent. Due to the high yielding and facile synthesis of **4-2**, it was chosen as an ideal entry point into [Cy-

PSiP]Co chemistry. Attempts to reduce the Co^{II} species **4-2** to the corresponding Co^{I} complex was met with little success, suggesting that further stabilization may be required to isolate such species. Reaction of **4-2** with PMe_3 resulted in the formation of [Cy-PSiP]Co(PMe_3)I (**4-3**), which was successfully reduced to the corresponding Co^{I} species [Cy-PSiP]Co(PMe_3)(N_2) (**4-5**), where N_2 was found to be coordinated to the metal center. Through comparison to the literature it was found that the degree of activation of the N_2 ligand was mild, and thusly it was proposed that the N_2 ligand may be labile, providing access to a potentially reactive 16-electron, Co^{I} species capable of oxidative addition reactions to form 18-electron Co^{III} products.

Attempts to oxidatively add iodobenzene and H_2 to [Cy-PSiP]Co(PMe_3)(N_2) did not result in the anticipated Co^{III} oxidative addition products. In the case of iodobenzene, the formation of what are postulated to be multiple paramagnetic Co^{II} species was observed. Treatment of **4-5** with H_2 resulted in the generation of a new species where the N_2 ligand in **4-5** had been displaced by H_2 to provide a nonclassical dihydrogen complex, as confirmed by the use of T_{1min} measurements. Thus it appears that although the electron-rich [Cy-PSiP]Co(PMe_3) species may be accessed in the course of such reactions, it does not readily undergo oxidative addition processes. Future studies will further explore the coordination chemistry of (PSiP)Co, with the goal of accessing new complexes that may more easily undergo such two-electron redox processes.

The synthesis of *N*-phosphinoamidine pro-ligands and their corresponding low-coordinate first-row transition metal complexes was the subject of Chapter 5. *N*-phosphinoamidine pro-ligands **5-1a** - **5-1c** were found to be readily accessible through the lithiation of easily prepared amidines and subsequent quenching with a

chlorophosphine. The ligation of such pro-ligands as neutral *N*-phosphinoamidines to iron centers was found to be unsuccessful, typically resulting in no reaction or an incomplete reaction. Alternatively, attempts at accessing monoanionic *N*-phosphinoamidinate ligation were met with considerable success. Ligation of $P(^tBu)_2$ substituted *N*-phosphinoamidine pro-ligands **5-1a** and **5-1b** via deprotometalation reactions resulted in the formation of the three-coordinate, high spin iron amido complexes **5-2a** - **5-2c** in moderate yields as crystalline solids.

Attempts at isolating (*N*-phosphinoamidinate)iron(alkyl) and (*N*-phosphinoamidinate)iron(chloride) complexes were met with less success as the reproducible synthesis of alkyl and chloride complexes **5-3** - **5-5** was elusive. Current efforts towards the isolation of (*N*-phosphinoamidinate)iron(halide) complex are focused on using $FeBr_2$ as the iron source. Attempted synthesis of an analogue of **5-2b** featuring less bulky $P(Ph)_2$ substitution resulted in the formation of the four-coordinate complex **5-6**, where two P,N ligands underwent ligation to the metal center. Such an observation suggests that bulky substitution at phosphorus is required for the isolation of three-coordinate complexes featuring *N*-phosphinoamidinate ligation. The investigation of alternatively substituted *N*-phosphinoamidinate ligands in the isolation of low-coordinate complexes is ongoing.

An investigation examining the catalytic utility of new three-coordinate Fe^{II} and Co^{II} *N*-phosphinoamidinate complexes was described in Chapter 6. Such complexes were found to be highly effective pre-catalysts in the challenging room temperature hydrosilylation of carbonyl compounds to alcohols. The superior performance of the well-defined Fe^{II} amido pre-catalyst (**5-2b**), which features sterically demanding *N*-2,6-

diisopropylphenyl and di(*tert*-butyl)phosphino moieties within the *N*-phosphinoamidinate ligand, was established in such applications. Notably, pre-catalyst **5-2b** operates at very low catalyst loadings (0.01-1.0 mol% Fe), requires the use of only one equivalent of phenylsilane reductant, and exhibits the broadest scope (37 examples total) of any reported iron pre-catalyst for carbonyl hydrosilylation at room temperature. Included for the first time in the room temperature catalytic survey are examples of iron-catalyzed hydrosilylations of benzophenones, sterically demanding acyclic dialkyl ketones, heteroaryl acetophenones, and esters en route to alcohols. Attempts to better understand the factors that contribute to the desirable catalytic profile exhibited by **5-2b** in carbonyl hydrosilylation reactions are ongoing.

The results presented in Chapter 7 establish the utility of the easily prepared, three-coordinate (*N*-phosphinoamidinate)cobalt(amido) pre-catalyst (**5-2c**) in challenging room temperature alkene hydroboration reactions that can be conducted in the presence or absence of added solvent. The efficient *anti*-Markovnikov addition of HBPin to linear and branched mono-substituted terminal alkenes, gem-disubstituted terminal alkenes, and linear internal octenes is reported, as is the hydroboration of cyclic alkenes and ketones. Particularly significant is the observation that **5-2c** promotes alkene isomerization/hydroboration processes involving both *cis*- and *trans*-4-octene, leading to the selective terminal addition of the BPin group. With the exception of a recent report that appeared while this thesis was in preparation,[142] such alkene isomerization/hydroboration chemistry is without precedent in base metal hydroboration catalysis, and underscores how appropriately ligated cobalt complexes can provide access

to challenging and synthetically useful reactivity manifolds that are normally reserved for the platinum-group metals.

8.2 Future Work

The research described in Chapters 2 and 3 indicated that the PSiN ligand framework is not ideal for the synthesis of robust late transition metal complexes featuring a hemilabile neutral donor. To this effect, it is proposed that the application of PSiP ligands featuring alternative substitution at the phosphorus centers may be a better approach for the synthesis of 'hemilabile' silyl pincer complexes. For example, one could envision synthesis of PSiP ligands of the type [Cy-PSiP-Ph] where the $P(Ph)_2$ substituent would be expected to more weakly coordinated to the metal center than the PCy_2 substituent. Such a difference in the electronic profiles of the phosphino substituents could potentially lead to PSiP ligands that exhibit hemilabile character. Alternatively, even without exhibiting any hemilabile character, such ligands are appealing targets as literature precedent suggests that changes in the nature of the phosphine substituents within the pincer ligand architecture can have a pronounced effect on the reactivity of the resulting complexes.[4] Such nonsymmetrical PSiP ligands should be easily prepared by the similar routes used to prepare PSiN pro-ligands in Chapter 3, where a (phosphinoaryl)chlorosilane is reacted with various lithium salts to synthesize the desired pro-ligand (Scheme 8-1). Furthermore, this technique could be applied to the synthesis of silyl pincer ligands containing alternative heteroatoms such as O and S, which would provide access to silyl pincer ligands containing a mixed set of P/S or P/O neutral donors. Once synthesized, attempts to cyclometalate such ligands to late

transition metal centers by some of the routes detailed in Chapters 2 and 3 of this document can be pursued. Once such complexes are synthesized, the stoichiometric reactivity of such species in the activation and functionalization of E-H bonds may be investigated.

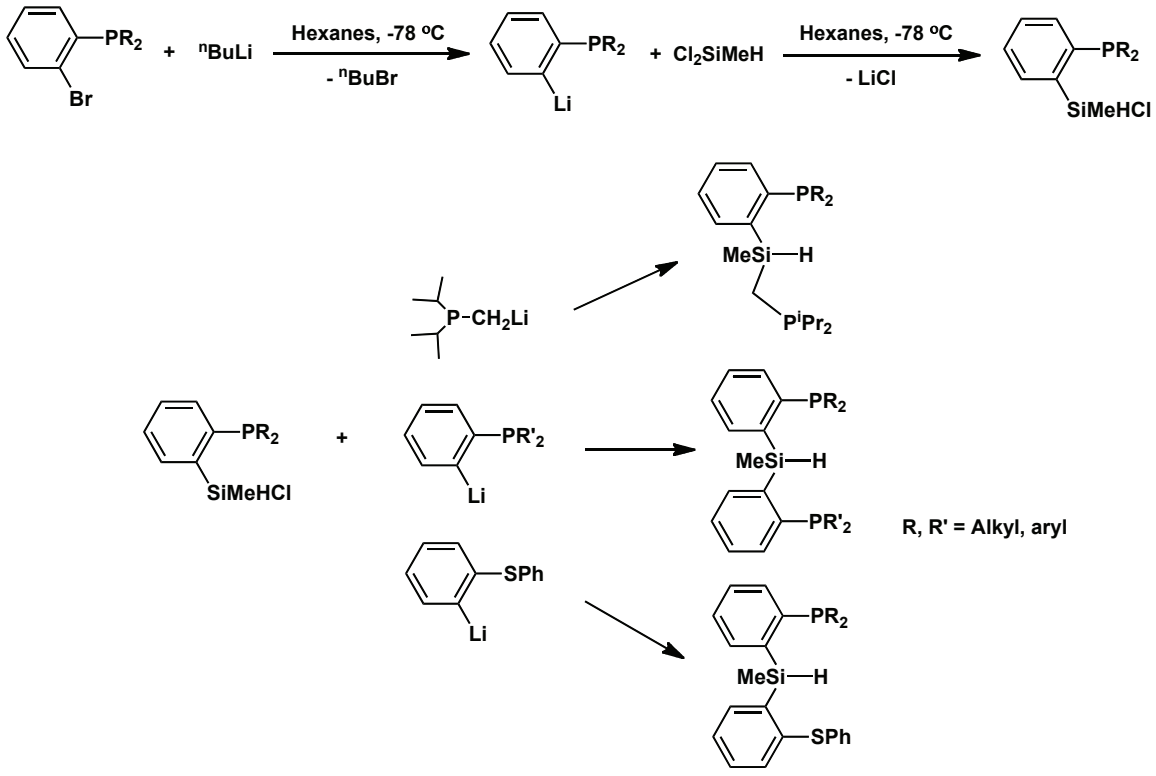

Scheme 8-1. Proposed synthesis of alternative PSiP and PSiS pro-ligands.

The results discussed in Chapter 4 suggest that the electron-rich [Cy-PSiP]Co(PMe_3) Co^I species is readily accessible, however it does not appear to be an optimal framework for the study of oxidative addition to cobalt centers. An extremely recent report form Chirik suggests that a key requirement for the oxidation of Co^I to Co^{III} is the use of extremely strong field ligands to promote such two-electron processes.[150] To this effect, it is proposed that replacing the PMe_3 in [Cy-PSiP]Co(PMe_3) with a CO ligand may provide a stronger ligand field that may promote two-electron chemistry at the cobalt center. Carbonyl ligands are amongst the strongest field ligands known, and thus

may be a more appropriate co-ligand for promoting two-electron oxidative addition processes than PMe_3 (a weaker field ligand than CO). Furthermore, CO may be a better ligand in this system due to its smaller size, which may facilitate the formation of the potential six-coordinate Co^{III} products due to the minimization of steric repulsion between the six ligands around the metal center. The proposed [Cy-PSiP]Co(CO) species should be readily accessed by syntheses analogous to those described in Chapter 4 (Scheme 8-2).

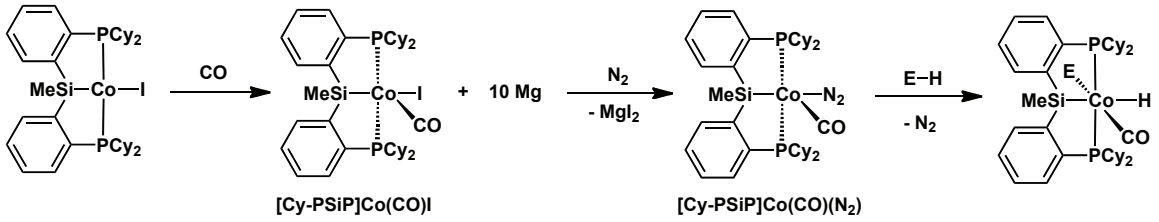

Scheme 8-2. Proposed synthesis of [Cy-PSiP]Co(CO)(N_2) and its potential reactivity in E-H bond activations.

The application of sterically demanding *N*-phosphinoamidinate ligation in the formation of low-coordinate Fe and Co complexes was the subject of Chapter 5. In subsequent chapters such Fe and Co complexes were demonstrated to be exceptional pre-catalysts for catalytic carbonyl hydrosilylation and alkene hydroboration reactions. Mechanistic studies of such systems are underway, however the application of such *N*-phosphinoamidinate ligated iron and cobalt complexes in alternative catalytic reactions is also highly desirable. Unfortunately, due to the involvement of an industrial collaborator in this project (CPChem), the exact nature of future research proposals cannot be disclosed at this time.

REFERENCES

(1) (a) Knowles, M. S. *Angew. Chem. Int. Ed.* **2002,** *41*, 2000. (b) Noyori, R. *Angew. Chem. Int. Ed.* **2002,** *41*, 2008. (c) Sharpless, K. B., *Angew. Chem. Int. Ed.* **2002,** *41*, 2024.

(2) (a) Schrock, R. R. *Angew. Chem. Int. Ed.* **2006,** *45*, 3748. (b) Grubbs, R. H. *Angew. Chem. Int. Ed.* **2006,** *45*, 3760. (c) Chauvin, Y. *Angew. Chem. Int. Ed.* **2006,** *45*, 3740.

(3) Wu, X. F.; Anbarasan, P.; Neumann, H.; Beller, M. *Angew. Chem. Int. Ed.* **2010,** *48*, 9047.

(4) (a) Albrecht, M.; van Koten, G. *Angew. Chem. Int. Ed.* **2001,** *40*. (b) van der Boom, M. E.; Milstein, D. *Chem. Rev.* **2003,** *103*, 1759. (c) Liang, L. C. *Coord. Chem. Rev.* **2006,** *150*, 1152. (d) Leis, W.; Meyer, H. A.; Kaska, W. C. *Coord. Chem. Rev.* **2008,** *252*, 1787. (e) Morales-Morales, D.; Jensen, C. M., Eds. *The Chemistry of Pincer Compunds*. Elsevier: Oxford: 2007. (f) van Koten, G.; Milstein, D. Eds. *Organometallic Pincer Chemistry*. Springer. 2013

(5) Jensen, C. M. *Chem. Commun.* **1999**, 2443.

(6) Fischer, J.; Schurmann, M.; Mehring, M.; Zachwieja, U.; Jurkschat, K. *Organometallics* **2006,** *25*, 2886.

(7) (a) Zim, D.; Gruber, A. S.; Ebeling, G.; Dupont, J.; Monteiro, A. L. *Org. Lett.* **2000,** *2*, 2281. (b) Espinet, P.; Garcia-Orodea, E.; Miguel, J. A. *Chem. Mater.* **2004,** *16*, 551.

(8) (a) Olsson, V. J.; Sevelius, S.; Selander, N.; Szabo, K. J. *J. Am. Chem. Soc.* **2006,** *128*, 4588. (b) Yao, Q.; Sheets, M. *J. Org. Chem.* **2006,** *71*, 5384.

(9) (a) Grundemann, S.; Albrecht, M.; Loch, J. A.; Faller, J. W.; Crabtree, R. H.; *Organometallics*. **2001**, *20*, 5485. (b) Bauer, E. B.; Andavan, G. T. S.; Hollis, T. K.; Rubio, R. J.; Cho, J.; Kuchenbeiser, G. R.; Helgert, T. R.; Letko, C. S.; Tham, F. S. *Org. Lett*. **2008**, *10*, 1175. (c) Raynal, M.; Cazin, C. S. J.; Vallee, C.; Olivier-Bourbigou, H.; Braunstein, P. *Chem. Commun*. **2008**, 3983. (d) Segawa, Y.; Yamashita, M.; Nozaki, K. *J. Am. Chem. Soc.* **2009,** *131*, 9201. (e) Schultz, K. M.; Goldberg, K. I.; Gusev, D. G.; Heinekey, D. M. *Organometallics*. **2011**, *30*, 1429. (f) Zuo, W. W.; Braunstein, P. *Organometallics*. **2012**, *31*, 2606. (g) Helgert, T. R; Hollis, K. T.; Valente, E. J. *Organometallics*. **2012**, *31*, 3002. (h) Helgert, T. R; Hollis, K. T.; Oliver, A. G.; Valle, H. U.; Wu, Y.; Webster, C. E. *Organometallics*. **2014**, *33*, 952. (i) Chianese, A. R.; Drance, M. J.; Jensen, K. H.; McCollum, Yusufova, N.; Shaner, S. E.; Shopov, D. Y., Tendler, J. A. *Organometallics*. **2014**, *33*, 457

(10) Hermann, W. A. *Angew. Chem. Int. Ed.* **2002,** *41*, 1290.

(11) (a) Moulton, C. J.; Shaw, B. L. *Dalton Trans.* **1976**, 1020. (b) Empsall, H. D.; Hyde, E. M.; Markam, R.; McDonald, W. S.; Norton, M. C.; Shaw, B. L.; Weeks, B. *J. Chem. Soc. Chem. Commun.* **1977,** 589. (c) Al-Salem, N. A.; Empsall, H. D.; Markam, R.; Shaw, B. L.; Weeks, B. *J. Chem. Soc. Dalton Trans.* **1979**, 1972. (d) Crocker, C.; Errington, R. J.; McDonald, W. S.; Odell, K. J.; Shaw, B. L. *J. Chem. Soc. Chem. Commun.* **1979**, 498. (e) Crocker, C.; Errington, R. J.; Moulton, C. J.; Odell, K. J.; Shaw, B. L. *J. Am. Chem. Soc.* **1980,** *102*, 4373.

(12) (a) Liu, F.; Goldman, A. S. *Chem. Commun.* **1999**, 655. (b) Gottker-Schnetmann, I.; White, P.; Brookhart, M. *J. Am. Chem. Soc.* **2004,** *126*, 1804.

(13) Kanzelberger, M.; Zhang, X.; Ernge, T. J.; Goldman, A. S.; Zhao, J.; Incarvito, C.; Hartwig, J. F. *J. Am. Chem. Soc.* **2003,** *125*, 13644.

(14) Watson, L. A.; V., O. O.; Pink, M.; Caulton, K. G. *J. Am. Chem. Soc.* **2003,** *125*, 8426.

(15) (a) Ben-Ari, E.; Leitus, G.; Shimon, L. J. W.; Milstein, D. *J. Am. Chem. Soc.* **2006,** *128*, 15390. (b) Ben-Ari, E.; Gandelman, M.; Rozenberg, H.; Shimon, L. J. W.; Milstein, D. *J. Am. Chem. Soc.* **2003,** *125*, 4714.

(16) Khaskin, E.; Iron, M. A.; Shimon, L. J. W.; Zhang, J.; Milstein, D. *J. Am. Chem. Soc.* **2010,** *132*, 8542.

(17) Braunstein, P.; Naud, F. *Angew. Chem. Int. Ed.* **2001,** *40*, 680.

(18) Helmchen, G.; Pfaltz, A. *Acc. Chem. Res.* **2000,** *33*, 336.

(19) Helmchen, G. *J. Organomet. Chem.* **1999,** *576*, 203.

(20) Loiseleur, O.; Hayashi, M.; Keenan, M.; Schmees, N.; Pfaltz, A. *J. Organomet. Chem.* **1999,** *576*, 16.

(21) Langer, T.; Helmchen, G. *Tetrahedron Lett.* **1996,** *37*, 1381.

(22) Pfaltz, A.; Blankenstein, J.; Hilgraf, R.; Hormann, E.; McIntyre, S.; Menges, F.; Schonleber, M.; Smidt, S.; Wusternburg, B.; Zimmerman, N. *Adv. Synth. Catal.* **2003,** *345*, 33.

(23) (a) Guiry, P. J.; Saunders, C. P. *Adv. Synth. Catal.* **2004,** *346*, 497. (b) Lundgren, R. J.; Stradiotto, M. *Chem. Eur. J.* **2012**, *18*, 9758.; (c) Carroll, M. P.; Guiry, P. J; *Chem. Soc. Rev*. **2014**, *43*, 819

(24) (a) Zhang, J.; Gandelman, M.; Shimon, L. J. W.; Milstein, D. *Organometallics* **2004,** *23*, 4026. (b) Zhang, J.; Leitus, G.; Ben-David, Y.; Milstein, D. *J. Am. Chem. Soc.* **2005,** *127*, 10840. (c) Vuzman, D.; Poverenov, E.; Shimon, L. J. W.; Diskin-Posner, Y.; Milstein, D. *Organometallics* **2008,** *27*, 2627. (d) Balaraman, E.; Gnanaprakasam, B.; Shimon, L. J. W.; Milstein, D. *J. Am. Chem. Soc.* **2010,** *132*, 16756. (e) Choualeb, A.; Lough, A. J.; Gusev, D. G. *Organometallics* **2007,** *26*, 5224. (f) Barrios-Francisco, R.; Balaraman, E.; Diskin-Posner, Y; Leitus, G.; Shimon, L. J. W.; Milstein, D. *Organometallics* **2013**, *32*, 2973.

(25) (a) Poverenov, E.; Gandelman, M.; Shimon, L. J. W.; Milstein, D. *Chem. Eur. J.* **2004,** *10*, 4673. (b) Gandelman, M.; Vigalok, A.; Shimon, L. J. W.; Milstein, D. *Organometallics* **1997,** *16*, 3981. (c) Poverenov, E.; Gandelman, M.; Shimon, L. J. W.; Rozenberg, H.; Ben-David, Y.; Milstein, D. *Organometallics* **2005,** *24*, 1082. (d) Spasyuk, D. M.; Zargarian, D.; van der Est, A. *Organometallics.*, **2009**, *28*, 6531. (e) Spasyuk, D. M.; Zargarian, D.; *Inorg. Chem*, **2010**, *49*, 6203. (f) Niu, J-L.; Chen, Q-T.; Hao, X-Q.; Zhao, Q-X.; Gong, J-F.; Song, M.P. *Organometallics* **2010**, *29*, 2148

(26) (a) Zhang, J.; Leitus, G.; Ben-David, Y.; Milstein, D. *Angew. Chem. Int. Ed.* **2006,** *45*, 1113. (b) Zhang, J.; Gandelman, M.; Shimon, L. J. W.; Milstein, D., *Dalton Trans.* **2007**, 107. (c) Guanathan, B.; Ben-David, Y.; Milstein, D. *Science* **2007,** *317*, 790. (d) Guanathan, B.; Shimon, L. J. W.; Milstein, D. *J. Am. Chem. Soc.* **2009,** *131*, 3146. (e) Gnanaprakasam, B.; Balaraman, E.; Ben-David, Y.; Milstein, D. *Angew. Chem. Int. Ed.* **2011**, *50*, 12240. (f) Balaraman, E.; Ben-David, Y.; Milstein, D. *Angew. Chem. Int. Ed.* **2011**, *50*, 11702. (g) Srimani, D.; Ben-David, Y.; Milstein, D. *Angew. Chem. Int. Ed.* **2013**, *52*, 4012.

(27) Smith, M. B. *Compendium of Organic Synthetic Methods*. Wiley: New York, **2001**; Vol. 9.

(28) Kohl, S. W.; Weiner, L.; Schwartsburd, L.; Konstantinovski, L.; Shimon, L. J. W.; Ben-David, Y.; Iron, M. A.; Milstein, D. *Science* **2009,** *324*, 74.

(29) (a) Lewis, N. S.; Nocera, D. G. *Proc. Natl. Acad. Sci. USA* **2006,** *103*, 15729. (b) Balzani, V.; Credi, A.; Ventura, M. *ChemSusChem* **2008,** *1*, 26.

(30) (a) Du, P.; Knowles, K.; Eisenberg, R. *J. Am. Chem. Soc.* **2008,** *130*, 12576. (b) Esswein, A. J.; Nocera, D. G. *Chem. Rev.* **2007,** *107*, 4022. (c) Fihri, A.; Artero, V.; Razavet, M.; Baffert, C.; Leibl, W.; Fontecave, M. *Angew. Chem. Int. Ed.* **2008,** *47*, 564.

(31) (a) Eisenberg, R.; Gray, H. B. *Inorg. Chem.* **2008,** *47*, 1697. (b) Liu, F.; Concepcion, J. J.; Jurss, J. W.; Cardolaccia, T.; Templeton, J. L.; Meyer, T. J. *Inorg. Chem.* **2008,** *47*, 1727. (c) Pecoraro, V. L.; Hsieh, W.-Y., *Inorg. Chem.* **2008,** *47*, 1765.

(32) Poverenov, E.; Efremenko, I.; Frenkel, A. I.; Y., B.-D.; Shimon, L. J. W.; Leitus, G.; Konstaninovski, L.; Martin, J. M.; Milstein, D. *Nature* **2008,** *455*, 1093.

(33) MacBeth, C. E.; Colombek, A. B.; Young, V. G.; Kuczera, K.; Hendrich, M. P.; Borovik, A. S. *Science* **2000,** *289*, 938.

(34) (a) Spaltenstein, E.; Conry, R. R.; Chrithlow, S. C.; Mayer, J. M. *J. Am. Chem. Soc.* **1989,** *111*, 8741.

(35) (a) Alstrum-Alcevedo, J. H.; Brennaman, M. K.; Meyer, T. J. *Inorg. Chem.* **2005,** *44*, 6802. (b) Hurst, J. K. *Coord. Chem. Rev.* **2005,** *249*, 313. (c) Ruettinger, W.; Dismukes, G. C., *Chem. Rev.* **1997,** *97*, 1. (d) Yagi, M.; Kaneko, M. *Chem. Rev.* **2001,** *101*, 21. (e) Yang, X.; Baik, M. H., *J. Am. Chem. Soc.* **2006,** *128*, 7476.

(36) Rostovtsev, V. V.; Labinger, J. A.; Bercaw, J. E.; Lasseter, T. L.; Goldberg, K. I. *Organometallics* **1998,** *17*, 4530.

(37) For some examples of pincer ligands featuring alternative anionic central donors please see: (a) Kameo, H.; Ishii, S.; Nakazawa, H. *Dalton Trans.* **2012**, *41*, 11386. (b) Takaya, J.; Nakamura, S.; Iwasawa, N. *Chem. Lett.* **2012**, *41*, 967. (c) Mazzeo, M.; Lamberti, M.; D'Auria, I.; Milione, S.; J. Peters, J. C.; C. Pellecchia, *J. Polym. Sci., Part A: Polym. Chem.* **2010**, *48*, 1374. (d) Derrah, E. J.; Ladeira, S.; Bouhadir, G.; Miqueu, K.; Bourissou, D. *Chem. Commun.* **2011**, *47*, 8611. (e) Day, G. S.; Pan, B.; Kellenberger, D. L.; Foxman, B. M.; Thomas, C. M. *Chem. Commun.* **2011**, *47*, 3634. (f) B. Pan, M. W. Bezpalko, B. M. Foxman, C. M. Thomas, *Organometallics* **2011**, *30*, 5560. (g) Derrah, E. J.; Martin, C.; Mallet-Ladeira, S.; Miqueu, K.; Bouhadir, G.; Bourissou, D. *Organometallics* **2013**, *32*, 1121. (h) Mazzeo, M.; Strianese, M.; Kuhl, O.; Peters, J. C. *Dalton Trans.* **2011**, *40*, 9026. (i) Mankad, N. P.; Rivard, E.; Harkins, S. B.; Peters, J. C. *J. Am. Chem. Soc.* **2005**, *127*, 16032. (j) Mazzeo, M.; Lamberti, M.; Massa, A.; Scettri, A.; Pellecchia, C.; Peters, J. C. *Organometallics* **2008**, *27*, 5741. (k) Bauer, R. C.; Gloaguen, Y.; Lutz, M.; Reek, J. N. H.; de Bruin, B.; van der Vlugt, J. I. *Dalton Trans.* **2011**, *40*, 8822. (l) Ogawa, H.; Yamashita, M. *Dalton Trans.* **2013**, *42*, 625. (m) El-Zaria, M. E.; Arii, H.; Nakamura, H. *Inorg. Chem.* **2011**, *50*, 4149. (n) Hill, A. F.; Lee, S. B.; Park, J.; Shang, R.; Willis, A. C. *Organometallics* **2010**, *29*, 5661. (o) Spokoyny, A. M.; Reuter, M. G.; Stern, C. L.; Ratner, M. A.; Seideman, T.; Mirkin, C. A. *J. Am. Chem. Soc.* **2009**, *131*, 9482. (p) Hasegawa, M.; Segawa, Y.; Yamashita, M.; Nozaki, K. *Angew. Chem. Int. Ed.* **2012**, *51*, 6956. (q) Segawa, Y.; Yamashita, M.; Nozaki, K.; *J. Am. Chem. Soc.* **2009**, *131*, 9201. (r) Segawa, Y.; Yamashita, M.; Nozaki, K. *Organometallics* **2009**, *28*, 6234.

(38) For a comparison of the *trans*-labilizing properties of silyl, a., and hydride ligated Ir complexes please see: Aizenberg, M.; Milstein, D. *J. Am. Chem. Soc.* **1995,** *117*, 6456.

(39) Auburn, M. J.; Stobart, S. R. *Inorg. Chem.* **1985,** *24*, 318.

(40) Gossage, R. A.; McLennan, G. D.; Stobart, S. R. *Inorg. Chem.* **1996,** *35*, 1729.

(41) Joslin, F. L.; Stobart, S. R. *J. Chem. Soc. Chem. Commun.* **1989**, 504.

(42) (a) Auburn, M. J.; Holmes-Smith, R. D.; Stobart, S. R.; Bakshi, P. K.; Cameron, T. S. *Organometallics* **1986,** *15*, 3032. (b) Brost, R. D.; Bruce, G. C.; Joslin, F. L.; Stobart, S. R. *Organometallics* **1997,** *16* (5669). (c) Zhou, X.; Stobart, S. R. *Organometallics* **2001,** *20,* 1898.

(43) (a) Sangtrirutnugul, P.; Stradiotto, M.; Tilley, T. D. *Organometallics* **2006,** *25*, 1607. (b) Sangtrirutnugul, P.; Tilley, T. D. *Organometallics* **2007,** *26*, 5557. (c) Sangtrirutnugul, P.; Tilley, T. D. *Organometallics* **2008,** *27*, 2223. (d) Stradiotto, M.; Fujdala, K. L.; Tilley, T. D. *Chem. Commun.* **2001**, 1200. (e) Yang, J.; Del Rosal, I.; Fasulo, M.; Sangtrirutnugul, P.; Maron, L.; Tilley, T. D. *Organometallics*, **2010**, *29*, 5544.

(44) (a) MacInnis, M. C.; MacLean, D. F.; Lundgren, R. J.; McDonald, R.; Turculet, L. *Organometallics* **2007,** *26*, 6522. (b) MacLean, D. F.; McDonald, R.; Ferguson, M. J.; Cadell, A. J.; Turculet, L. *Chem. Commun.* **2008**, 5146. (c) Mitton, S. J.; McDonald, R.; Turculet, L. *Organometallics* **2009,** *28*, 5122. (d) Mitton, S. J.; McDonald, R.; Turculet, L. *Angew. Chem. Int. Ed.* **2009,** *48*, 8568. (e) Morgan, E.; MacLean, D. F.; McDonald, R.; Turculet, L. *J. Am. Chem. Soc.* **2009,** *131*, 14234. (f) Macinnis, M. C.; McDonald, R.; Ferguson, M. J.; Tobisch, S.; Turculet, L. *J. Am. Chem. Soc.* **2011***, 133,* 13622. (g) Mitton, S.; Turculet, L.; *Chem. Eur. J.* **2012**, *18*, 12258.

(45) (a) Ito, M.; Hirakawa, M.; Osaku, A.; Ikariya, T. *Organometallics* **2003**, *22*, 4190. (b) Ito, M.; Ikariya, T. *Chem. Commun*. **2007**, 5134. (c) Ito, M.; Osaku, I.; Kobayashi, C.; Shiibashi, A. Ikariya, T. *Organometallics*. **2009,** *28*, 390. (d) Lee, W-C.; Sears, J. M.; Enow, R. A.; Eads, K.; Krogstad, D. A.; Frost, B. J. *Inorg. Chem*. **2013**, *52*, 1737.

(46) Baker, R. T.; Gordon, J. C.; Hamilton, C. W.; Henson, N. J.; Lin P-H., Maguire, S.; Murugesu, M.; Scott, B. L.; Nathan C. Smythe. *J. Am. Chem. Soc.* **2012**, *134*, 5598.

(47) (a) Bourget-Merle, L. Lappert, M. F.; Severn, J. R. *Chem. Rev.*, **2002**, *102*, 3031. (b) Mindiola, D. J.; Holland, P. L.; Warren, T. H. *Inorganic Syntheses*, **2010**, *35*, 1.

(48) Sydora, O. L.; Jones, T. C.; Small, B. L.; Nett, A. J.; Fischer, A. A.; Carney, M. J. *ACS Catal.* **2012**, *2*, 2452.

(49) Murata, M.; Buchwald, S. L. *Tetrahedron* **2004,** *60*, 7397.

(50) (a) Rankin, M. A.; Schatte, G.; McDonald, R.; Stradiotto, M. *J. Am. Chem. Soc.* **2007,** *129*, 6390. (b) Rankin, M. A.; McDonald, R.; Ferguson, M. J.; Stradiotto, M. *Angew. Chem. Int. Ed.* **2005,** *44*, 3603. (c) Rankin, M. A.; MacLean, D. F.; McDonald, R.; Ferguson, M. J.; Lumsden, M. D.; Stradiotto, M. *Organometallics* **2009,** *28*, 74. (d) Rankin, M. A.; McDonald, R.; Ferguson, M. J.; Stradiotto, M. *Organometallics* **2005**, *24*, 4981.

(51) (a) Mauthner, K.; Soldouzi, K. M.; Mereiter, K.; Schmid, R.; Kirchner, K. *Organometallics* **1999,** *18*, 4681. (b) Pasch, R.; Koelle, U.; Ganter, B.; Englert, U. *Organometallics* **1997,** *16*, 3950.

(52) Consiglio, G. *Chem. Rev.* **1987,** *87*, 761.

(53) (a) Zhao, J.; Goldman, A. S. Hartwig, J. F. *Science* **2005,** *307*, 1080. (b) Morgan, E.; MacLean, D. F.; McDonald, R.; Turculet, L. *J. Am. Chem. Soc.* **2009,** *131*, 14234.

(54) (a) Albinati, A.; Bakhmutov, W. I.; Caulton, K. G.; Clot, E.; Eckert, J.; Eisenstein, O.; Gusev, D. G.; Grushin, V. V.; Hauger, B. E.; Klooster, W. T.; Koetzle, T. F.; McMullan, R. K.; O'Loughlin, T. J.; Pelisier, M.; Ricci, J. S.; Sigalais, M. P.; Vymenits, A. B. *J. Am. Chem. Soc.* **1993,** *115*, 7300. (b) Riehl, J.-F.; Jean, Y.; Eisenstein, O.; Pelissier, M. *Organometallics* **1992,** *11*, 729. (c) Thorn, D. L.; Hoffmann, R. *New J. Chem.* **1979,** *3*, 39.

(55) Lachaize, S.; Sabo-Etienne, S. *Eur. J. Inorg. Chem.* **2006**, 2115.

(56) Lindner, R.; van den Bosch, B.; Lutz, M.; Reek, J. N. H.; van der Vlugt, J. I. *Organometallics* **2011,** *30*, 499.

(57) Ruddy, A. J.; Mitton, S. J.; McDonald, R.; Turculet, L. *Chem. Commun.* **2012**, 48, 1159.

(58) Morgan, E.; Lindeperg, F.; Turculet, L. *Unpublished Results*.

(59) (a) Arndsten, B. A.; Bergman, R. G. *Science* **1995,** *270*, 1970; (b) Bromberg, S. E.; Yang, H.; Asolund, M. C.; Lian, T.; McNamara, B. K.; Kotz, K. T.; Yeston, J. S.; Wilkens, M.; Frei, H.; Bergman, R. G. *Science* **1997,** *278*, 260. (c) Janowicz, A. H.; Bergman, R. G. *J. Am. Chem. Soc* **1982,** *104*, 352.

(60) Dreyfuss, M. P.; Pruckmayr, G. *Tetrahydrofuran Polymers in Encyclopedia of Polymer Science and Engineering*. John Wiley and Sons: New York, **1985,** *16,* 649.

(61) Li, Z.; Iida, K.; Tomisaka, Y.; Yoshimura, A.; Hirao, T.; Nomoto, A.; Ogawa, A. *Organometallics* **2007**, *26*, 1212.

(62) Lindner, R.; van den Bosch, B.; Lutz, M.; Reek, J. N. H.; van der Vlugt, J. I. Organometallics **2011**, *30*, 499.

(63) Hernández-Molina, R.; Mederos, A. *Acyclic and Macrocyclic Schiff Base Ligands In Comprehensive Coordination Chemistry II*. Pergamon: Oxford, UK. 2003.

(64) Tasker, S. Z., Standley, E. A.; Jamison, T, F. *Nature* **2014**, *509*, 299.

(65) (a) Kloek, S, M.; Goldberg, K. I. *J. Am. Chem. Soc.*, **2007**, *129*, 3460; (b) Fekl, U.; Kaminsky, W.; Goldberg, K. I. *J. Am. Chem. Soc.*, **2001**, *123*, 6423; (c) Reinartz, S.; White, S. P.; Brookhart, M.; Templeton, J. *J. Am. Chem. Soc.* **2001**, *123*, 6425.

(66) (a) Rotar, A.; Varga, R. A.; Jurkschat, K; Silvestru, C. *J. Organomet. Chem.* **2009**, 694, 1385. (b) Vergnaud, J.; Ayed, T.; Hussein, K.; Vendier, L.; Grellier, M.; Bouhadir, G.; Barthelat, J.-C.; Sabo-Etienne, S.; Bourissou, D. *Dalton Trans*. **2007**, 2370.

(67) Hartwig, J. F. *Organotransition metal chemistry: from bonding to catalysis;* University of Science Books: Sausalito, CA, 2010.

(68) While the +1 and +3 oxidation states are readily available to the heavier group 9 congeners Rh and Ir, the +2 oxidation state is rare in Rh and Ir complexes.[4] Such M^{II} (M = Rh, Ir) species have a propensity to undergo disproportionation reaction, generating more stable M^{I} and M^{III} species. See (a) DeWitt, D. G. *Coord*. *Chem*. *Rev*. **1996**, *147*, 209. (a) Pandey, K. K. *Coord*. *Chem*. *Rev*. **1992**, *121*, (c) Poli, R.; *Chem. Rev*. **1996**, *96*, 2135. (d) de Bruin, B.; Hetterscheid, D. J. H.; Koekkoek, H.; A. J. J.; H. Grützmacher, *Prog. Inorg. Chem*. **2007**, *55*, 247.

(69) (a) Rakowski, M. C.; Meutterties, E. L. *J. Am. Chem. Soc*. **1977**, *99*, 739. (b) Mock, M. T.; Potter, R. G.; O'Hagan, M. J.; Camaioni, D. M.; Dougherty, W. G.; Kassel, W. D.; DuBois, D. L. *Inorg. Chem*. **2011**, *50*, 11914. (c) Ingleson, M.; Fan, H.; Pink, M.; Tomaszewski, J.; Caulton, K. G. *J. Am. Chem. Soc*. **2006**, *128*, 1804 (d) Ingleson, M.; Pink, M.; Fan, H.; Caulton, K. G. *J. Am. Chem. Soc*. **2008**, *130*, 4262. (e) Lin, T.-P.; Peters, J. C. *J. Am. Chem. Soc*., **2013**, *135*, 15310. (f) Rozenel, S. S.; Padilla, R.; Camp C.; Arnold, J. *Chem. Commun*. **2014**, *50*, 2612. (g) Semproni, S. P.; Atienza, C. C. H.; Chirik, P. J. *Chem. Sci*. **2014**, *5*, 1956.

(70) Crabtree, R. H. *The Organometallic Chemistry of the Transition Metals, Fourth Edition*, Wiley, Hoboken, 2005.

(71) Ingleson, M.; Pink, M.; Caulton, K. G. *J. Am. Chem. Soc*. **2006**, *128*, 4248.

(72) Adams, D. M. *Metal-ligand and Related Vibrations; A Critical Survey of the Infrared and Raman Spectra of Metallic and Organometallic Compounds*; Edward Arnold, London, 1967; p 379.

(73) Denney, M. C.; Pons, V.; Hebden, T. J.; Heinekey, D. M.; Goldberg, K. I. *J. Am. Chem. Soc***. 2006**, *128*, 12048.

(74) Hebden, T. J.; St. John, A. J.; Gusev, D. G.; Kaminsky, W.; Goldberg, K. I.; Heinekey, D. M. *Angew. Chem. Int. Ed*. **2011**, *50*, 1873.

(75) During the course of these studies [Ph-PSiP]Co complexes in the +2 and +3 oxidation states were reported by Sun using alternative synthetic protocols than those that are reported herein: Wu, S.; Li, X.; Xiong, Z.; Xu, W.; Lu, Y.; Sun, H. *Organometallics*. **2013**, *32*, 3227.

(76) Fryzuk, M. D.; Leznoff, D. B.; Thompson, R. C.; Rettig, S. J. *J. Am. Chem. Soc.* **1998***, 120,* 10126.

(77) (a) Whited, M. T.; Mankad, N. P.; Lee, Y.; Oblad, P. F.; Peters, J. C. *Inorg. Chem*. **2009**, 48, 2507. (b) Suess, D. L. M.; Tsay, C.; Peters, J. C. *J. Am. Chem. Soc.* **2012**, *134*, 14158.

(78) Ding, K.; Pierpont, A. W.; Brennessel, W. W.; Lukat-Rodgers, G.; Rodgers, K. R.; Cundari, T. R.; Bill, E.; Holland, P. L. *J. Am. Chem. Soc.* **2009**, *131*, 9471.

(79) Due to the complex ^{1}H NMR spectrum obtained for this reaction mixture, the unambiguous presence of **4-3** in the product mixture has yet to be verified.

(80) (a) Losse, S.; Vos, J. G.; Rau, S. *Coord. Chem. Rev*. **2010**, *254*, 2492. (b) Dinca, M; Long, J. R. *Angew. Chem. Int. Ed*. **2008**, 47, 6766. (c) Suh, M. P.; Park, H. J.; Prasad, T. K.; Lim, D.-W. *Chem. Rev*. **2012**, *112*, 782. (d) Hebrard, F.; Kalck, P. *Chem. Rev*. **2009**, *109*, 4272.

(81) Keaton, R. J.; Blacquiere, J. M.; Baker, R. T. *J. Am. Chem. Soc*. **2007**, 129, 1844.

(82) (a) Hamilton, D. G.; Crabtree, R. H. *J. Am. Chem. Soc*. **1988**, *110*, 4126. (b) Crabtree, R. H. *Acc. Chem. Res*. **1990**, *23*, 95.

(83) Bain G, A.; Berry, J. F. *J. Chem. Educ.* **2008**, *85*, 532.

(84) Schrauzer, G. N. *Angew. Chem. Int. Ed*. **1975**, *14*, 514.

(85) Bradley, D. C.; Chisholm, M. H. *Acc. Chem. Res.* **1976**, *9*, 273.

(86) (a) LaPointe, R. E.; Wolczanski, P. T.; Mitchell, J. F. *J. Am. Chem. Soc.* **1986**, *108*, 6382. (b) Cummins, C. C.; Baxter, S. M.; Wolczanski, P. T. *J. Am. Chem. Soc.* **1988**, *110*, 8731. (c) Schaller, C. P.; Wolczanski, P. T. *Inorg. Chem.* **1993**, *32*, 131.

(87) Laplaza, C. E.; Cummins, C. C. *Science.* **1995**, *268*, 861.

(88) Holland, P. L. *Acc. Chem. Res.* **2008**, *41*, 905.

(89) Vela, J.; Smith, J. M.; Yu, Y.; Ketterer, N. A.; Flaschenriem, C. J.; Lachicotte, R. J.; Holland, P. L. *J. Am. Chem. Soc.* **2005**, *127*, 7857.

(90) Cowley, R. E.; Eckert, N. A.; Elkaik, J.; Holland, P. L. *Chem. Commun.* **2009**, 1760.

(91) Hitchcock, P. B.; Lappert, M. F.; Merle, P. G. *Dalton Trans.* **2007**, 585.

(92) Hill, M. S.; Hitchcock, P. B. *J. Organomet. Chem.* **2004**, *689*, 3163.

(93) (a) Eckert, N. A.; Smith, J. M.; Lachicotte, R. J.; Holland, P. L. *Inorg. Chem.* **2004**, *43*, 3306. (b) Cowley, R. E.; Holland, P. L. *Inorg. Chem.* **2012**, *51*, 8352.

(94) Baker, R. T.; Gordon, J. C.; Hamilton, C. W.; Henson, N. J.; Lin, P. H.; Maguire, S.; Murugesu, M.; Scott, B. L.; Smythe, N. C. *J. Am. Chem. Soc.* **2012**, *134*, 5598.

(95) Anderson, R. A.; Faegri Jr, K.; Green J. C.; Haaland, A.; Lappert, M. F.; Leung, W-P.; Rypdal, K. *Inorg. Chem.* **1988**, *27*, 1782.

(96) Campora, J.; Naz, A. M.; Palma, P.; Alvarez, E.; Reyes, M. L. *Organometallics* **2005**, *24*, 4878.

(97) Bürger, H.; Wannagat, U. *Montash. Chem*. **1963**, *94*, 1007.

(98) Abdel-Magid, A. F. *Reductions in Organic Synthesis, Recent Advances and Practical Applications*; ACS Symp. Ser., Vol. 641; American Chemical Society: Washington D.C., 1996.

(99) Magano, J.; Dunetz, J. R. *Org. Process Res. Dev.* **2012**, *16*, 1156.

(100) Riener, K.; Högerl, M. P.; Gigler, P.; Kühn, F. E. *ACS Catal.* **2012**, *2*, 613.

(101) Enthaler, S.; Junge, K.; Beller, M. *Angew. Chem. Int. Ed.* **2008**, *47*, 3317.

(102) (a) Junge, K.; Schroeder, K.; Beller, M. *Chem. Commun.* **2011**, *47*, 4849. (b) Le Bailly, B. A. F.; Thomas, S. P. *RSC Adv.* **2011**, *1*, 1435. (c) Gopalaiah, K. *Chem. Rev.* **2013**, *113*, 3248.

(103) Marciniec, B. *Hydrosilylation: A Comprehensive Review on Recent Advances*; Advances in Silicon Science; Springer Science, 2009.

(104) Morris, R. H. *Chem. Soc. Rev.* **2009**, *38*, 2282.

(105) (a) Nishiyama, H.; Furuta, A. *Chem. Commun.* **2007**, 760. (b) Furuta, A.; Nishiyama, H. *Tetrahedron Lett.* **2008**, *49*, 110. (c) Hosokawa, S.; Ito, J.-i.; Nishiyama, H. *Organometallics* **2010**, *29*, 5773. (d) Inagaki, T.; Ito, A.; Ito, J.-i.; Nishiyama, H. *Angew. Chem. Int. Ed.* **2010**, *49*, 9384. (e) Inagaki, T.; Phong, L. T.; Furuta, A.; Ito, J.; Nishiyama, H. *Chem. Eur. J.* **2010**, *16*, 3090.

(106) (a) Shaikh, N. S.; Junge, K.; Beller, M. *Org. Lett.* **2007**, *9*, 5429. (b) Shaikh, N. S.; Enthaler, S.; Junge, K.; Beller, M. *Angew. Chem. Int. Ed.* **2008**, *47*, 2497. (c)

Addis, D.; Shaikh, N.; Zhou, S.; Das, S.; Junge, K.; Beller, M. *Chem. Asian J.* **2010**, *5*, 1687.

(107) Langlotz, B. K.; Wadepohl, H.; Gade, L. H. *Angew. Chem. Int. Ed.* **2008**, *47*, 4670.

(108) Gutsulyak, D. V.; Kuzmina, L. G.; Howard, J. A. K.; Vyboishchikov, S. F.; Nikonov, G. I. *J. Am. Chem. Soc.* **2008**, *130*, 3732.

(109) (a) Buitrago, E.; Zani, L.; Adolfsson, H. *Appl. Organomet. Chem.* **2011**, *25*, 748. (b) Buitrago, E.; Tinnis, F.; Adolfsson, H. *Adv. Synth. Catal.* **2012**, *354*, 217.

(110) (a) Castro, L. C. M.; Bezier, D.; Sortais, J. B.; Darcel, C. *Adv. Synth. Catal.* **2011**, *353*, 1279. (b) Jiang, F.; Bezier, D.; Sortais, J.-B.; Darcel, C. *Adv. Synth. Catal.* **2011**, *353*, 239. (c) Bezier, D.; Jiang, F.; Roisnel, T.; Sortais, J.-B.; Darcel, C. *Eur. J. Inorg. Chem.* **2012**, 1333. (d) Zheng, J.; Misal, C. L. C.; Roisnel, T.; Darcel, C.; Sortais, J.-B. *Inorg. Chim. Acta* **2012**, *380*, 301.

(111) Hashimoto, T.; Urban, S.; Hoshino, R.; Ohki, Y.; Tatsumi, K.; Glorius, F. *Organometallics* **2012**, *31*, 4474.

(112) Bhattacharya, P.; Krause, J. A.; Guan, H. *Organometallics* **2011**, *30*, 4720.

(113) Dieskau, A. P.; Begouin, J. M.; Plietker, B. *Eur. J. Org. Chem.* **2011**, 5291.

(114) (a) Kandepi, V. V. K. M.; Cardoso, J. M. S.; Peris, E.; Royo, B. *Organometallics* **2010**, *29*, 2777. (b) Warratz, S.; Postigo, L.; Royo, B. *Organometallics* **2013**, *32*, 893.

(115) Blom, B.; Enthaler, S.; Inoue, S.; Irran, E.; Driess, M. *J. Am. Chem. Soc.* **2013**, *135*, 6703.

(116) (a) Tondreau, A. M.; Lobkovsky, E.; Chirik, P. J. *Org. Lett.* **2008**, *10*, 2789. (b) Tondreau, A. M.; Darmon, J. M.; Wile, B. M.; Floyd, S. K.; Lobkovsky, E.; Chirik, P. J. *Organometallics* **2009**, *28*, 3928.

(117) Yang, J.; Tilley, T. D. *Angew. Chem. Int. Ed.* **2010**, *49*, 10186.

(118) Bezier, D.; Venkanna, G. T.; Castro, L. C. M.; Zheng, J.; Roisnel, T.; Sortais, J.-B.; Darcel, C. *Adv. Synth. Catal.* **2012**, *354*, 1879.

(119) Junge, K.; Wendt, B.; Zhou, S.; Beller, M. *Eur. J. Org. Chem.* **2013**, *2013*, 2061.

(120) The iron-catalyzed reduction of esters to aldehydes under mild conditions employing UV irradiation has been reported recently: Li, H.; Misal Castro, L. C.; Zheng, J.; Roisnel, T.; Dorcet, V.; Sortais, J. B.; Darcel, C. *Angew. Chem. Int. Ed.* **2013**, *52*, 8045.

(121) Holland, P. L. *Acc. Chem. Res.* **2008**, *41*, 905.

(122) Hatano, M.; Suzuki, S.; Ishihara, K. *J. Am. Chem. Soc.* **2006**, *128*, 9998.

(123) Driver, T. G.; Harris, J. R.; Woerpel, K. A. *J. Am. Chem. Soc.* **2009**, *129*, 3836.

(124) Dieskau, A. P.; Begouin, M-P.; Plietker, B. *Eur. J. Org. Chem.* **2011**, *129*, 5291.

(125) Consiglio G.B.; Queval, P.; Harrison-Marchand A.; Mordini A.; Lohier, J-L.; Delacroix, O.; Gaumont A-C.; Gérard, H.; Maddaluno, J.; Oulyadi, H. *J. Am. Chem. Soc.* **2011**, *133*, 6472.

(126) Kim, J. W.; Koike, T.; Yamaguchi, T.; Mizuno, N. *Chem. Eur. J.* **2008**, *14,* 4104.

(127) Castro, L. C. M.; Bezier, D.; Sortais, J-B.; Darcel, C. *Adv. Synth. Catal.* **2011**, *353,* 1279.

(128) Findlay, N. J.; Park, S. R.; Schoenebeck, F.; Cahard, E.; Zhou, S.; Berlouis, L. E. A.; Spicer, M. D.; Tuttle, T.; Murphy, J. A. *J. Am. Chem. Soc.* **2010**, *132*, 15462.

(129) Snead, D. R.; Ghiviriga, I.; Abboud, K. A.; Hong, S. *Org. Lett*. **2009**, *11*, 3274.

(130) Anton, D. R.; Crabtree, R. H. *Organometallics.* **1983**, *2*, 855.

(131) Blaquiere, J.; Diallo-Garcia, S.; Gorelsky, S. I.; Black, D. A.; Fagnou, K. *J. Am. Chem. Soc.* **2008***, 130,* 14034.

(132) Shaikh, O.; Junge, K.; Beller, M. *Org. Lett.* **2009**, *9*, 5429.

(133) Bauerlein, P. S.; Jairlanb, I. J. S.; Jarvis, A. J.; Lee, A. F.; Muller, C.; Slattery, J. M.; Thatcher, R. J.; Vogt, D.; Whitwood, J. C. *Chem. Commun.* **2009***,* 5734.

(134) Query, I. P.; Squier, P. A.; Larson, E. M.; Isley, N. A.; Clark. T. B. *J. Org. Chem*. **2011**, *76*, 6452.

(135) Vogels, C. M.; Westcott, S. A. *Curr. Org. Chem.* **2005**, *9*, 687.

(136) (a) Suzuki, A. *Angew. Chem. Int. Ed.* **2011**, *50*, 6722. (b) Jana, R.; Pathak, T. P.; Sigman, M. S. *Chem. Rev.* **2011**, *111*, 1417.

(137) Crudden, C. M.; Edwards, D. *Eur. J. Org. Chem.* **2003**, 4695.

(138) (a) Sherry, B. D.; Fuerstner, A. *Acc. Chem. Res.* **2008**, *41*, 1500. (b) Junge, K.; Schroeder, K.; Beller, M. *Chem. Commun.* **2011**, *47*, 4849.

(139) Wu, J. Y.; Moreau, B.; Ritter, T. *J. Am. Chem. Soc.* **2009**, *131*, 12915.

(140) (a) Zhang, L.; Peng, D.; Leng, X.; Huang, Z. *Angew. Chem. Int. Ed.* **2013**, *52*, 3676. (b) Obligacion, J. V.; Chirik, P. J. *Org. Lett.* **2013**, *15*, 2680. (c) Zheng, J.; Sortais, J.-B.; Darcel, C. *Chemcatchem* **2014**, *6*, 763. (d) Greenhalgh, M. D.; Thomas, S. P. *Chem. Commun.* **2013**, *49*, 11230.

(141) (a) Zaidlewicz, M.; Meller, J., *Tetrahedron Lett.* **1997**, *38*, 7279. (b) Zaidlewicz, M.; Meller, J., *Main Group Met. Chem.* **2000**, *23*, 765.

(142) Obligacion, J. V.; Chirik, P. J. *J. Am. Chem. Soc.* **2013**, *135*, 19107.

(143) Zhang, L.; Zuo, Z.; Leng, X.; Huang, Z. *Angew. Chem. Int. Ed.* **2014**, *53*, 2696.

(144) Ruddy, A. J.; Kelly, C. M.; Crawford, S. M; Wheaton, C. A.; Sydora, O. L.; Small, B. L.; Stradiotto, M.; Turculet, L. *Organometallics* **2013**, *32*, 5581.

(145) (a) Tucker, C. E.; Davidson, J.; Knochel, P. *J. Org. Chem.* **1992**, *57*, 3482. (b) Pereira, S.; Srebnik, M. *J. Am. Chem. Soc.* **1996**, *118*, 909. (c) Yamamoto, Y. Fujikawa, R.; Umemoto, T.; Miyaura, N. *Tetrahedron* **2004**, *60*, 10695. (d) Hadebe, S. W.; Robinson, R. S. *Tetrahedron Lett.* **2006**, *47*, 1299. (e) Lata, C. J.; Crudden, C. M. *J. Am. Chem. Soc.* **2010**, *132*, 131.

(146) (a) Casey, C. P.; Cyr, C. R. *J. Am. Chem. Soc*. **1973**, *95*, 2248. (b) Kochi, T.; Hamasaki, T.; Aoyama, Y.; Kawasaki, J.; Kakiuchi, F.; *J. Am. Chem. Soc*. **2012**, *134*, 16544.

(147) Caballero, A.; Sabo-Etienne, S. *Organometallics* **2007**, *26*, 1191.

(148) Dieskau, A. P.; Begouin, J. M; Plietker, B. *Eur. J. Org. Chem.* **2011**, 5291.

(149) Consiglio, G. B.; Queval, P.; Harrison-Marchand, A.; Mordini, A.; Lohier, J. F.; Delacroix, O.; Gaumont, A. C.; Gerard, H.; Maddaluno, J.; Oulyadi, H. *J. Am. Chem. Soc.* **2011**, *133*, 6472.

(150) Semproni, S. P.; Hojilla Atienza, C. C.; Chirik, P. J. *Chem. Sci*. **2014**, *5*, 1956.

APPENDIX A: Crystallographic Experimental Details

Table A-1. Crystallographic Experimental Details for [^{t}Bu-PSiC]Ru(η^3-C_8H_{13}) (**2-5**)

A. Crystal Data

formula	$C_{31}H_{46}NPRuSi$
formula weight	592.82
crystal dimensions (mm)	0.30 x 0.25 x 0.14
crystal system	triclinic
space group	$P\bar{1}$
unit cell parameters[a]	
a (Å)	9.3387 (3)
b (Å)	10.1491 (3)
c (Å)	15.4308 (5)
α (deg)	91.6768 (4)
β (deg)	90.8227 (4)
γ (deg)	99.6424 (3)
V (Å^3)	1440.97 (8)
Z	2
ρ_{calcd} (g cm^{-3})	1.366
μ (mm^{-1})	0.661

B. Data Collection and Refinement Conditions

diffractometer	Bruker D8/APEX II CCD[b]
radiation (λ [Å])	graphite-monochromated Mo Kα (0.71073)
temperature (°C)	–100
scan type	w scans (0.3°) (15 s exposures)
data collection 2θ limit (deg)	54.98
total data collected	12772 (-12 ≤ h ≤ 12, -13 ≤ k ≤ 13, -20 ≤ l ≤ 20)

independent reflections	6561 (R_{int} = 0.0120)
number of observed reflections (*NO*)	6135 [$F_o^2 \geq 2\sigma(F_o^2)$]
structure solution method *2008*[c])	Patterson/structure expansion (*DIRDIF–*
refinement method *97*[d])	full-matrix least-squares on F^2 (*SHELXL–*
absorption correction method	Gaussian integration (face-indexed)
range of transmission factors	0.9102–0.8283
data/restraints/parameters	6561 / 0 / 317
goodness-of-fit (*S*)[e] [all data]	1.034
final *R* indices[f]	
R_1 [$F_o^2 \geq 2\sigma(F_o^2)$]	0.0224
wR_2 [all data]	0.0608
largest difference peak and hole	0.493 and –0.258 e Å^{-3}

[a]Obtained from least-squares refinement of 6716 reflections with 4.42° < 2θ < 53.66°.

[b]Programs for diffractometer operation, data collection, data reduction and absorption correction were those supplied by Bruker.

[c]Beurskens, P. T.; Beurskens, G.; de Gelder, R.; Smits, J. M. M; Garcia-Granda, S.; Gould, R. O. (2008). The *DIRDIF-2008* program system. Crystallography Laboratory, Radboud University Nijmegen, The Netherlands.

[d]Sheldrick, G. M. *Acta Crystallogr.* **2008**, *A64*, 112–122.

[e]$S = [\Sigma w(F_o^2 - F_c^2)^2/(n - p)]^{1/2}$ (n = number of data; p = number of parameters varied; $w = [\sigma^2(F_o^2) + (0.0327P)^2 + 0.5985P]^{-1}$ where $P = [\mathrm{Max}(F_o^2, 0) + 2F_c^2]/3$).

[f]$R_1 = \Sigma||F_o| - |F_c||/\Sigma|F_o|$; $wR_2 = [\Sigma w(F_o^2 - F_c^2)^2/\Sigma w(F_o^4)]^{1/2}$.

Table A-2. Crystallographic Experimental Details for [^{t}Bu-PSiC]Ru(η^3-C_8H_{13}) (**2-6**)

A. Crystal Data

formula	$C_{29}H_{40}NPRuSi$
formula weight	562.75
crystal dimensions (mm)	0.47 x 0.27 x 0.15
crystal system	monoclinic
space group	$P2_1/c$ (No. 14)
unit cell parameters[a]	
a (Å)	10.3542 (5)
b (Å)	16.6143 (8)
c (Å)	15.3008 (8)
β (deg)	94.3988 (5)
V (Å^3)	2624.4 (2)
Z	4
ρ_{calcd} (g cm^{-3})	1.424
μ (mm^{-1})	0.722

B. Data Collection and Refinement Conditions

diffractometer	Bruker D8/APEX II CCD[b]
radiation (λ [Å])	graphite-monochromated Mo Kα (0.71073)
temperature (°C)	–100
scan type	w scans (0.3°) (15 s exposures)
data collection 2θ limit (deg)	55.00
total data collected	23253 (-13 ≤ h ≤ 13, -21 ≤ k ≤ 21, -19 ≤ l ≤ 19)
independent reflections	6037 (R_{int} = 0.0127)

number of observed reflections (*NO*)	5727 [$F_o^2 \geq 2\sigma(F_o^2)$]
structure solution method	Patterson/structure expansion (*DIRDIF–2008*[c])
refinement method	full-matrix least-squares on F^2 (*SHELXL–97*[d])
absorption correction method	Gaussian integration (face-indexed)
range of transmission factors	0.8988–0.7259
data/restraints/parameters	6037 / 0 / 299
goodness-of-fit (*S*)[e] [all data]	1.047
final *R* indices[f]	
$R1$ [$F_o^2 \geq 2\sigma(F_o^2)$]	0.0195
$wR2$ [all data]	0.0537
largest difference peak and hole	0.559 and –0.334 e Å^{-3}

[a]Obtained from least-squares refinement of 9921 reflections with $4.64° < 2\theta < 54.98°$.

[b]Programs for diffractometer operation, data collection, data reduction and absorption correction were those supplied by Bruker.

[c]Beurskens, P. T.; Beurskens, G.; de Gelder, R.; Smits, J. M. M; Garcia-Granda, S.; Gould, R. O. (2008). The *DIRDIF-2008* program system. Crystallography Laboratory, Radboud University Nijmegen, The Netherlands.

[d]Sheldrick, G. M. *Acta Crystallogr.* **2008**, *A64*, 112–122.

[e]$S = [\Sigma w(F_o^2 - F_c^2)^2/(n - p)]^{1/2}$ (n = number of data; p = number of parameters varied; $w = [\sigma^2(F_o^2) + (0.0327P)^2 + 0.5985P]^{-1}$ where $P = [\mathrm{Max}(F_o^2, 0) + 2F_c^2]/3$).

[f]$R1 = \Sigma||F_o| - |F_c||/\Sigma|F_o|$; $wR2 = [\Sigma w(F_o^2 - F_c^2)^2/\Sigma w(F_o^4)]^{1/2}$.

Table A-3. Crystallographic Experimental Details for [^{t}Bu-PSiN-Me]Rh(H)(Cl) (**2-7**)

A. Crystal Data

formula	$C_{23}H_{36}ClNPRhSi$
formula weight	523.95
crystal dimensions (mm)	0.34 x 0.30 x 0.27
crystal system	monoclinic
space group	$P2_1/c$ (No. 14)
unit cell parameters[a]	
a (Å)	15.8620 (4)
b (Å)	10.3058 (2)
c (Å)	16.0399 (4)
β (deg)	113.0811 (2)
V (Å^3)	2412.16 (10)
Z	4
ρ_{calcd} (g cm^{-3})	1.443
μ (mm^{-1})	0.944

B. Data Collection and Refinement Conditions

diffractometer	Bruker D8/APEX II CCD[b]
radiation (λ [Å])	graphite-monochromated Mo Kα (0.71073)
temperature (°C)	–100
scan type	w scans (0.3°) (15 s exposures)
data collection 2θ limit (deg)	55.02
total data collected	21050 (-20 ≤ h ≤ 20, -13 ≤ k ≤ 13, -20 ≤ l ≤ 20)
independent reflections	5548 (R_{int} = 0.0113)
number of observed reflections (NO)	5351 [$F_o^2 \geq 2\sigma(F_o^2)$]

structure solution method	Patterson/structure expansion (*DIRDIF–2008*[c])
refinement method	full-matrix least-squares on F^2 (*SHELXL–97*[d])
absorption correction method	Gaussian integration (face-indexed)
range of transmission factors	0.7859–0.7402
data/restraints/parameters	5548 / 0 / 257
goodness-of-fit (S)[e] [all data]	1.045
final R indices[f]	
R_1 [$F_o^2 \geq 2\sigma(F_o^2)$]	0.0197
wR_2 [all data]	0.0574
largest difference peak and hole	0.673 and –0.497 e Å^{-3}

[a]Obtained from least-squares refinement of 9952 reflections with $4.82° < 2\theta < 54.78°$.

[b]Programs for diffractometer operation, data collection, data reduction and absorption correction were those supplied by Bruker.

[c]Beurskens, P. T.; Beurskens, G.; de Gelder, R.; Smits, J. M. M; Garcia-Granda, S.; Gould, R. O. (2008). The *DIRDIF-2008* program system. Crystallography Laboratory, Radboud University Nijmegen, The Netherlands.

[d]Sheldrick, G. M. *Acta Crystallogr.* **2008**, *A64*, 112–122.

[e]$S = [\Sigma w(F_o^2 - F_c^2)^2/(n-p)]^{1/2}$ (n = number of data; p = number of parameters varied; $w = [\sigma^2(F_o^2) + (0.0327P)^2 + 0.5985P]^{-1}$ where $P = [\mathrm{Max}(F_o^2, 0) + 2F_c^2]/3$).

[f]$R_1 = \Sigma||F_o| - |F_c||/\mathrm{S}|F_o|$; $wR_2 = [\Sigma w(F_o^2 - F_c^2)^2/\Sigma w(F_o^4)]^{1/2}$.

Table A-4. Crystallographic Experimental Details for [^{t}Bu-PSiN-Me]Ir(H)(Cl) (**2-8**)

A. Crystal Data

formula	$C_{23}H_{36}ClIrNPSi$
formula weight	613.24
crystal dimensions (mm)	0.33 x 0.18 x 0.15
crystal system	monoclinic
space group	$P2_1/c$ (No. 14)
unit cell parameters[a]	
a (Å)	15.8428 (16)
b (Å)	10.3414 (11)
c (Å)	16.0067 (16)
β (deg)	112.8869 (10)
V (Å^3)	2416.0 (4)
Z	4
ρ_{alcd} (g cm^{-3})	1.686
μ (mm^{-1})	5.762

B. Data Collection and Refinement Conditions

diffractometer	Bruker D8/APEX II CCD[b]
radiation (λ [Å])	graphite-monochromated Mo Kα (0.71073)
temperature (°C)	–100
scan type	w scans (0.3°) (15 s exposures)
data collection 2θ limit (deg)	55.02
total data collected	20958 (-20 ≤ h ≤ 20, -13 ≤ k ≤ 13, -20 ≤ l ≤ 20)
independent reflections	5559 (R_{int} = 0.0162)

number of observed reflections (*NO*)	5254 [$F_o^2 \geq 2\sigma(F_o^2)$]
structure solution method	Patterson/structure expansion (*DIRDIF–2008*[c])
refinement method	full-matrix least-squares on F^2 (*SHELXL–97*[d])
absorption correction method	Gaussian integration (face-indexed)
range of transmission factors	0.4746–0.2522
data/restraints/parameters	5559 / 0 / 257
goodness-of-fit (*S*)[e] [all data]	1.037
final *R* indices[f]	
$R1$ [$F_o^2 \geq 2\sigma(F_o^2)$]	0.0161
$wR2$ [all data]	0.0415
largest difference peak and hole	0.945 and –0.514 e Å^{-3}

[a]Obtained from least-squares refinement of 9903 reflections with $4.82° < 2\theta < 54.72°$.

[b]Programs for diffractometer operation, data collection, data reduction and absorption correction were those supplied by Bruker.

[c]Beurskens, P. T.; Beurskens, G.; de Gelder, R.; Smits, J. M. M; Garcia-Granda, S.; Gould, R. O. (2008). The *DIRDIF-2008* program system. Crystallography Laboratory, Radboud University Nijmegen, The Netherlands.

[d]Sheldrick, G. M. *Acta Crystallogr.* **2008**, *A64*, 112–122.

[e]$S = [\Sigma w(F_o^2 - F_c^2)^2/(n-p)]^{1/2}$ (n = number of data; p = number of parameters varied; $w = [\sigma^2(F_o^2) + (0.0327P)^2 + 0.5985P]^{-1}$ where $P = [\mathrm{Max}(F_o^2, 0) + 2F_c^2]/3$).

[f]$R1 = \Sigma||F_o| - |F_c||/\Sigma|F_o|$; $wR2 = [\Sigma w(F_o^2 - F_c^2)^2/\Sigma w(F_o^4)]^{1/2}$.

Table A-5. Crystallographic Experimental Details for [^{t}Bu-PSiN-Me]Rh(H)(Cl)(PMe_3) (**2-9**)

A. Crystal Data

formula	$C_{26}H_{45}ClNP_2RhSi$
formula weight	600.02
crystal dimensions (mm)	0.41 x 0.34 x 0.29
crystal system	triclinic
space group	$P\bar{1}$
unit cell parameters[a]	
a (Å)	8.5401 (6)
b (Å)	9.8992 (7)
c (Å)	18.8502 (13)
a (deg)	93.9595 (7)
b (deg)	100.2991 (7)
g (deg)	106.6562 (7)
V (Å^3)	1489.85 (18)
Z	2
ρ_{calcd} (g cm^{-3})	1.338
μ (mm^{-1})	0.825

B. Data Collection and Refinement Conditions

diffractometer	Bruker D8/APEX II CCD[b]
radiation (λ [Å])	graphite-monochromated Mo Kα (0.71073)
temperature (°C)	–100
scan type	*w* scans (0.4°) (10 s exposures)
data collection 2σ limit (deg)	55.02
total data collected	13114 (-11 ≤ *h* ≤ 11, -12 ≤ *k* ≤ 12, -24 ≤ *l* ≤

24)

independent reflections	6763 (R_{int} = 0.0115)
number of observed reflections (*NO*)	6418 [$F_o^2 \geq 2\sigma(F_o^2)$]
structure solution method *2008*[c])	Patterson/structure expansion (*DIRDIF–*
refinement method *97*[d])	full-matrix least-squares on F^2 (*SHELXL–*
absorption correction method	Gaussian integration (face-indexed)
range of transmission factors	0.7941–0.7290
data/restraints/parameters	6763 / 0 / 293
goodness-of-fit (*S*)[e] [all data]	1.057
final *R* indices[f]	
$R1$ [$F_o^2 \geq 2\sigma(F_o^2)$]	0.0204
$wR2$ [all data]	0.0553
largest difference peak and hole	0.509 and –0.348 e Å^{-3}

[a]Obtained from least-squares refinement of 7626 reflections with 4.60° < 2θ < 54.96°.

[b]Programs for diffractometer operation, data collection, data reduction and absorption correction were those supplied by Bruker.

[c]Beurskens, P. T.; Beurskens, G.; de Gelder, R.; Smits, J. M. M; Garcia-Granda, S.; Gould, R. O. (2008). The *DIRDIF-2008* program system. Crystallography Laboratory, Radboud University Nijmegen, The Netherlands.

[d]Sheldrick, G. M. *Acta Crystallogr.* **2008**, *A64*, 112–122.

[e]$S = [\Sigma w(F_o^2 - F_c^2)^2/(n - p)]^{1/2}$ (n = number of data; p = number of parameters varied; $w = [\sigma^2(F_o^2) + (0.0327P)^2 + 0.5985P]^{-1}$ where $P = [\mathrm{Max}(F_o^2, 0) + 2F_c^2]/3$).

[f]$R1 = \Sigma||F_o| - |F_c||/\mathrm{S}|F_o|$; $wR2 = [\Sigma w(F_o^2 - F_c^2)^2/\Sigma w(F_o^4)]^{1/2}$.

Table A-6. Crystallographic Experimental Details for [^{t}Bu-PSiN-Me]Rh(H)(OTf) (**2-10**)

A. Crystal Data

formula	$C_{24}H_{36}F_3NO_3PRhSSi$
formula weight	637.57
crystal dimensions (mm)	0.25 x 0.22 x 0.09
crystal system	monoclinic
space group	*C*2/*c* (No. 15)
unit cell parameters[a]	
a (Å)	18.1669 (7)
b (Å)	10.9167 (4)
c (Å)	29.9817 (12)
β (deg)	106.7449 (5)
V (Å3)	5693.9 (4)
Z	8
ρ_{calcd} (g cm^{-3})	1.487
μ (mm^{-1})	0.817

B. Data Collection and Refinement Conditions

diffractometer	Bruker D8/APEX II CCD[b]
radiation (λ [Å])	graphite-monochromated Mo Kα (0.71073)
temperature (°C)	–100
scan type	*w* scans (0.3°) (15 s exposures)
data collection 2θ limit (deg)	52.90
total data collected	22434 (-22 ≤ *h* ≤ 22, -13 ≤ *k* ≤ 13, -37 ≤ *l* ≤ 37)
independent reflections	5875 (R_{int} = 0.0438)
number of observed reflections (*NO*)	4585 [$F_o^2 \geq 2\sigma(F_o^2)$]

structure solution method	Patterson/structure expansion (*DIRDIF–2008*[c])
refinement method	full-matrix least-squares on F^2 (*SHELXL–97*[d])
absorption correction method	Gaussian integration (face-indexed)
range of transmission factors	0.9331–0.8213
data/restraints/parameters	5875 / 0 / 320
goodness-of-fit (S)[e] [all data]	1.021
final R indices[f]	
R_1 [$F_o^2 \geq 2\sigma(F_o^2)$]	0.0289
wR_2 [all data]	0.0720
largest difference peak and hole	0.415 and –0.542 e Å^{-3}

[a]Obtained from least-squares refinement of 8157 reflections with $4.42° < 2\theta < 50.38°$.

[b]Programs for diffractometer operation, data collection, data reduction and absorption correction were those supplied by Bruker.

[c]Beurskens, P. T.; Beurskens, G.; de Gelder, R.; Smits, J. M. M; Garcia-Granda, S.; Gould, R. O. (2008). The *DIRDIF-2008* program system. Crystallography Laboratory, Radboud University Nijmegen, The Netherlands.

[d]Sheldrick, G. M. *Acta Crystallogr.* **2008**, *A64*, 112–122.

[e]$S = [\Sigma w(F_o^2 - F_c^2)^2/(n-p)]^{1/2}$ (n = number of data; p = number of parameters varied; $w = [\sigma^2(F_o^2) + (0.0327P)^2 + 0.5985P]^{-1}$ where $P = [\mathrm{Max}(F_o^2, 0) + 2F_c^2]/3$).

[f]$R_1 = \Sigma||F_o| - |F_c||/\mathrm{S}|F_o|$; $wR_2 = [\Sigma w(F_o^2 - F_c^2)^2/\Sigma w(F_o^4)]^{1/2}$.

Table A-7. Crystallographic Experimental Details for [^{t}Bu-PSiN-Me]Ir(H)(OTf) (**2-11**)

A. Crystal Data

formula	$C_{24}H_{36}F_3IrNO_3PSSi$
formula weight	726.86
crystal dimensions (mm)	0.20 x 0.14 x 0.09
crystal system	monoclinic
space group	*C*2/*c* (No. 15)
unit cell parameters[a]	
a (Å)	18.1791 (13)
b (Å)	10.9325 (8)
c (Å)	29.924 (2)
β (deg)	106.6346 (8)
V (Å3)	5698.2 (7)
Z	8
ρ_{calcd} (g cm^{-3})	1.695
μ (mm^{-1})	4.903

B. Data Collection and Refinement Conditions

diffractometer	Bruker D8/APEX II CCD[b]
radiation (λ [Å])	graphite-monochromated Mo Kα (0.71073)
temperature (°C)	–100
scan type	*w* scans (0.3°) (20 s exposures)
data collection 2θ limit (deg)	52.86
total data collected	22263 (-22 ≤ *h* ≤ 22, -13 ≤ *k* ≤ 13, -37 ≤ *l* ≤ 37)
independent reflections	5865 (R_{int} = 0.0644)
number of observed reflections (*NO*)	4093 [$F_o^2 \geq 2\sigma(F_o^2)$]

structure solution method	Patterson/structure expansion (*DIRDIF–2008*[c])
refinement method	full-matrix least-squares on F^2 (*SHELXL–97*[d])
absorption correction method	Gaussian integration (face-indexed)
range of transmission factors	0.6585–0.4405
data/restraints/parameters	5865 / 1[e] / 319
goodness-of-fit (S)[f] [all data]	1.009
final R indices[g]	
R_1 [$F_o^2 \geq 2\sigma(F_o^2)$]	0.0327
wR_2 [all data]	0.0719
largest difference peak and hole	0.620 and –1.059 e Å^{-3}

[a]Obtained from least-squares refinement of 5451 reflections with $4.40° < 2\theta < 46.20°$.

[b]Programs for diffractometer operation, data collection, data reduction and absorption correction were those supplied by Bruker.

[c]Beurskens, P. T.; Beurskens, G.; de Gelder, R.; Smits, J. M. M; Garcia-Granda, S.; Gould, R. O. (2008). The *DIRDIF-2008* program system. Crystallography Laboratory, Radboud University Nijmegen, The Netherlands.

[d]Sheldrick, G. M. *Acta Crystallogr.* **2008**, *A64*, 112–122.

[e]The Ir–H1 distance was fixed at 1.55(1) Å during refinement.

[f]$S = [\Sigma w(F_o^2 - F_c^2)^2/(n-p)]^{1/2}$ (n = number of data; p = number of parameters varied; $w = [\sigma^2(F_o^2) + (0.0327P)^2 + 0.5985P]^{-1}$ where $P = [\mathrm{Max}(F_o^2, 0) + 2F_c^2]/3$).

[g]$R_1 = \Sigma||F_o| - |F_c||/\mathrm{S}|F_o|$; $wR_2 = [\Sigma w(F_o^2 - F_c^2)^2/\Sigma w(F_o^4)]^{1/2}$.

Table A-8. Crystallographic Experimental Details for [Cy-PSiP]Co(Cl) (**4-1•C_7H_8**)

A. Crystal Data

formula	$C_{44}H_{63}ClCoP_2Si$
formula weight	776.35
crystal dimensions (mm)	0.30 x 0.24 x 0.07
crystal system	monoclinic
space group	$P2_1/n$ (an alternate setting of $P2_1/c$ [No.14])
unit cell parameters[a]	
a (Å)	16.2894 (2)
b (Å)	14.1617 (2)
c (Å)	18.2009 (3)
β (deg)	99.9420 (10)
V (Å^3)	4135.63 (10)
Z	4
ρ_{calcd} (g cm^{-3})	1.247
μ (mm^{-1})	5.065

B. Data Collection and Refinement Conditions

diffractometer	Bruker D8/APEX II CCD[b]
radiation (λ [Å])	graphite-monochromated Cu Kα (1.54178)
temperature (°C)	–100
scan type	w scans (0.8°) (8 s exposures)
data collection 2θ limit (deg)	135.46
total data collected	26156 (-19 ≤ h ≤ 19, -16 ≤ k ≤ 16, -21 ≤ l ≤ 21)
independent reflections	7331 (R_{int} = 0.0351)
number of observed reflections (*NO*)	6574 [$F_o^2 \geq 2\sigma(F_o^2)$]

structure solution method	direct methods (*SHELXS–97*[c])
refinement method	full-matrix least-squares on F^2 (*SHELXL–97*[c])
absorption correction method	Gaussian integration (face-indexed)
range of transmission factors	0.7182–0.3137
data/restraints/parameters	7331 / 0 / 444
goodness-of-fit (*S*)[d] [all data]	1.027
final *R* indices[e]	
R_1 [$F_o^2 \geq 2\sigma(F_o^2)$]	0.0320
wR_2 [all data]	0.0828
largest difference peak and hole	0.398 and –0.224 e Å^{-3}

[a]Obtained from least-squares refinement of 9073 reflections with $6.72° < 2\theta < 134.70°$.

[b]Programs for diffractometer operation, data collection, data reduction and absorption correction were those supplied by Bruker.

[c]Sheldrick, G. M. *Acta Crystallogr.* **2008**, *A64*, 112–122.

[d]$S = [\Sigma w(F_o^2 - F_c^2)^2/(n - p)]^{1/2}$ (n = number of data; p = number of parameters varied; $w = [\sigma^2(F_o^2) + (0.0327P)^2 + 0.5985P]^{-1}$ where $P = [\mathrm{Max}(F_o^2, 0) + 2F_c^2]/3$).

[e]$R_1 = \Sigma||F_o| - |F_c||/\mathrm{S}|F_o|$; $wR_2 = [\Sigma w(F_o^2 - F_c^2)^2/\Sigma w(F_o^4)]^{1/2}$.

Table A-9. Crystallographic Experimental Details for [Cy-PSiP]Co(I) (**4-2•C_7H_8**)

A. Crystal Data

formula	$C_{44}H_{63}CoIP_2Si$
formula weight	867.80
crystal dimensions (mm)	0.34 x 0.27 x 0.14
crystal system	orthorhombic
space group	$Pca2_1$ (No. 29)
unit cell parameters[a]	
a (Å)	17.6444 (7)
b (Å)	13.3291 (5)
c (Å)	17.9305 (7)
V (Å^3)	4217.0 (3)
Z	4
ρ_{calcd} (g cm^{-3})	1.367
μ (mm^{-1})	1.273

B. Data Collection and Refinement Conditions

diffractometer	Bruker D8/APEX II CCD[b]
radiation (λ [Å])	graphite-monochromated Mo Kα (0.71073)
temperature (°C)	–100
scan type	w scans (0.3°) (20 s exposures)
data collection 2θ limit (deg)	55.00
total data collected	36116 (-22 ≤ h ≤ 22, -17 ≤ k ≤ 17, -23 ≤ l ≤ 23)
independent reflections	9672 (R_{int} = 0.0325)
number of observed reflections (*NO*)	8961 [$F_o^2 \geq 2\sigma(F_o^2)$]
structure solution method	Patterson/structure expansion (*DIRDIF*–

2008[c])	
refinement method	full-matrix least-squares on F^2 (*SHELXL–97*[d])
absorption correction method	Gaussian integration (face-indexed)
range of transmission factors	0.8460–0.6744
data/restraints/parameters	9672 / 0 / 444
Flack absolute structure parameter[e]	–0.062(9)
goodness-of-fit (*S*)[f] [all data]	1.081
final *R* indices[g]	
R_1 [$F_o^2 \geq 2\sigma(F_o^2)$]	0.0263
wR_2 [all data]	0.0650
largest difference peak and hole	0.625 and –0.614 e Å^{-3}

[a]Obtained from least-squares refinement of 8447 reflections with $4.46° < 2\theta < 42.02°$.

[b]Programs for diffractometer operation, data collection, data reduction and absorption correction were those supplied by Bruker

[c]Beurskens, P. T.; Beurskens, G.; de Gelder, R.; Smits, J. M. M.; Garcia-Granda, S.; Gould, R. O. (2008). The *DIRDIF-2008* program system. Crystallography Laboratory, Radboud University Nijmegen, The Netherlands.

[d]Sheldrick, G. M. *Acta Crystallogr.* **2008**, *A64*, 112–122.

[e]Flack, H. D. *Acta Crystallogr.* **1983**, *A39*, 876–881; Flack, H. D.; Bernardinelli, G. *Acta Crystallogr.* **1999**, *A55*, 908–915; Flack, H. D.; Bernardinelli, G. *J. Appl. Cryst.* **2000**, *33*, 1143–1148. The Flack parameter will refine to a value near zero if the structure is in the correct configuration and will refine to a value near one for the inverted configuration.

[f]$S = [\Sigma w(F_o^2 - F_c^2)^2/(n-p)]^{1/2}$ (n = number of data; p = number of parameters varied; $w = [\sigma^2(F_o^2) + (0.0327P)^2 + 0.5985P]^{-1}$ where $P = [\mathrm{Max}(F_o^2, 0) + 2F_c^2]/3$).

[g]$R_1 = \Sigma||F_o| - |F_c||/\mathrm{S}|F_o|$; $wR_2 = [\Sigma w(F_o^2 - F_c^2)^2/\Sigma w(F_o^4)]^{1/2}$.

Table A-10. Crystallographic Experimental Details for [Cy-PSiP]Co(Cl)(PMe_3) (**4-4**)

A. Crystal Data

formula	$C_{40}H_{64}ClCoP_3Si$
formula weight	760.29
crystal dimensions (mm)	0.59 x 0.12 x 0.12
crystal system	triclinic
space group	$P\bar{1}$ (No. 2)
unit cell parameters[a]	
a (Å)	12.2174 (8)
b (Å)	18.3157 (13)
c (Å)	18.5118 (13)
α (deg)	85.9947 (10)
β (deg)	85.0880 (10)
γ (deg)	77.8534 (10)
V (Å^3)	4029.1 (5)
Z	4
ρ_{calcd} (g cm^{-3})	1.253
μ (mm^{-1})	0.668

B. Data Collection and Refinement Conditions

diffractometer	Bruker D8/APEX II CCD[b]
radiation (λ [Å])	graphite-monochromated Mo Kα (0.71073)
temperature (°C)	–100
scan type	*w* scans (0.3°) (20 s exposures)
data collection 2θ limit (deg)	53.00
total data collected	32851 (-15 ≤ *h* ≤ 15, -22 ≤ *k* ≤ 22, -23 ≤ *l* ≤

23)

independent reflections	16622 (R_{int} = 0.0445)
number of observed reflections (*NO*)	11272 [$F_o^2 \geq 2\sigma(F_o^2)$]
structure solution method	direct methods/dual space (*SHELXD*[c])
refinement method	full-matrix least-squares on F^2 (*SHELXL–97*[d])
absorption correction method	Gaussian integration (face-indexed)
range of transmission factors	0.9247–0.6940
data/restraints/parameters	16622 / 0 / 892
goodness-of-fit (*S*)[e] [all data]	1.014
final *R* indices[f]	
R_1 [$F_o^2 \geq 2\sigma(F_o^2)$]	0.0405
wR_2 [all data]	0.0908
largest difference peak and hole	0.508 and –0.355 e Å^{-3}

[a]Obtained from least-squares refinement of 8100 reflections with 4.42° < 2θ < 49.12°.

[b]Programs for diffractometer operation, data collection, data reduction and absorption correction were those supplied by Bruker.

[c]Schneider, T. R.; Sheldrick, G. M. *Acta Crystallogr.* **2002**, *D58*, 1772-1779.

[d]Sheldrick, G. M. *Acta Crystallogr.* **2008**, *A64*, 112–122.

[e]$S = [\Sigma w(F_o^2 - F_c^2)^2/(n - p)]^{1/2}$ (n = number of data; p = number of parameters varied; $w = [\sigma^2(F_o^2) + (0.0327P)^2 + 0.5985P]^{-1}$ where $P = [\mathrm{Max}(F_o^2, 0) + 2F_c^2]/3$).

[f]$R_1 = \Sigma||F_o| - |F_c||/\mathrm{S}|F_o|$; $wR_2 = [\Sigma w(F_o^2 - F_c^2)^2/\Sigma w(F_o^4)]^{1/2}$.

Table A-11. Crystallographic Experimental Details for **5-1b**

formula	$C_{27}H_{41}N_2P$
formula weight	424.59
crystal dimensions (mm)	0.56 x 0.39 x 0.22
crystal system	monoclinic
space group	$P2_1/c$
unit cell parameters	
a (Å)	15.6183 (7)
b (Å)	11.6578 (5)
c (Å)	29.7284 (2)
σ (deg)	90
β (deg)	104.4940 (10)
γ (deg)	90
V (Å^3)	5240.5 (4)
Z	8
ρ_{calcd} (g cm^{-3})	1.076
μ (mm^{-1})	0.12
total data collected	74295 ($-19 \le h \le 19$, $-14 \le k \le 14$, $-37 \le l \le 37$)
independent reflections	10794 (R_{int} = 0.0391)
number of observed reflections (*NO*)	8416 [$F_o^2 \ge 2\sigma(F_o^2)$]
absorption correction method	Gaussian integration (face-indexed)
range of transmission factors	0.9247–0.6940
data/restraints/parameters	10794 / 2 / 569
goodness-of-fit (S)[e] [all data]	1.02
final R indices[f]	

R_1 [$F_o^2 \geq 2\sigma(F_o^2)$]	0.042
wR_2 [all data]	0.111
largest difference peak and hole	0.24 and –0.35 e Å^{-3}

Table A-12. Crystallographic Experimental Details for **5-2a**

Empirical formula	$C_{29}H_{50}FeN_3PSi_2$	
Formula weight	583.72	
Temperature	173(2) K	
Wavelength	1.54178 Å	
Crystal system	Triclinic	
Space group	$P\bar{1}$	
Unit cell dimensions	a = 10.5120(2) Å b = 10.5164(2) Å c = 18.0374(4) Å	α= 77.5920(10)° β= 75.604(2)° γ = 61.6840(10)°
Volume	1689.27(6) $Å^3$	
Z	2	
Density (calculated)	1.148 Mg/m^3	
Absorption coefficient	4.852 mm^{-1}	
F(000)	628	
Crystal size	0.29 x 0.16 x 0.07 mm^3	
θ range for data collection	2.55 to 70.23°	
Index ranges	-12<=h<=12, -12<=k<=12, -21<=l<=22	
Reflections collected	11252	
Independent reflections	6108 [R(int) = 0.0405]	
Completeness to theta = 70.23°	95.0 %	
Absorption correction	Semi-empirical from equivalents	
Max. and min. transmission	0.7154 and 0.3345	
Refinement method	Full-matrix least-squares on F^2	

Data / restraints / parameters	6108 / 0 / 339
Goodness-of-fit on F^2	1.047
Final R indices [I>2sigma(I)]	$R_1 = 0.0421$, $wR^2 = 0.1068$
R indices (all data)	$R_1 = 0.0513$, $wR^2 = 0.1122$
Largest diff. peak and hole	0.461 and -0.496 e $Å^{-3}$

Table A-13. Crystallographic Experimental Details for **5-2b**

Empirical formula	$C_{33}H_{58}FeN_3PSi_2$	
Formula weight	639.82	
Temperature	173(2) K	
Wavelength	0.71073 Å	
Crystal system	Monoclinic	
Space group	P2(1)/n	
Unit cell dimensions	a = 17.7285(11) Å b = 19.4132(12) Å c = 22.7688(14) Å	α= 90° β= 107.5410(10)° γ = 90°
Volume	7471.9(8) $Å^3$	
Z	8	
Density (calculated)	1.138 Mg/m^3	
Absorption coefficient	0.535 mm^{-1}	
F(000)	2768	
Crystal size	0.55 x 0.36 x 0.18 mm^3	
θ range for data collection	1.60 to 26.47°.	
Index ranges	-22<=h<=22, -24<=k<=24, -28<=l<=28	
Reflections collected	112770	
Independent reflections	15396 [R(int) = 0.0535]	
Completeness to θ = 26.47°	99.7 %	
Absorption correction	Semi-empirical from equivalents	
Max. and min. transmission	0.9099 and 0.7586	
Refinement method	Full-matrix least-squares on F^2	

Data / restraints / parameters	15396 / 0 / 753
Goodness-of-fit on F^2	1.010
Final R indices [$I>2\sigma(I)$]	$R_1 = 0.0365$, $wR^2 = 0.0875$
R indices (all data)	$R_1 = 0.0544$, $wR^2 = 0.0980$
Largest diff. peak and hole	0.452 and -0.339 e $Å^{-3}$

Table A-14. Crystallographic Experimental Details for **5-2c**

Empirical formula	$C_{33}H_{58}CoN_3PSi_2$	
Formula weight	642.90	
Temperature	173(2) K	
Wavelength	0.71073 Å	
Crystal system	Monoclinic	
Space group	P2(1)/n	
Unit cell dimensions	a = 17.6220(13) Å b = 19.4261(14) Å c = 22.7710(16) Å	α= 90° β= 107.3280(10)° γ = 90°
Volume	7441.3(9) $Å^3$	
Z	8	
Density (calculated)	1.148 Mg/m^3	
Absorption coefficient	0.593 mm^{-1}	
F(000)	2776	
Crystal size	0.34 x 0.32 x 0.23 mm^3	
θ range for data collection	1.29 to 26.44°.	
Index ranges	-22<=h<=22, -24<=k<=24, -28<=l<=28	
Reflections collected	117084	
Independent reflections	15313 [R(int) = 0.0724]	
Completeness to θ = 26.44°	99.8 %	
Absorption correction	Semi-empirical from equivalents	
Max. and min. transmission	0.8737 and 0.8239	
Refinement method	Full-matrix least-squares on F^2	

Data / restraints / parameters	15313 / 0 / 753
Goodness-of-fit on F^2	1.035
Final R indices [$I>2\sigma(I)$]	$R_1 = 0.0415$, $wR^2 = 0.0931$
R indices (all data)	$R_1 = 0.0670$, $wR^2 = 0.1071$
Largest diff. peak and hole	0.478 and -0.341 e $Å^{-3}$

Table A-15. Crystallographic Experimental Details for **5-3**

Empirical formula	$C_{36}H_{56}FeN_3PSi$	
Formula weight	645.75	
Temperature	173(2) K	
Wavelength	0.71073 Å	
Crystal system	Monoclinic	
Space group	P2(1)/*c*	
Unit cell dimensions	a = 17.995(3) Å b = 21.202(3) Å c = 19.245(16) Å	α= 90° β= 107.3280(10)° γ = 90°
Volume	7342(2) $Å^3$	
Z	8	
Density (calculated)	1.168 Mg/m^3	
Absorption coefficient	0.51 mm^{-1}	
F(000)	2784	
Crystal size	0.34 x 0.26 x 0.16 mm^3	
θ range for data collection	2.57 to 26.37°	
Index ranges	-22<=h<=22, -26<=k<=26, -24<=l<=24	
Reflections collected	90448	
Independent reflections	15002 [R(int) = 0.086]	
Absorption correction	Multi scan	
Max. and min. transmission	0.923 and 0.853	
Refinement method	Full-matrix least-squares on F^2	
Data / restraints / parameters	15002 / 0 / 783	

Goodness-of-fit on F^2	1.02
Final R indices [$I>2\sigma(I)$]	$R_1 = 0.0452$, $wR^2 = 0.1051$
R indices (all data)	$R_1 = 0.0776$, $wR^2 = 0.1251$
Largest diff. peak and hole	0.37 and -0.43 e $Å^{-3}$

Table A-16. Crystallographic Experimental Details for **5-4•0.5C_7H_8**

Empirical formula	$C_{35.5}H_{49}ClFeN_3P$	
Formula weight	640.05	
Temperature	173(2) K	
Wavelength	0.71073 Å	
Crystal system	Triclinic	
Space group	$P\bar{1}$	
Unit cell dimensions	a = 9.0284(10) Å b = 11.8863(13) Å c = 17.2264(19) Å	α= 87.3600(10)° β= 84.2880(10)° γ = 71.3770(10)°
Volume	1742.9(3) $Å^3$	
Z	2	
Density (calculated)	1.220 Mg/m^3	
Absorption coefficient	0.582 mm^{-1}	
F(000)	682	
Crystal size	0.48 x 0.25 x 0.15 mm^3	
θ range for data collection	1.19 to 27.59°	
Index ranges	-11<=h<=11, -15<=k<=15, -22<=l<=22	
Reflections collected	30858	
Independent reflections	8017 [R(int) = 0.0347]	
Completeness to θ = 27.59°	99.2 %	
Absorption correction	Semi-empirical from equivalents	
Max. and min. transmission	0.9177 and 0.7658	
Refinement method	Full-matrix least-squares on F^2	

Data / restraints / parameters	8017 / 0 / 417
Goodness-of-fit on F^2	1.052
Final R indices [$I>2\sigma(I)$]	$R_1 = 0.0328$, $wR^2 = 0.0769$
R indices (all data)	$R_1 = 0.0430$, $wR^2 = 0.0871$
Largest diff. peak and hole	0.369 and -0.304 e $Å^{-3}$

Table A-17. Crystallographic Experimental Details for **5-5**

Empirical formula	$C_{66}H_{104}Cl_4Fe_2Li_2N_4O_3P_2$	
Formula weight	1330.85	
Temperature	296(2) K	
Wavelength	0.71073 Å	
Crystal system	Monoclinic	
Space group	P2(1)	
Unit cell dimensions	a = 10.7319(3) Å b = 27.4315(7) Å c = 12.4002(3) Å	α= 90° β= 102.55° γ = 90°
Volume	3563.30(16) $Å^3$	
Z	2	
Density (calculated)	1.240 Mg/m^3	
Absorption coefficient	0.646 mm^{-1}	
F(000)	1416	
Crystal size	0.38 x 0.28 x 0.22 mm^3	
θ range for data collection	1.48 to 27.51°.	
Index ranges	-13<=h<=13, -35<=k<=35, -16<=l<=16	
Reflections collected	77946	
Independent reflections	16332 [R(int) = 0.0259]	
Completeness to θ = 27.51°	99.9 %	
Absorption correction	Semi-empirical from equivalents	
Max. and min. transmission	0.8693 and 0.7936	
Refinement method	Full-matrix least-squares on F^2	

Data / restraints / parameters	16332 / 1 / 769
Goodness-of-fit on F^2	1.041
Final R indices [$I>2\sigma(I)$]	$R_1 = 0.0293$, $wR^2 = 0.0791$
R indices (all data)	$R_1 = 0.0305$, $wR^2 = 0.0800$
Largest diff. peak and hole	1.813 and -0.283 e $Å^{-3}$

Table A-18. Crystallographic Experimental Details for **5-6•Et_2O**

Empirical formula	$C_{66}H_{74}FeN_4OP_2$	
Formula weight	1057.08	
Temperature	173(2) K	
Wavelength	1.54178 Å	
Crystal system	Triclinic	
Space group	$P\bar{1}$	
Unit cell dimensions	a = 12.2849(2) Å b = 12.9845(2) Å c = 20.4504(3) Å	α= 104.210(1)° β= 92.628(1)° γ = 112.489(1)°
Volume	2866.03(8) $Å^3$	
Z	2	
Density (calculated)	1.216 Mg/m^3	
Absorption coefficient	2.962 mm^{-1}	
F(000)	1124	
Crystal size	0.29 x 0.27 x 0.07 mm^3	
θ range for data collection	3.84 to 71.46°	
Index ranges	-22<=h<=22, -26<=k<=26, -24<=l<=24	
Reflections collected	88146	
Independent reflections	10636 [R(int) = 0.058]	
Absorption correction	Multi scan	
Max. and min. transmission	0.829 and 0.477	
Refinement method	Full-matrix least-squares on F^2	
Data / restraints / parameters	10636 / 0 / 677	

Goodness-of-fit on F^2	1.04
Final R indices [$I>2\sigma(I)$]	$R_1 = 0.0329$, $wR^2 = 0.0851$
R indices (all data)	$R_1 = 0.0358$, $wR^2 = 0.0864$
Largest diff. peak and hole	0.47 and -0.32 e $Å^{-3}$

APPENDIX B: Representative NMR Spectra

^{1}H NMR (300.1 MHz, $CDCl_3$) 1-Phenylethanol (6-1a)

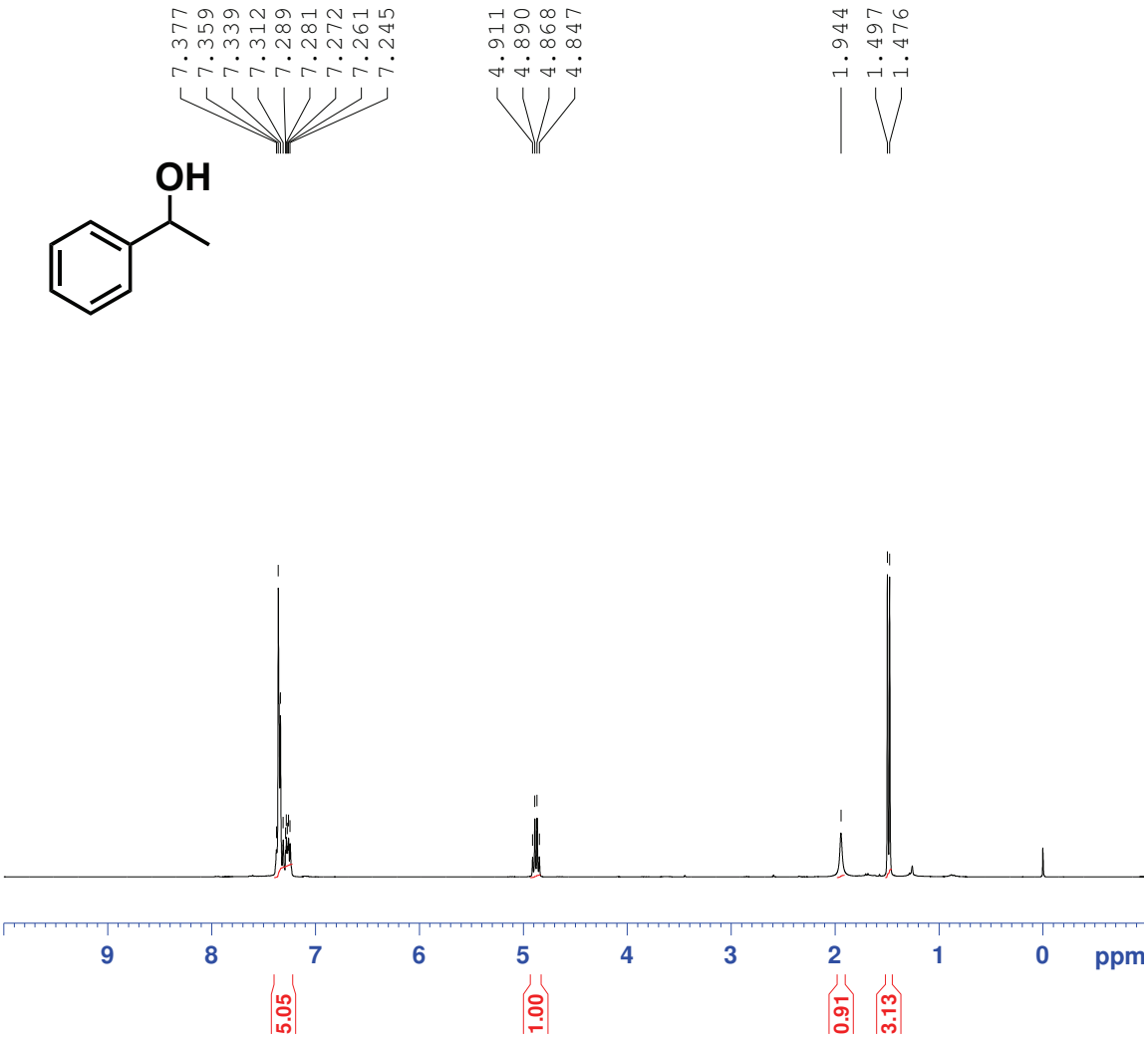

^{13}C NMR (75.5 MHz, $CDCl_3$) 1-Phenylethanol (6-1a)

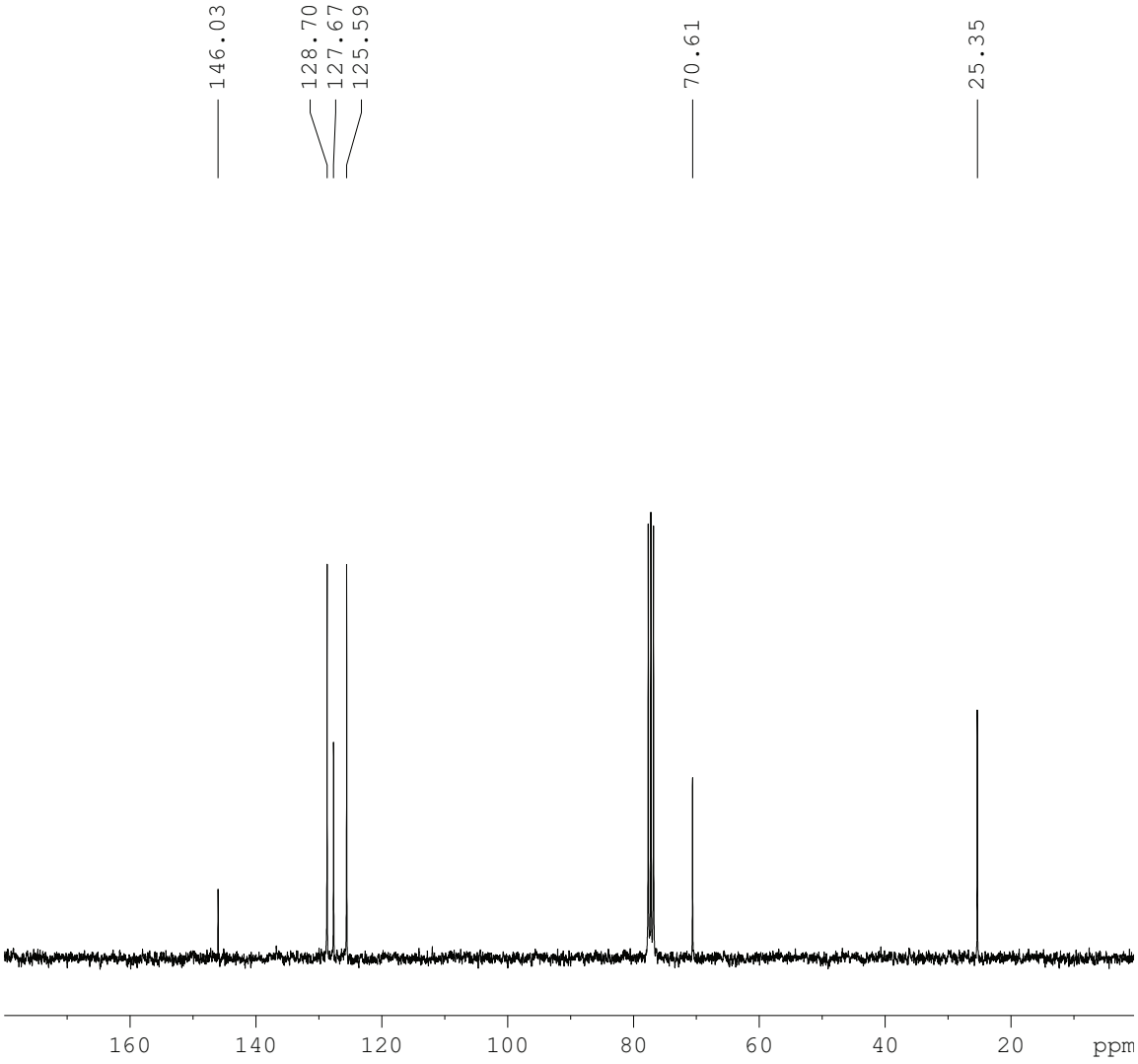

^{1}H NMR (300.1 MHz, $CDCl_3$) 1-(4-Chlorophenyl)ethanol (6-1b)

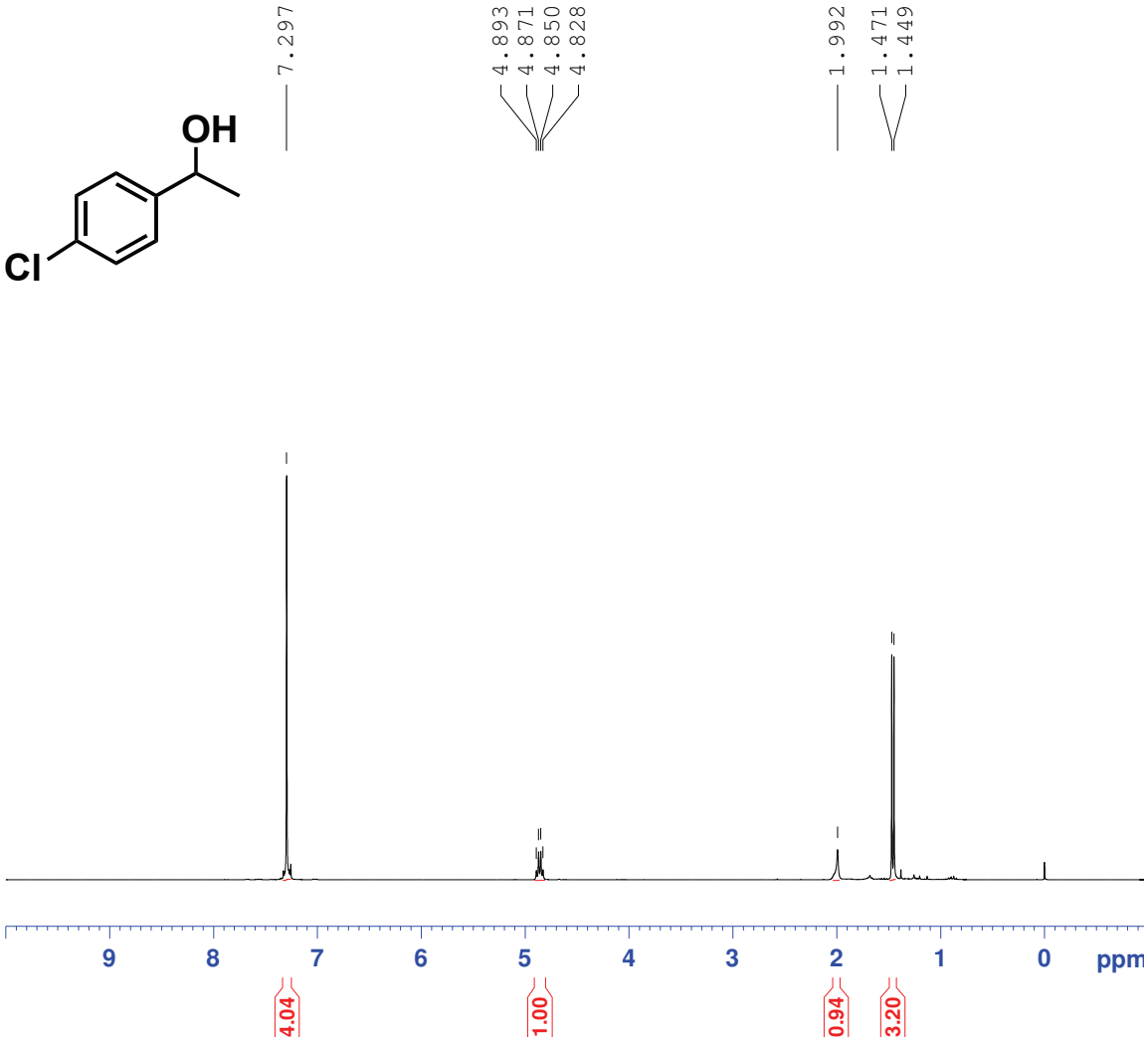

^{13}C NMR (75.5 MHz, $CDCl_3$) 1-(4-Chlorophenyl)ethanol (6-1b)

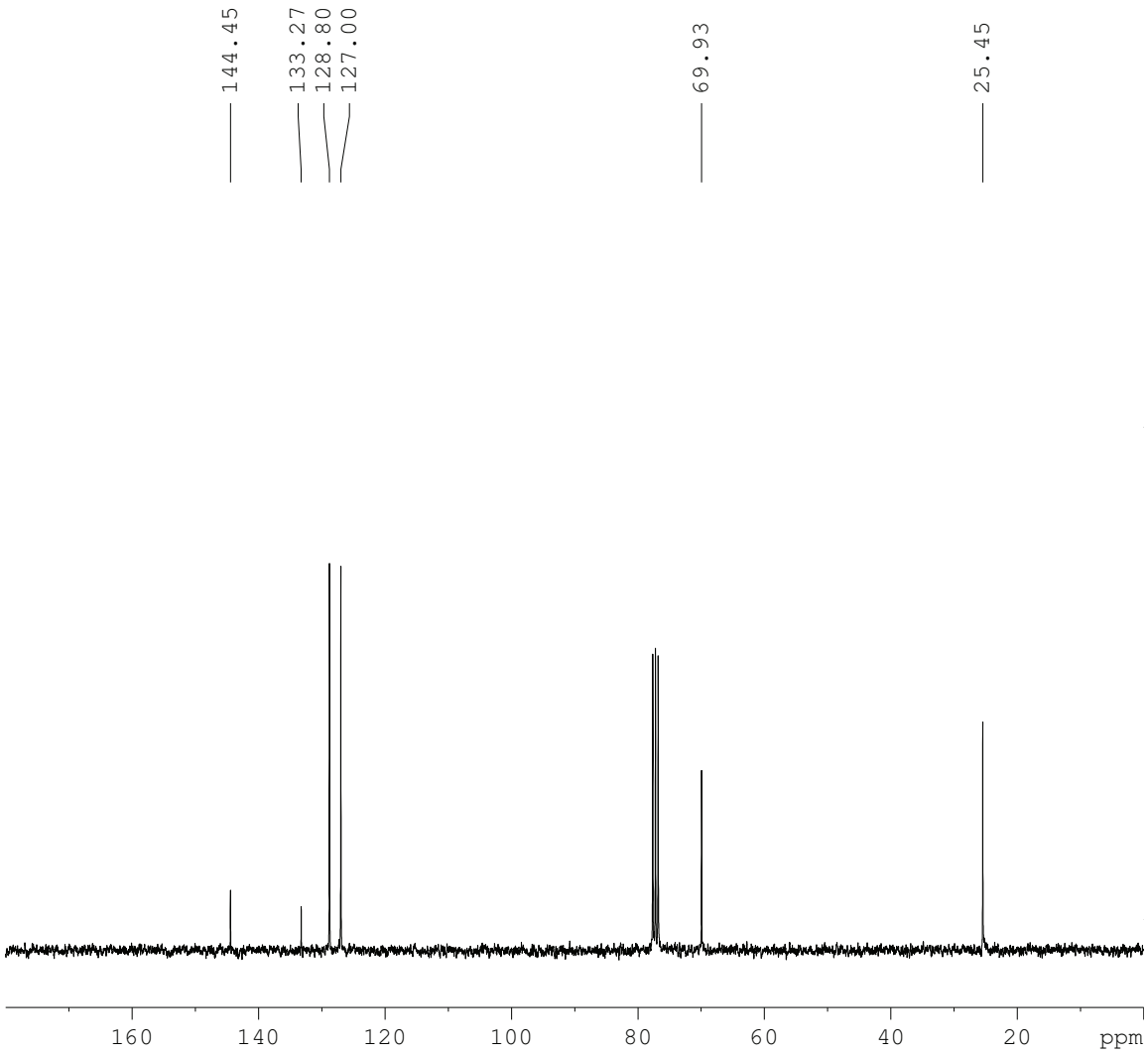

^{1}H NMR (300.1 MHz, $CDCl_3$) 1-(4-Pyridyl)ethanol (6-1e)

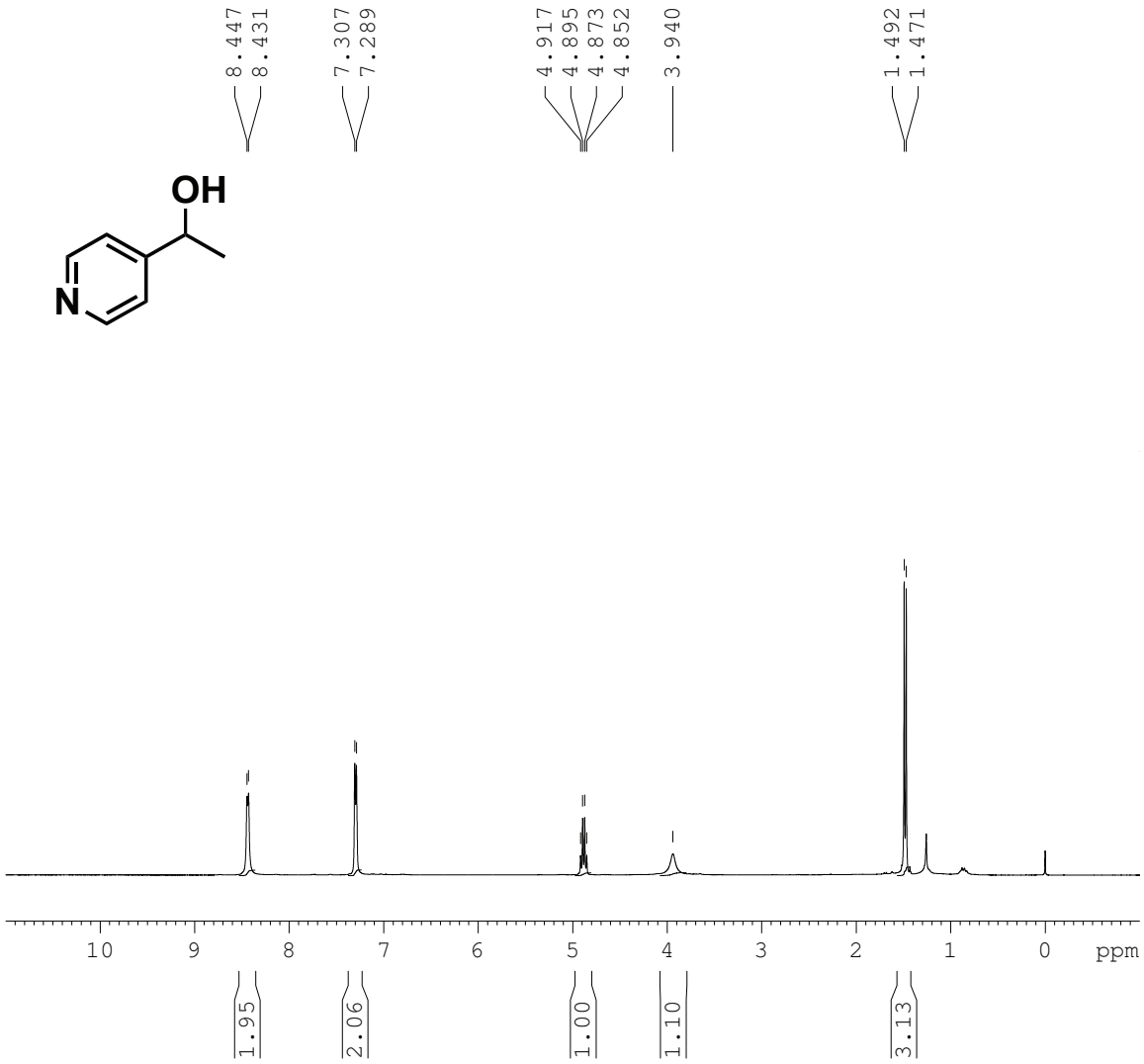

^{13}C NMR (75.5 MHz, $CDCl_3$) 1-(4-Pyridyl)ethanol (6-1e)

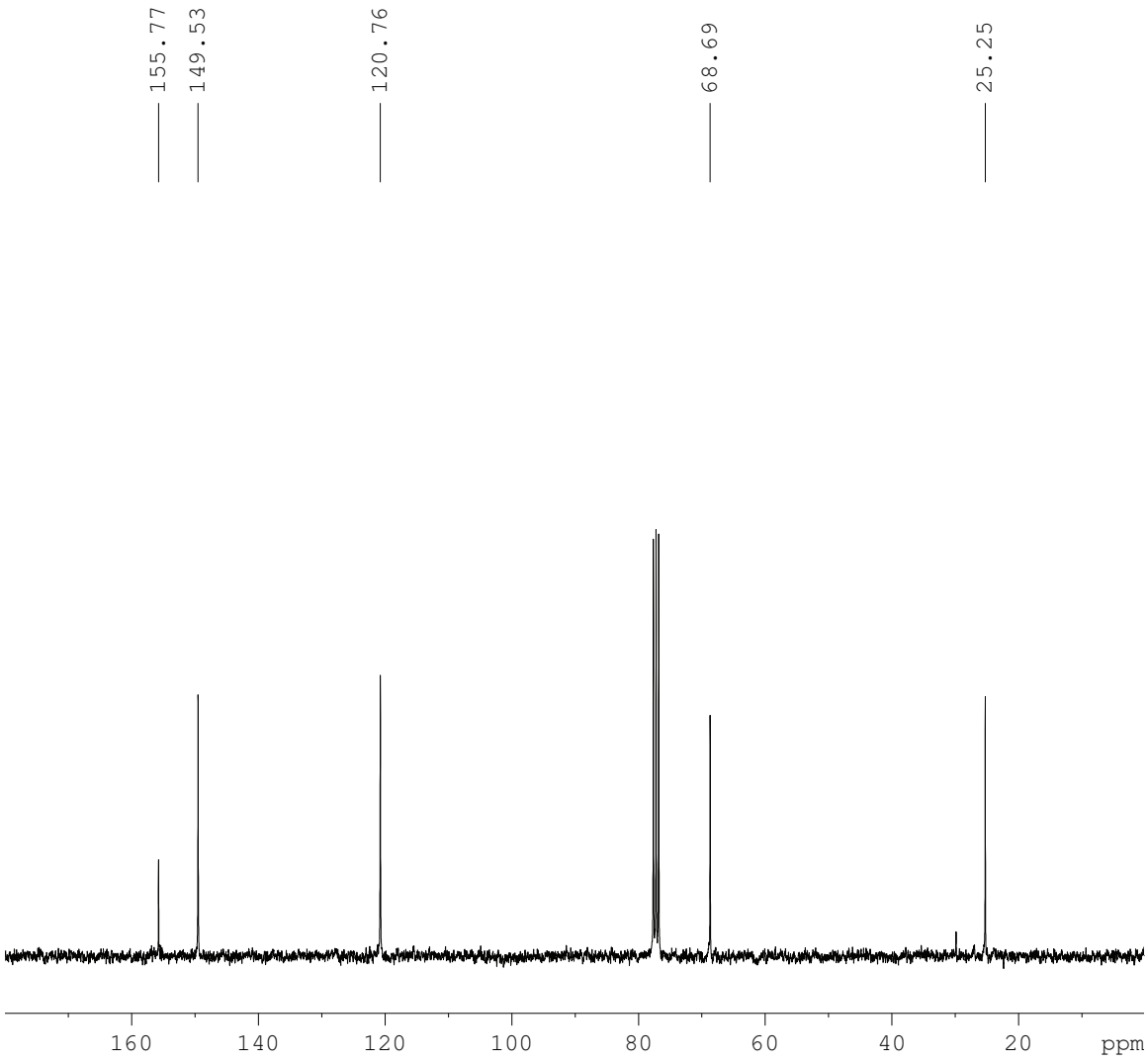

^{1}H NMR (300.1 MHz, $CDCl_3$) Cylohexanol (6-1m)

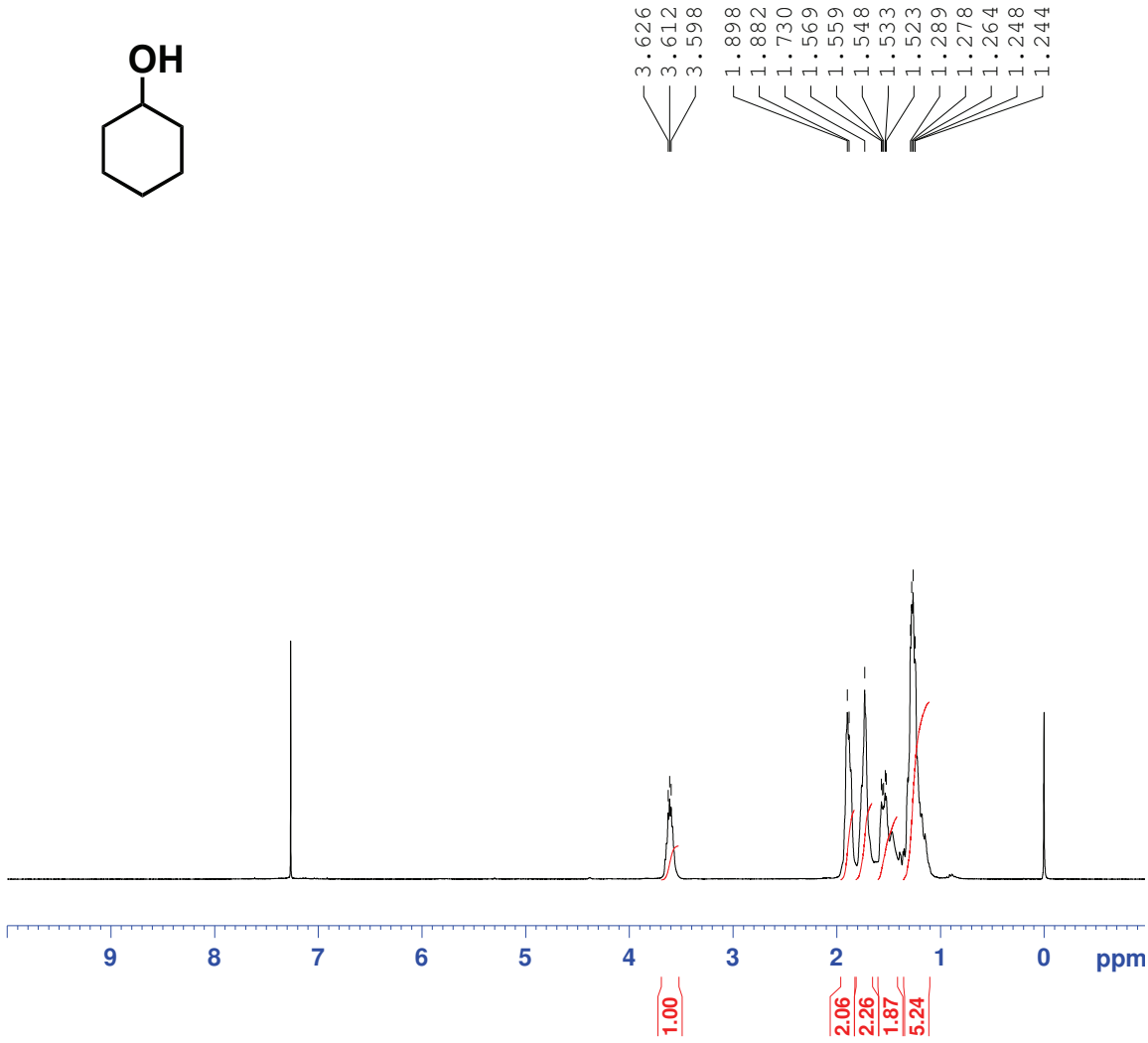

^{13}C NMR (75.5 MHz, $CDCl_3$) Cyclohexanol (6-1m)

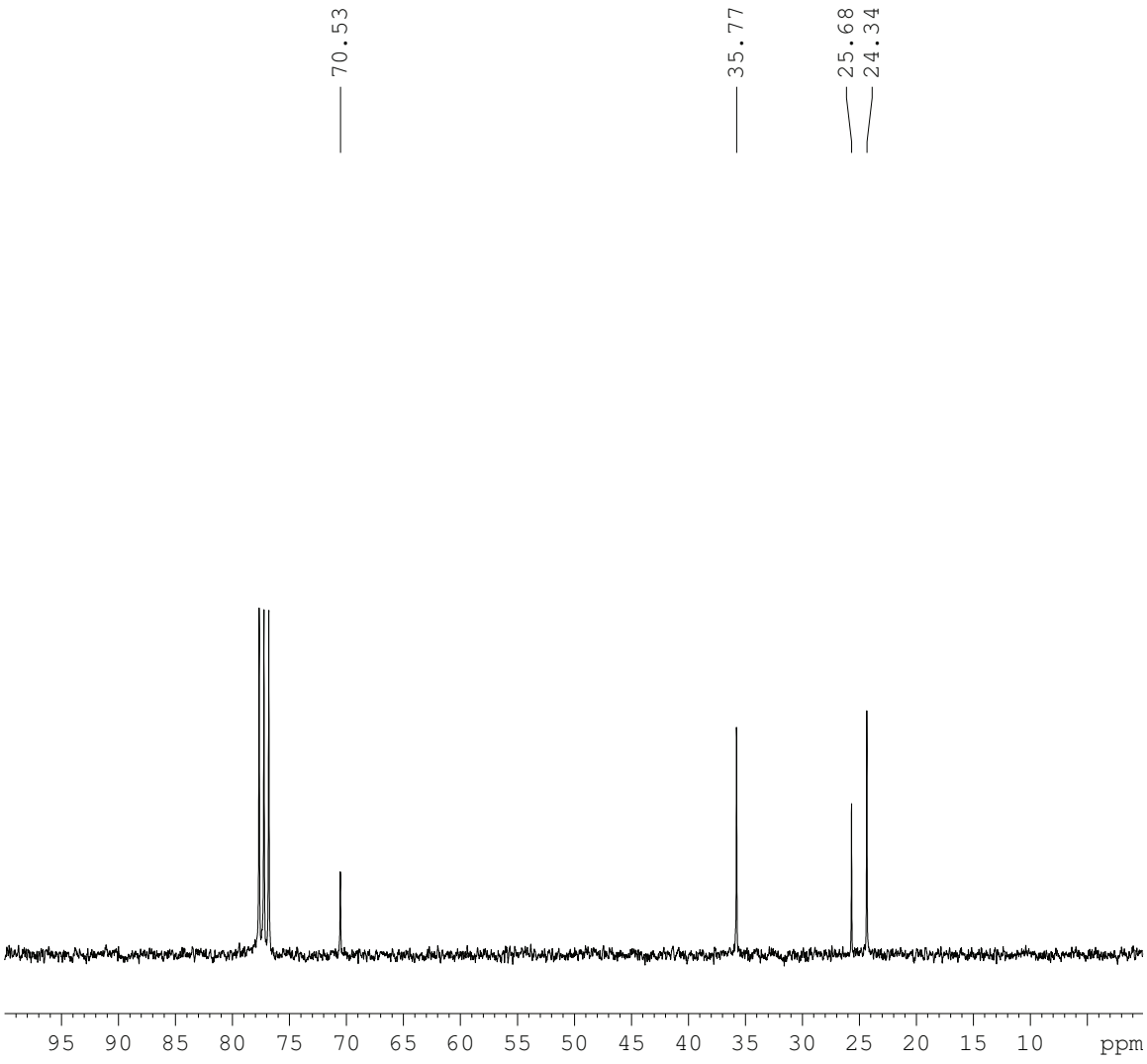

^{1}H NMR (300.1 MHz, $CDCl_3$) 2-Heptanol (6-1r)

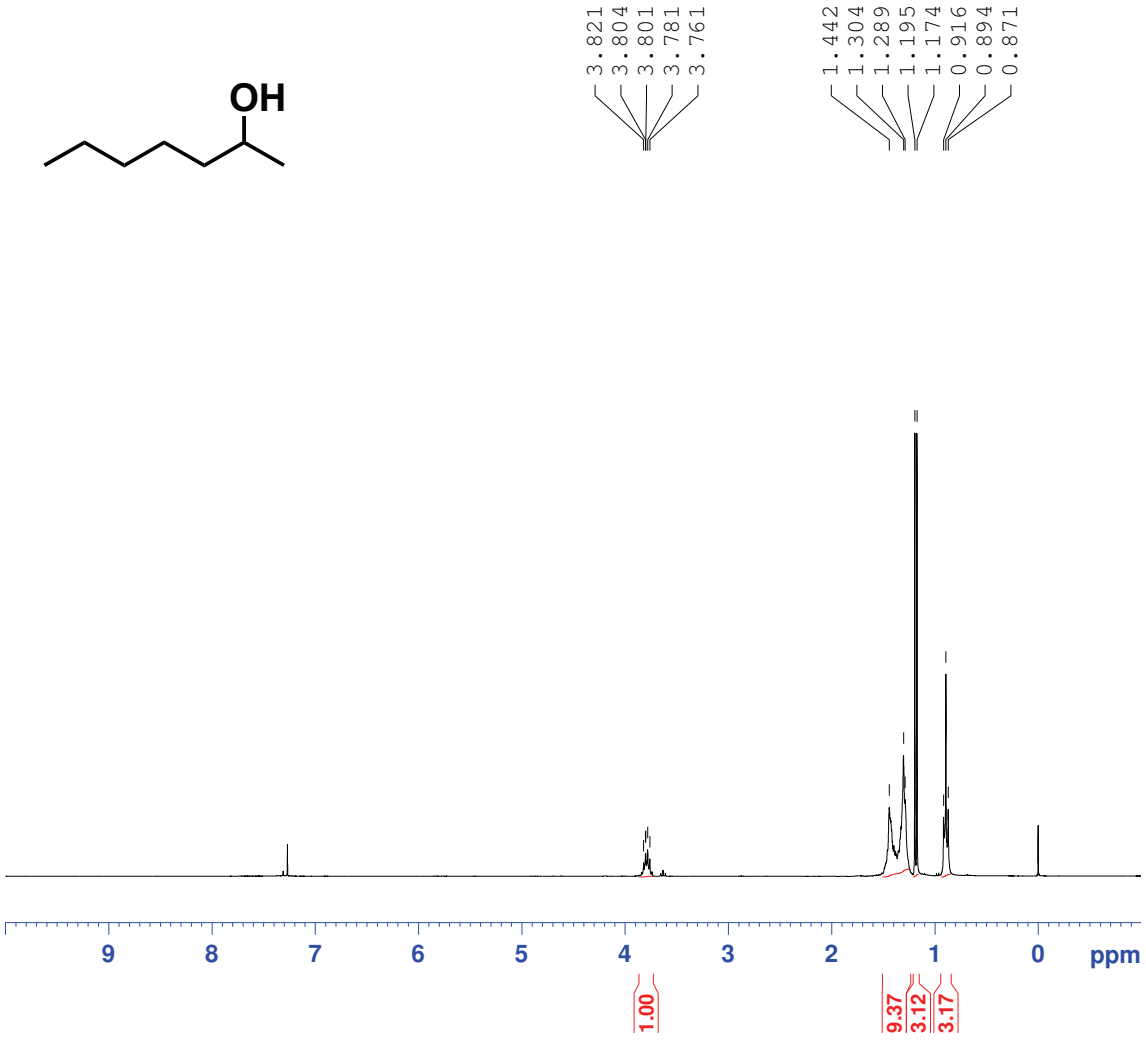

^{13}C NMR (75.5 MHz, $CDCl_3$) 2-Heptanol (6-1r)

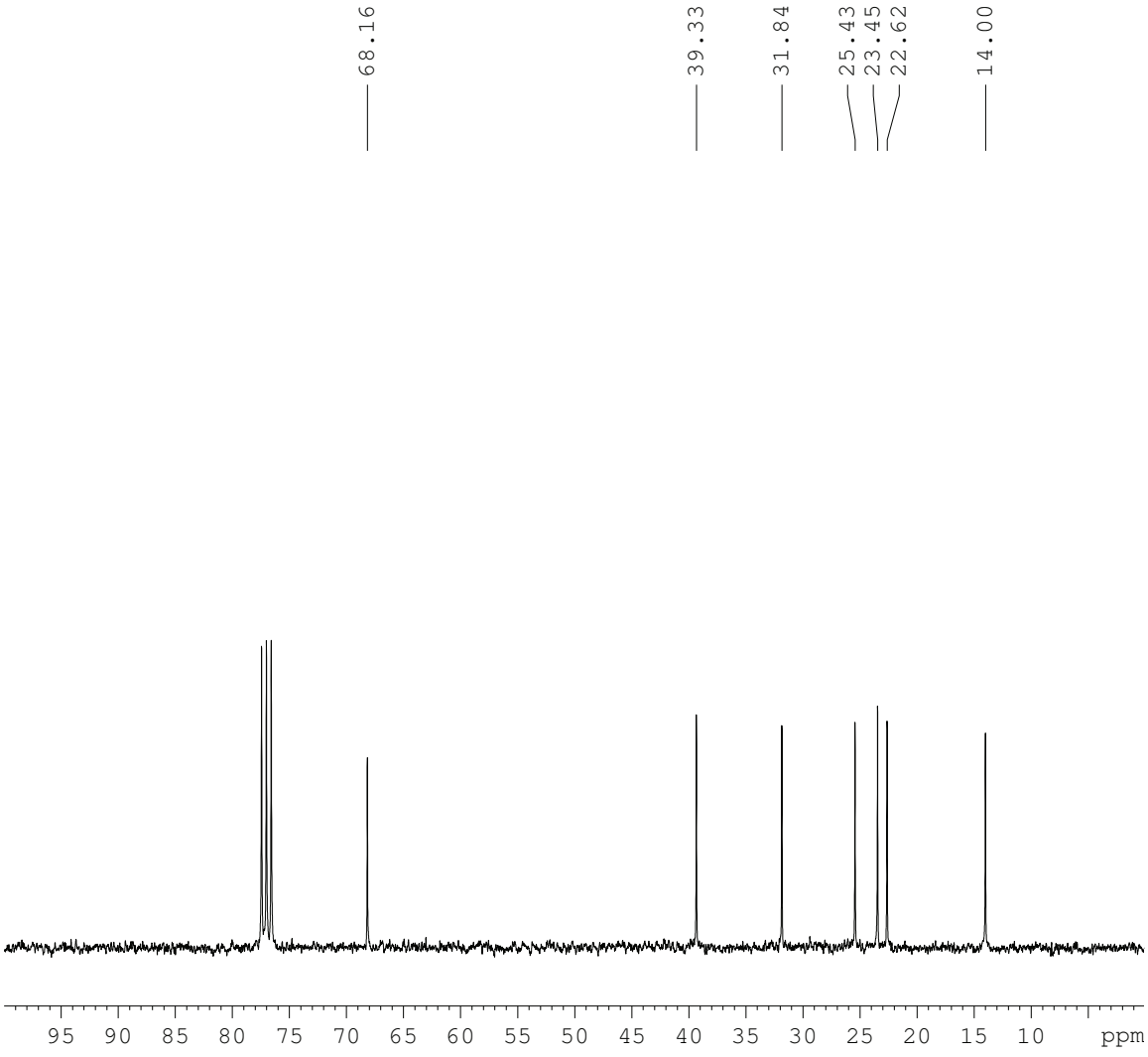

^{1}H NMR (300.1 MHz, $CDCl_3$) Diphenylmethanol (6-1u)

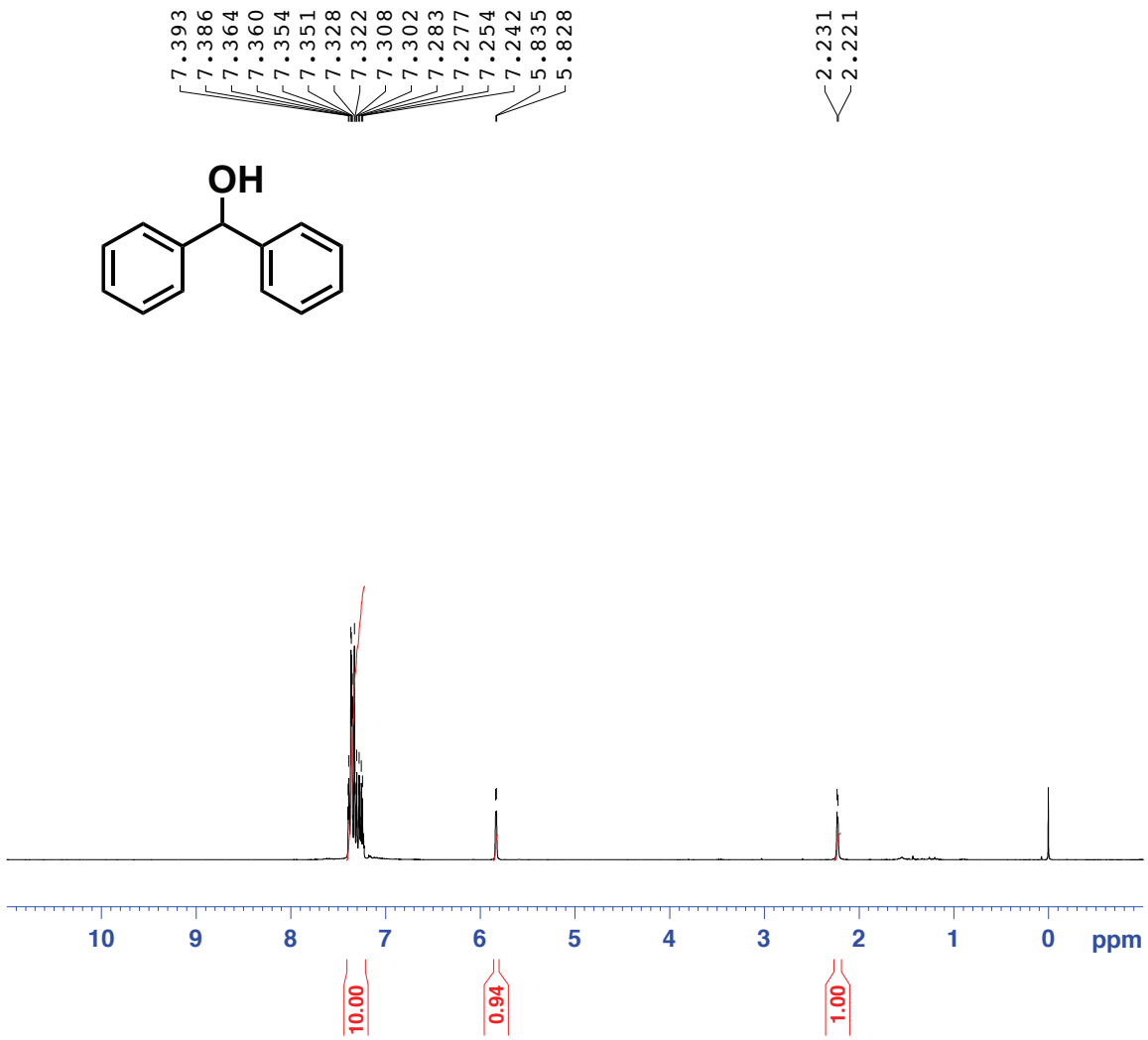

^{13}C NMR (75.5 MHz, $CDCl_3$) Diphenylmethanol (6-1u)

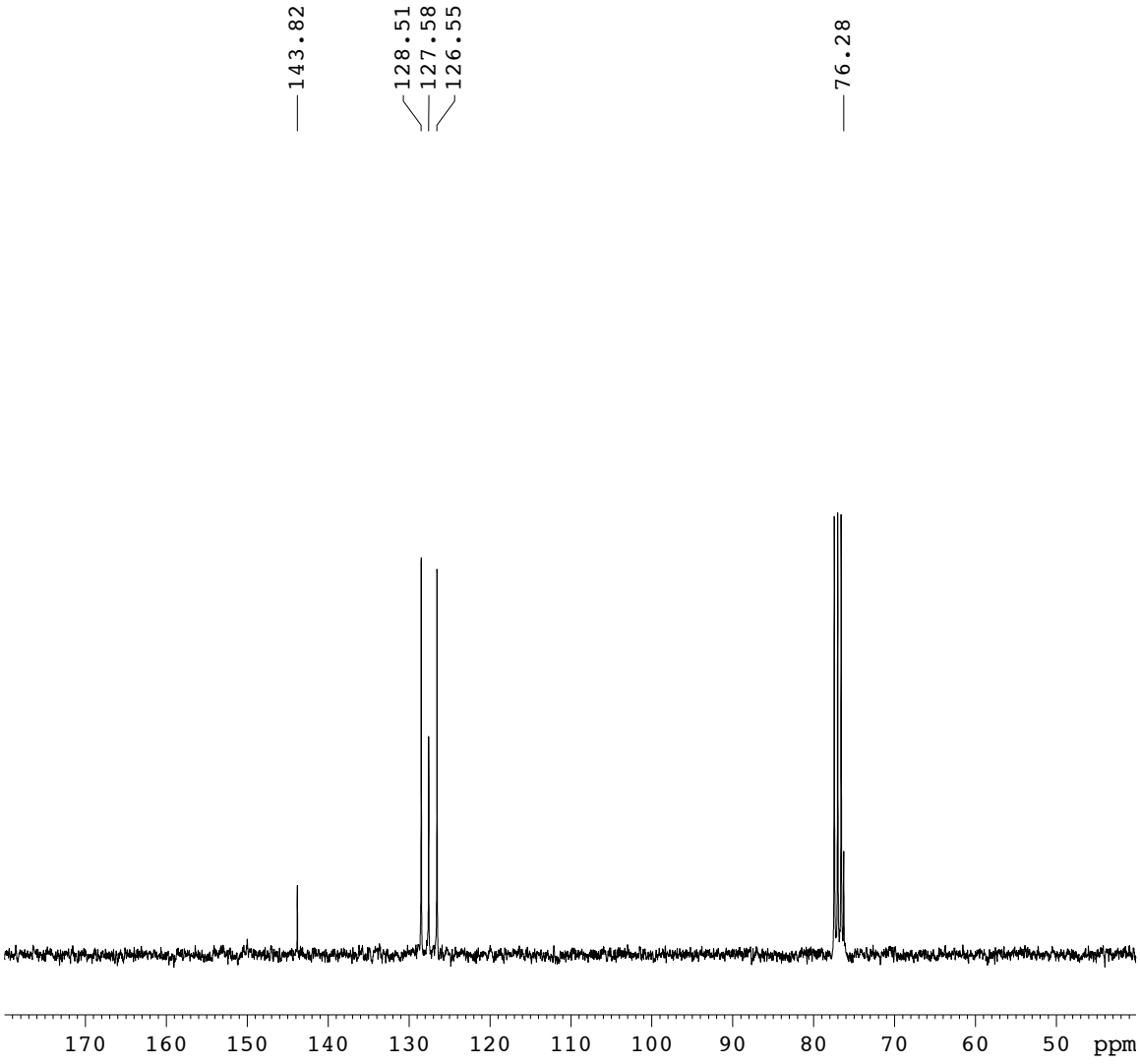

^{1}H NMR (300.1 MHz, $CDCl_3$) 2-Methylbenzyl alcohol (6-1x)

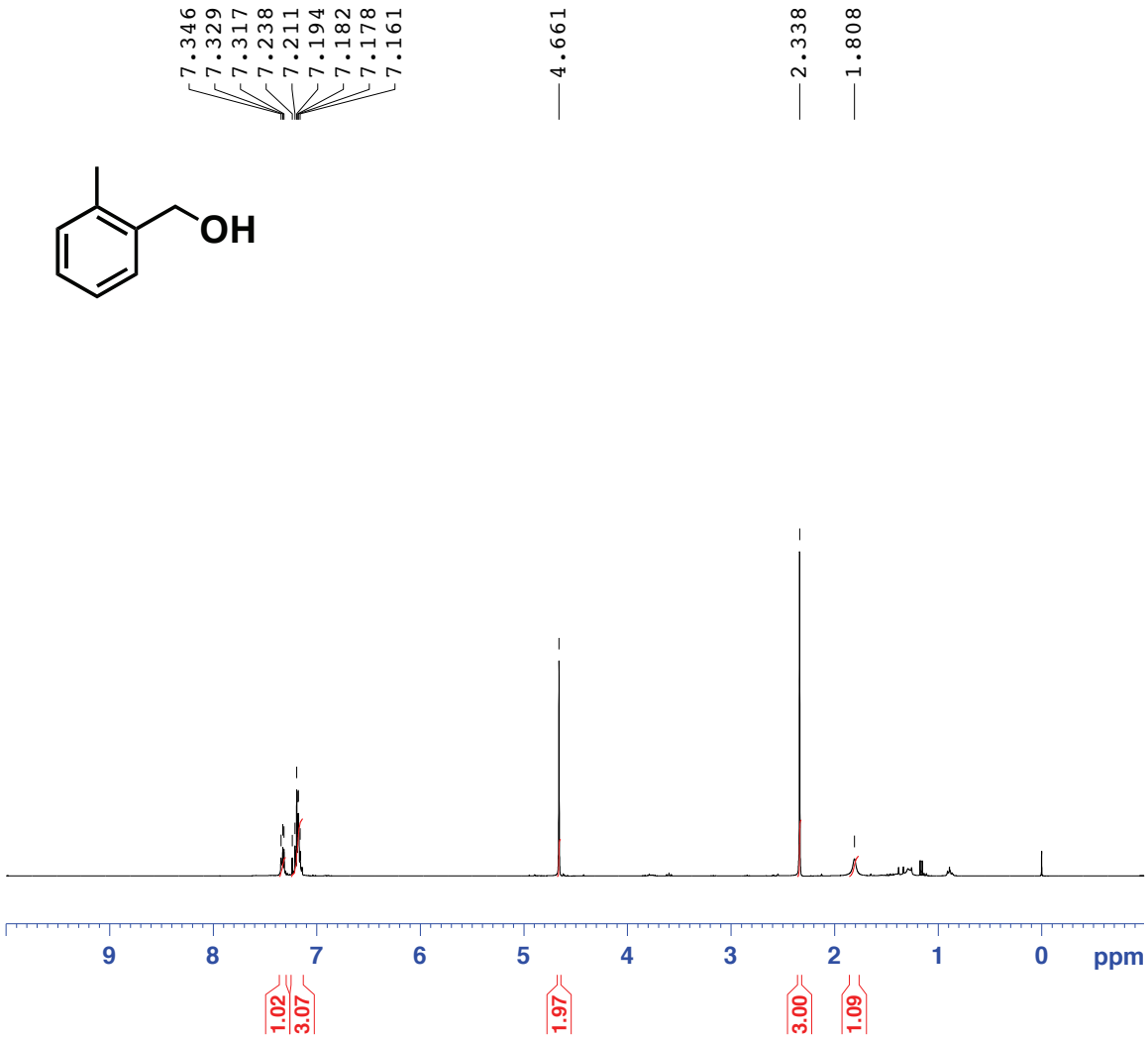

^{13}C NMR (75.5 MHz, $CDCl_3$) 2-Methylbenzyl alcohol (6-1x)

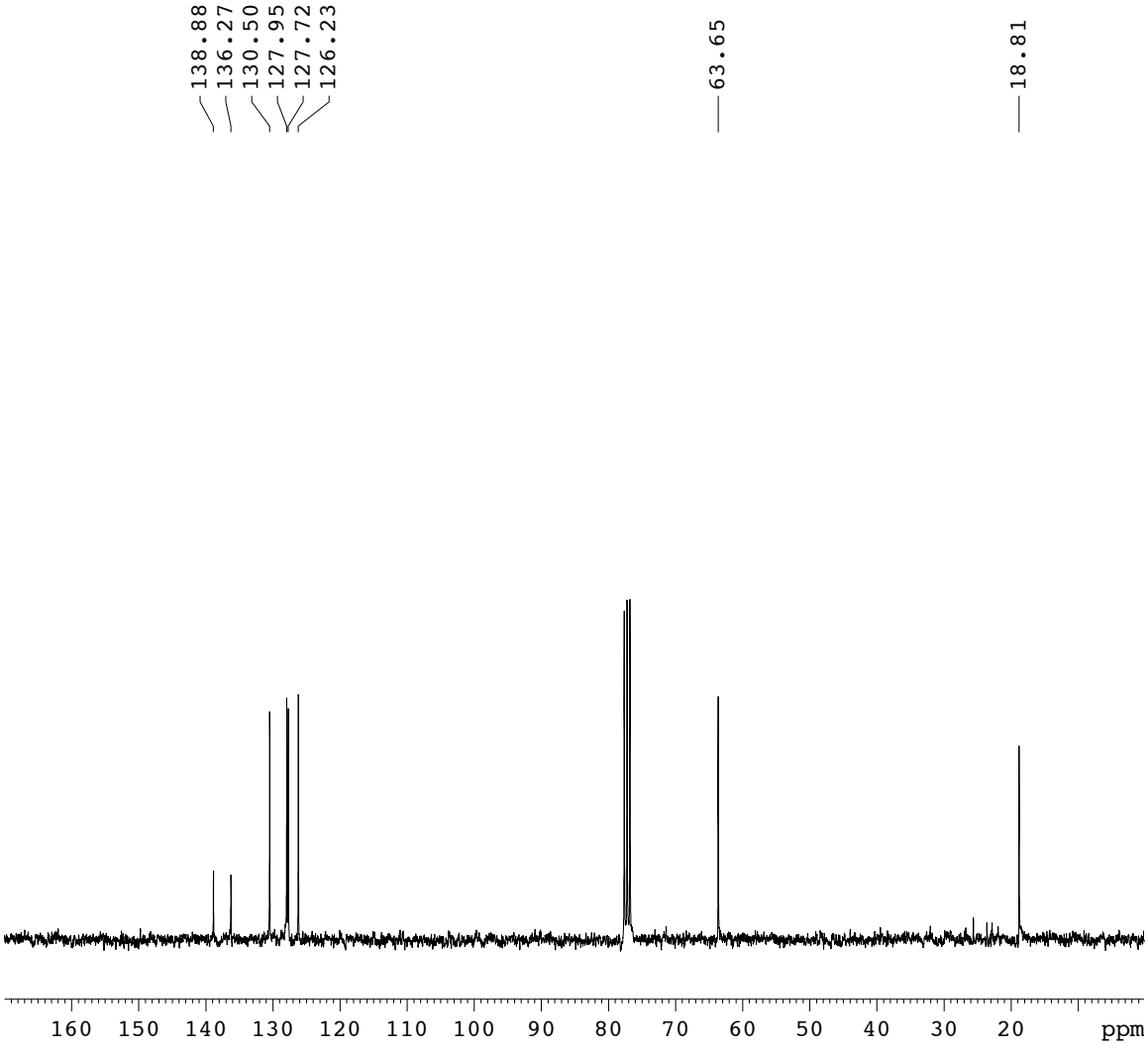

^{1}H NMR (300.1 MHz, $CDCl_3$) 2-Cyclohexen-1-ol (6-2a)

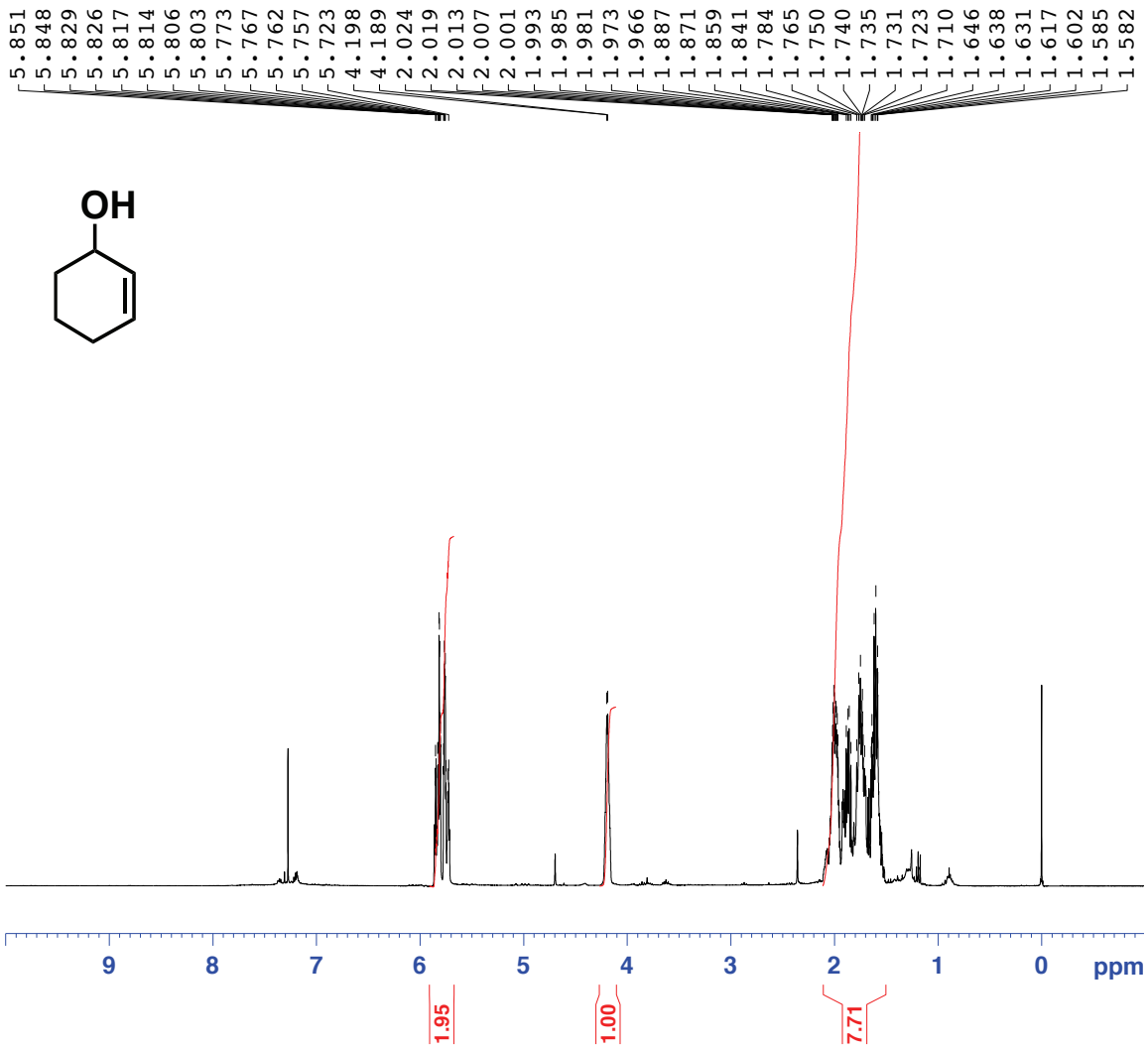

^{13}C NMR (75.5 MHz, $CDCl_3$) 2-Cyclohexen-1-ol (6-2a)

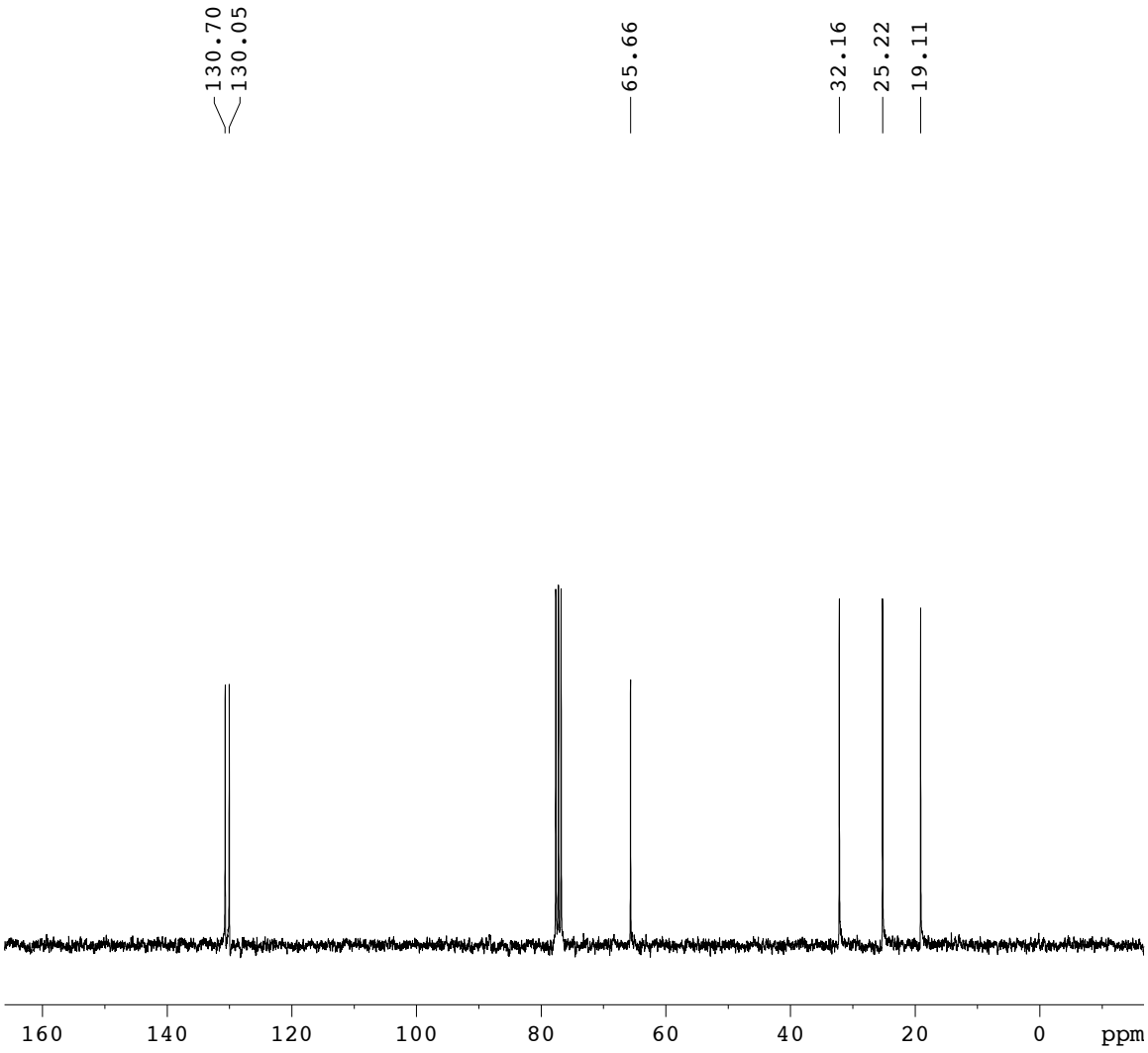

^{1}H NMR (300.1 MHz, $CDCl_3$) 5-Hexen-2-ol (6-2b)

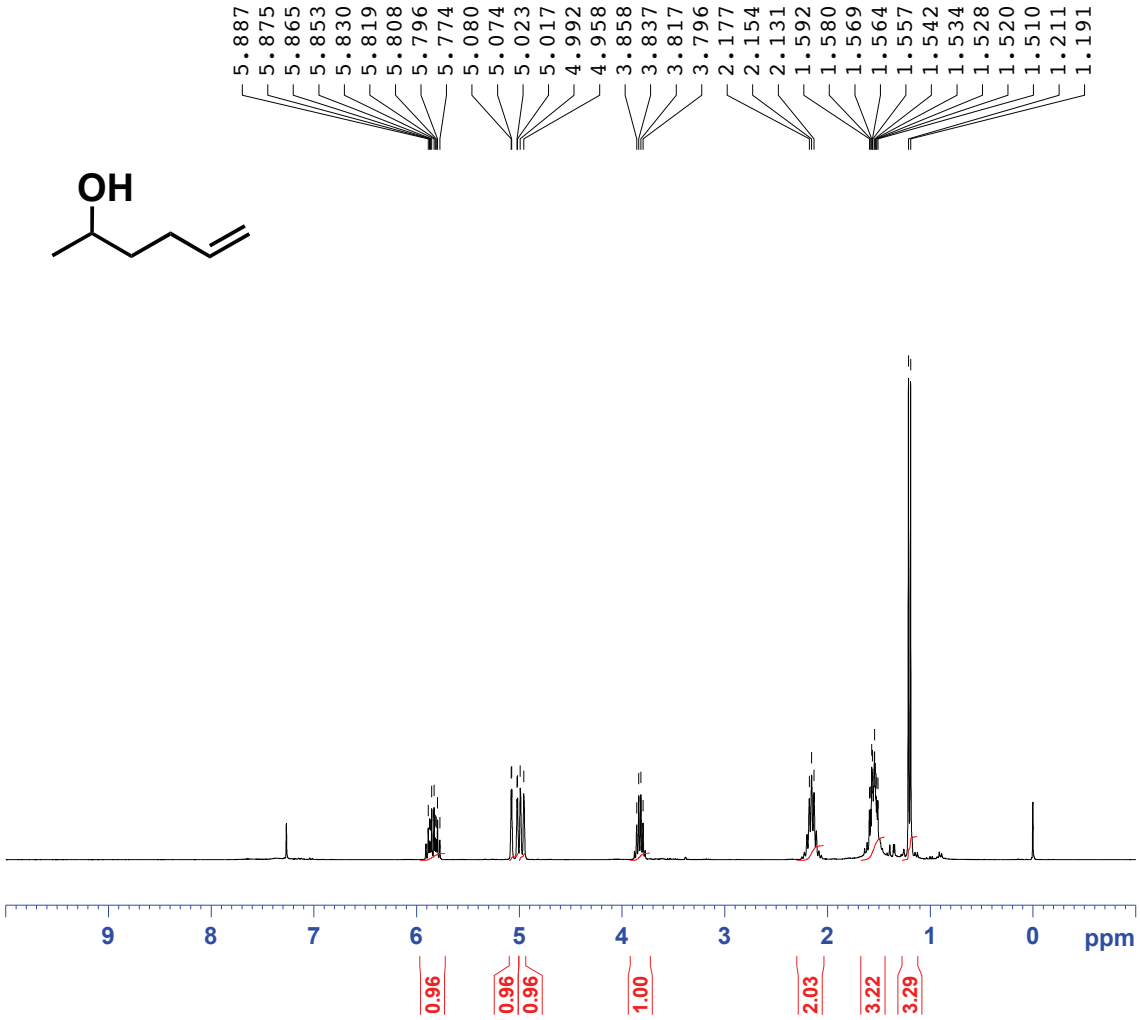

^{13}C NMR (75.5 MHz, $CDCl_3$) 5-Hexen-2-ol (6-2b)

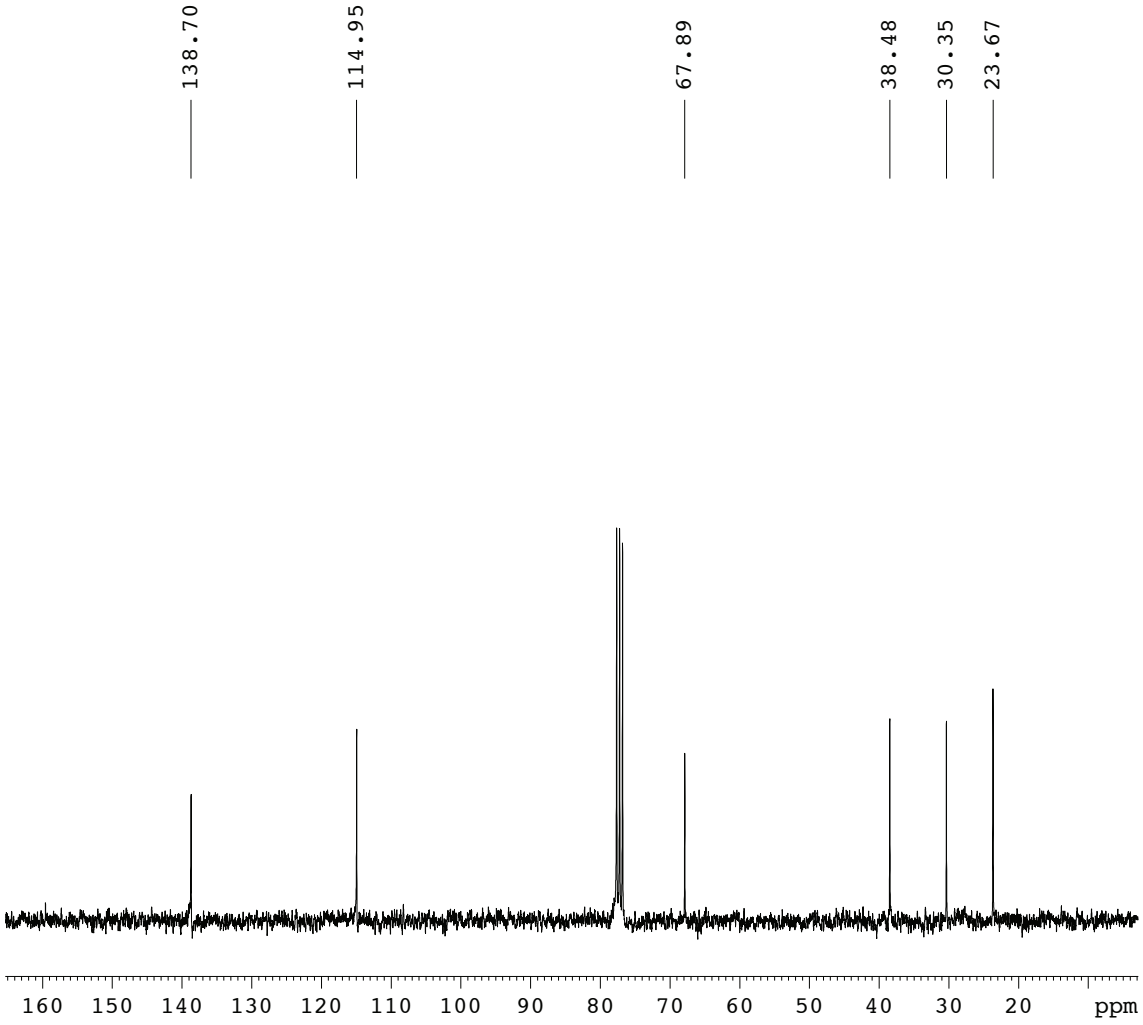

^{1}H NMR (300.1 MHz, $CDCl_3$) 2-Phenylethanol (6-3a)

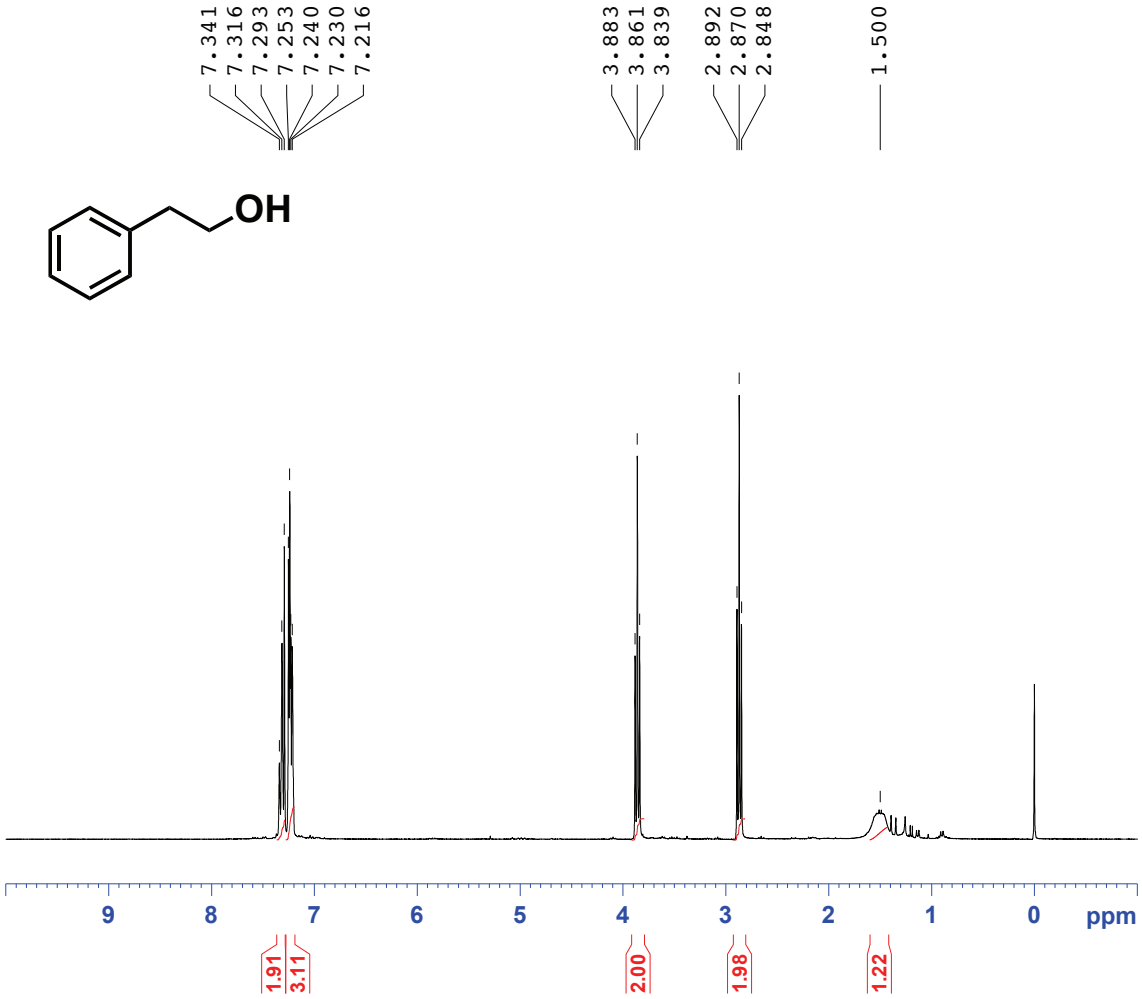

^{13}C NMR (75.5 MHz, $CDCl_3$) 2-Phenylethanol (6-3a)

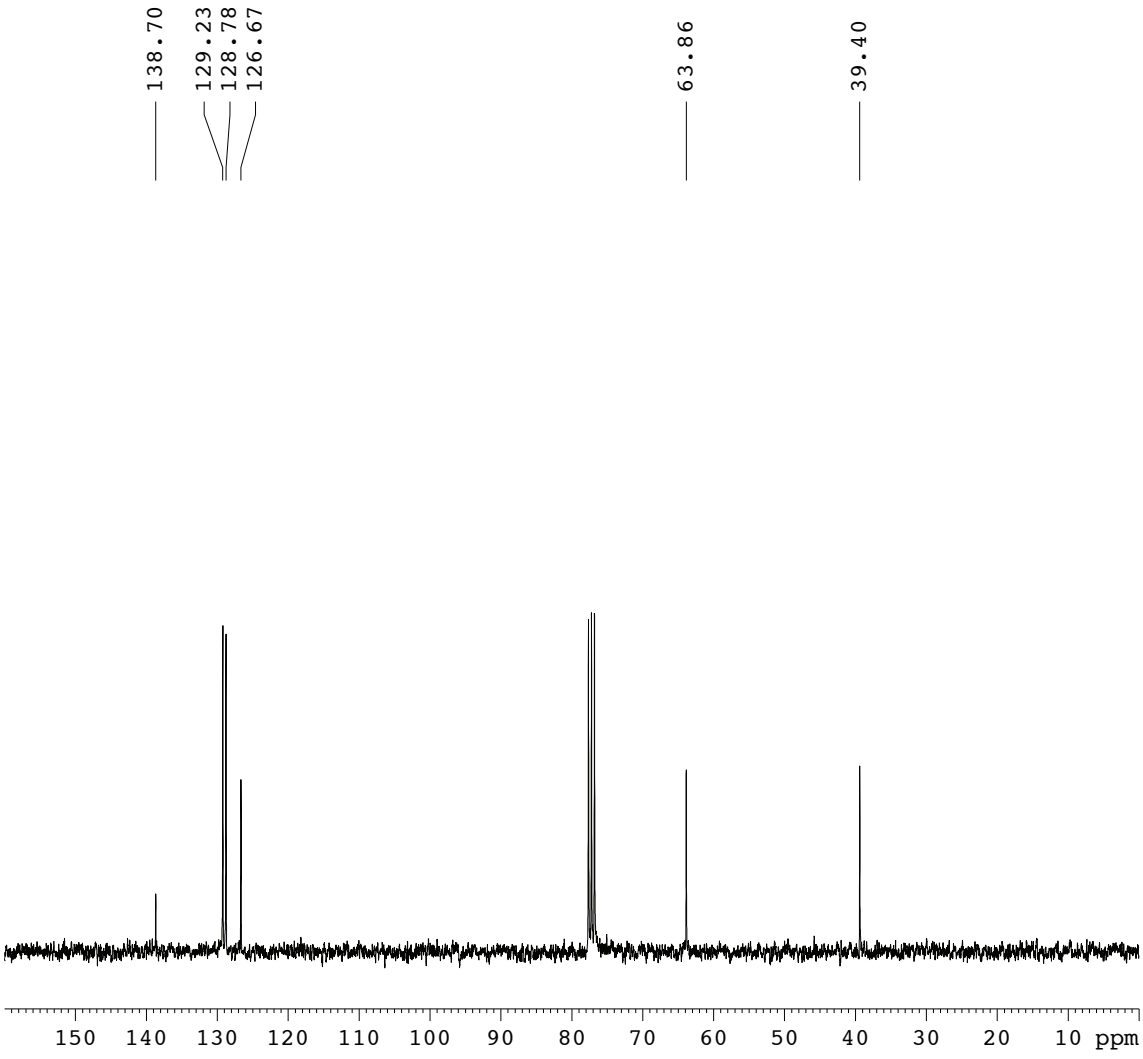

^{1}H NMR (300.1 MHz, $CDCl_3$) Benzyl alcohol (6-3b)

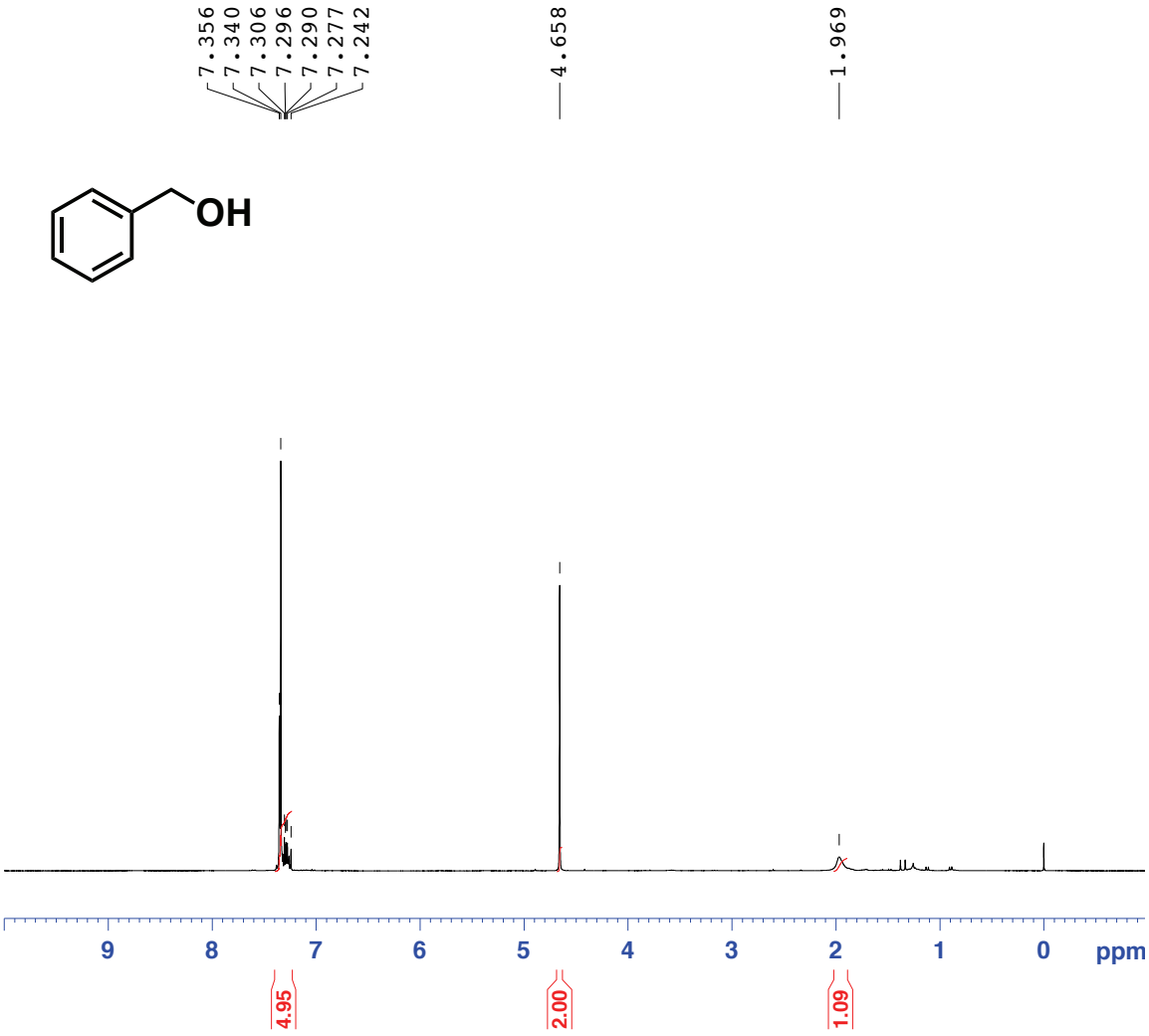

^{13}C NMR (75.5 MHz, $CDCl_3$) Benzyl alcohol (6-3b)

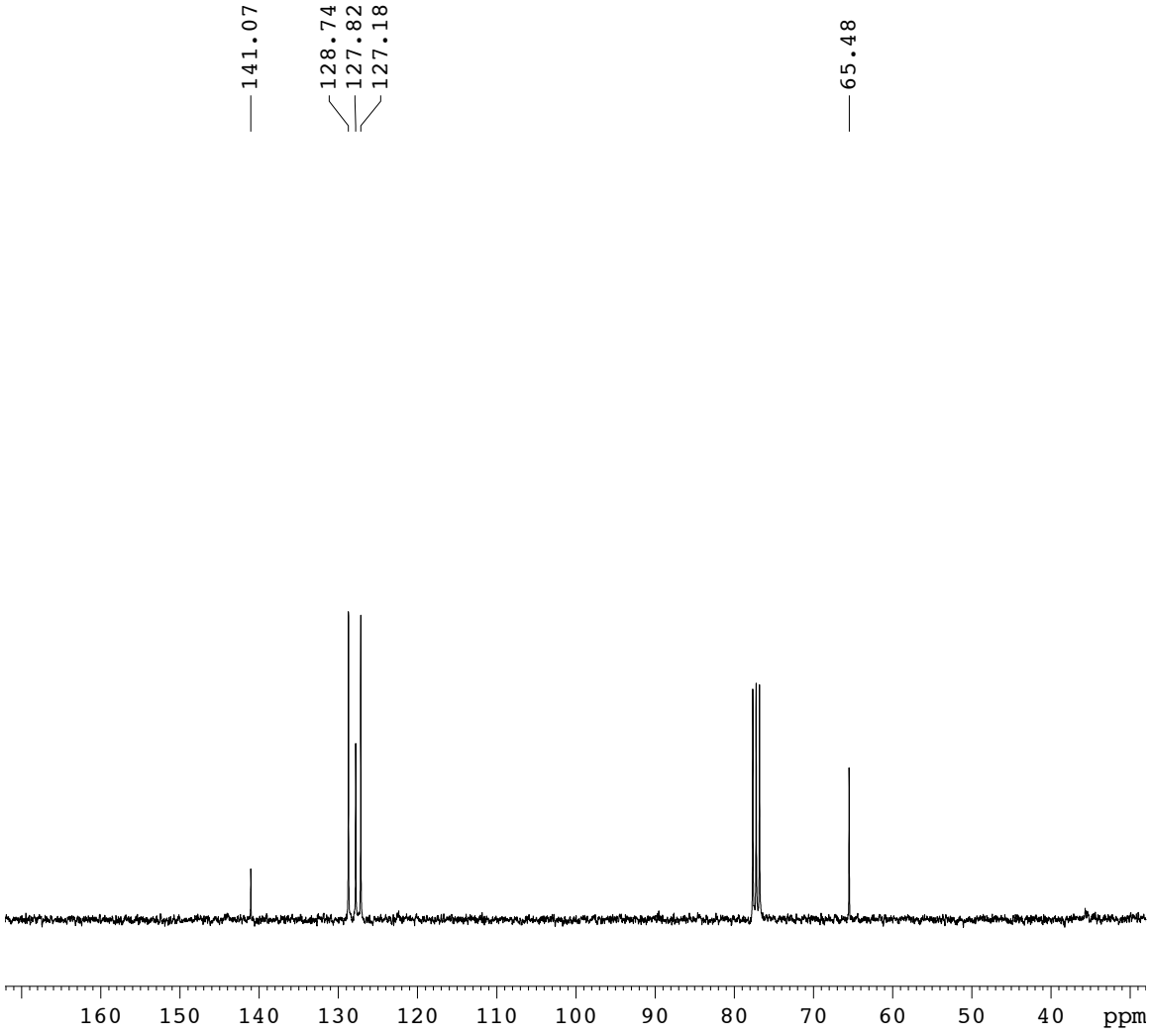

^{1}H NMR (300.1 MHz, $CDCl_3$) 4-Methoxybenzyl alcohol (6-3d)

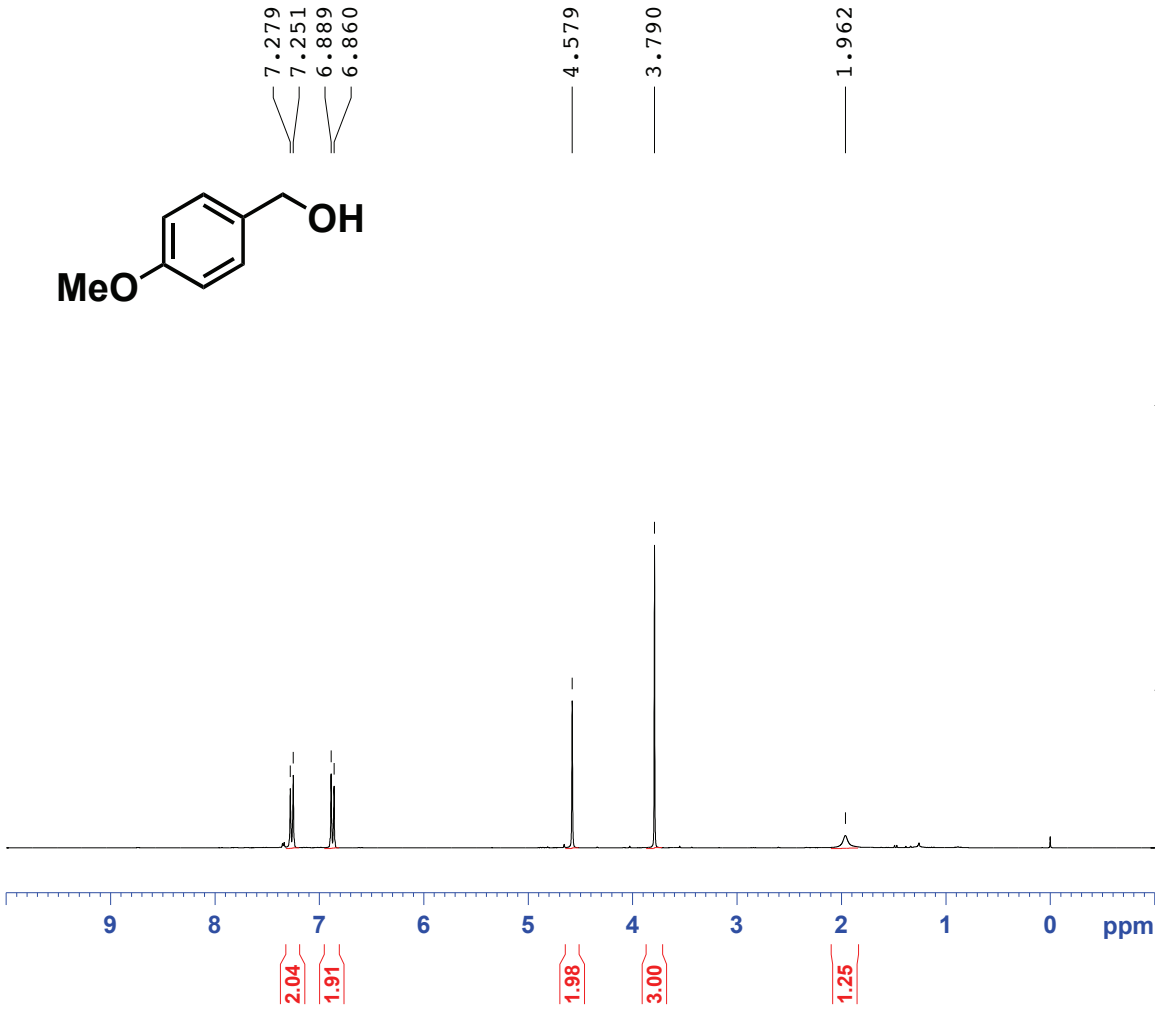

^{13}C NMR (75.5 MHz, $CDCl_3$) 4-Methoxybenzyl alcohol (6-3d)

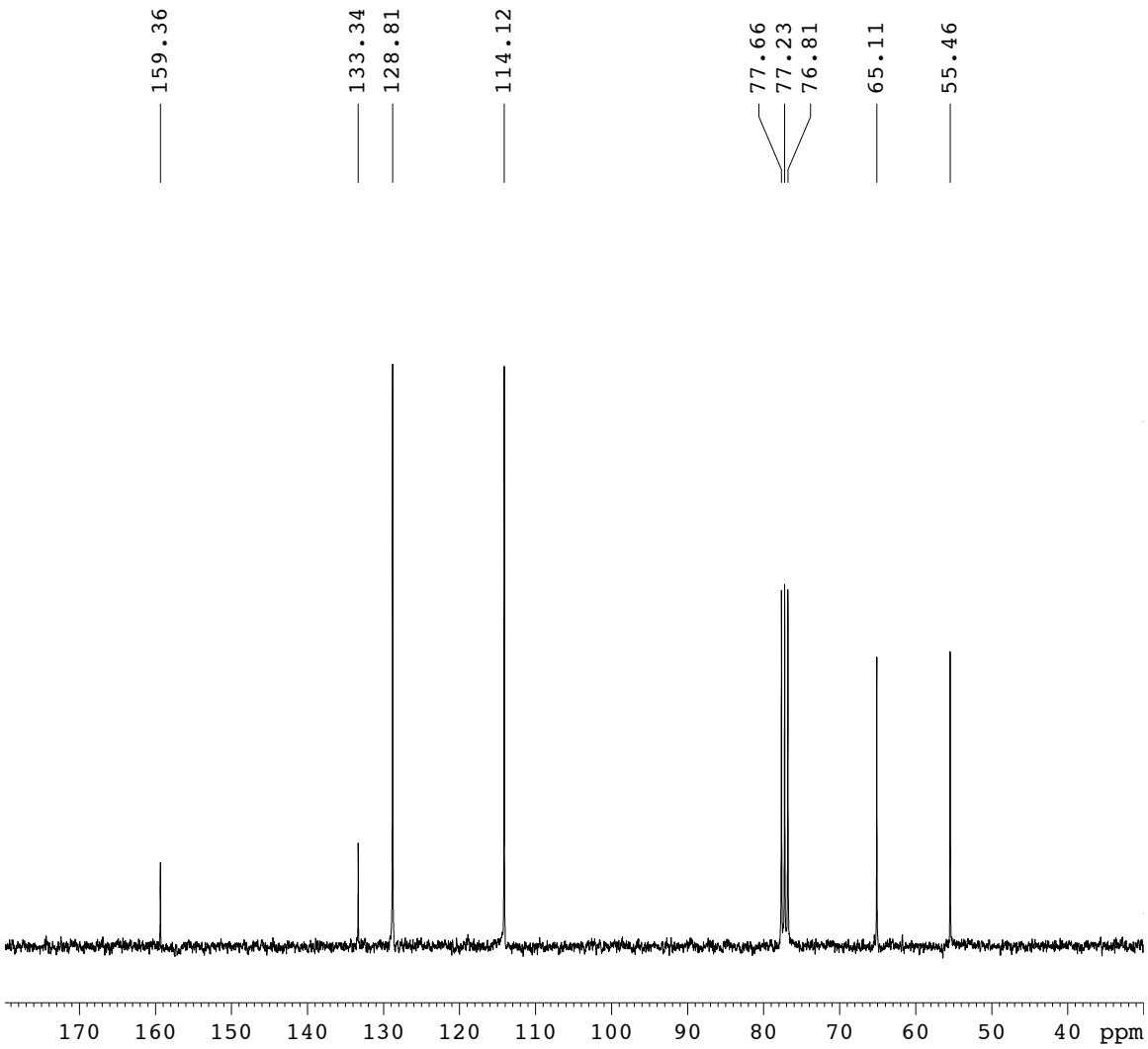

^{1}H NMR (300.1 MHz, $CDCl_3$) 1-Octanol (6-3g)

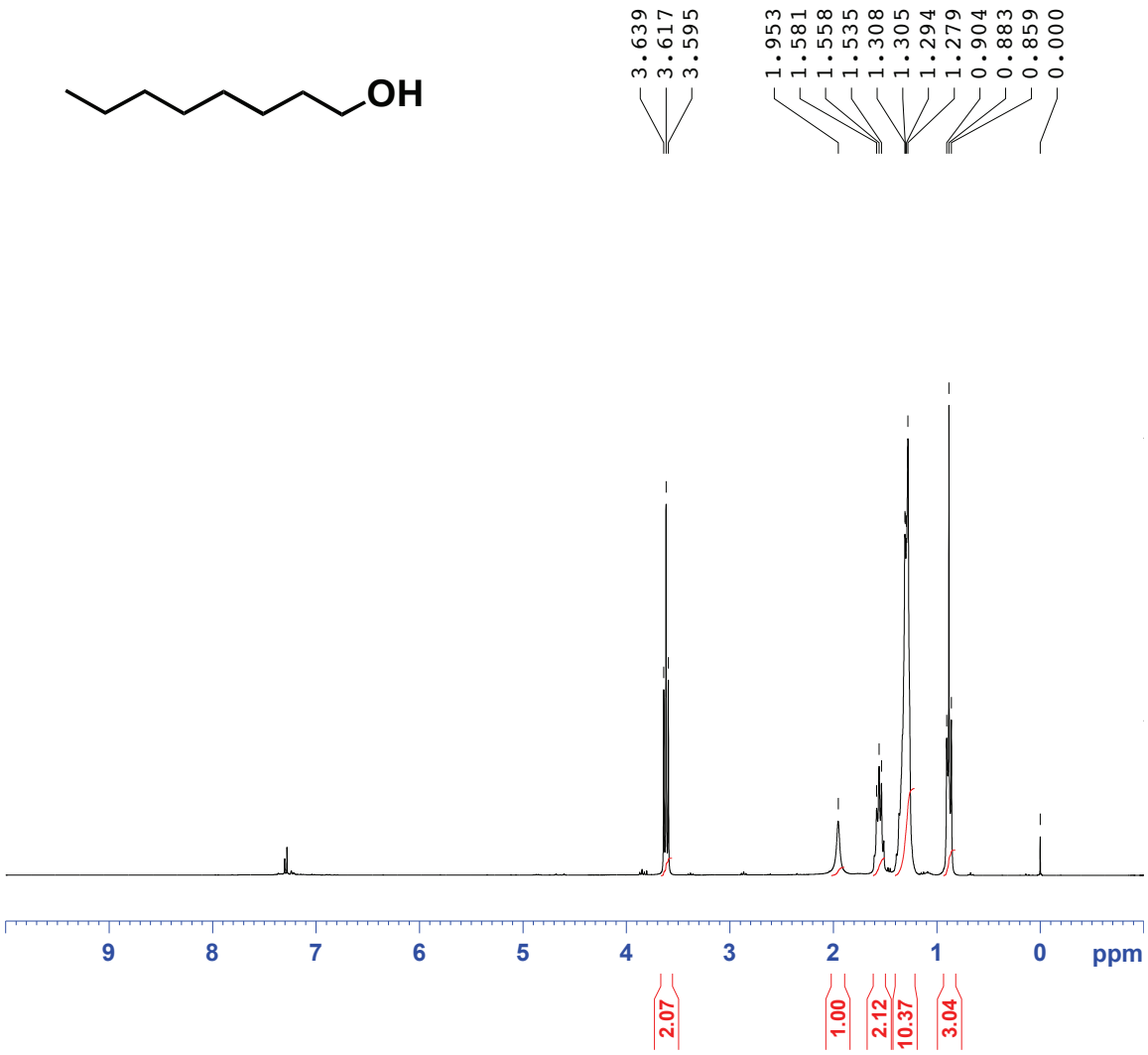

^{13}C NMR (75.5 MHz, $CDCl_3$) 1-Octanol (6-3g)

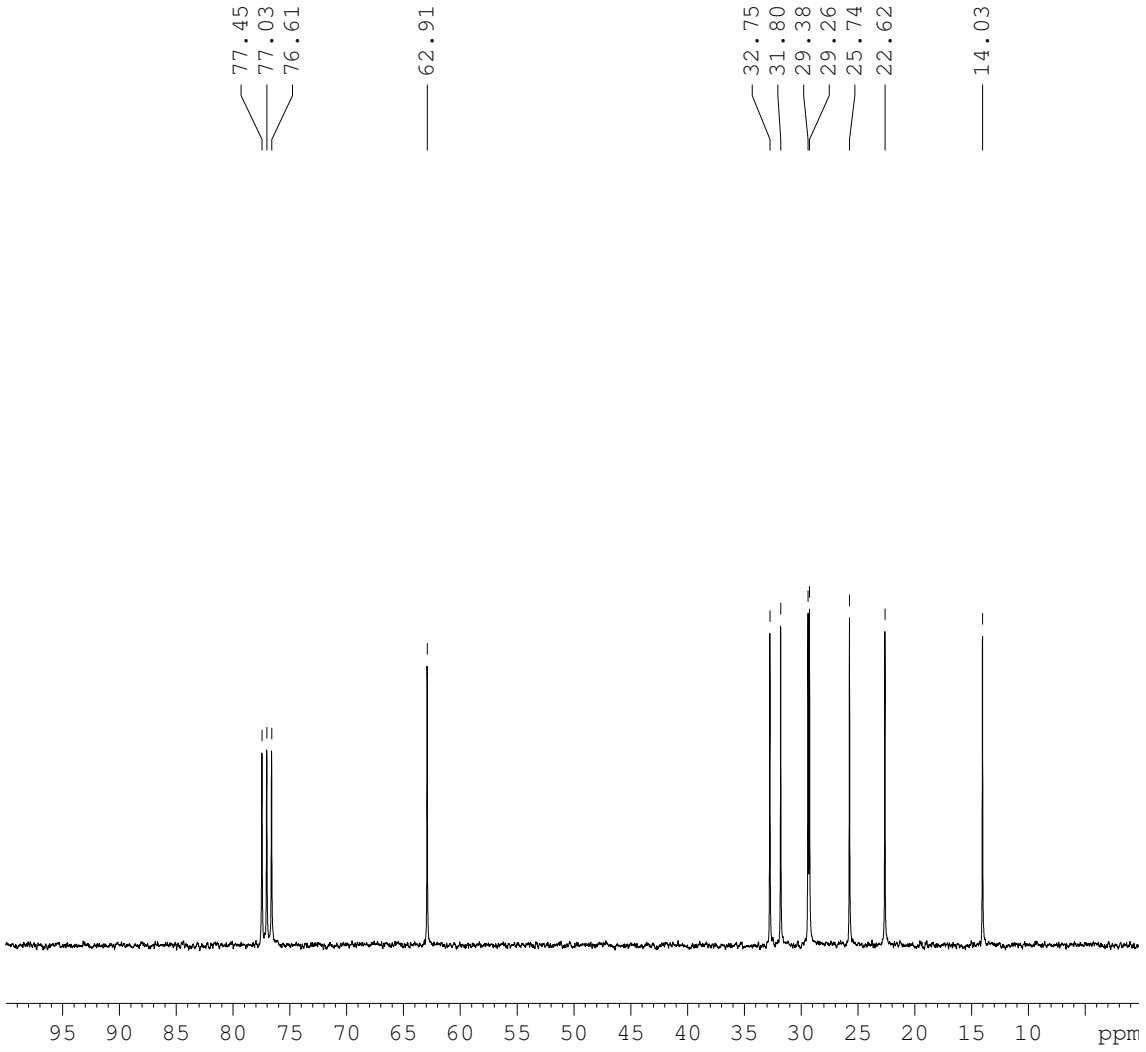

^{1}H NMR (300.1 MHz, $CDCl_3$) 2-octyl-4,4,5,5-tetramethyl-1,3,2-dioxaborolane (7-1)

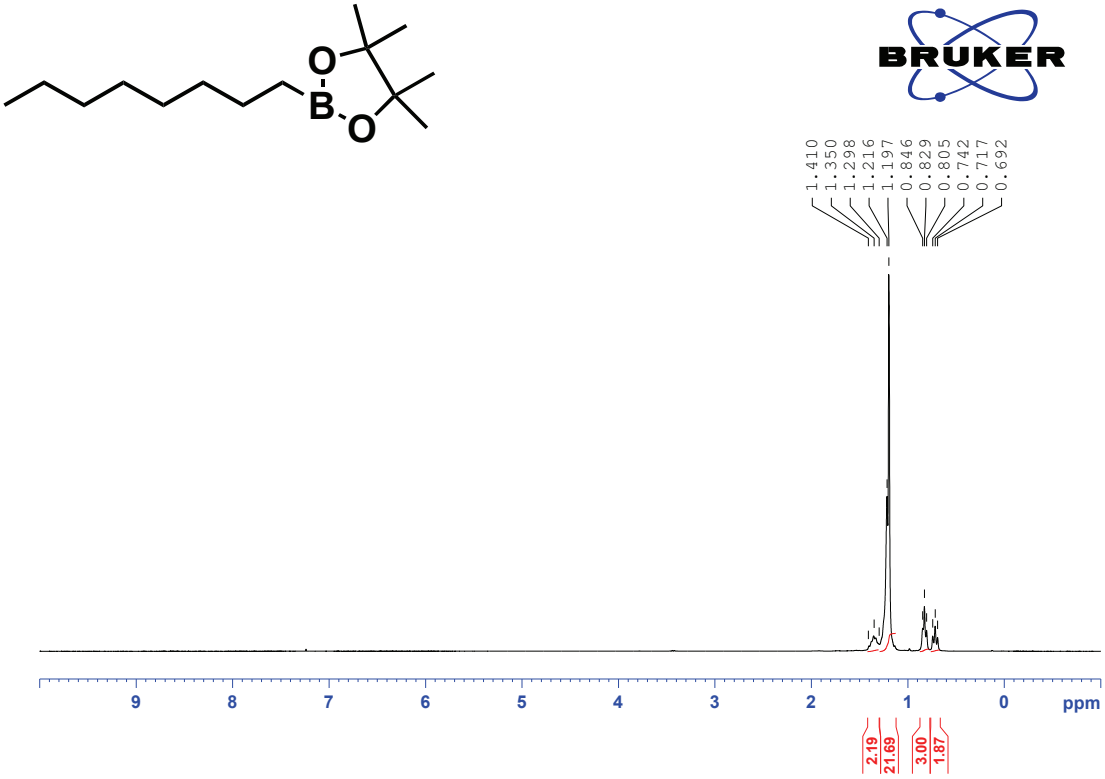

^{13}C DEPT-Q NMR (75.5 MHz, $CDCl_3$) 2-octyl-4,4,5,5-tetramethyl-1,3,2-dioxaborolane (7-2)

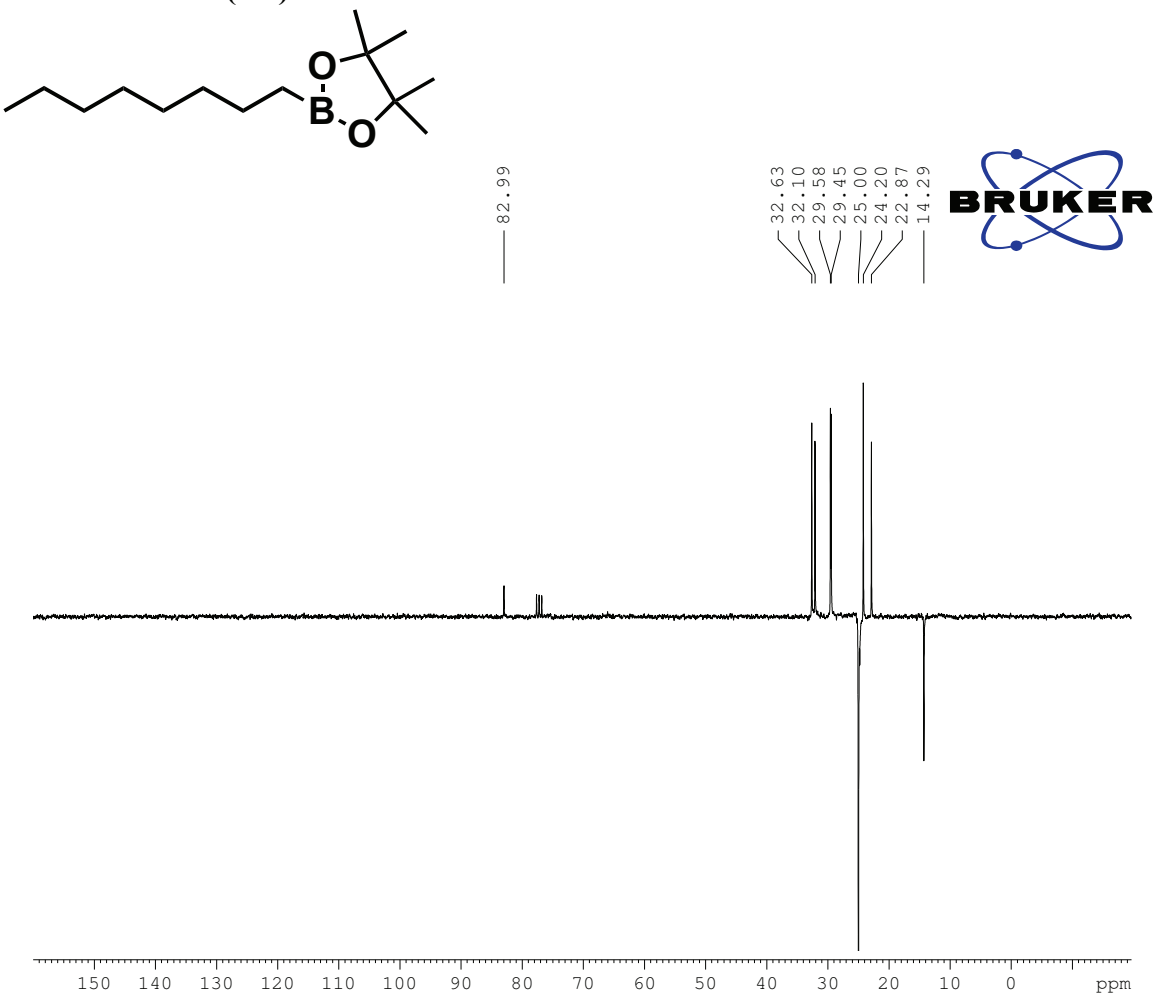

^{1}H NMR (300.1 MHz, $CDCl_3$) 2-hexyl-4,4,5,5-tetramethyl-1,3,2-dioxaborolane (7-3)

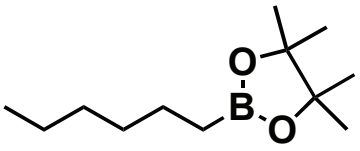

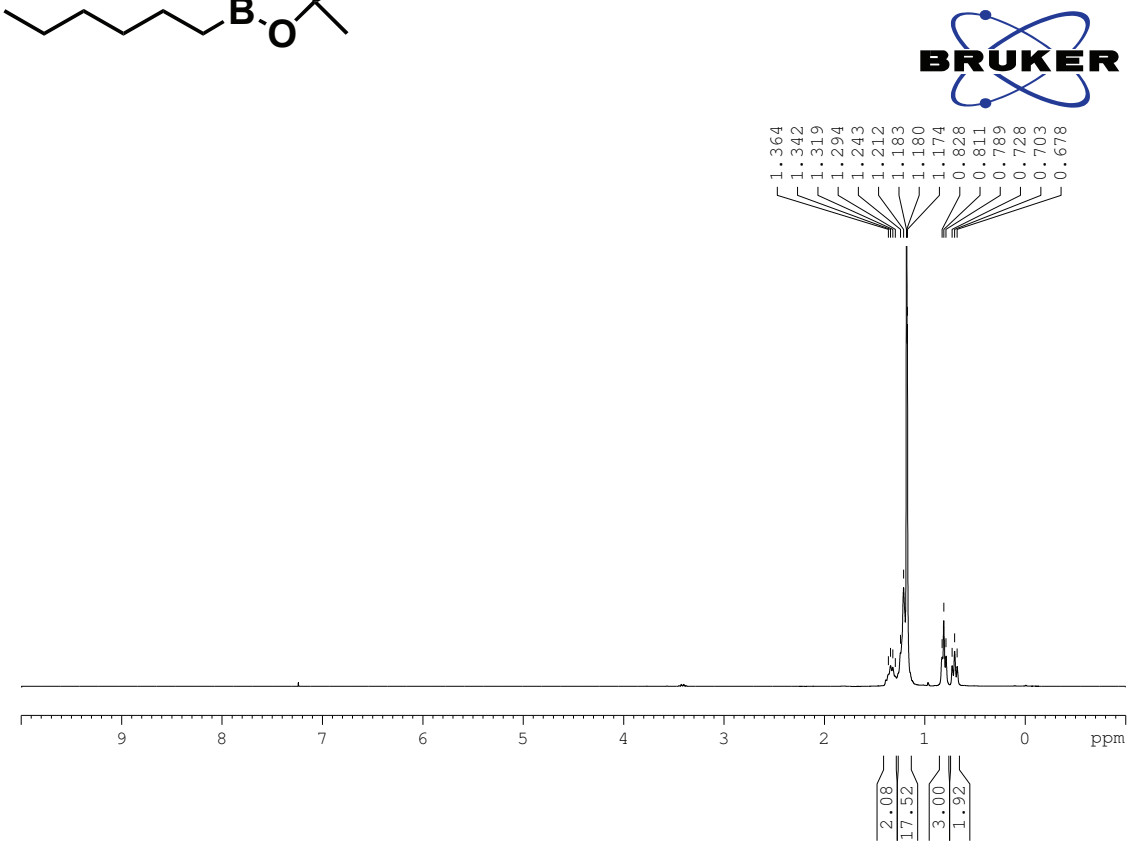

^{13}C DEPT-Q NMR (75.5 MHz, $CDCl_3$) 2-hexyl-4,4,5,5-tetramethyl-1,3,2-dioxaborolane (7-3)

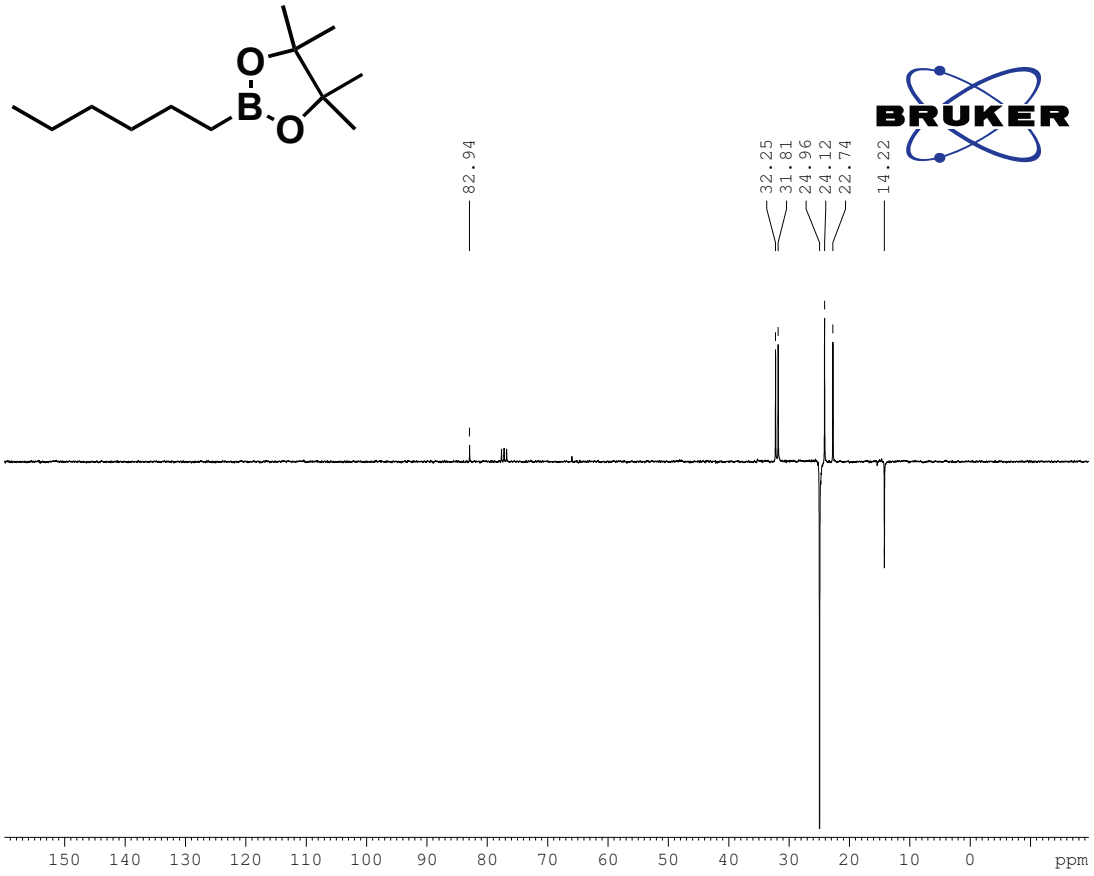

^{1}H NMR (300.1 MHz, $CDCl_3$) 2-(4-methylpentyl)-4,4,5,5-tetramethyl-1,3,2-dioxaborolane (7-4)

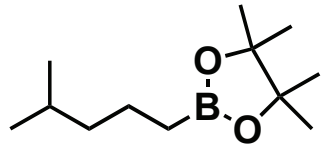

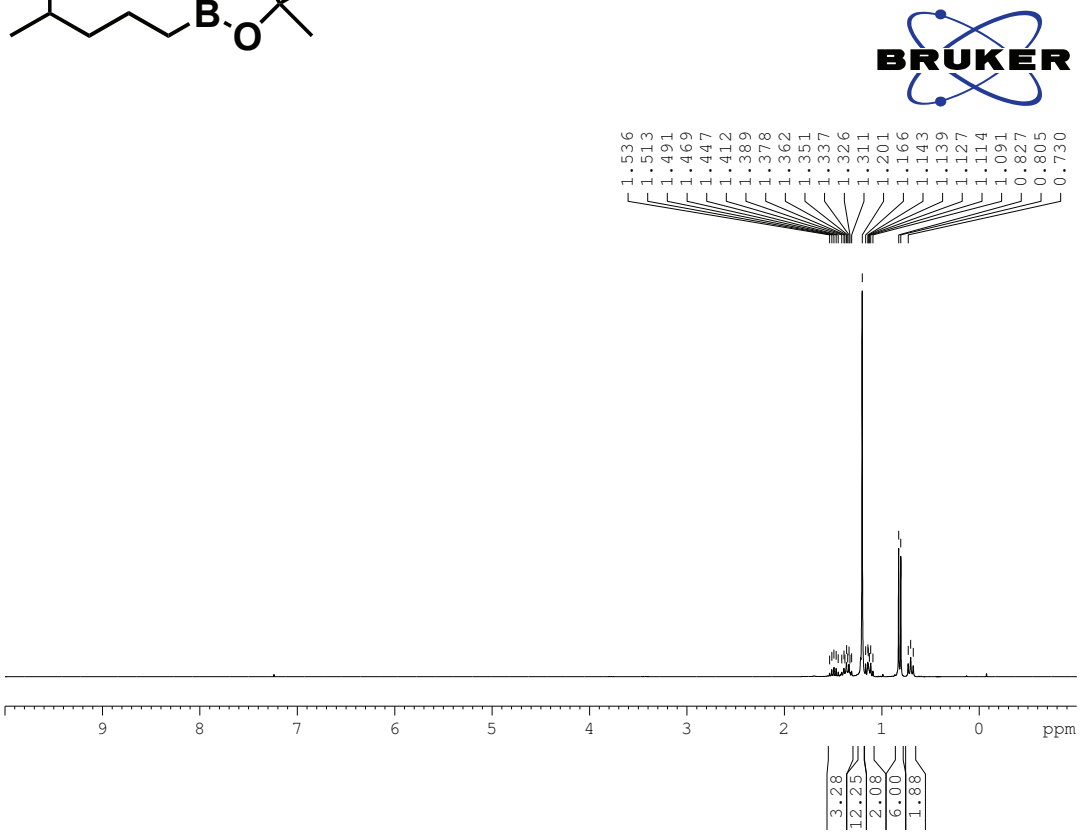

^{13}C DEPT-Q NMR (75.5 MHz, $CDCl_3$) 2-hexyl-4,4,5,5-tetramethyl-1,3,2-dioxaborolane (7-4)

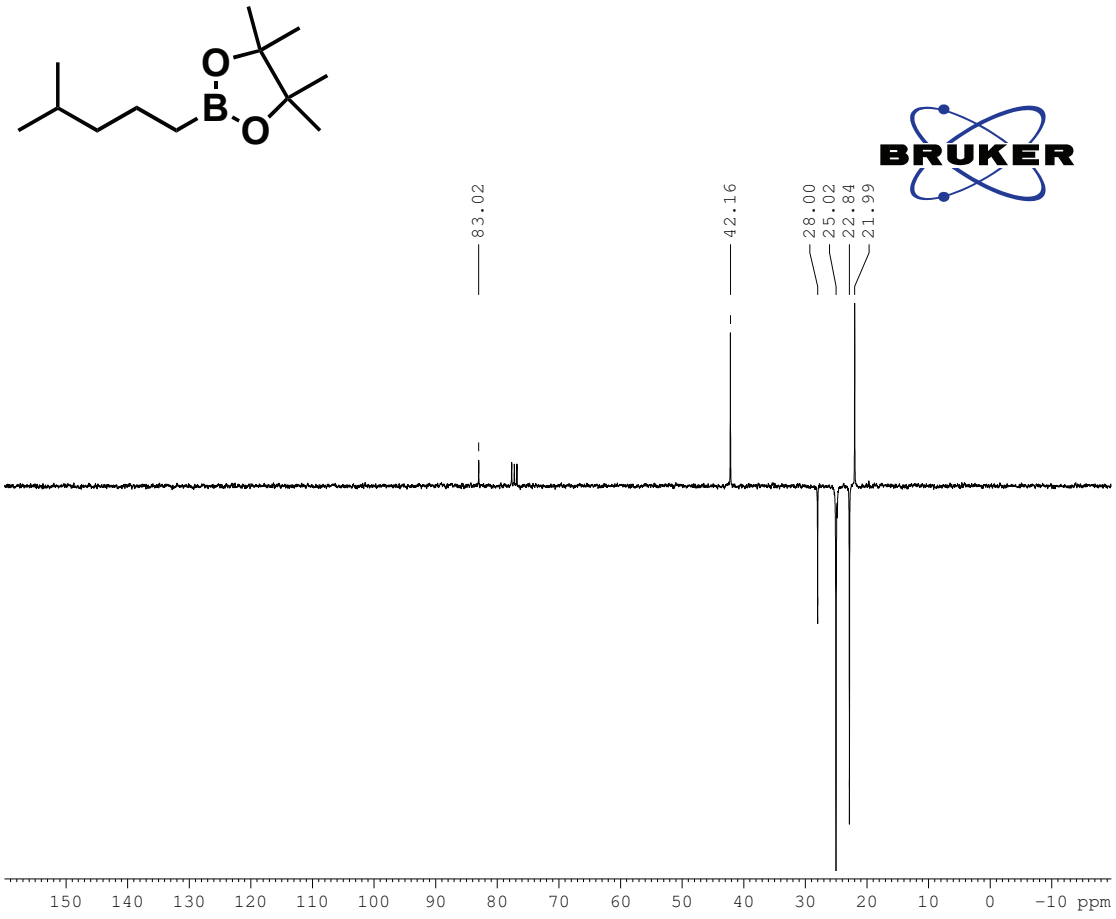

^{1}H NMR (300.1 MHz, $CDCl_3$) trimethyl(3-(4,4,5,5-tetramethyl-1,3,2-dioxaborolan-2-yl)propyl)silane (7-5)

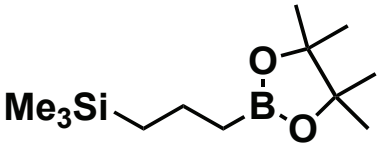

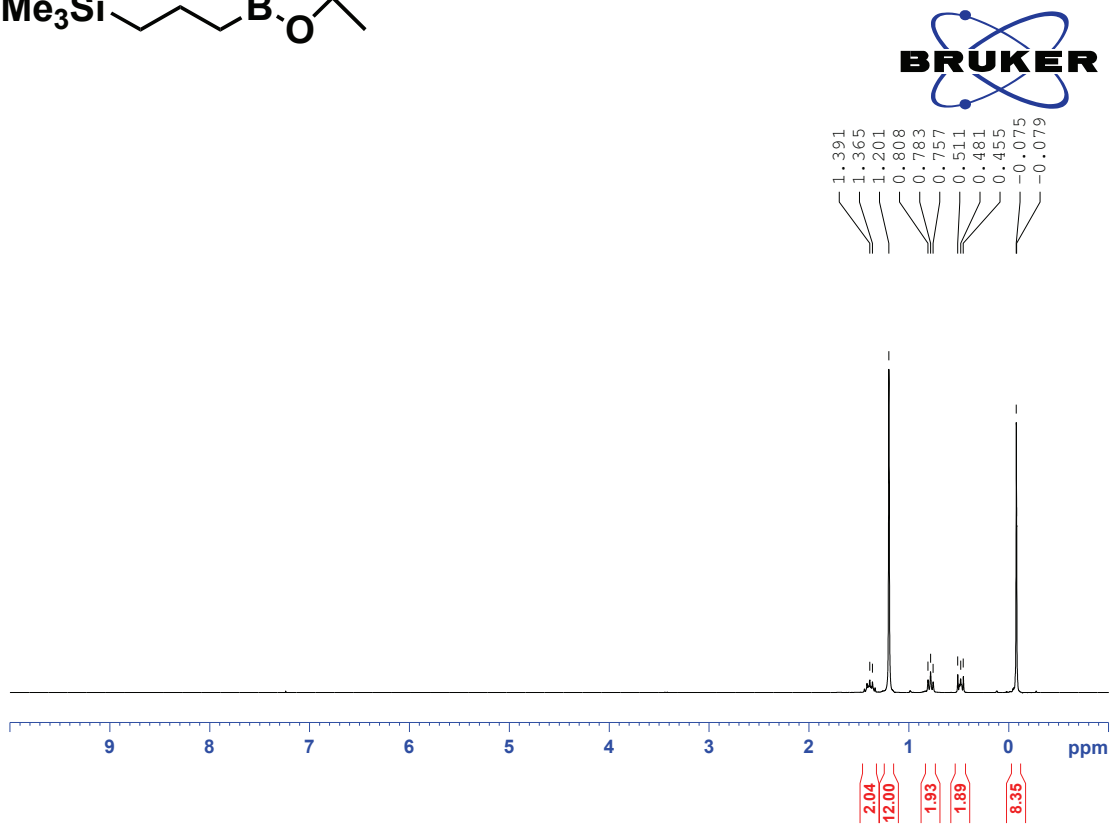

^{13}C DEPT-Q NMR (75.5 MHz, $CDCl_3$) trimethyl(3-(4,4,5,5-tetramethyl-1,3,2-dioxaborolan-2-yl)propyl)silane (7-5)

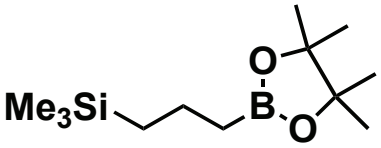

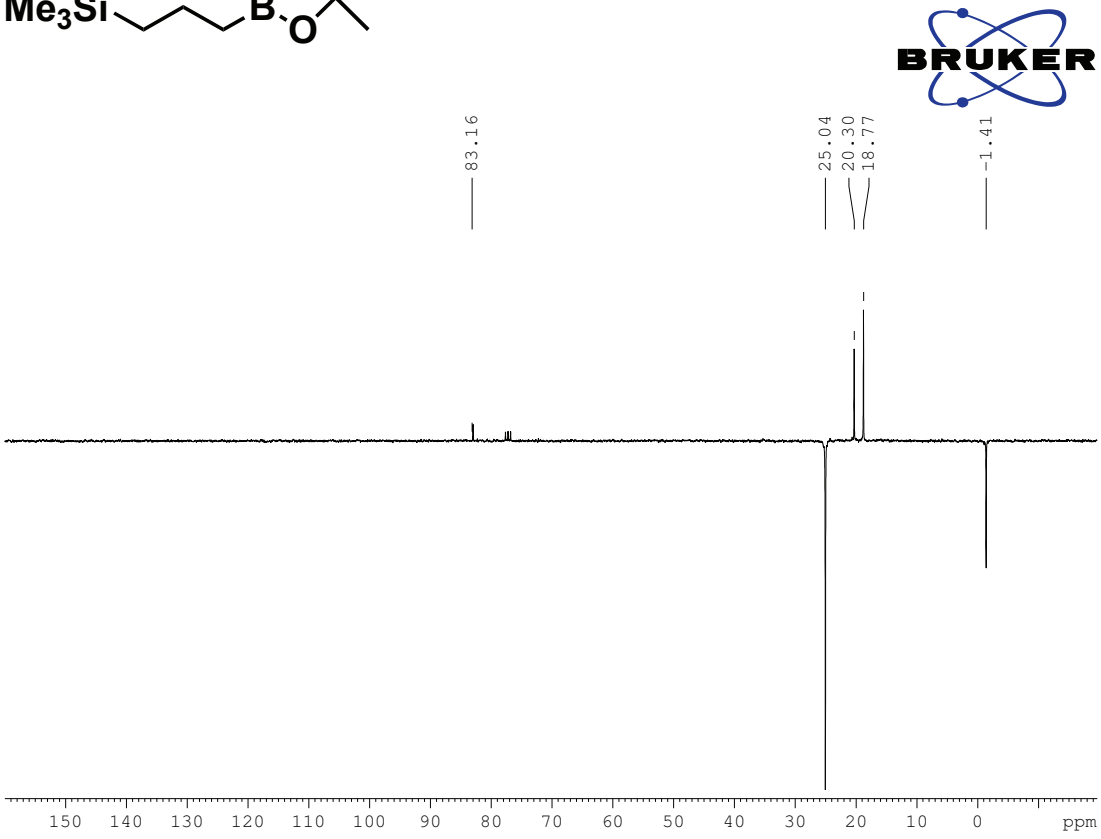

^{1}H NMR (300.1 MHz, $CDCl_3$) 2-(3,3-dimethylbutyl)-4,4,5,5-tetramethyl-1,3,2-dioxaborolane (7-6)

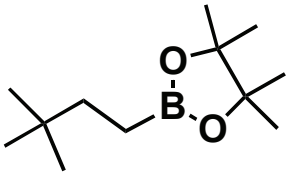

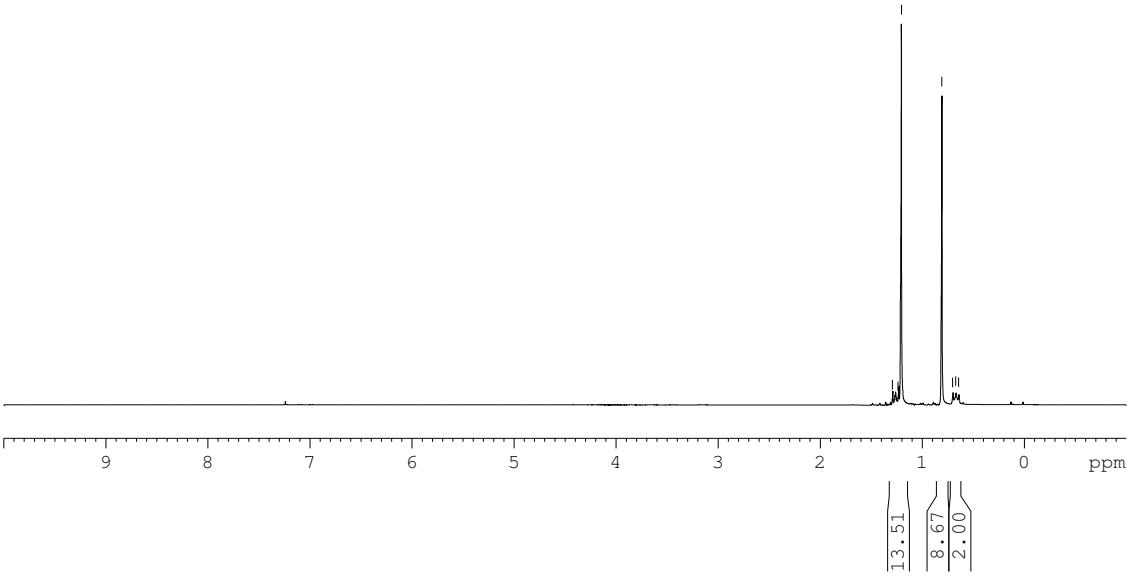

^{13}C DEPT-Q NMR (75.5 MHz, $CDCl_3$)) 2-(3,3-dimethylbutyl)-4,4,5,5-tetramethyl-1,3,2-dioxaborolane (7-6)

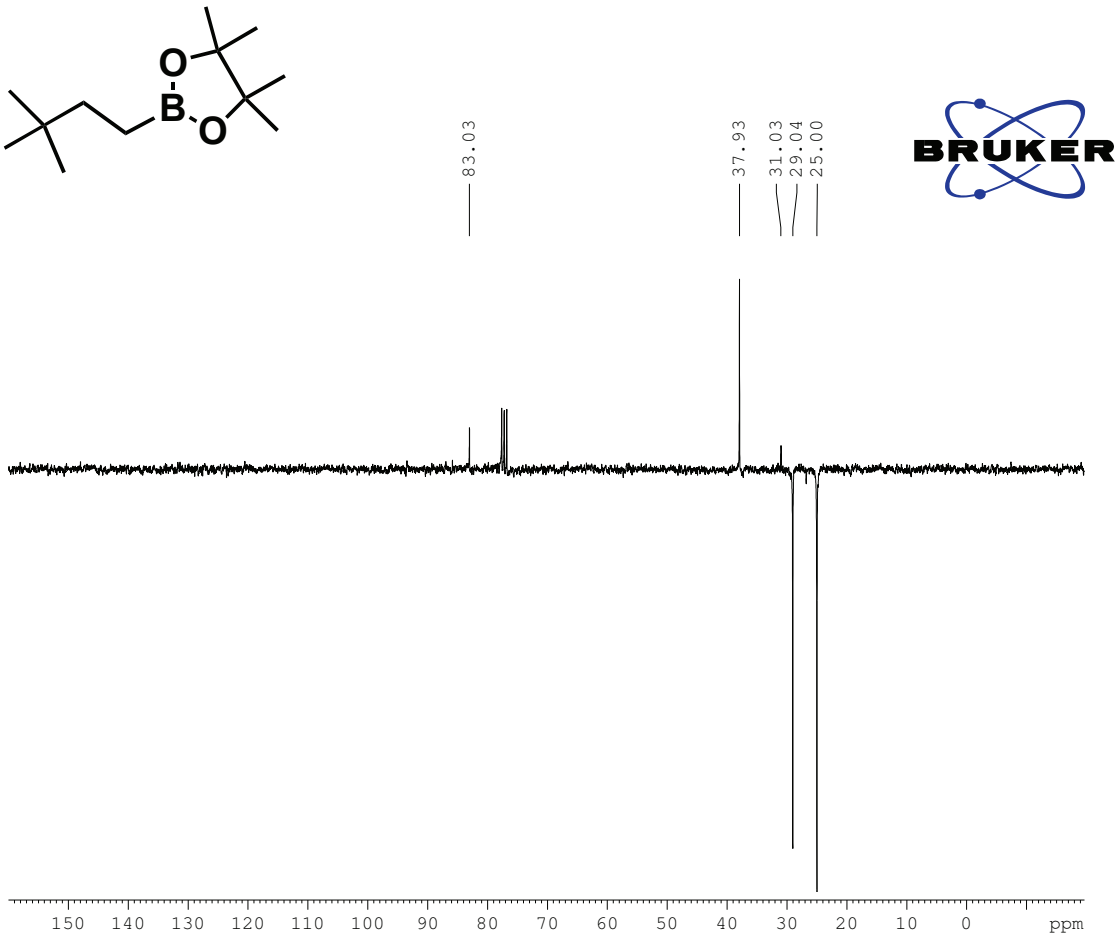

^{1}H NMR (300.1 MHz, $CDCl_3$) 2-(2-methylpentyl)-4,4,5,5-tetramethyl-1,3,2-dioxaborolane (7-7)

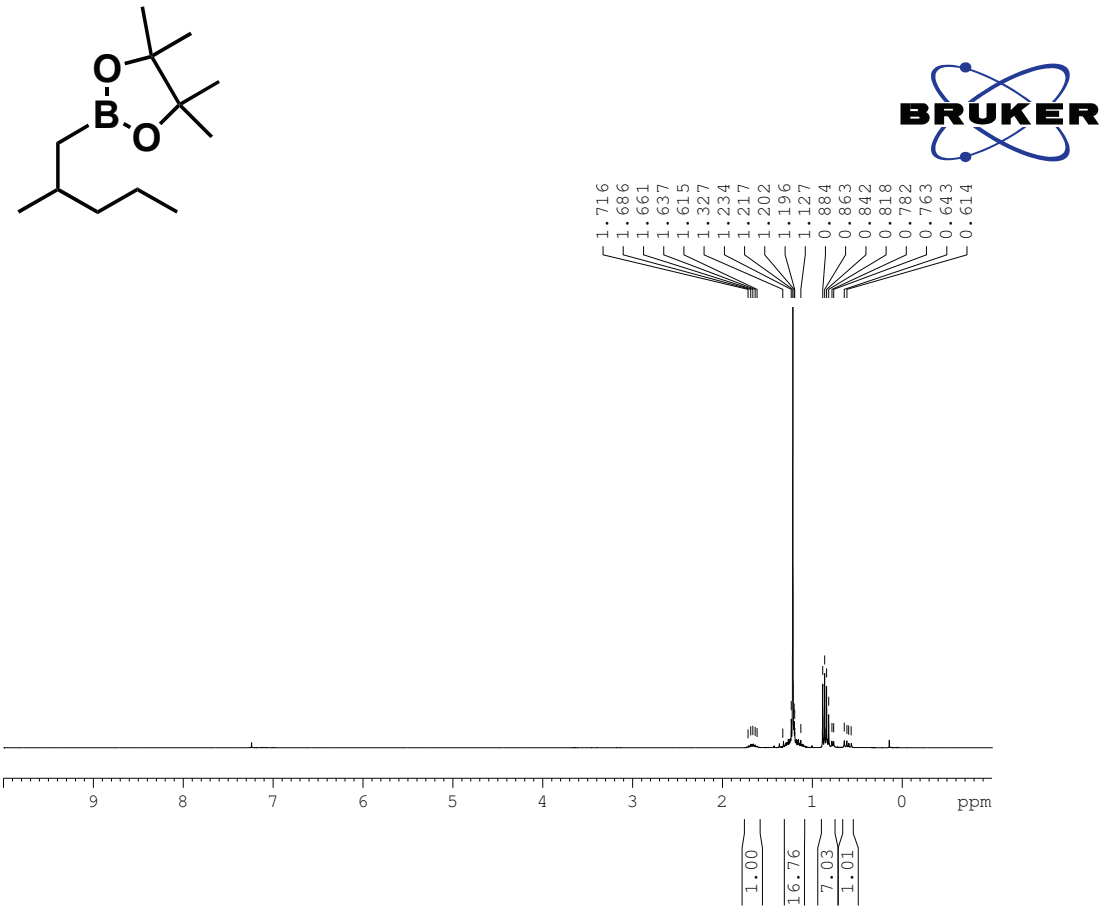

^{13}C DEPT-Q NMR (75.5 MHz, $CDCl_3$) 2-(2-methylpentyl)-4,4,5,5-tetramethyl-1,3,2-dioxaborolane (7-7)

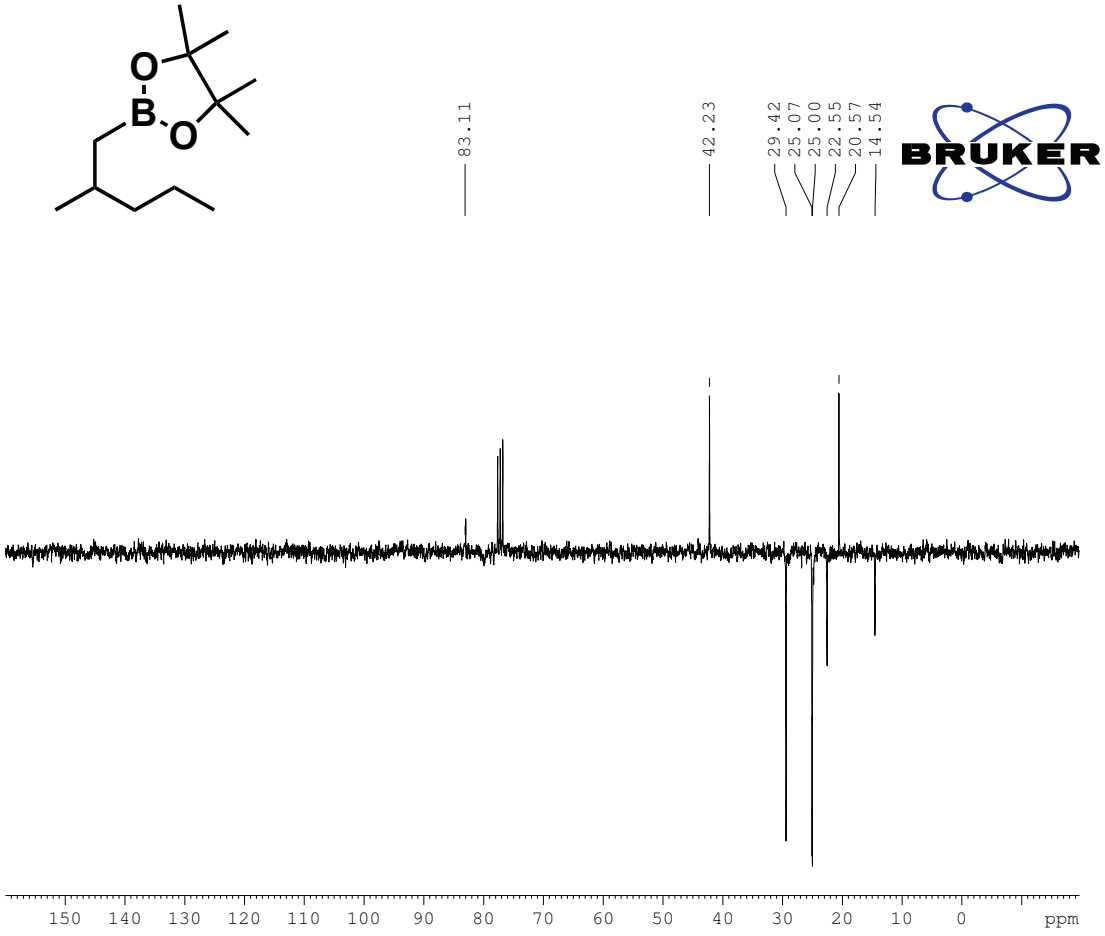

^{1}H NMR (300.1 MHz, $CDCl_3$) 2-cyclohexyl-4,4,5,5-tetramethyl-1,3,2-dioxaborolane (7-8)

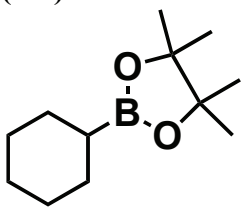

^{13}C DEPT-Q NMR (75.5 MHz, $CDCl_3$) 2-cyclohexyl-4,4,5,5-tetramethyl-1,3,2-dioxaborolane (7-8)

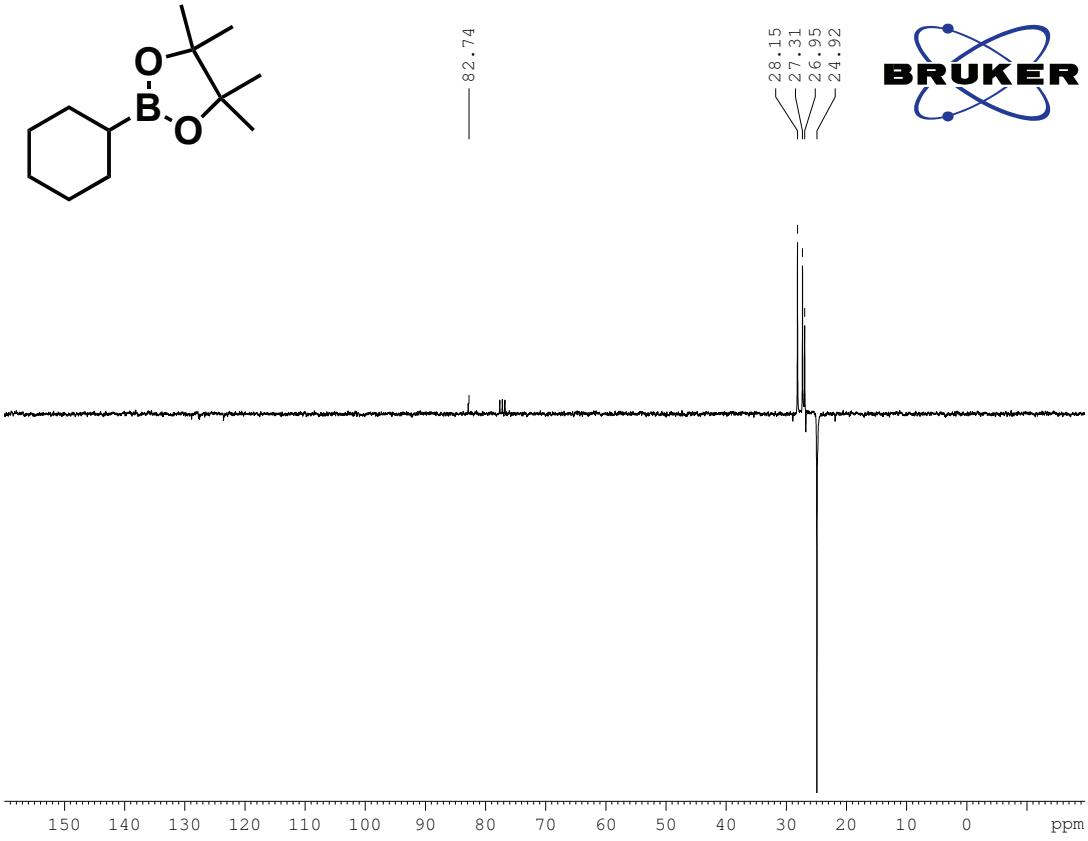

^{1}H NMR (300.1 MHz, $CDCl_3$) 2-cyclooctyl-4,4,5,5-tetramethyl-1,3,2-dioxaborolane (7-9)

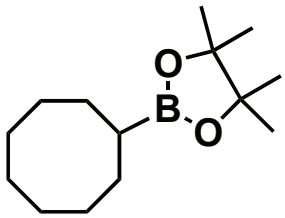

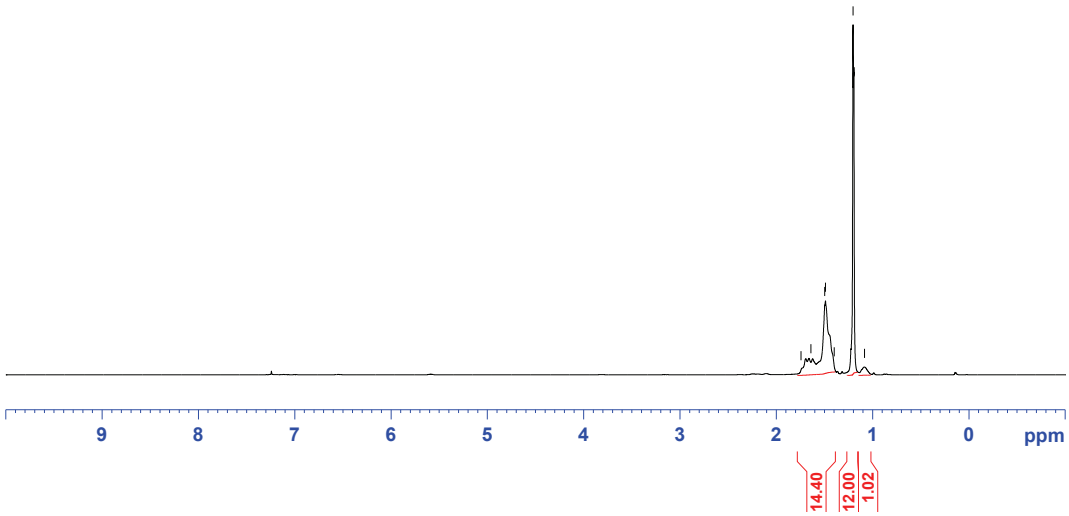

^{13}C DEPT-Q NMR (75.5 MHz, $CDCl_3$) 2-cyclooctyl-4,4,5,5-tetramethyl-1,3,2-dioxaborolane (7-9)

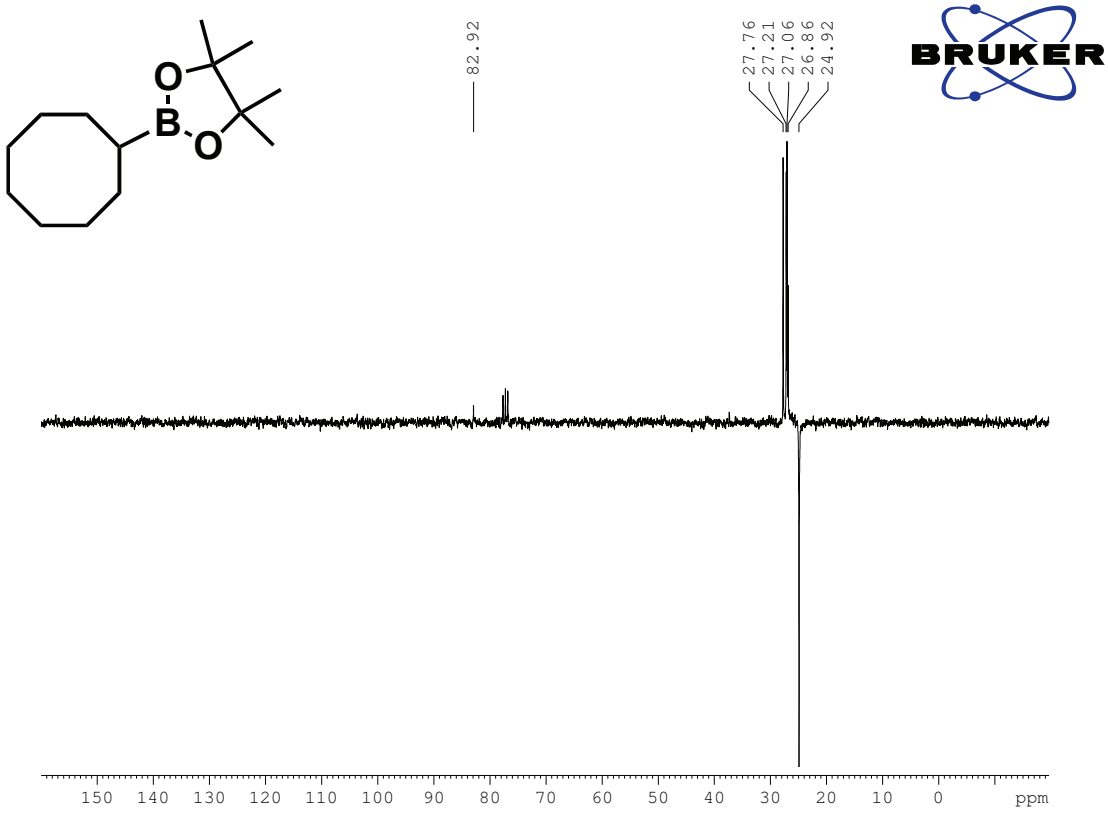

^{1}H NMR (300.1 MHz, $CDCl_3$) 1-phenylethanol (7-10)

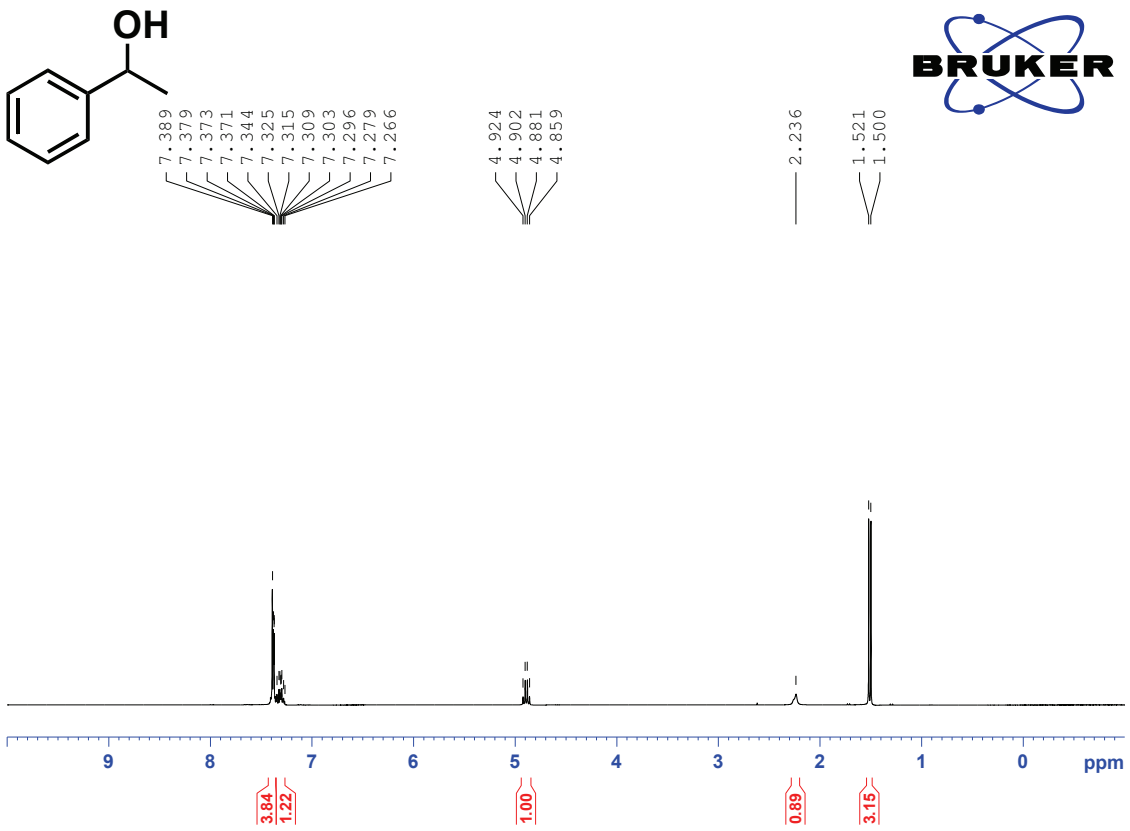

^{13}C DEPT-Q NMR (75.5 MHz, $CDCl_3$) 1-phenylethanol (7-10)

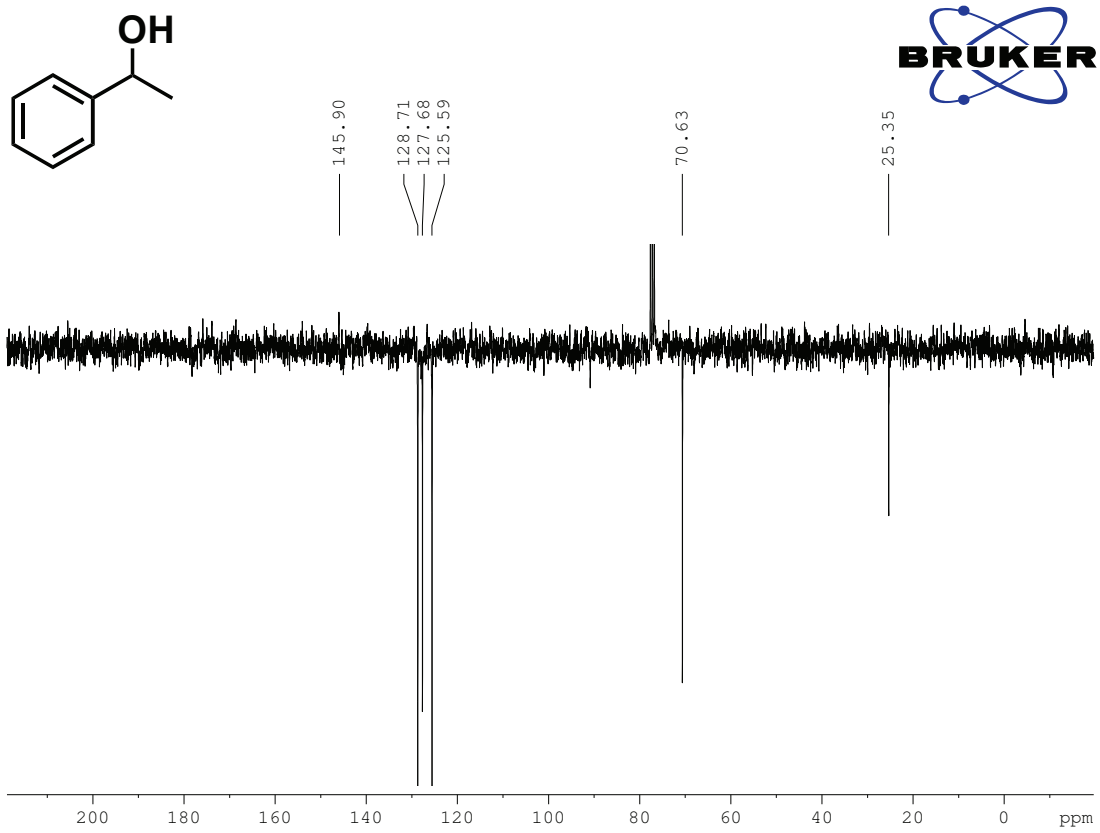

^{1}H NMR (300.1 MHz, $CDCl_3$) Cyclohexanol (7-11)

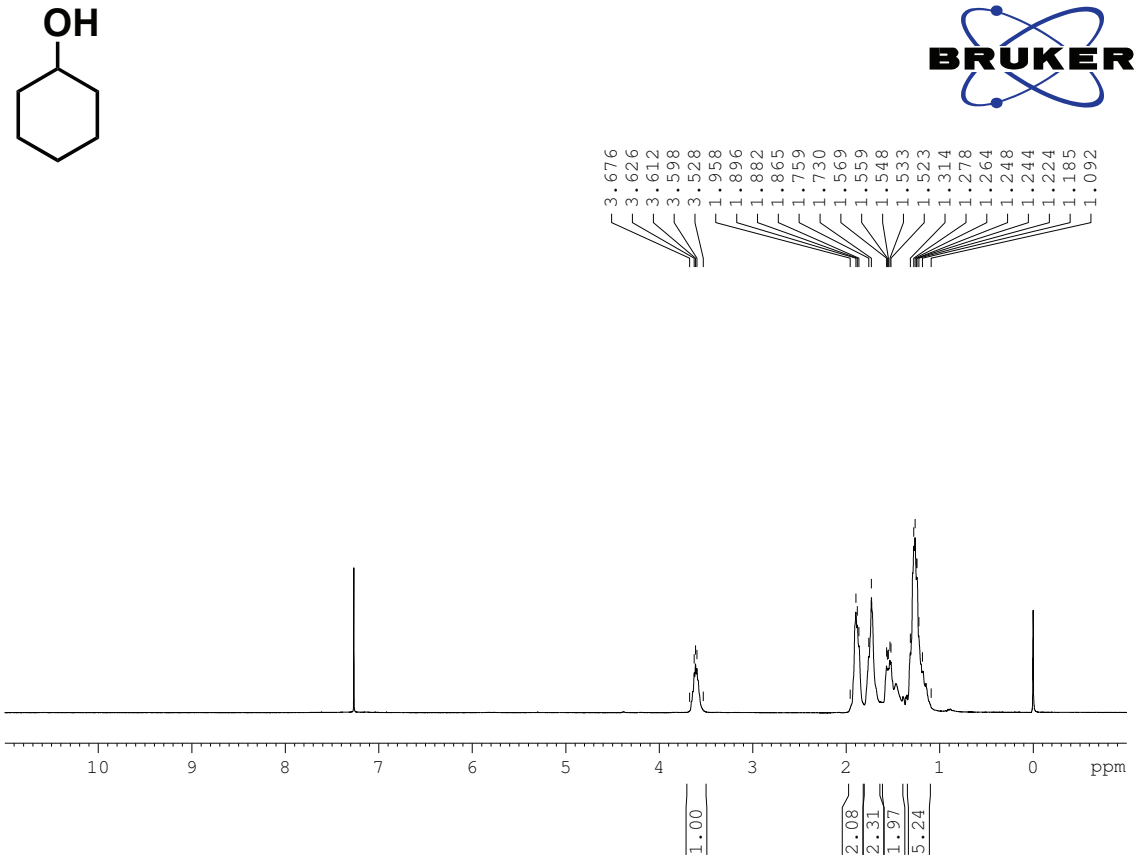

^{13}C DEPT-Q NMR (75.5 MHz, $CDCl_3$) Cyclohexanol (7-11)

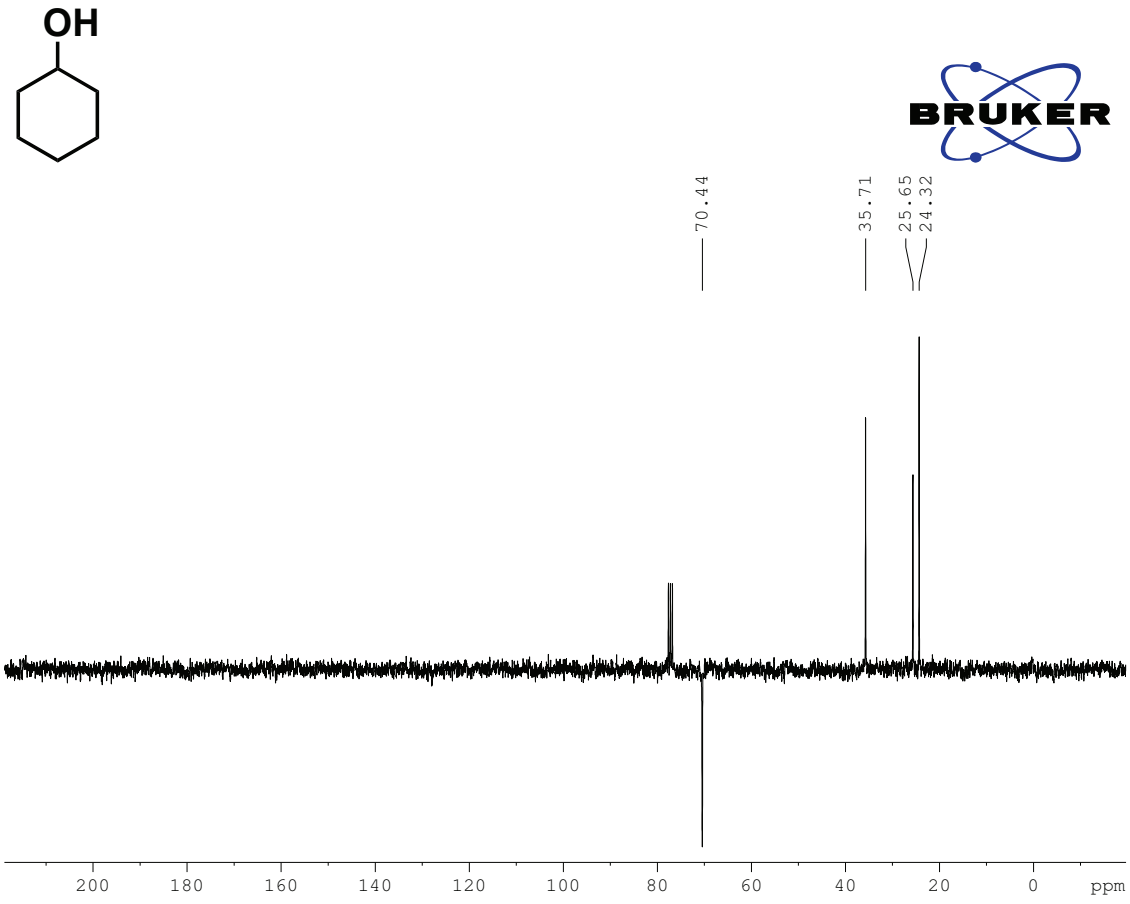

^{1}H NMR (300.1 MHz, $CDCl_3$) 2-heptanol (7-12)

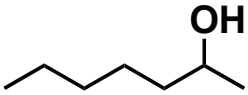

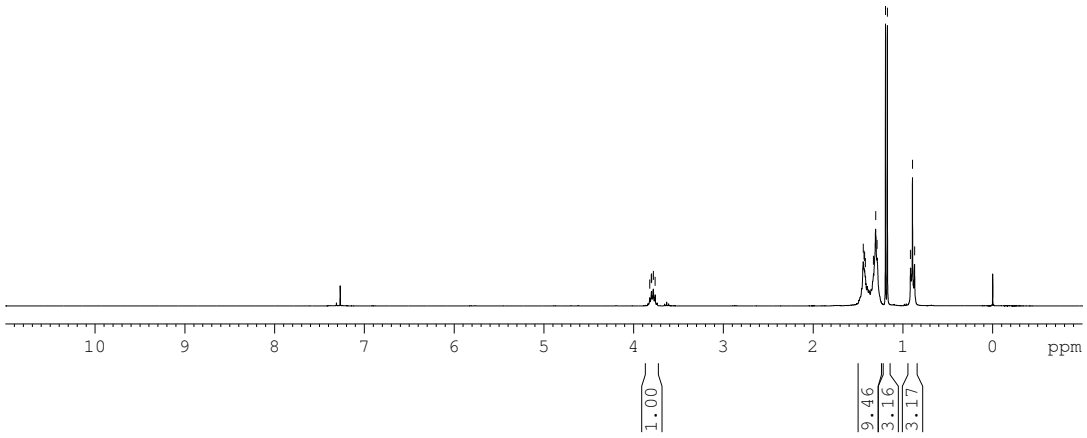

^{13}C DEPT-Q NMR (75.5 MHz, $CDCl_3$) 2-heptanol (7-12)